UNIVERSITY OF OKLAHOMA

GRADUATE COLLEGE

METAL-ENHANCED FLUORESCENCE OF GOLD NANOPARTICLE AND QUANTUM DOT INCORPORATED SILICA NANOPARTICLE AGGREGATES

A DISSERTATION

SUBMITTED TO THE GRADUATE FACULTY

in partial fulfillment of the requirements for the

Degree of

DOCTOR OF PHILOSOPHY

By

SARAVANAN RAMASAMY
Norman, Oklahoma
2015

METAL-ENHANCED FLUORESCENCE OF GOLD NANOPARTICLE AND QUANTUM DOT INCORPORATED SILICA NANOPARTICLE AGGREGATES

A DISSERTATION APPROVED FOR THE
DEPARTMENT OF CHEMISTRY AND BIOCHEMISTRY

BY

_____
Dr. Ronald L. Halterman, Chair

_____
Dr. Daniel T. Glatzhofer

_____
Dr. Kenneth M. Nicholas

_____
Dr. Wai Tak Yip

_____
Dr. Mark A. Nanny

I dedicate this dissertation to my parents, my brother, and my wife for their endless love and support

Acknowledgements

I want to take this opportunity to thank my advisor Dr. Ronald Halterman for his excellent guidance and encouragement. I really appreciate the patience Dr. Halterman had with me through all these years of my learning. This work would have not been possible without his vision.

I would also like to thank my committee members, Dr. Glatzhofer, Dr. Nicholas, Dr. Yip and Dr. Nanny for their valuable advice and constructive feedback throughout my graduate study. My special thanks to all of my lab mates, Shawna Ellis, Justin Garrett, Nathan Green, Kalani Gunawardana, Robinson James, Shekar Mekala, Anuradha Singh and the undergraduate researchers. I would also like to thank the Department of Chemistry and Biochemistry for providing me teaching assistantship throughout my study.

I would like to extent my special thanks to Greg Strout in the Samuel Robert Nobel Electron Microscopy Laboratory for training me with the TEM instrument. I would also like to thank many of my Indian friends at OU and back in India for their motivation.

I am greatly indebted to my parents Kannagi M. and Ramasamy M. and my brother Kathiranvan Ramasamy for all their sacrifices in their life to be able to send me to USA to pursue my higher education. Most importantly I would like to thank my wife Shanmugapriya Dharmarajan for her wisdom, patience, and love throughout this process.

Table of Contents

List of Tables

List of Figures

Abstract

The enhancement of fluorescence intensity due to the proximity of metal nanoparticles is of great interest in enabling the detection of low concentration biomarkers. Although the recent developments in the optical sensor techniques pushed the sensitivity to the single-molecular detection, there is still an immense need for smaller and brighter sensor probes. Metal-enhanced fluorescence (MEF) is a promising strategy to amplify the signal from fluorophores by coupling to metal nanoparticles and significantly improve the potential of fluorescence based technology in bioapplications.

Gold nanoparticles are known for their ability to manipulate the incident light and generate a localized charge density oscillation called surface plasmon resonance (SPR). The concentrated electric field created around the metal surface by the SPR can dramatically increase the fluorescence brightness of nearby fluorophores by opening up additional excitation and emission pathways. Our research goal is to develop a solution based approach to study the metal-enhanced fluorescence by aggregating metal and fluorophore nanoparticles using organic linker molecules, which would ultimately lead to the ultra-bright fluorescent probes.

In the first part of our research, monodisperse gold nanoparticles (GNPs) of various diameters (15 - 60 nm) were synthesized using citrate reduction method and their photophysical properties were analyzed. The GNPs absorb and scatter in the visible light region with λ_{max} between 515-545 nm. The place exchange efficacies of thiol and disulfide based hydrophobic ligand to replace water stabilizing citrate ions on the GNP surface were investigated. The amount of surface modified gold nanoparticles phase transferred from the aqueous to organic phase was measured using absorption

spectroscopy to determine the efficacy of the place exchange. It took about 1 mM of 1,2-didodecyldisulfide to phase transfer 89% of GNPs.

The surface plasmon resonances of nearby GNPs can combine to generate even more concentrated electric field at their interparticle gap and the phenomenon is called plasmon coupling. This would cause a red-shift of absorbance band for the aggregated GNPs. We used this red shift in absorbance spectra to monitor the aggregation of gold nanoparticles. We developed a method of organic molecules mediated GNP aggregation in aqueous solution. We synthesized alkane chain ligand with amine and disulfide terminal groups to coat on GNPs' surface and promote GNP aggregation by spontaneous or photo triggered activation of dithiocarbamate (DTC) moiety. The DTC mediated robust aggregates of GNP caused a red shift of absorbance peak from ~530 nm to beyond 580 nm. This red shifted scattering component of GNP aggregates can also be used to enhance the fluorescence brightness of the fluorophores placed in the interparticle gap.

Quantum dots (QDs) are fluorescent semiconductors with high photostability, high quantum efficiency and size tunable emission. They are attractive alternatives to the common organic dyes as the QDs have a broad excitation band and a narrow emission band. Since the MEF depends on the degree of spectral overlap between the metal and fluorophore, QDs with tunable emission would best fit for the study of MEF. Therefore, in the second part of our research we focused on synthesizing various size CdSe quantum dots cores (diameter 2.6 – 4.6 nm) and coated them with ZnS shell (overall diameter 7 nm) to create a highly stable and bright CdSe-ZnS core-shell QDs. In order to introduce water compatibility to the QDs, we developed a silica scaffold to

encapsulate the CdSe-ZnS core. We produced different size silica nanoparticles (diameter 35 nm and 100 nm) by varying the thickness of the silica shell around the QD core in order to study the metal-fluorophore distance dependency of MEF. The silica nanoparticles were surface functionalized with various ligands containing dithiocarbamate terminal that have preferential affinity to gold surface to produce silica-gold heteroaggregation.

In the last part of our research we investigated the effect of size and concentration of silica and gold nanoparticle on the fluorescence enhancement. We were able to achieve a notable 3-fold fluorescence enhancement from the dithiocarbamate mediated heteroaggregates of 25 nm diameter gold nanoparticles and 100 nm diameter QD-doped-silica nanoparticles in aqueous solution. TEM images verified that the heteroaggregates of GNP and QD-doped-SiNP were enabled by the organic linker ligands. The excitation and emission spectra indicated that the fluorescence enhancement was due to the aggregation of multiple GNP around the SiNPs. The effect of different binding methods of gold to silica on MEF was investigated.

The construction and the controlled aggregation of functionalized gold and fluorophore-doped-silica nanoparticles would give an opportunity to advance the field of fluorescence based sensors. Our focus has been to take advantage of the fine-tuned synthetic control to synergize the special optical properties of the gold nanoparticles and quantum dots in a solution based approach to study MEF.

Chapter I: Introduction

1.1.1. Surface plasmon resonance of gold nanoparticles

Surface plasmon resonance (SPR) is a light induced collective oscillation of surface electrons of a metal film or a metal nanoparticle.[1] When a light interacts with a metal nanoparticle the electric field of the light stimulates the conduction electrons on the metal surface to polarize with respect to the nanoparticle's positive ionic core. When the displacement of the surface electrons from the immobile positive charge occurs, a net charge difference arises at the interface of the metal and the surrounding medium.[2] If the movement of electrons are in-phase, a dipolar oscillation will be generated and is called surface plasmon oscillation or surface plasmon resonance. When the frequency of the surface plasmon resonance falls within the frequency range of the visible light, the nanoparticles absorb the photons of the light and scatter. Although this loosely bound electrons exist on the surface of bulk metals, they cannot be excited to plasmons under normal conditions.[3]

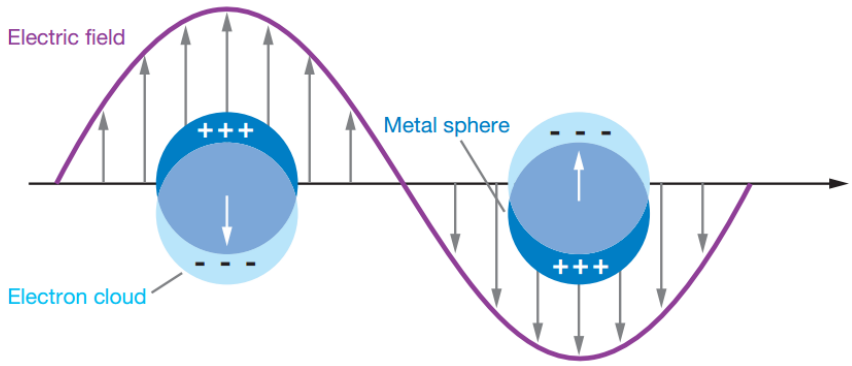

Figure 1.1. Generation of surface plasmon resonance on metal nanospheres under the influence of the electric field. (Image from Willets et al.)[4]

The surface plasmon resonance is responsible for the characteristic colors of metal nanoparticles. For gold nanoparticles the oscillation frequency of the surface

electrons is in the visible region and leads to a strong SPR absorption. The oscillation frequency and the extent of polarization depends on the material, size and shape of the nanoparticles.[5] Therefore changing any those parameters will cause a change in structure of the absorbance band. Since the ability to create dipole oscillation depends on the polarizability of the nanoparticle surface, varying the dielectric constant of the surface or the surrounding material can affect the SPR frequency and thus alter the absorbance band.[6]

The absorbance spectrum of the metal nanoparticles is a collective result of both absorption and scattering. Absorption is due to the plasmons that cannot radiate but dissipate as heat and the scattering is due to the plasmons that radiate energy. The combined effect is called extinction.[7] The plasmon scattering is an attractive phenomenon of nanoparticle as it can affect the nearby optically active materials.

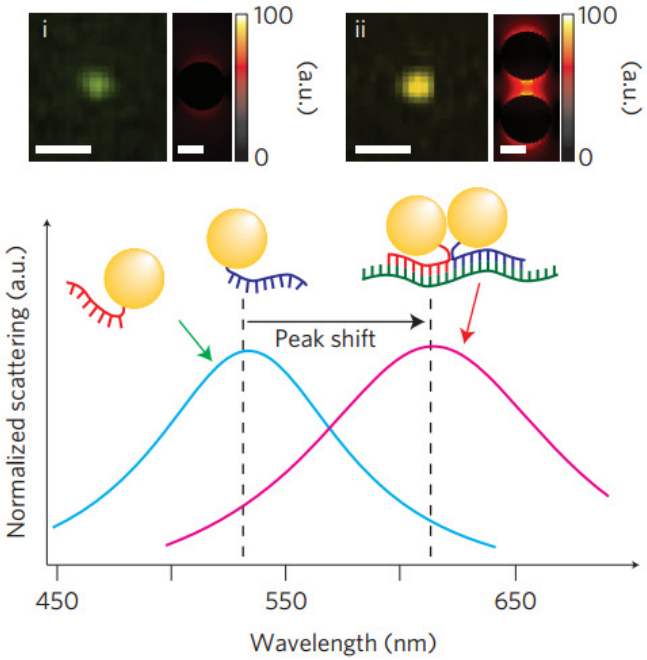

Figure 1.2. Bottom: Normalized absorbance spectra of monomer and dimer gold nanoparticles bound to mRNA, Top: Real-color images and finite-difference time-domain (FDTD) simulation of monomer and dimer GNPs. (Image from Lee et al)[8]

The electric field caused by the SPR of nearby metal nanoparticles or metal aggregates can combine to create more concentrated local electric field in that interparticle region, and the phenomenon is called plasmon coupling.[9] The plasmon coupling of gold nanoparticle aggregates causes a red-shift of the absorbance band due to the combination of different energy levels of SPR from multiple GNPs. This spectral shift can be used as a signal in various nanoscale applications where the size and concentration of the sensor probe are very limited.[8] In a recent study Lee et al., have used the coupled plasmonic resonance of gold nanoparticles to monitor the mRNA splice variants in cells (Figure 1.3).[8]

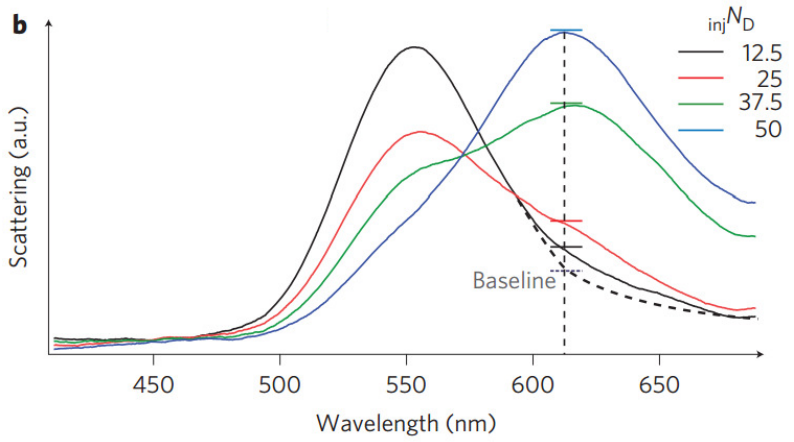

Figure 1.3. a) Absorbance spectra shows increases in scattering at ~610 nm due to coupled plasmonic resonance of aggregated GNPs (12.5, 25, 37.5 and 50 numbers) injected in a cell to monitor mRNA splicing. (Image from Lee et al)[8]

Gold nanoparticles (GNPs) are very attractive as they can be readily synthesized, shape engineered, surface functionalized and plasmon tuned.[1] Gold nanoparticles are highly stable under atmospheric conditions, and absorb and scatter visible light at ~520 nm. The field of synthesis and surface modification of gold nanoparticles are a very active area of research.[5] We aim to take advantage of these special photophysical properties of gold nanoparticles, by synthesizing high quality of

nanospheres, for investigating the energy interactions between gold nanoparticles and fluorophores in solution phase.

1.1.2. Metal-fluorescence enhancement

When a fluorophore is placed in the region of a metal's surface plasmonic electric field, a dramatic increase in fluorescence brightness can be observed due to the increased excitation events and the additional emission pathways. This phenomenon is called metal-enhanced fluorescence (MEF).[10] The absorption cross section of a metal is about 10^5 times greater than that of a typical organic fluorophore.[11] Thus, metals can strongly interact with the incident light and produce concentrated SPR electric field around the surface within a nanometer scale range. The fluorophores placed in that region would feel the effect of the SPR. This non-radiative energy transfer between metal and fluorophore depends on the strength of the electric field, degree of spectral overlap and the distance between the metal surface and the fluorophore.[11]

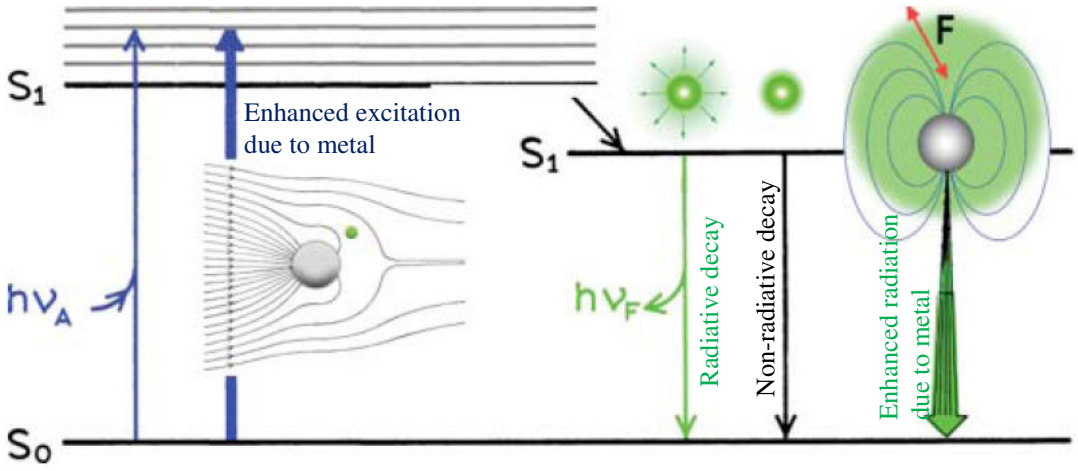

Figure 1.4. Jablonski diagram of a fluorophore placed near the surface of a metal nanoparticles. (Image from Lakowicz et al.)[11]

Figure 1.4 displays the standard and metal SPR influenced excitation and emission pathways. The thicker excitation arrow indicates the enhanced number of

excitations due to the proximity of metal. The presence of metal near the fluorophore increases the rate of excitation and emission cycle, and thus increase the brightness of the fluorescence.

The fluorescence enhancement can be further improved by placing a fluorophore in the region of coupled plasmonic resonance called "hotspot" of metal nanoparticle aggregates.[11] Thus it would be beneficial to construct a metal nanoparticle aggregates system with optimal metal-fluorophore distance as a means to achieve maximum enhancement.[12]

Fluorescence based sensors can be used to report specific molecular events in chemical and biological studies.[13] In those analyses the size of the probes and signal intensity is often a great challenge and thus investigations of techniques, such as MEF, that can produce amplified fluorescence signals are required. Recent developments in the field of optical sensors pushes the sensitivity to a single-molecular detection limit.[14] There is always an immense need for "smaller and brighter" fluorescent probes in the area of *in vitro* and *in vivo* imaging.[14] The surface plasmon resonance based sensors are highly sensitive to the size, shape and local environment of metal nanoparticles, and also offer tunable detection limits. Because of the nanometer size SPR electric field decay range, a single-nanoparticle sensor can offer a high spatial resolution.

1.1.3. Nanoparticle scaffolds to promote MEF

Metal-enhanced fluorescence has been broadly studied on solid phase substrates where the fluorophores can be easily placed at a controlled distance from metal surface.[15] The solid substrate platforms provide an excellent insight to the underlying factors like plasmonic hotspots and distance dependency of metal-enhanced fluorescence. However the solid substrates have strong limitations in biological applications as they cannot be used as sensor probes for bioimaging or biodetection.[16] To achieve solution phase MEF it is necessary to investigate a robust methods to create a scaffold of metal nanoparticle and fluorophore.

Our research group has been developing gold nanoparticle and dye-doped-silica nanoparticle aggregate system in order to promote MEF in aqueous solution. Different sizes and shapes of gold nanoparticles were prepared and their physical and optical properties were studied by our group. Nathan Green has synthesized organic dye-doped-silica nanoparticle of various sizes and aggregated those assemblies to gold nanoparticles by mean of organic bindings.[12] Kalani Gunawardana demonstrated a 200-fold fluorescence enhancement from propyl dithiocarbamate (DTC) mediated aggregates of rhodamine B doped silica nanoparticles and gold nanoparticles.[17]

In this study we focus on adapting the previously designed nanoparticle aggregate model to produce MEF from inorganic quantum dots (QDs). Quantum dots are nano size semiconductors possessing attractive properties like size tunable emission, high photostability and high extinction coefficient.[18] In contrast to common organic dyes, quantum dots have a broad excitation range, and a narrow and symmetric emission range, which allow production of multicolor fluorescence simultaneously from

different size QDs using a single excitation source.[19] However, the toxicity of the heavy metal restricts the use of QDs in biological systems. So it is essential to encapsulate the QDs in a non-toxic and chemically inert shell.[20] Several literature reports show that microemulsion silica coating on quantum dots produces highly monodisperse silica nanoparticles with single QD core. The silica shell introduces water compatibility to the QDs. Adjusting the thickness of the silica shell varies the distance between the metal surface and fluorophore core.[21]

In order to create the gold and silica nanoparticle scaffolds in solution phase a strong binding between the gold and silica surface needs to be investigated. Surface modification of gold and silica nanoparticles allows the exploration of various aggregation motifs. Our group has been investigating the installation of thiol, disulfide, amine, dithiocarbamate and carboxylic acid derivatives on gold and silica nanoparticles.

To characterize the nanoparticles and measure the degree of aggregation a suitable imaging method is required. Transition electron microscopy (TEM) is an excellent method to measure the size and monodispersity of the nanoparticles, and monitor the change in morphology due to aggregation of the nanoparticles. The ability of a material to stop an electron depends on its density, thickness, and the energy of the accelerated electrons. Gold has larger ability to stop the electrons and produce darker shadow on the image compared to silica nanoparticles. This image contrast allows us to differentiate the gold and silica. However to view the quantum dot core in silica nanoparticles (to increase the contrast between core and shell), the samples should be coated on a slimmer grid and the acceleration energy of the electron beam should be higher.

1.3. Research focus

The focus of our research is to develop a robust metal-enhanced fluorescence (MEF) system by aggregating gold nanoparticles with quantum dot encapsulated silica nanoparticles in solution phase. Based on the key literature reports of MEF from solid substrates, our hypothesis is that similar MEF can be produce in solution phase by placing a fluorophore in close proximity to metal nanoparticles. The metal-fluorophore nanoparticle aggregates would emit brighter fluorescence due the plasmon induced faster excitation and emission cycles.

We aimed to synthesize and characterize gold nanoparticles and quantum dots, and then functionalize their surface in order to integrate them in an aggregate system. In the first part of our research we synthesized various size gold nanoparticles using different methods and characterized the particles using absorption spectroscopy and transition electron microscopy. Then we synthesized various ligands and examined their place exchange efficacy on GNP surface. Then the GNPs were tethered with multifunctional ligands to study the efficacy of formation of nanoparticle aggregates in aqueous solution. In the second part of our research we focused on synthesizing various size quantum dots and encapsulate them in silica shells of various thickness. We studied the surface functionalization of these silica nanoparticles with ligands that preferentially bind to gold surface. We investigated the binding conditions to form gold-silica heteroaggregation in aqueous phase. Then in the last part of the research we focused on optimizing the conditions to maximize the gold-silica heteroaggregation, and applying our nanoparticle scaffold system to produce metal-enhanced fluorescence. We investigated the effects of size and concentration of gold and silica nanoparticles, and

different binding methods between them to produce MEF. Throughout our study we used techniques like TEM imaging to characterize the nanoparticle scaffolds, absorption spectroscopy to measure the degree of heteroaggregation, and fluorescence spectroscopy to measure the fluorescence enhancement.

1.3. References

1. Ghosh, S. K.; Pal, T., Interparticle Coupling Effect on the Surface Plasmon Resonance of Gold Nanoparticles: From Theory to Applications. *Chem. Rev. (Washington, DC, U. S.)* **2007,** *107* (11), 4797-4862.

2. Adams, A.; Moreland, J.; Hansma, P. K.; Schlesinger, Z., Light emission from surface-plasmon and waveguide modes excited by nitrogen atoms near a silver grating. *Phys. Rev. B: Condens. Matter* **1982,** *25* (6), 3457-61.

3. Adams, A.; Rendell, R. W.; West, W. P.; Broida, H. P.; Hansma, P. K.; Metiu, H., Luminescence and nonradiative energy transfer to surfaces. *Phys. Rev. B: Condens. Matter* **1980,** *21* (12), 5565-71.

4. Willets, K. A.; Van Duyne, R. P., Localized surface plasmon resonance spectroscopy and sensing. *Annu. Rev. Phys. Chem.* **2007,** *58*, 267-297.

5. Eustis, S.; El-Sayed, M. A., Why gold nanoparticles are more precious than pretty gold: Noble metal surface plasmon resonance and its enhancement of the radiative and nonradiative properties of nanocrystals of different shapes. *Chem. Soc. Rev.* **2006,** *35* (3), 209-217.

6. Aslan, K.; Gryczynski, I.; Malicka, J.; Matveeva, E.; Lakowicz, J. R.; Geddes, C. D., Metal-enhanced fluorescence: an emerging tool in biotechnology. *Curr. Opin. Biotechnol.* **2005,** *16* (1), 55-62.

7. Quinten, M.; Leitner, A.; Krenn, J. R.; Aussenegg, F. R., Electromagnetic energy transport via linear chains of silver nanoparticles. *Opt. Lett.* **1998,** *23* (17), 1331-1333.

8. Lee, K.; Cui, Y.; Lee, L. P.; Irudayaraj, J., Quantitative imaging of single mRNA splice variants in living cells. *Nat. Nanotechnol.* **2014,** *9* (6), 474-480.

9. Su, K. H.; Wei, Q. H.; Zhang, X.; Mock, J. J.; Smith, D. R.; Schultz, S., Interparticle Coupling Effects on Plasmon Resonances of Nanogold Particles. *Nano Lett.* **2003,** *3* (8), 1087-1090.

10. Lakowicz, J. R.; Geddes, C. D.; Gryczynski, I.; Malicka, J.; Gryczynski, Z.; Aslan, K.; Lukomska, J.; Matveeva, E.; Zhang, J.; Badugu,

R.; Huang, J., Advances in Surface-Enhanced Fluorescence. *J. Fluoresc.* **2004,** *14* (4), 425-441.

11. Lakowicz, J. R.; Ray, K.; Chowdhury, M.; Szmacinski, H.; Fu, Y.; Zhang, J.; Nowaczyk, K., Plasmon-controlled fluorescence: a new paradigm in fluorescence spectroscopy. *Analyst (Cambridge, U. K.)* **2008,** *133* (10), 1308-1346.

12. Green, N. S., Plasmonic Properties of Enhanced Fluorescence of Gold and Dye-doped SIlica Nanoparticles Aggregates. **2013**.

13. Deng, W.; Xie, F.; Baltar, H. T. M. C. M.; Goldys, E. M., Metal-enhanced fluorescence in the life sciences: here, now and beyond. *Phys. Chem. Chem. Phys.* **2013,** *15* (38), 15695-15708.

14. Anker, J. N.; Hall, W. P.; Lyandres, O.; Shah, N. C.; Zhao, J.; Van Duyne, R. P., Biosensing with plasmonic nanosensors. *Nat. Mater.* **2008,** *7* (6), 442-453.

15. (a) Jackson, J. B.; Halas, N. J., Surface-enhanced Raman scattering on tunable plasmonic nanoparticle substrates. *Proc. Natl. Acad. Sci. U. S. A.* **2004,** *101* (52), 17930-17935; (b) Dragan, A. I.; Golberg, K.; Elbaz, A.; Marks, R.; Zhang, Y.; Geddes, C. D., Two-color, 30 second microwave-accelerated Metal-Enhanced Fluorescence DNA assays: A new Rapid Catch and Signal (RCS) technology. *J. Immunol. Methods* **2011,** *366* (1-2), 1-7.

16. Geddes, C. D., Metal-enhanced fluorescence. *Phys. Chem. Chem. Phys.* **2013,** *15* (45), 19537.

17. (a) Gunawardana, K. B., Study of metal-enhanced fluorescence of dye doped silica nanoparticles. *Uinversity of Oklahoma* **2012**; (b) Gunawardana, K. B.; Green, N. S.; Bumm, L. A.; Halterman, R. L., Metal-Enhanced Fluorescence of Dye-Doped Silica Nano Particles. *J. Fluoresc.* **2015,** *25* (2), 311-317.

18. Alivisatos, A. P., Semiconductor clusters, nanocrystals, and quantum dots. *Science (Washington, D. C.)* **1996,** *271* (5251), 933-7.

19. Gao, X.; Nie, S., Quantum Dot-Encoded Mesoporous Beads with High Brightness and Uniformity: Rapid Readout Using Flow Cytometry. *Anal. Chem.* **2004,** *76* (8), 2406-2410.

20. Gao, X.; Cui, Y.; Levenson, R. M.; Chung, L. W. K.; Nie, S., In vivo cancer targeting and imaging with semiconductor quantum dots. *Nat. Biotechnol.* **2004,** *22* (8), 969-976.

21. Darbandi, M.; Thomann, R.; Nann, T., Single quantum dots in silica spheres by microemulsion synthesis. *Chem. Mater.* **2005,** *17* (23), 5720-5725.

Chapter II: Synthesis of gold nanoparticles and place exchange study of ligands on gold surface

2.1. Chapter Overview

In this chapter we discuss our effort to synthesize various size gold nanoparticles and modify their surface with multifunctional ligands. To examine the size and shape sensitive optical properties of gold nanoparticles (GNPs), it is essential to synthesize various sizes of highly monodisperse GNPs. We focused on the controlled nucleation and the seeded growth method of reducing gold (III) chloride using sodium citrate to produce different diameter gold nanospheres. The citrate ions capped on the GNPs supports the stability of the particles in aqueous medium. Replacing the citrate ions on the surface of the GNPs with more useful ligand is vital to utilize the attractive photophysical properties of GNPs in diverse applications. We aimed to investigate the surface functionalization of the GNPs with several ligands. We considered the organic moieties that have great affinity to gold surface, and installed those moieties in larger ligand structures. Thiol and disulfide based hydrophobic ligands were synthesized and used for place exchanging the citrate ions on GNPs in a biphasic solution. The amount of GNPs phase transferred from aqueous to organic phase can be used to assess the place exchange efficacy of the ligands. We also analyzed the ligand facilitated aggregation of GNPs in aqueous solution as a preliminary step in our pursuit to produce metal-fluorophore aggregates system in solution phase. The high affinity of dithiocarbamate group towards the gold surface can be employed to fabricate the GNP aggregates in solution. We performed an initial study of photo triggered aggregation of GNPs by applying photolabile ligands on the gold surface and activating it by UV light.

2.2. Introduction

Rapid developments in nanotechnology have increased the possibility of eventual contact of engineered nanomaterials with humans and the environment. Nanoparticles are tiny particles made of several thousands of atoms and the particles size usually range between 1-100 nm. They possess numerous attractive properties depending on the composite materials such as strong optical absorption (e.g., gold nanoparticles), fluorescence (e.g., CdSe quantum dots) phosphorescence (e.g. yttrium oxide), and magnetic moment (e.g. iron oxide or cobalt nanoparticles).[1] Innovations in synthesizing and functionalizing nanoparticles is an essential for any significant improvements of nonmaterial based application.[2] The special properties of nanostructures, due to the presence of high percentage of constituent atoms on the surface, make them behave distinct from the bulk materials.[3] Modifying the nanoparticle surface with organic ligands is an emerging area of research with potential applications in the fields like biosensors, optoelectronic devices, light-energy conversation system and data storage system.[4] Subbiah et al., has reported the early clinical studies suggested that a nanoparticle coated with special targeting chemical moieties yielded enhanced efficacy of cellular uptake at the same time with reduced side effects.[2a]

Variety of chemical methods have been developed in recent years to conjugate chemical moieties on bulk metal surfaces, but tethering ligands on metal nanoparticles is fairly a new field.[5] The focus of our research is to develop a solution based approach to study metal-enhanced fluorescence by aggregating fluorescent semiconductor quantum dots (QDs) doped-silica nanoparticles to gold nanoparticles. In order to

produce a controlled aggregate system of nanoparticles in aqueous solution it is essential to investigate the ability of surface modification of gold nanoparticles with various ligands.

Gold nanoparticles (GNPs) are considered to be one of the stable metal nanoparticles and have attracted photo-chemists and biologists due to the GNPs' interesting plasmonic properties caused by the collective oscillation of surface electrons and also due to the biological inertness and stability. Although gold nanoparticles possess interesting and useful properties, they have poor dispersibility in solvents without being coated with appropriate phase compatible ligands. So in most cases the GNPs are surface modified during the synthesis to promote dispersiblity of the particles.[6] The GNP surface has a great affinity to adsorb organic molecules since this enable to lower the charge separation potential at the interface between the metal and the surrounding environment. The organic molecules can also prevent nanoparticle aggregation, decrease the reactivity of surface atoms and act as an insulating film. Organic molecules with appropriate moiety can spontaneously self-assemble on gold surfaces, but functionalizing GNP surface with a random organic materials is not very helpful in the advancement of nano devices. Gold nanoparticles are commonly synthesized in aqueous suspension with the assistance of citrate ions or CTAB (cetyltrimethylammonium bromide) surfactant.

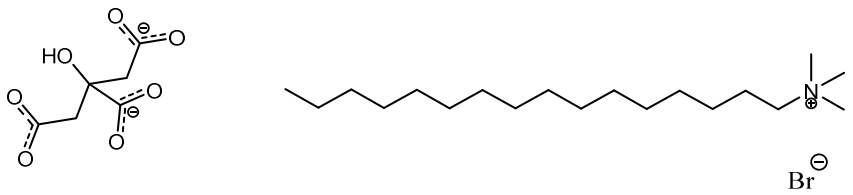

Citrate ion CTAB surfactant

Figure 2.1. Structures of citrate ion and CTAB surfactant.

The loosely bound citrate and CTAB adsorbents can be easily replaced by molecules with functionality showing higher affinity for gold surface. The most commonly used functional group is thiol, not just because of its strong binding to gold surface but also the ease of installation of thiols in large structures of ligands. The organic ligand capped GNPs are highly advantageous to carry out the desired chemistry on a nanoparticle surface in the solution phase. Sperling et al., compared the structures of various thiolated ligand commonly used to surface modify inorganic nanoparticles.[1] Figure 2.2 shows the size comparison of different thiolated ligands to a 5 nm diameter nanoparticle. The space filling structures were drawn to scale with the nanoparticle.

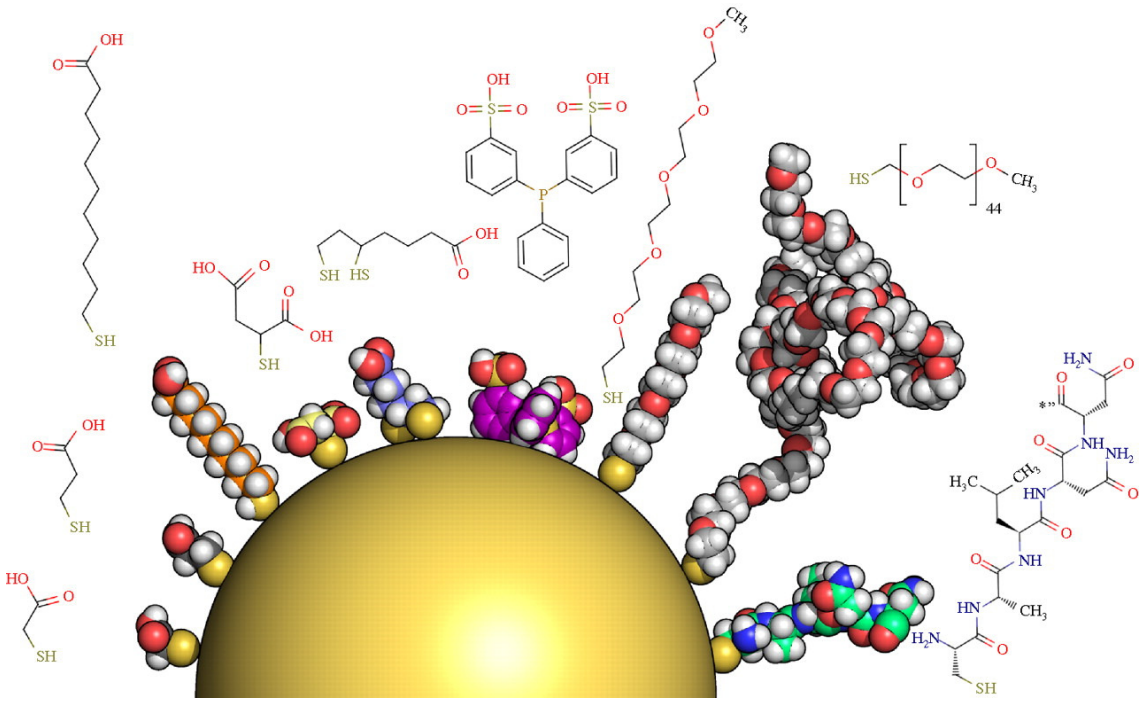

Figure 2.2. Various ligand molecules with thiol functionality adsorbed on the surface of a 5 nm diameter nanoparticles (drawn to scale). The molecules are "mercaptoacetic acid (MAA), mercaptopropionic acid (MPA), mercaptoundecanoic acid (MUA), mercaptosuccinic acid (MSA), dihydrolipid acid (DHLA), bis-sulphonated triphenylphosphine, mPEG5-SH, mPEG45-SH (2000 g mol−1) and a short peptide of the sequence CALNN." (image obtained from Sperling et al)[1]

The attractive photophysical properties of the gold nanoparticles can be explored by surface coating the particles with thiolated ligand carrying a useful functionality on the other end. The composition of the ligand can be modified in several ways such as by synthesizing the nanoparticles with a ligand of desired functionality, place exchanging an impractical ligand with a desired ligand, or modifing (deprotect or activate) the structure of the coated ligand.

In our lab Aunradha Singh has synthesized various ligand with thiol and disulfide functionality to produce well-ordered self-assembled monolayer on gold surface.[7] Kalani Gunawardana has investigated the place exchange of thiolated dyes on 13 nm gold nanoparticles to study the variation of molar fluorescence of the dyes.[8] Nathaniel Green and Kalani Gunawardana have achieved metal-enhanced fluorescence in aqueous solution by forming dithiocarbamate mediated aggregates of gold and dye-doped-silica nanoparticles.[9]

In this study we synthesized various size gold nanoparticle using citrate reduction method and investigated the place exchange efficacy of citrate ions with ligands carrying thiol, disulfide or dithiocarbamate (DTC) functionality.

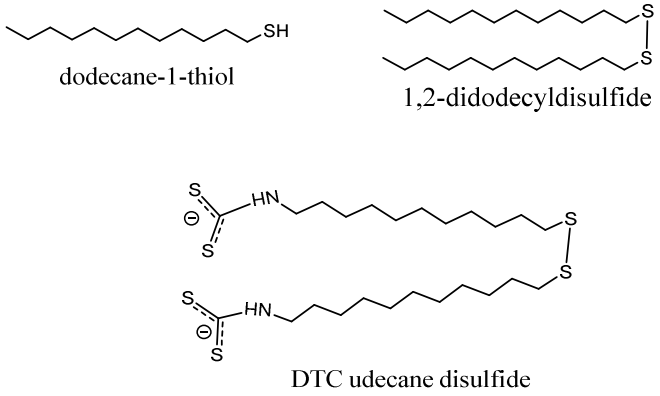

Figure 2.3. Structure of thiol, disulfide and dithiocarbamate ligands used in this work.

We also used the spontaneous DTC activation of ligand containing terminal amine to promote aggregation of gold nanoparticles. The absorbance band of GNPs is highly sensitive to shape and size of the particles. The organic ligand facilitated aggregation of gold nanoparticles would change the morphology of the GNPs and that would alter the structure of absorbance band. The absorbance λ_{max} of free GNPs corresponds to the surface plasmon resonance and ranges between of 520 – 550 nm. But for the aggregated GNP the surface plasmons of individual particles are coupled to produce an enhanced absorbance at >570 nm with a simultaneous drop in absorbance from free GNPs (between 520-2550 nm). This morphology influenced change in absorbance spectrum can be used to assess the place exchange efficacy of the particular organic ligands.

Based on these key literature precedents we investigated the synthesis of different size gold nanoparticles, place exchange efficacy, surface functionalization and aggregation of GNPs.

2.3. Results and Discussion

2.3.1. Synthesis of various size gold nanoparticles

Gold nanoparticles (GNPs) of various sizes were synthesized by controlled nucleation and seeded growth methods. Those methods emerged from the standard aqueous phase reduction of gold (III) chloride with sodium citrate initially developed by Turkevich et al.[10] In these methods the citrate ions act as the reducing agents as well as the capping agents. The center carboxylate group in the citrate ion would be oxidized to carbon dioxide. The negatively charged citrate ions form a loose shell around the gold nanoparticles and keep them from aggregating. Moreover, the citrate ions can be easily replaced with other ligands by place exchange. Frens et al., modified the standard citrate reduction method by altering the concentration of sodium citrate to obtain gold nanospheres of various diameters.[11]

For our study we first used the controlled nucleation method to get two different size gold nanoparticles. Based on the Frens procedure, we calculated the amount of sodium citrate required to create 16 nm and 100 nm diameter gold nanoparticles. In two separate reactions setups 50 mL of aqueous solution of $HAuCl_4$ (tetracholoauric acid, 0.25 mM) was brought to boil in a clean round bottom flask. To the boiling solutions, 1 mL and 0.16 mL of $Na_3C_6H_5O_7$ (sodium citrate, 34 mM) were added to synthesize 16 nm and 100 nm particles respectively. By changing the relative concentration of the reactants, the rate of nucleation and particle growth processes can be altered. The smaller concentration of sodium citrate would slow down the nucleation process and thus decrease the number of nucleation cites. That causes the available gold precursor divided over fewer nuclei and result in considerably larger diameter particles. Simply,

decreasing the concentration of sodium citrate would increase the size of the gold nano particles. Within 2 min after the addition of sodium citrate, the color of the solutions was turned pale blue. In about 6 minutes the color of the solution turned red due to the SPR scattering of gold nanoparticles and indicating the completion of the reaction. Then the reaction was cooled, and the final volume was made up to 50 mL by adding milipore water.

The following TEM images (Figure 2.4) show that the change in concentration of sodium citrate clearly made an effect on the shape, size and size distribution of the gold nanoparticles. The greater amount of sodium citrate produced highly monodisperse GNPs with average diameter of 14 nm. However the lesser amount of sodium citrate produced irregular shapes of GNPs with large size distribution (10 nm to 80 nm). This may be due to the insufficient concentration of sodium citrate to protect the growth of spherical shape particles. The absorbance spectra (Figure 2.5) also show the shortcomings of our experiment to synthesize 100 nm particles using the controlled nucleation method. Since the wavelength of absorbance band is directly proportional to the size of the particles, the absorbance λ_{max} is highly size sensitive. As size of the gold nanoparticles increases, the absorbance λ_{max} would red-shift. In our case the 14 nm gold nanoparticles synthesized with greater amount of sodium citrate resulted in λ_{max} at 527 nm as expected. But the blue-shift of λ_{max} for lesser concentration of sodium citrate indicates that the average size of the (irregular) particles was actually smaller than 14 nm. We were unable to reproduce the Frens et al., literature results (larger monodisperse GNPs), and we didn't spend much time to analyze it, as we had the alternate seeded growth technique (by Bastus et al.,) to synthesize various size GNPs.

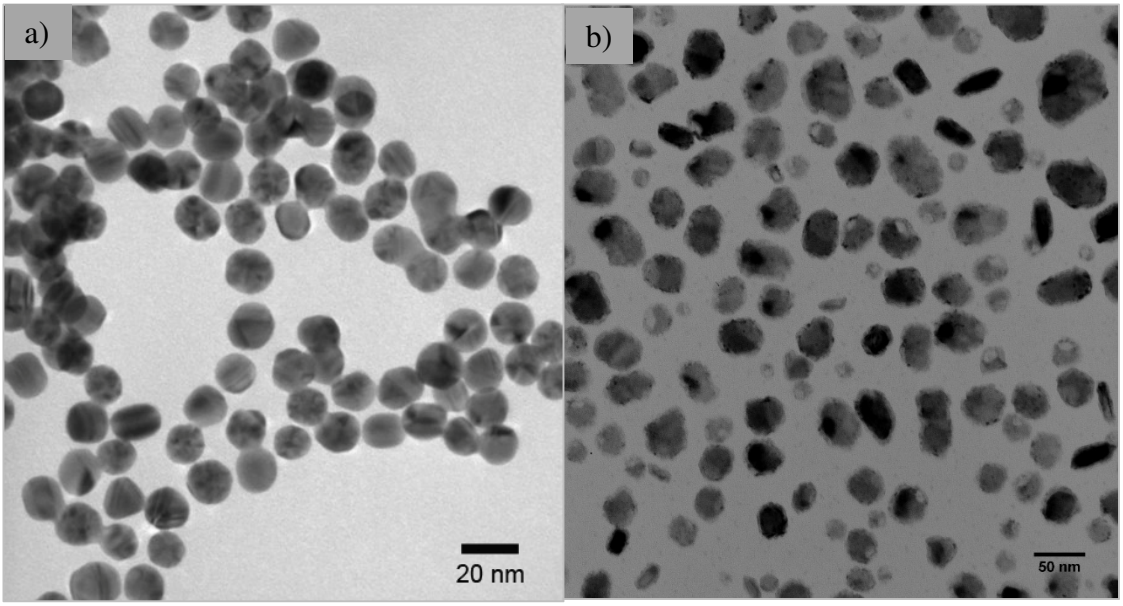

Figure 2.4. TEM images of gold nanoparticles synthesized by controlled nucleation method using a) more citrate and b) less citrate

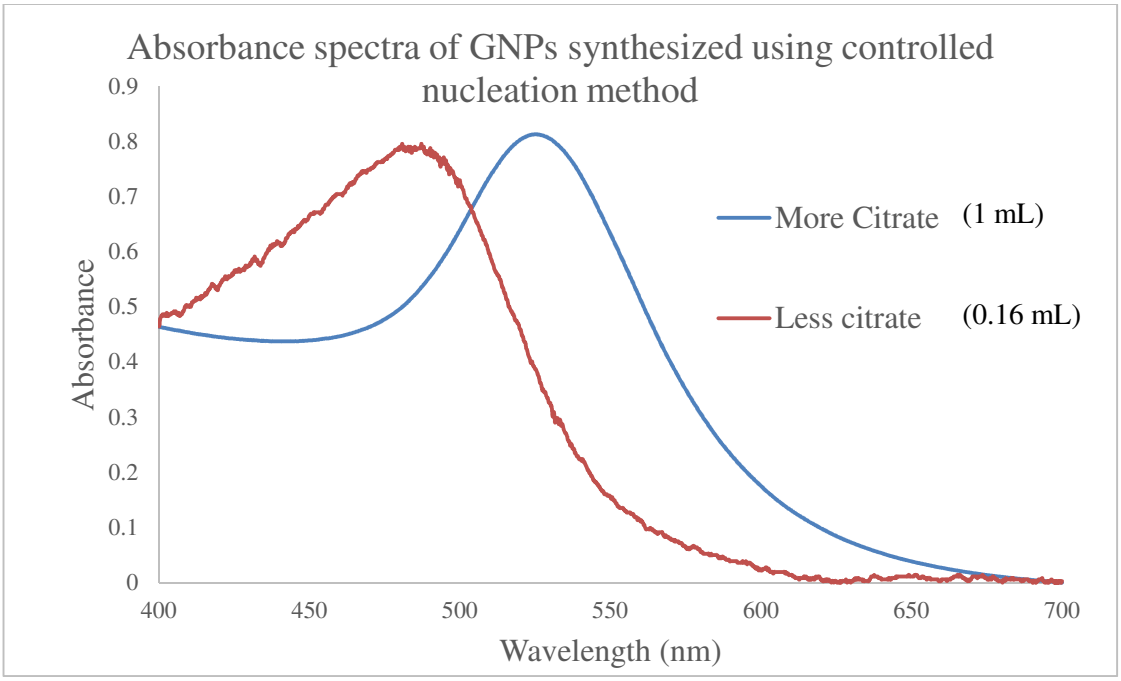

Figure 2.5. Absorbance spectra of GNPs synthesized using controlled nucleation method

Bastus et al., developed the seeded growth method by modifying Turkevich/Frens reaction system to synthesize highly monodisperse spherical gold nanoparticles.[12] In this method the inhibition of secondary nucleation was controlled by changing the gold precursor to seed particle concentration in order to obtain homogeneous growth. Enlargement of pre-synthesized gold nanoparticles was achieved by surface-catalyzed reduction of Au^{3+} by sodium citrate. Figure 2.6 describes our scheme of kinetically controlled seeded growth synthesis of different generation (size) gold nanoparticles in a single pot.

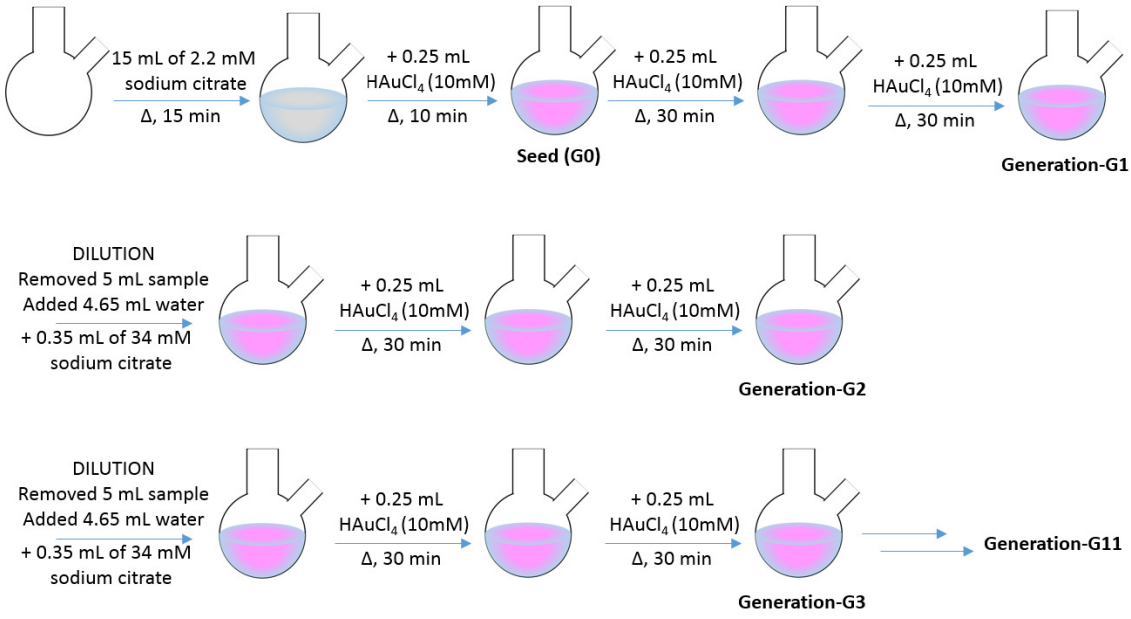

Figure 2.6. Seeded growth synthesis of different size gold nanoparticles in a single pot. (Image from this work)

The gold seeds were prepared by adding $HAuCl_4$ precursor solution into a boiling sodium citrate solution. The mixture was vigorously stirred at boiling temperature until it reached a red color indicating GNP nuclei were formed. Then the temperature of the reaction was decreased to 90 °C to stop nucleation. To this seed

suspension more $HAuCl_4$ precursor was injected under vigorous stirring. The reaction was continued for 30 min at decreased temperature (90 °C) to maintain a slow growth of particles. We repeated the addition of $HAuCl_4$ precursor and 30 min stirring before removing an aliquot of generation-1 gold nanoparticle suspension. From the same pot, new generations of gold nanoparticles were obtained every hour by diluting the previous generation GNP suspension, adding more sodium citrate and $HAuCl_4$ precursor, and stirring at 90 °C. The gold nanoparticles obtained in new generations were larger and monodisperse. Figure 2.7 shows the cuvettes containing aqueous suspensions of G1 to G11 gold nanoparticle generations. The increase in the intensity of pink color as the generations grows is due to the size influenced absorbance of the particles. Larger particles absorb and scatter longer wavelength light.

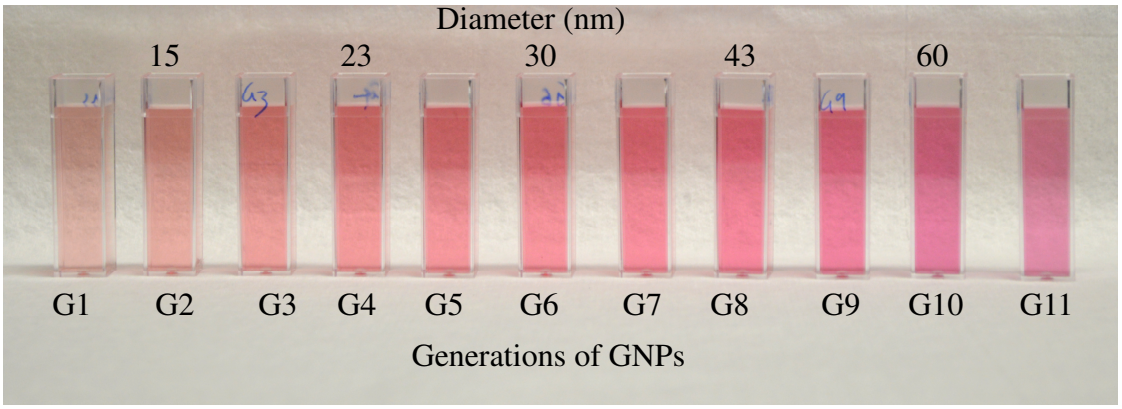

Figure 2.7. Image of aqueous suspensions of different generation gold nanoparticles (from this work).

The TEM images (Figure 2.8) on the following page are obtained from GNP generations G2, G4, G6, G8 and G10. It is clearly seen that the size of the particle was increased as the generations (number of growth steps) grew and also the particles are fairly monodisperse. The average sizes of the gold nanoparticles in each generation were measured from the TEM images.

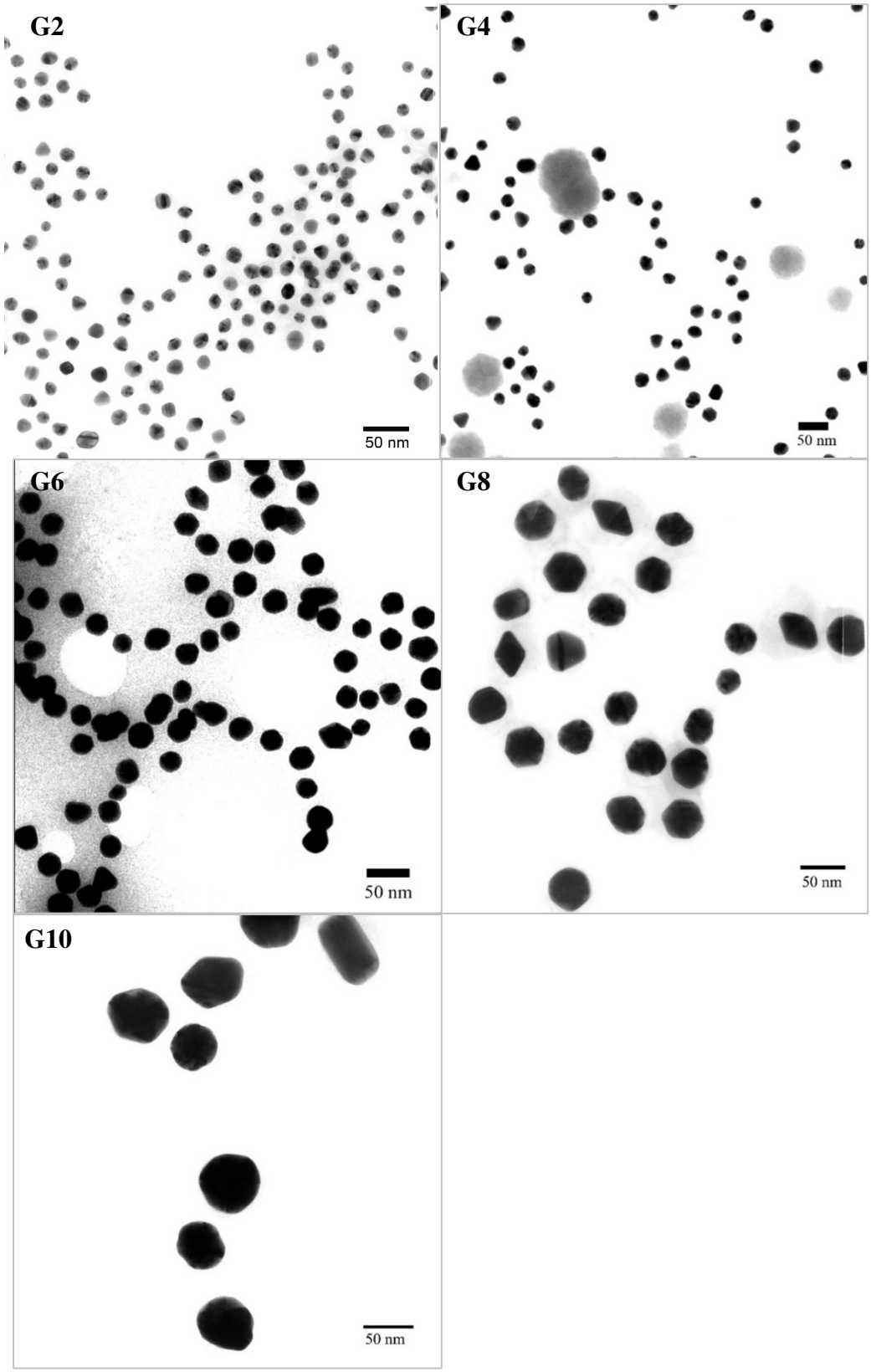

Figure 2.8. TEM images of various generation of gold nanoparticles

Figure 2.9 shows the absorbance spectra of gold nanoparticle obtained from different generations of seeded growth method. The absorbance due to surface plasmon resonance is highly sensitive to the size of GNPs. A gradual red-shift of the absorbance λ_{max} from 520 nm (for G1) to 542 nm (for G11) indicates the increase in diameter of the particles. The concentration of the GNP suspensions were calculated using the extinction coefficient and Beer's law. Liu et al., studied the extinction coefficient of different size GNPs capped with different ligands.[13] Their findings indicates that a linear relationship exists between the double logarithm of extinction coefficient and the diameter of nanoparticles. We used that linear equation to calculate the extinction coefficient of citrate-capped GNP suspensions.

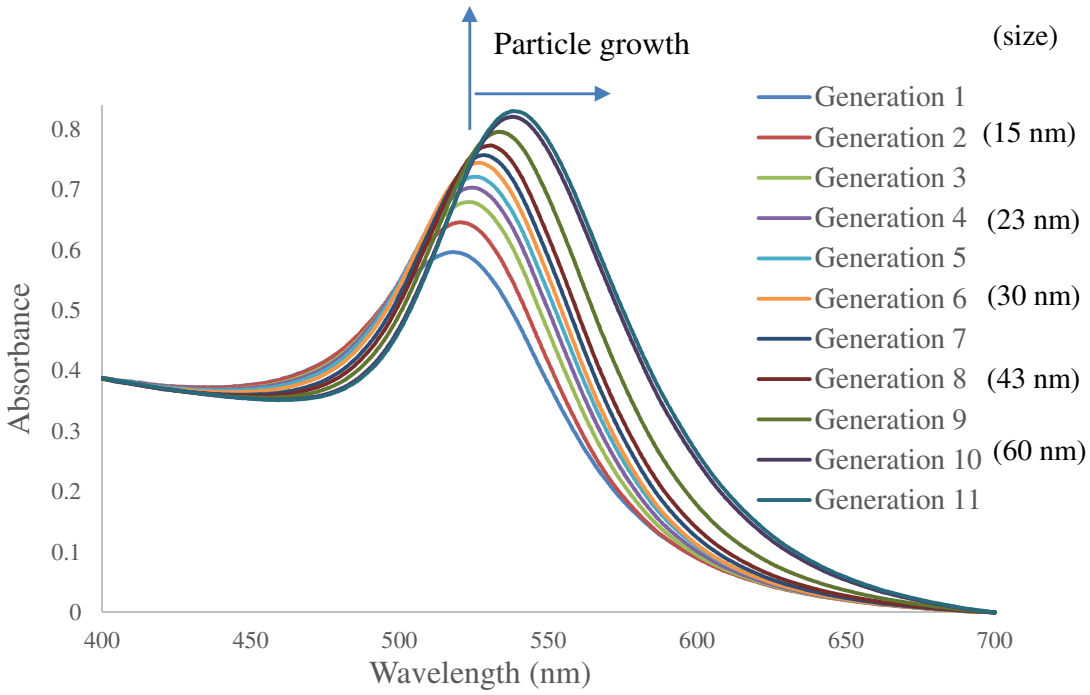

Figure 2.9. Normalized absorbance spectra of different size gold nanoparticles show the increase in size of the particles caused the red-shift of the λ_{max} of the absorbance peak.

The equation relating the GNPs' extinction coefficient and diameter.[13]

$$ln\varepsilon = k \ln D + a$$

Where,

ε = extinction coefficient

D = diameter of the particles

k = 3.3211 (constant)

a = 10.80505 (constant)

Beer's law relating the absorbance and the concentration of the GNP suspension

$$A = \varepsilon\, b\, c$$

Where,

A = absorbance

b = path length

c = concentration

GNP generations	Average particle size from TEM image	λ_{max} (nm)	Absorbance	Extinction coefficient ($M^{-1}cm^{-1}$)	Concentration of the GNP suspension (M)
G2	15 nm	520.6	0.6461	3.96×10^{8}	1.63×10^{-9}
G4	23 nm	523.8	0.7036	1.64×10^{9}	4.28×10^{-10}
G6	30 nm	526	0.7446	3.97×10^{9}	1.88×10^{-10}
G8	43 nm	530.6	0.7734	1.31×10^{10}	5.90×10^{-11}
G10	60 nm	537.6	0.8204	3.96×10^{10}	2.07×10^{-11}

Table 2.1. GNP particle size, absorbance, extinction coefficient and concentration.

Theoretically larger gold nanoparticles possess stronger surface plasmon resonance and thus absorb/scatter more light. This phenomenon leads to the greater extinction coefficient (how strongly a species absorb light at given wavelength) of larger diameter GNP particles. Table 2.1 shows the average diameter, absorbance and extinction coefficient of GNPs from different generations. A noticeable increase in extinction coefficient is seen for the increase in size of GNPs. Also the concentration of the GNP particles decreased as the size increased. It is worthy to note that the number of gold atoms was increased in the suspension as particle size was increased. Number of nucleation sites was constant during the particle growth time in this kinetically controlled seeded growth method. In this single pot synthesis, we removed samples and added more $HAuCl_4$ precursor solution after each generation, which resulted in less concentration of larger gold nanoparticles. In our lab we were able to reproduced monodisperse citrated capped GNPs of different sizes as in literature reports. The effect of various sizes of gold nanoparticles on the spectral overlap with quantum dots would be investigated in order to produce metal-enhanced fluorescence.

2.3.2. Study of place exchange of citrate by thiol and disulfide ligands on gold nanoparticle surface

Gold nanoparticles with interesting surface plasmon resonance property can be used for various applications in medicine, light harvesting, data storage and optical sensors only if the surface of the gold was derived with useful ligands.[4] Gold nanoparticles tethered with thiolated DNA, proteins, antibodies and peptide are currently used in applications in the fields like diagnosis, therapy, drug delivering and sensing.[12, 14] In the previous step we synthesized citrate-capped gold nanoparticles in aqueous suspension. The citrate ions bound to gold surface prevent the particle aggregation by loosely insulate the gold surface. The citrate ions can be replaced by thiolated molecules that "pseudocovalently bind (~45nKcal/mol) to gold surface" (Bastus et al).[12]

We investigated the place exchange of citrate ions by thiol and disulfide molecules on gold nanoparticle surface. We preferred a highly hydrophobic molecules with thiol and disulfide functional group to replace the citrate ion, so that we could examine the efficiency of the place exchange by measuring the concentration of gold nanoparticles phase transferred from aqueous to organic phase. Citrate coated GNPs are highly stable in aqueous medium, when thiol or disulfide molecules with longer hydrocarbon chain replace the citrate ions, the GNPs are incompatible with aqueous phase and thus move into organic phase. This phase transfer of organic ligand coated gold nanoparticle is useful in investigating the efficiency of ligand recoating or self-assembly on gold surface.

Place exchange of citrate *ion with alkanethiol:* We used different concentrations dodecane-1-thiol in the place exchange study to assess the amount of alkanethiol molecules needed to saturate the surface of gold nanoparticles. For this experiment we estimated the approximate concentration of dodecane-1-thiol required to saturate 15 nm diameter gold nanoparticle suspension of specific concentration and volume. From the surface area of a single GNP and the concentration of GNP suspension, we calculated the total surface area of gold in the reaction volume. Using the surface density of thiols on gold surface (4.5 x 10^{14} molecules/cm^2, obtained from literature)[5] we calculated the required concentration of dodecane-1-thiol to use.

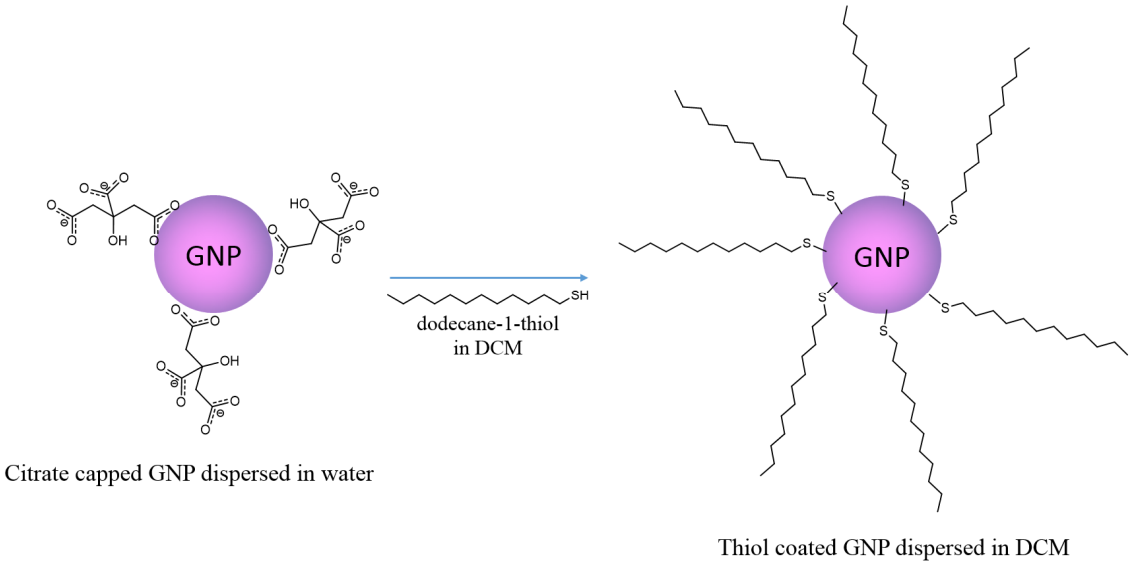

Figure 2.10. Schematic illustration of place-exchange of citrate by dodecane-1-thiol on GNP surface.

Concentration of aqueous suspension of GNP (# moles of particles / L)	1.63 nM
Diameter of GNP	15 nm
Number of 15 nm GNPs in (200 μL) aqueous suspension	1.96×10^{11} particles
Surface area of one 15 nm GNP sphere	706.5 nm^2
Total surface area of gold in the reaction volume	1.39×10^{14} nm^2
Surface density of thiols on gold surface[5]	4.5×10^{14} molecules/cm^2
Number of thiol molecules per GNP	3180 molecules
Number of thiol molecules needed for the reaction volume (200 μL)	6.24×10^{14} molecules
Moles of thiol needed for the reaction volume (200 μL)	1.04 nmol
Concentration of dodecane-1-thiol in 200 μL of DCM (assuming that the reaction yield is 100%)	> 5.18 μM

Table 2.2. Calculation of concentrations of dedecane-1-thiol needed to place exchange the citrate.

For the place exchange experiment we took 200 µL of aqueous suspension of citrate-capped 15 nm GNPs in different micro centrifuge tubes. To that, 1 mM KOH was added to adjust the pH to ~9. Then to each tube we added 200 µL different concentrations (0, 0.125, 0.25, 0.5, 1, 2, 3 mM) of dodecane-1-thiol dissolved in dichloromethane to create biphasic solutions. After 12 h of rotation the microtubes were incubated to separate the aqueous and organic phases. Figure 2.11 shows the biphasic solution of water (top) and dichloromethane (bottom). The phase transfer of gold nanoparticles was occurred only with the highest concentration (3 mM) of dodecane-1-thiol. The pink color organic phase in 3 mM tube contains the dodecane-1-thiol coated gold nanoparticles.

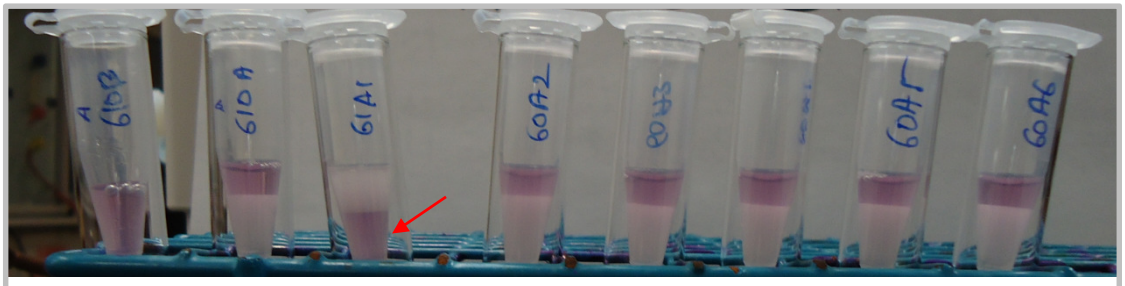

No DCM 0mM 3mM 2mM 1mM 0.5mM 0.25mM 0.125mM

Concentrations of dodecane-1-thiol in DCM

Figure 2.11. Place-exchange study of citrate by dodecane-1-thiol on GNP surface

The aqueous layers was extracted by adding 800 µL of water to each microtube and removing the top aqueous layer. Absorbance spectra of the diluted aqueous portions are shown in Figure 2.12. The 81% drop in absorbance was seen for the 3 mM sample corresponds to the decrease in concentration of gold nanoparticles due to phase transfer. But the samples with lower concentrations of thiol didn't show any significant phase transfer. The experimental data suggests that we need alkane thiol of 3 mM concentration to completely place exchange the citrate ions on 15 nm diameter GNP of

1.63 nM concentration (keeping the aqueous and organic volume ratio 1:1). This large difference between the experimental result and theoretical prediction of thiol concentration (5.18 μM) may be due our yield assumption (yield = 100%) in calculating the theoretical concentration of thiol.

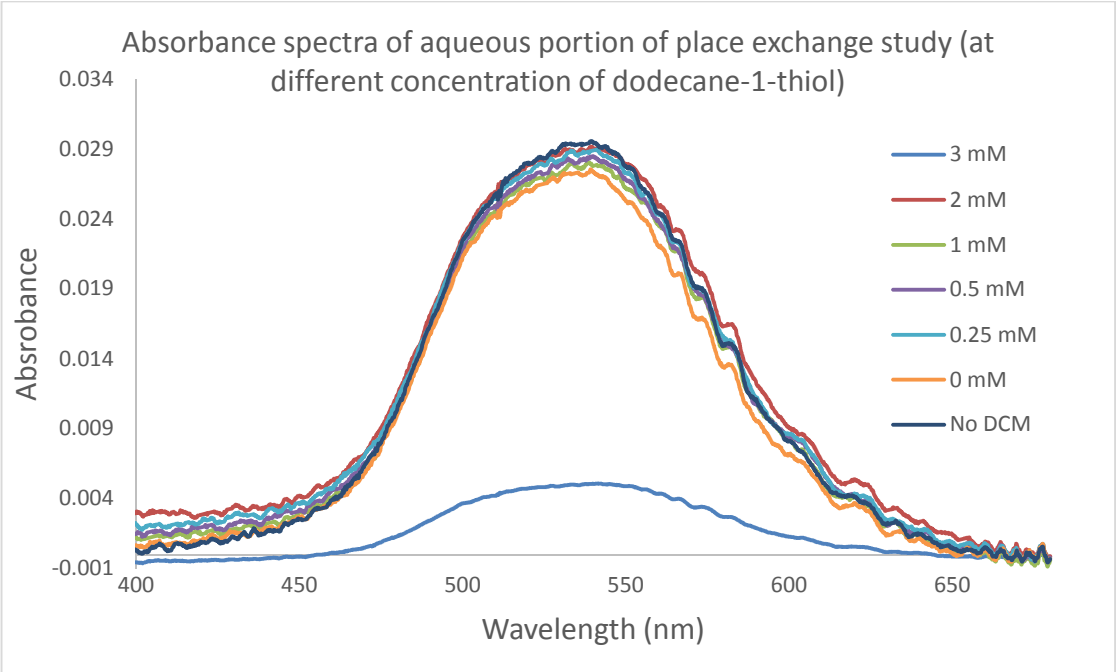

Figure 2.12. Absorbance spectra of aqueous portion extracted from the place exchange study of citrate by different concentration dodecane-1-thiol on GNP surface

Place exchange of citrate ion with disulfide ligand: In our study of possibilities of functionalizing gold nanoparticle surface, next we assessed the place exchange efficacy of disulfide. For that we synthesized 1,2-didodecyldisulfide from the dodecane-1-thiol used in previous step.

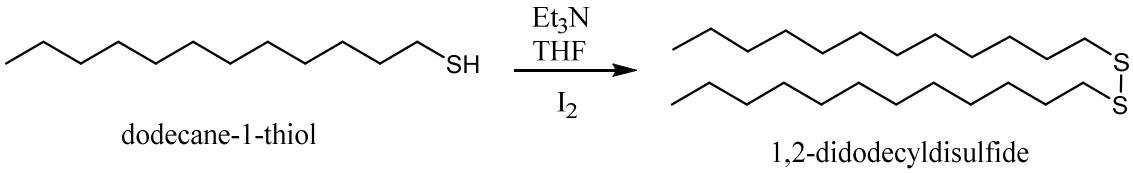

Figure 2.13. Synthesis scheme of 1,2-didodecyldisulfide.[15]

The systematic photophysical studies of gold nanoparticles functionalized with thiol and disulfide by Navarro et al., suggests that disulfides have apparent higher affinity for gold nanoparticles.[16] The tendency of disulfide to self-assemble on GNPs at low concentration indicates that this stronger multidentate ligand is better suited when robust metal-organic binding is required.

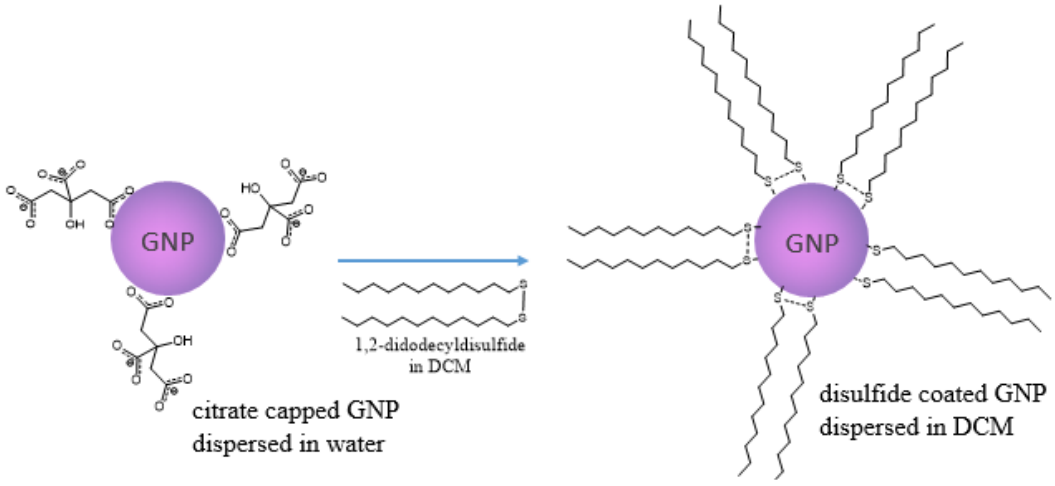

Figure 2.14. Schematic illustration of place-exchange of citrate by 1,2-didodecyldisulfide on GNP surface.

Figure 2.14 shows our scheme of place exchanging citrate ion with disulfide. For this experiment we took 200 μL of 1.63 nM aqueous suspension of citrate-capped 15 nm GNPs in different micro centrifuge tubes. To that, 1 mM KOH was added to adjust the pH to ~9. Then to each tube we added 200 μL different concentrations (0, 0.02, 0.2, 0.5, 1 mM) of 1,2-didodecyldisulfide in dichloromethane to create biphasic solutions. After 12 h of rotation the microtubes were incubated to separate the aqueous and organic phases. Figure 2.15 shows the biphasic solutions of water (top) and dichloromethane (bottom). The increasing concentration of disulfide in DCM caused the darker color of organic phase. The decreased intensity of pink color in the aqueous portion of 1 mM sample visually proves that the phase transfer of gold nanoparticles was occurred with the 1 mM of 1,2-didodecyldisulfide.

The aqueous and organic portions were extracted by adding 800 μL of water and 800 μL of DCM to the microtubes. Absorbance spectra (Figure 2.16) of the aqueous phases show a gradual decrease in concentration of gold nanoparticles due to phase transfer. The % phase transfer was calculated from decrease in absorbance at ~520 nm.

Initial concentration of GNP in 200 μL aqueous phase	Concentration disulfide in 200 μL organic phase	Ratio GNP to disulfide	% decrease in concentration of GNPs in aq. phase
1.63 nM	0.02 mM	1: 12300	33.2%
1.63 nM	0.2 mM	1:123000	37.9%
1.63 nM	0.5 mM	1:307000	49.3%
1.63 nM	1 mM	1:613000	88.6%

Table 2.3. Efficiency of place exchange of citrate by disulfide

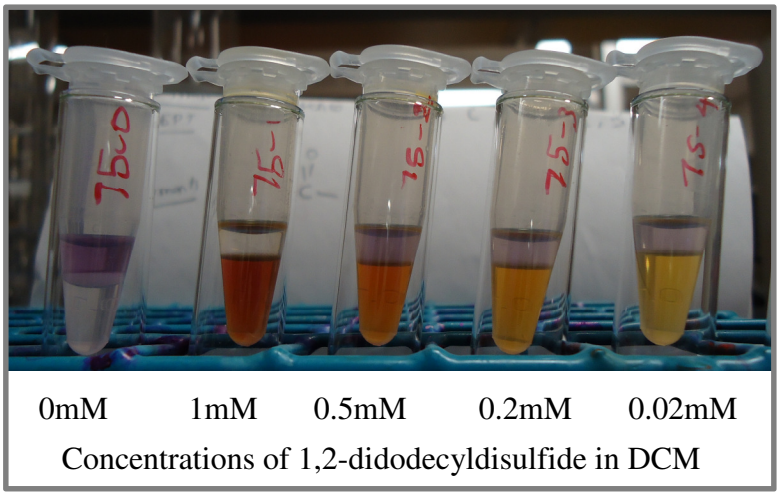

Figure 2.15. Place-exchange study of citrate by 1,2-didodecyldisulfide on GNP surface

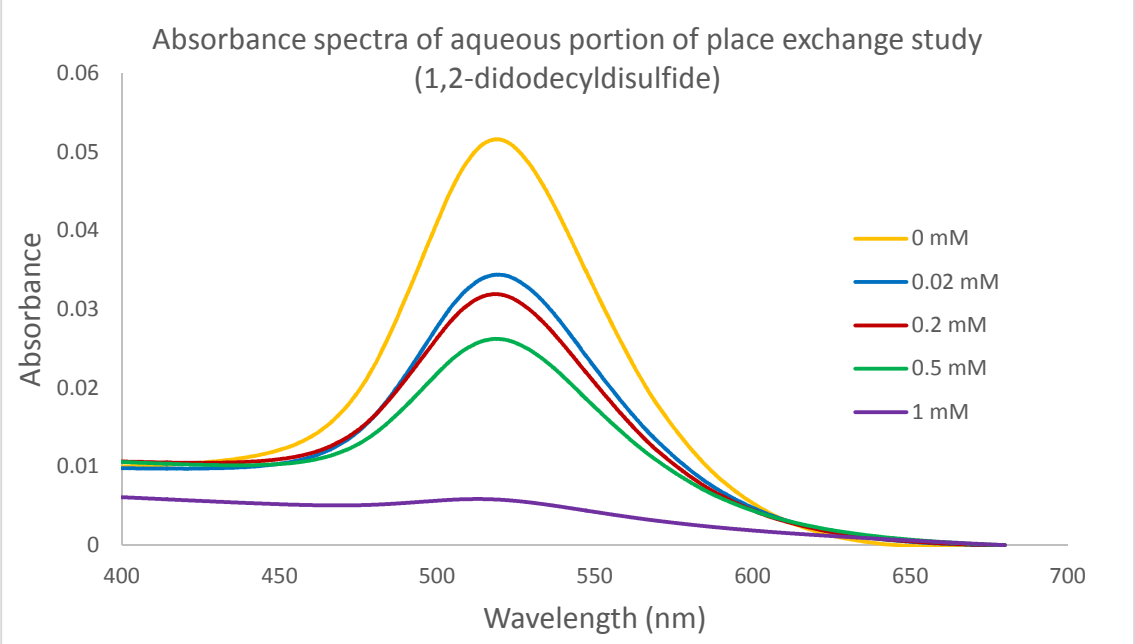

Figure 2.16. Absorbance spectra of aqueous portion of place exchange study of citrate by different concentration of 1,2-didocyldisulfance on gold surface

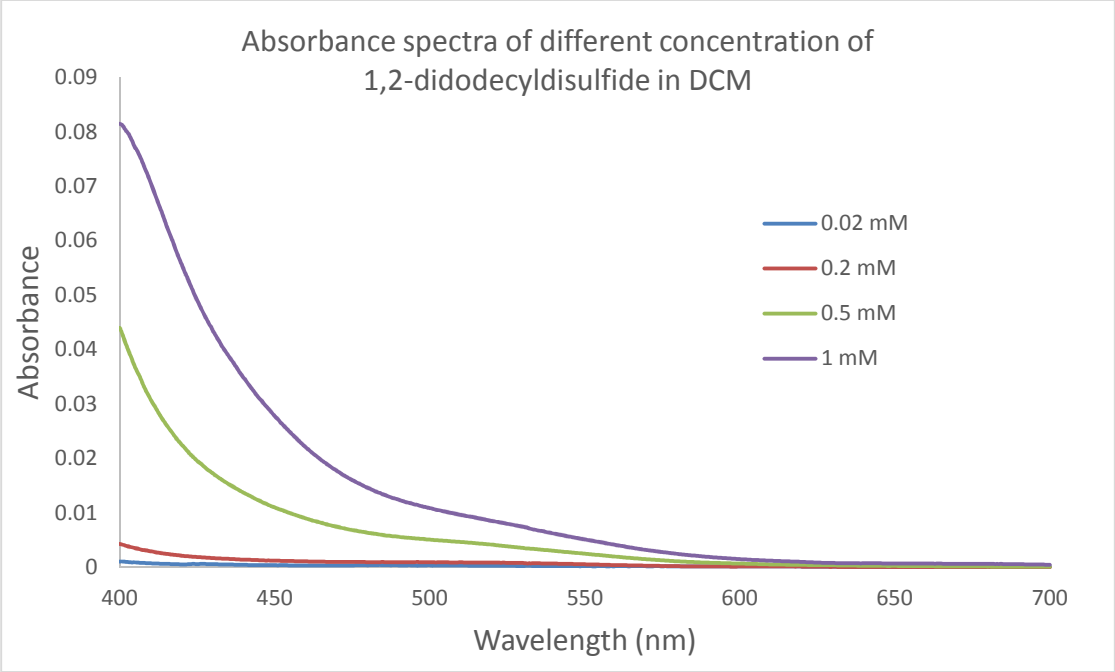

Figure 2.17. Absorbance spectra of different concentration of 1,2-didodecyldisulfide in DCM

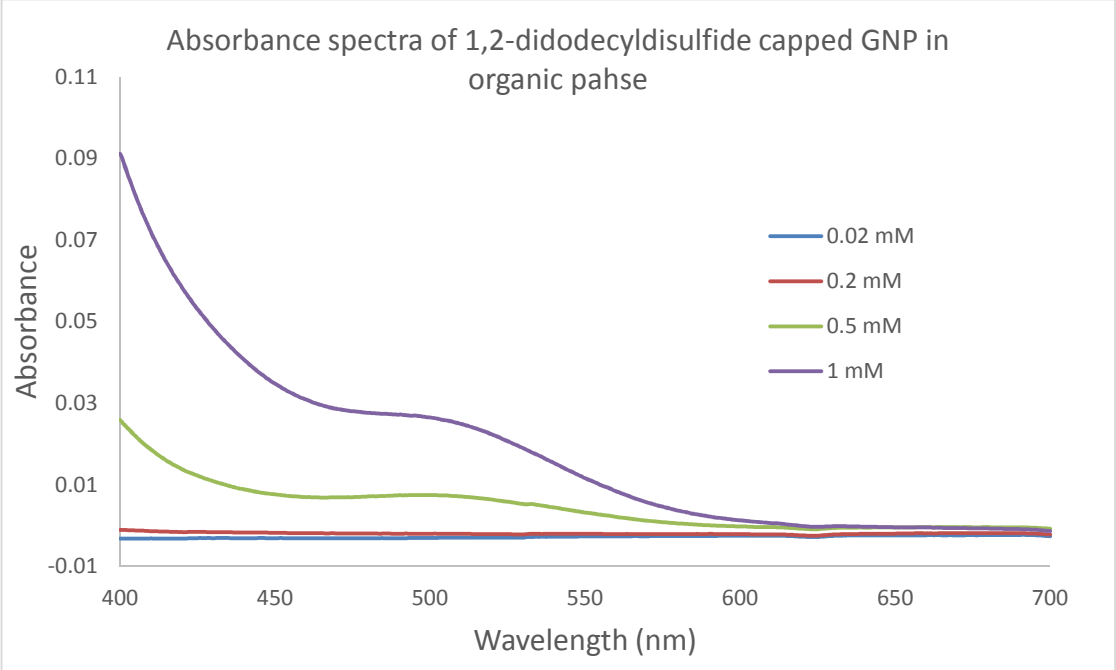

Figure 2.18. Absorbance spectra of organic portion of place exchange study of citrate by different concentration of 1,2-didocyldisulfance on gold surface

The spectra (Figure 2.18) of extracted organic phases show a steady increase in absorbance (compared to the controls) at ~515 nm corresponds to the increase in concentration of GNP. The % increase of absorbance of GNPs could not be accurately calculated, since the absorbance of the disulfide or CS_2 is dominant at <550 nm. But we can see the change in structure of the absorbance bands (purple and green lines) of the samples with higher disulfide concentrations (1 mM and 0.5 mM).

The percentages of GNP phase transferred due to the place exchange of citrate ion by different concentration of disulfide were in the Table 2.3. The experimental data demonstrates that disulfide has a somewhat higher affinity to gold compared to thiol. For thiol it took 3 mM to phase transfer 81% of gold nanoparticles from aqueous to organic phase, but for disulfide it took about 1 mM to phase transfer the same amount of GNPs. Thus it is better to employ multidentate ligands like disulfide for stronger binding between fluorophore to metal nanoparticles. In **Chapter 3** and **4** we discussed the application of organic ligands in designing the gold and silica nanoparticles aggregate system in order to promote metal-enhanced fluorescence in aqueous solution.

2.3.3. Dithiocarbamate ligand mediated aggregation of gold nanoparticles

Following the place exchange study of thiol and disulfide on gold surface, we investigated the efficacy of disulfide derivative in promoting gold nanoparticle aggregation in aqueous solution. For that we reproduced the "diamino disulfide" ligand initially synthesized by Anuradha Singh in our lab.[7a] Although amines have affinity for gold surface, dithiocarbamate (DTC) are known to be better ligands for gold binding.[11] The full negative charges on DTC creates a great tendency for stronger binding with the positively charged gold surface. Also the ease of spontaneous activation of DTC make it a useful candidate for controlled binding of GNPs in solution phase.

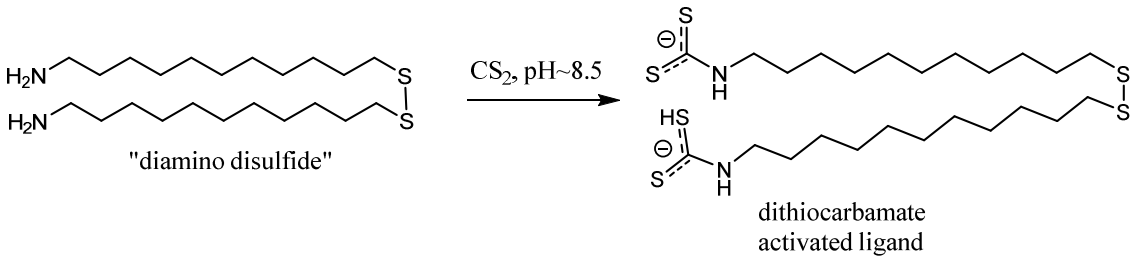

Figure 2.19. Spontaneous conversion of amine into dithiocarbamate in aqueous solution.

Our early studies showed that diamino disulfide coated gold nanoparticles are not stable in aqueous phase at higher pH. The longer alkane chain with neutral amine terminals make the ligand highly hydrophobic and thus the ligand coated GNPs migrate into organic phase. Figure 2.20 shows the pH controlled phase transfer of diamino disulfide coated gold nanoparticles. At pH~7, the ammonium ions of the ligands tend to keep the particles in aqueous phase, but when the pH is changed to ~10, the particles transfer into organic phase. To avoid this solubility problem, we pre-coated the gold nanoparticles with a water compatible ligands to keep them dispersed in aqueous solution.

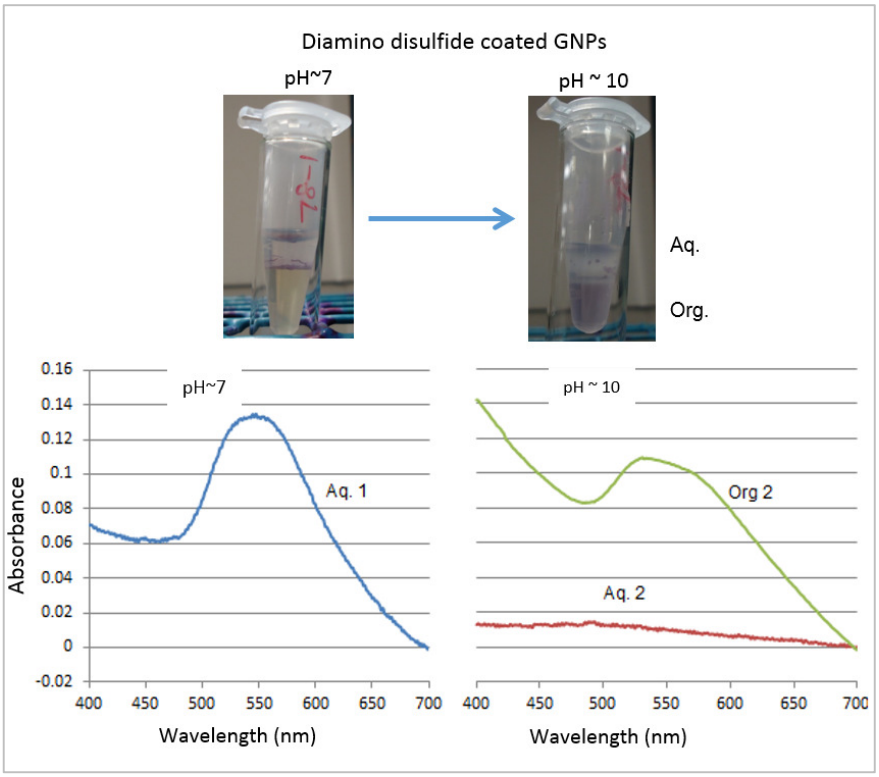

Figure 2.20. pH controlled phase transfer of diamino disulfide coated GNPs

To maintain the water compatibility of gold nanoparticles throughout our study we place exchanged the loosely bound citrate ions with a strongly binding thiolated ligand carrying the hydrophilic ether moiety. For this purpose we used the "ether thiol" ligand prepared by Anuradha Singh.[17]

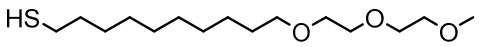

"Ether thiol"

Diluted ether thiol solution (5 mL) at pH~9.5 was added to the citrate-capped gold nanoparticle suspension (15 nm diameter, 10 mL) in a scintillation vial and the sol was incubated overnight to allow the place exchange of citrate by ether thiol to happen. Then we partially place exchanged the ether thiol with diamino disulfide to study the DTC mediated aggregation of gold nanoparticle as shown in the following scheme.

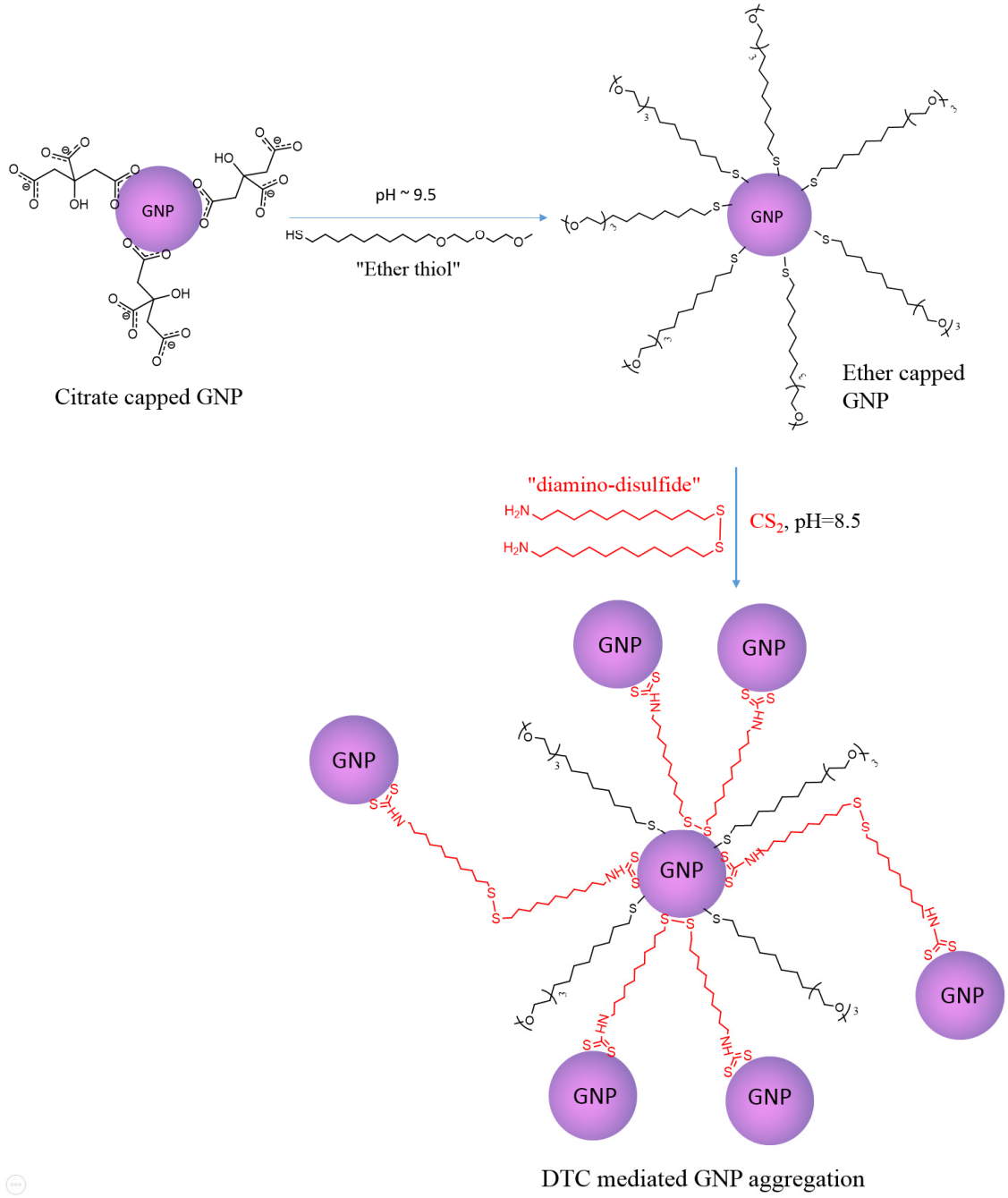

Figure 2.21. Scheme of "ether thiol" coating on GNP surface for better aqueous dispersibility and DTC disulfide mediated GNP aggregation

Since disulfides bind stronger with gold surface, they can replace the relatively weaker ether-thiol ligands on the gold nanoparticles.[9a] At the same time we need some of the aqueous compatible ether-thiol ligand on gold surface to keep the particles dispersed in aqueous phase. So we used a lesser concentration of disulfide to partially replace the ether thiol on GNP surface. In a cuvette, we took 3 mL of the ether-capped GNP, adjusted the pH to ~8.5 and added diamino sulfide (0.5 mM, 200 µL) and CS_2 (1 mM, 200 µL). Control samples were prepared in separate cuvettes as shown in the Figure 2.22 (taken after the overnight reaction). The cuvettes were tightly capped and sealed with parafilm to any avoid evaporation of solvent. The reaction mixture was stirred overnight.

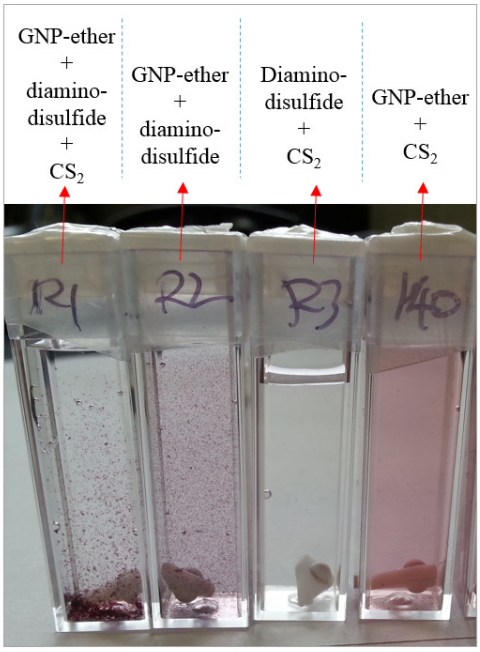

Figure 2.22. Investigation of DTC and amine mediated GNP aggregation

Aggregation of gold nanoparticle caused the particle sinking and is clearly seen in the first two cuvettes containing the mixture of ether-capped GNP and diamino disulfide ligand with CS_2 (cuvette R1) and without CS_2 (cuvette R2). The result shows

both dithiocarbamate and amine moieties facilitated the gold-gold aggregation. But the GNP aggregates were seen unstable in aqueous solution. This result may be due to the decreased concentration of aqueous compatible ether-thiol ligand on the GNP surface. The disulfide and dithiocarbamate moieties might have replaced most of the ether thiols before and after DTC activation respectively. The absorbance spectra show a drop in absorbance at ~520 nm (green and red lines) that corresponds to the decrease in concentration of free gold nanoparticles in the solution. Also the increase in absorbance at >570 nm corresponds to the coupled plasmon resonance supports presence of GNP aggregates. The greater absorbance enhancement at > 570 nm was observed for the sample containing DTC ligand.

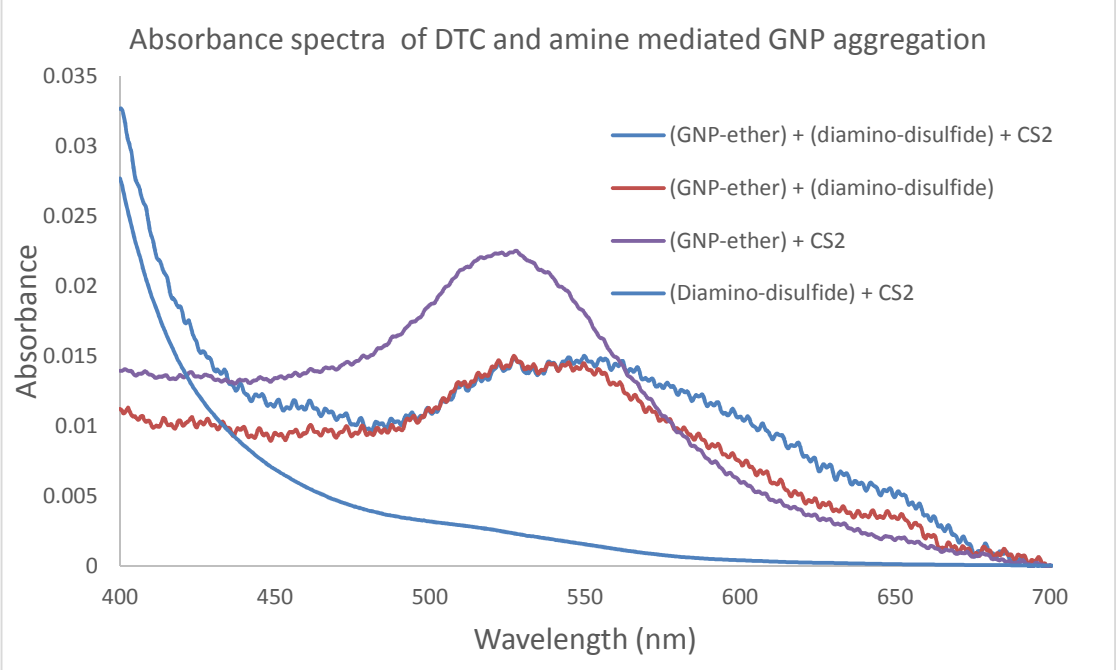

Figure 2.23. Absorbance spectra from DTC and amine mediated GNP aggregation study.

Thus, ligands containing DTC or amine terminal can promote the aggregation gold nanoparticles in aqueous solution. These promising results led us to investigate more on designing and controlling nanoparticle aggregation systems in solution phase.

2.3.4. Photo-triggered aggregation of gold nanoparticles in aqueous solution

We synthesized a photolabile ligand for gold surface and performed an initial study on the efficacy of photo-triggered aggregations of gold nanoparticle. In recent years there has been a growing interest in the promising application of photolabile protecting groups in various fields such as photolithography, targeted delivery, photo-triggered drug release, etc.[1] The possibility of smoothly breaking bonds without the need of any reagent is an attractive feature of the photolabile protecting groups. This could solve the problems associated with harsh conditions (acids and bases) usually required for the deprotection in vivo applications.[18]

Photolabile ligands coated on gold nanoparticles can be activated to produce controlled GNP aggregates in aqueous solution and this method can be adapted to various applications. Also the aqueous based gold aggregate system can be used as a method of testing the efficienty the photolabile ligands. We used 2-(2-nitrophenyl) propyloxycarbonyl (NPPOC) protecting group to protect the primary amines of diamino disulfide ligands. Bhushan et al., has been used the NPPOC group in photolithographic solid-phase peptide synthesis as a photolabile protecting group for amino acids.[19] Upon irradiation with UV light (~365 nm) the amines can be deprotected.

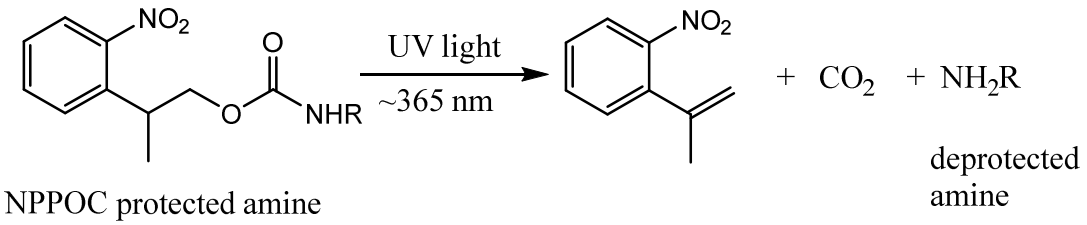

Figure 2.24. Scheme of photo-deprotection of amine[19]

We synthesized the photolabile protecting group (NPPOC chloride) from 1-ethyl-2-nitrobenzene following the literature procedure.[19] Titron B (organic base) was

used to deprotonate the benzylic carbon of 1-ethyl-2-nitrobezene followed by the addition of formaldehyde and reflux for 6 h. After extraction and purification steps we obtained 2-(2-nitrophenyl)-propan-1-ol with 98% yield. Treating that with 20% phosgene in toluene at 0 °C for 3 h resulted in NPPOC chloride. Because of the high reactivity and light sensitivity of this compound we moved on to next step without further purification. Under dark condition the previously synthesized diamino disulfide was mixed with sodium carbonate in 1:1 dioxane-water mixture followed by dropwise addition of NPPOC chloride in THF solution at 0 °C for 20 min. Then the reaction mixture was stirred for 24 h at room temperature. After extraction and purification steps we obtained the "photolabile diamino disulfide". NMR and Mass spectra were obtained to confirm the structure of the product. Throughout the synthesis we tool measures to avoid the exposure of this product to light.

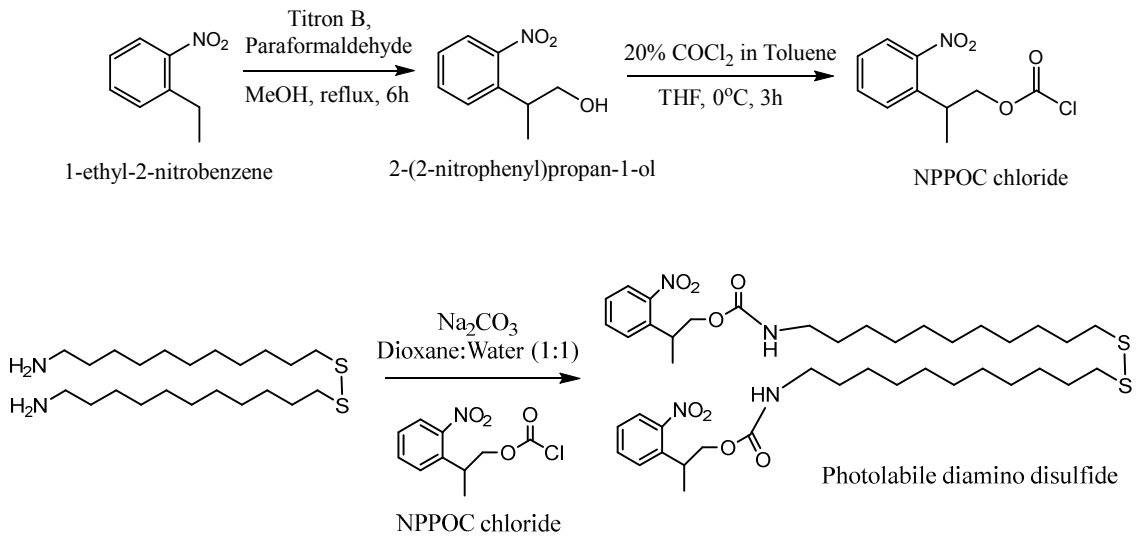

Figure 2.25. Scheme of synthesizing photolabile diamino disulfide ligand

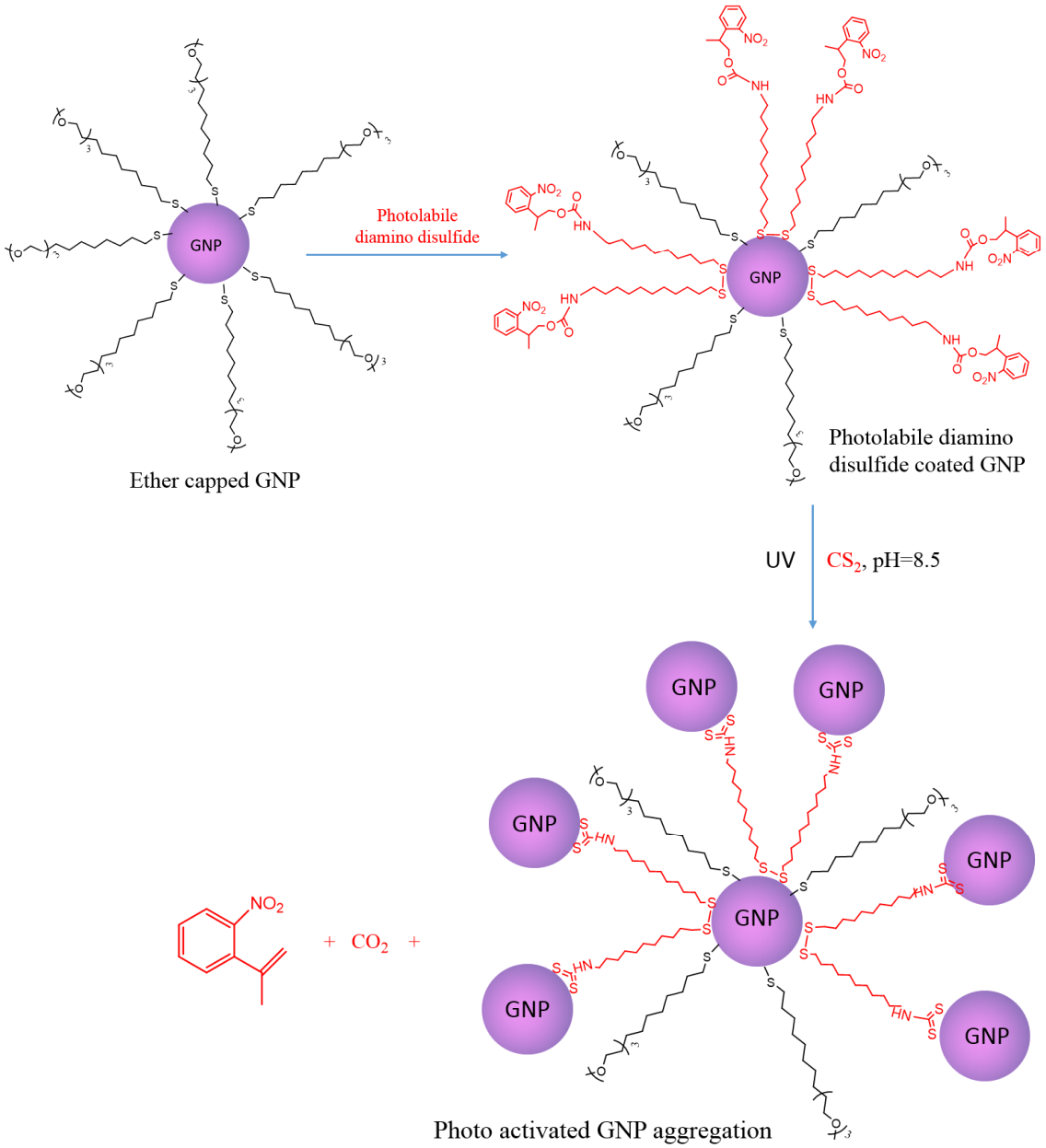

Figure 2.26. Place exchange of ether thiol by photolabile ligand and photo activation of the ligand to promote GNP aggregation

An advantage of using amine protected ligand is that we can avoid amine to gold binding and selectively form disulfide to gold binding. That would increase the possibility of DTC mediated gold aggregation. The NPPOC protected diamino disulfide was dissolved in DCM to get 1 mM concentration. In a quartz cuvette 3 mL of

ethanol water suspension ether-capped GNP was taken and the pH was adjusted to ~9. Then 200 µL of 1 mM NPPOC protected diamino disulfide as added to the cuvette. The sample was incubated overnight under dark condition. Absorbance spectra were taken before deprotecting the ligand. To activate the ligand, we added 200 µL of 1 mM CS_2 to the sample and exposed the sample filled quarts cuvette to UV light for 4 h. Then the sample was gently mixed and incubated for 6 h. Absorbance spectra were obtained to measure the amount of photo-triggered gold nanoparticle aggregation taken place.

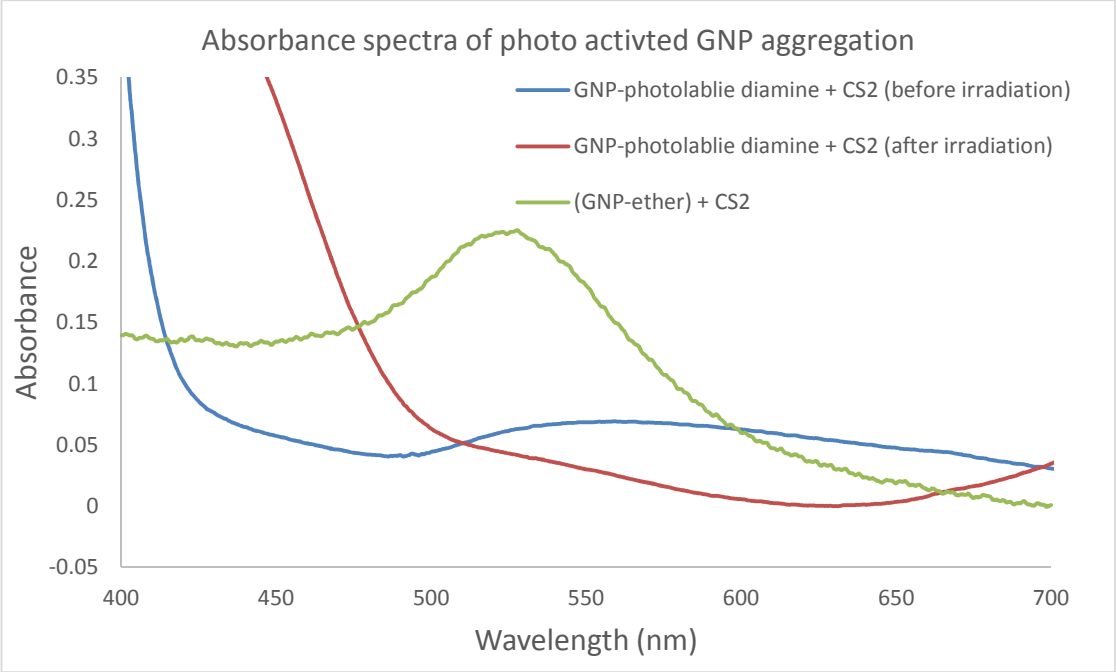

Figure 2.27. Absorbance spectra of photo-activated GNP aggregation

Absorbance spectra (Figure 2.27) indicates a drop in concentration of gold nanoparticles even before the photo activation step (blue line). We speculate that a robust place exchange of ether thiol with the photolabile ligand decreased the water compatibility of the GNPs. So the photolabile ligand coated GNPs might have sunk even before the photo-triggered aggregation. A further drop in absorbance after irradiation may be due to the aggregation of GNPs or decrease in concentration of

GNPs due to water incompatibility. The increase in absorbance at > 570 due to GNP aggregation is not seen in the after irradiation spectrum. So the particles were most likely settled due to poor dispersibility even before the irradiation. Although we were unable to achieve the photo triggered GNP aggregation in this experiment, this initial results encouraged us to explore optimal conditions to test the photolabile linkers.

This promising results from organic ligand based aggregation of gold nanoparticles drives us to use similar method to promote heteroaggregation of metal (gold) and fluorophore (QD-doped-silica) nanoparticles in solution phase. In the next chapter we discuss the synthesis of QD-doped-silica nanoparticles and surface modification of them with the organic ligands.

2.4. Chapter Summary

In this chapter we discuss the synthesis of various size gold nanoparticles and the place exchange study of thiol, disulfide and dithiocarbamate ligands on the surface of gold nanoparticles.

Gold nanoparticles were synthesized by reduction of gold (III) chloride by sodium citrate in a boiling aqueous solution. Using this standard citrate reduction method we produced highly monodisperse 14 nm diameter gold nanospheres. We also attempted to produce larger gold nanoparticles by the controlled nucleation method developed by Frens,[11] where a lesser concentration of sodium citrate was used to create fewer nucleation sites. But the results showed that this method produced only irregular and polydisperse GNPs. However, in a kinetically controlled single pot seeded growth method we were able to produce various sizes of monodisperse gold nanoparticles. In the seeded growth method, by slow addition of gold (III) chloride and sodium citrate to a GNP seed solution, any secondary nucleation was inhibited. Eleven generations of GNPs were synthesized with size range from 15 nm to 60 nm. These different size particles would be used in the second part of our research to investigate the degree of spectral overlap with quantum dots in order to produce metal-enhanced fluorescence.

We functionalized the surface of GNPs with thiol and disulfide ligands. The citrate ions on the GNPs were place exchanged with the hydrophobic dodecane-1-thiol ligand in a biphasic solution. Absorbance spectra of the aqueous phase were obtained to measure the amount of GNPs phase transferred to organic layer and thus measure the place exchange efficacy of the ligands. The results suggest that 3 mM concentration of dodecan-1-thiol was need to phase transfer 81% of 1.63 nM GNPs.

Then we investigated the efficacy of disulfide ligand to place exchange the citrate ion on GNP surface. For that we synthesized 1,2-didodecyldisulfide in our lab. Theoretically disulfide ligands, compared to thiols, have higher affinity for gold because of the possibility of multidentate binding with gold surface. Our results showed that it requires less than 1mM concentration of disulfides (one third of the concentration of thiols) to phase transfer the same amount of GNPs. Therefore, we synthesized disulfide based multifunctional ligands for further studies.

We attempted to produce dithiocarbamate (DTC) mediated GNP aggregation system in aqueous solution. For that we reproduced the diamino disulfide ligand initially synthesized by Anuradha Singh in our lab. Also we used the TEG derived ether-thiol ligand (that has more hydrophilic moiety) to cap the GNPs in order to increase the water compatibility of GNPs. We performed a place exchange of the ether-thiol with minimum amount of diamino disulfide and a spontaneous DTC activation to produce GNP aggregates in aqueous solution. The absorbance spectra of samples containing DTC ligands showed a decrease in concentration of free GNPs and an increase in concentration of aggregated GNP in the solution. However similar result was also observed for the amine ligand. The hydrophobic nature of these ligands could decreased the water dispersibility of the GNPs, so that the amount of aggregation was not accurately reflected in the absorbance spectra.

We attempted to produce a photo triggered GNP aggregation in aqueous solution. For that we synthesized the photolabile 2-(2-nitrophenyl) propyloxycarbonyl (NPPOC) protecting group to protect the primary amines of diamino disulfide ligands. The protected diamino disulfide ligands were place exchanged on ether-capped GNPs.

The sample was irradiated with UV light to deprotect and spontaneously convert the amines into DTC with the intention of promoting GNP aggregations. However, the results showed that a significant drop in concentration of GNPs occurred even before the irradiation. This may be due to the poor aqueous dispersibility of the photolabile ligand coated GNPs or the instability of the protecting group. This initial study provided a path for further optimization of conditions to examine the efficacy of a photolabile ligand in the study of optical properties of GNPs.

2.5. Experimental and Methods

2.5.1. Synthesis of gold nanoparticles using controlled nucleation method [11]

For this experiment all glassware were washed with aqua-regia (HNO_3:HCl, 1:3) and milipore water (17.8 M) before use. Gold (III) chloride trihydrate ($HAuCl_4$ $3H_2O$) and trisodium citrate ($Na_3C_6H_5O_7$) were purchased from Sigma-Aldrich and used without any further purification. Based on the Frens procedure, we calculated the amount of sodium citrate required for synthesizing16 nm and 100 nm diameter gold nanoparticles. To prepare 16 nm diameter gold nanoparticles, aqueous solution of gold (III) chloride trihydrate (50 mL, 0.25 mM) was added to a round bottom reactions flasks along with a magnetic stir bar. The solution was brought to boil before an aqueous solution of trisodium citrate $Na_3C_6H_5O_7$ (1 mL, 34 mM) was added. Within 2 min the solution gradually turned a dark blue color before becoming the dark red color, which indicates the complete formation of GNP (approximately 5 min after boiling). Then the reaction was cooled and the final volume was made up to 50 mL by adding milipore water. To synthesize 100 nm gold nanoparticles, we used the same procedure but with 0.16 mL of 34 mM trisodium citrate. Size of the particles were measured from the TEM images and the concentration of the suspension were calculated from the absorbance spectra.

2.5.2. Synthesis of gold nanoparticles using seeded growth method [12, 14]

All glassware were washed with aqua-regia (HNO_3:HCl, 1:3) and milipore water (17.8 M) before use. Aqueous solution of trisodium citrate (15 mL, 2.2 mM) was added to a two neck round bottom flask along with a magnetic stir bar. The flask was connected to a water condenser and the solution was boiled for 15 min before reducing the temperature to 90 °C. Then an aqueous solution of gold (III) chloride trihydrate (0.25

mL, 10 mM) was injected into the flask and continued stirring at 90 °C for 10 min to obtain the seed solution or generation G0. To the seed solution in the same pot gold (III) chloride trihydrate (0.25 mL, 10 mM) was injected and stirred for 30 min at 90 °C. Then again gold (III) chloride trihydrate (0.25 mL, 10 mM) was injected and stirred for 30 min at 90 °C to obtain the G1 generation gold nanoparticles. Using glass syringe 5 mL of the G1 sample was removed. Then to obtain 5 mL of every new generation from the same pot, trisodium citrate (0.35 mL, 34 mM) and water (4.65 mL) was added once and repeated the process of adding gold (III) chloride trihydrate (0.25 mL, 10 mM) and stirring for 30 min at 90 °C twice. The single pot reaction was continued up to eleven generations of GNPs. Size of the particles were measured from the TEM images and the concentration of the suspension were calculated from the absorbance spectra.

2.5.3. Synthesis of 1,2-didodecyldisulfide ligand [15]

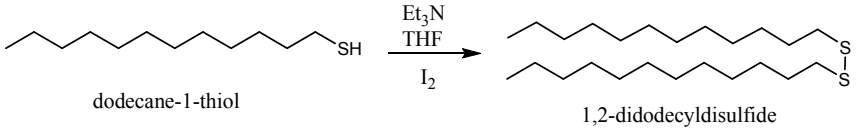

Figure 2.28. Synthetic scheme of 1,2-didodecyldisulfide

In a 5 mL reaction flask THF (0.75 mL), 1-dodecanethiol (0.1 g, 0.49 mmol), and Et3N (0.08 mL, 0.54 mmol) were placed under nitrogen atmosphere. Iodine (0.1379 g, 0.54 mmol) was then added to the solution at 0 °C. After being stirred at 25 °C for 6 h, the mixture was poured into a sodium thiosulfate solution (1 M, 2 mL). The product was extracted with EtOAc (3 × 2 mL) and the combined organic layers were dried over Na_2SO_4 and concentrated under vacuum. The residue was purified by silica gel column

chromatography (hexane) to yield 1,2-didodecyldisulfide (0.18 g, 89%). ^{1}H NMR (300 MHz, $CDCl_3$): δ 2.69 (t, 4H), 1.67 (p, 4H), 1.27 (m, 36H), 0.39 (t, 6H).

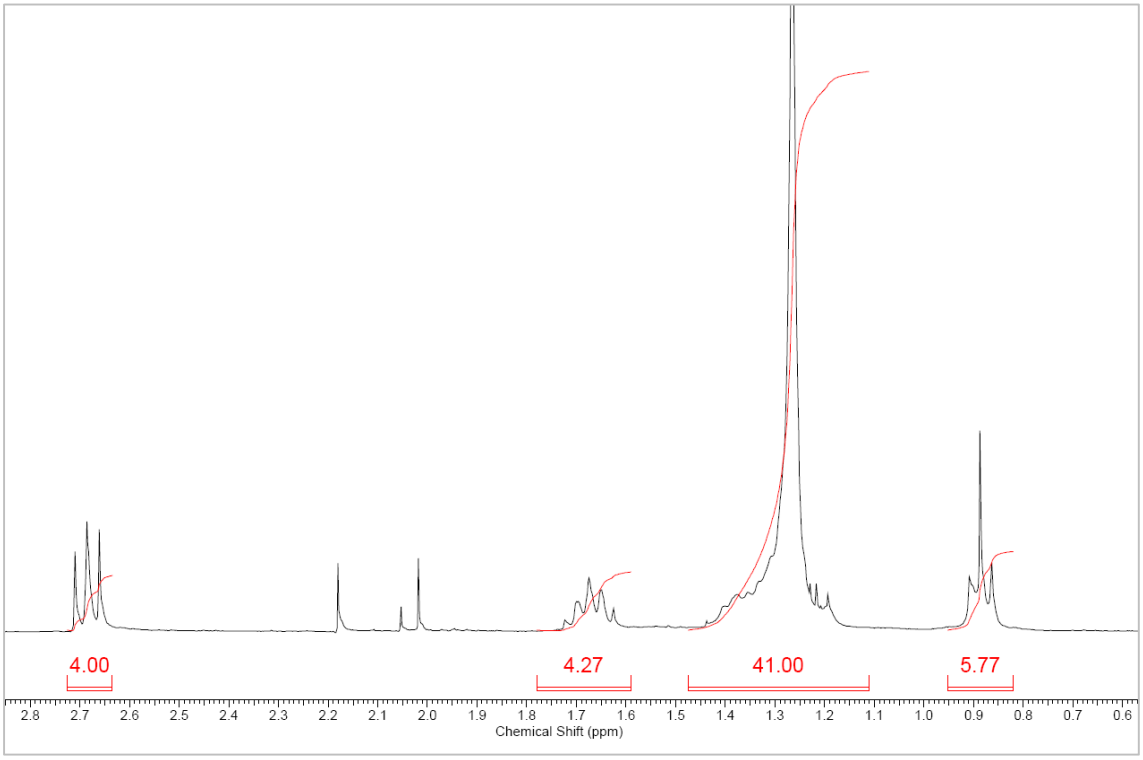

Figure 2.29. ^{1}H NMR of 1,2-didodecyldisulfide

2.5.4. Synthesis of "diamino disulfide" ligand [7a, 20]

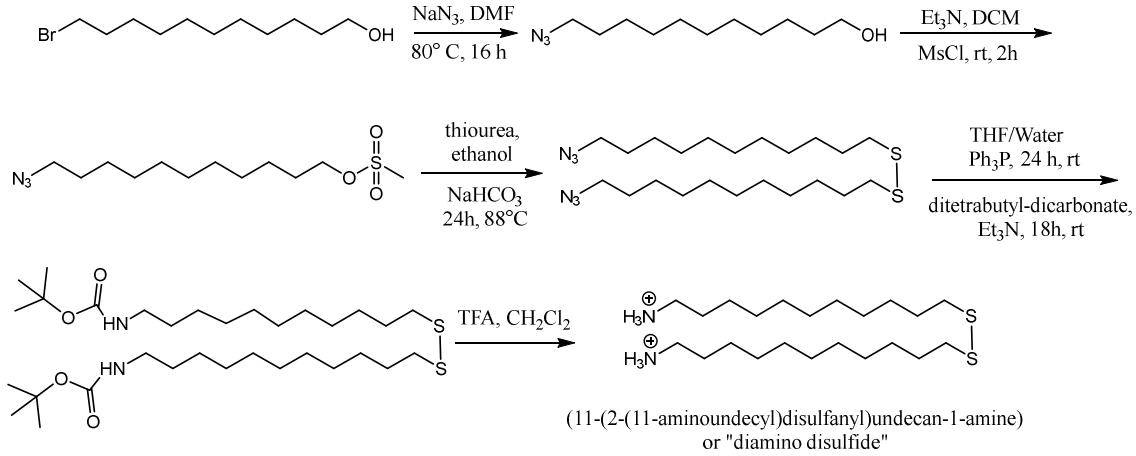

Figure 2.30. Synthetic route of diamino disulfide

To a 250 mL reaction flask, 11-bromoundecanol (10 g, 39.8 mmol), sodium azide (7.7 g, 119 mmol), and DMF (80 mL) were added and stirred for 24 h at 80 °C. 200 mL of distilled water was added and stirred it for 30 minutes and extracted with dichloromethane (3×20 mL). The organic portion was combined and washed with water (2× 20mL) and brine solution (1× 20 mL). The organic phase was dried over anhydrous $MgSO_4$, filtered and concentrated to obtain pure 11-azidoundecanol (8.3 g, 39 mmol, 98%) as a colorless oily liquid. The NMR spectrum matched with literature. To a 250 mL reaction flask, 11- azidoundecanol (8.35 g, 39 mmol), methanesulfonyl chloride (12 g, 108 mmol), dichloromethane (250 mL) were added and stirred at 0 °C. The solution of triethylamine (10.89 mL, 108 mmol) was added to the cooled reaction flask dropwise through syringe over 5 min and stirred it for overnight at room temperature. The reaction was quenched by the adding ice-cold water (50 mL) and stirred for 15 min. The organic phase was separated and the aqueous phase was further extracted with dichloromethane (2×30 mL). The organic portions were combined, washed with 1M

HCl (1×20 mL), NaHCO3 (1×20 mL), brine (1×20 mL), and water (2×20 mL), dried over anhydrous sodium sulfate, filtered, and evaporated the solvent via rotary evaporation to provide pale orange oily liquid (100% yield, 12.27g). The obtained 1-azidoundecanemesylate (12.27 g, 42.16 mmol) was refluxed with thiourea (6.41 g, 84.32 mmol), and ethanol (50 mL) for 4h. Then aqueous sodium bicarbonate (3M, 50 mL) was added and stirred at room temperature for 24 h. The flask was cooled and concentrated. The residue was treated with water (50 mL) and extracted with dichloromethane (3×20 mL). The combined organic phase was dried over Na_2SO_4 and concentrated to obtain bis-(azidoundecane)disulfide (8.7 g, 91%) as a colorless liquid. Azidoundecanedisulfide (8.7 g, 19.21 mmol) was reduced to amine by stirring with triphenyl phosphine (50.3 g, 192.07 mmol) in THF (200 mL)/ water (8 mL) at room temperature for 24 h. Triethylamine (10.07 g, 109.48 mmol) and di-t-butyl dicarbonate (20.1 g, 92.2 mmol) were added to the same flask and continued stirring at room temperature for more 18 h. The crude was extracted with ether (3×60 mL), and washed with water (2×60 mL). The combined organic phase was dried over $MgSO_4$ and concentrated via rotary evaporation. The boc protected diamino disulfide was purified through silica gel column chromatography (9:1 CH_2Cl_2/ MeOH) to provide pure compound (8.7 mg, 75%) as a colorless solid. Boc was deprotected by stirring boc protected disulfide (0.390 g, 0.64 mmol) with TFA (5 mL) and dichloromethane (5 mL) at room temperature for more 0.5 h. The TFA was removed through vacuum evaporation in the presence of methanol couple of times to provide pure diamino disulfide (0.395 g, 97%) as a colorless oily liquid. ^{1}H NMR (300 MHz, $CDCl_3$): δ 7.86 (b, 6H), 2.9 (m, 4H), 2.7 (t, 4H,), 1.66 (m, 8H), 1.28 (m, 28 H).

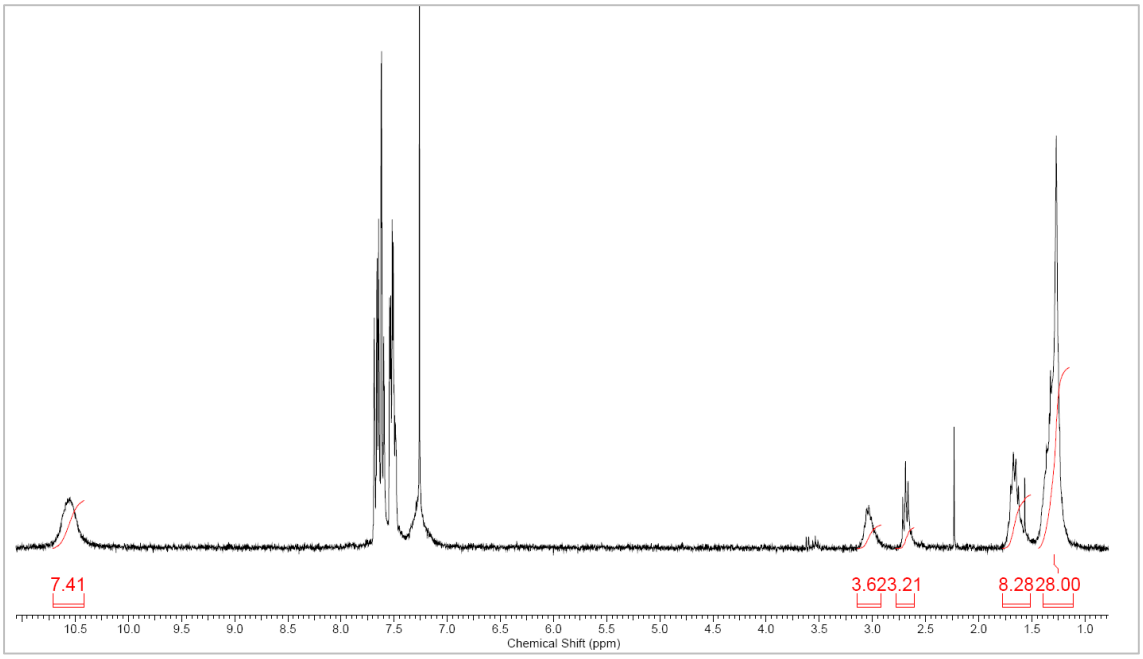

Figure 2.31. ^{1}H NMR of diamino disulfide

2.5.5. Synthesis of NPPOC chloride (photolabile protecting group) [19]

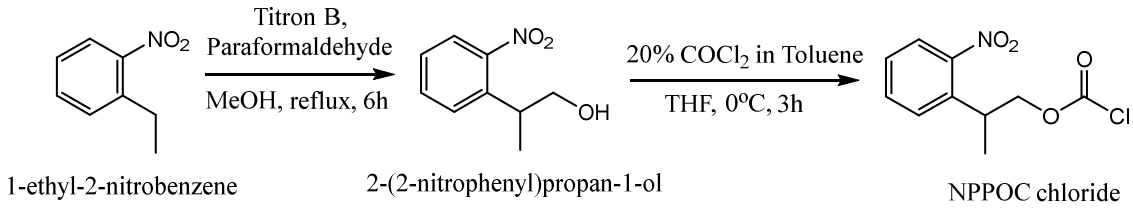

Figure 2.32. Synthetic route of NPPOC chloride

Preparation of 2 -(2 -nitrophenyl)propanol: Triton B (40% in MeOH, 13.9 mL, 33.3 mmol) was added to 2-ethylnitrobenzene (5 g, 33.3 mmol) and paraformaldehyde (1.0 g, 33.6 mmol), and the mixture was heated at reflux for 6 h. After concentration under vacuum, the reaction mixture was neutralized using 5% aqueous HCl. The mixture was extracted with ethyl acetate (3×25 mL), dried over Na_2SO_4 and concentrated under vacuum. The residue was purified by silica gel flash chromatography using hexane–

ethyl acetate (4:1) to give compound 2 (11.2 g, 98%, red oil). ^{1}H NMR (300 MHz, $CDCl_3$): δ 7.74 (d, 1H), 7.57 (t, 1H), 7.49 (d, 1H), 7.36 (t, 1H), 3.78 (d, 2H), 3.52 (m, 1H), 1.80 (br s, 1H, OH), 1.33 (d, 3H)

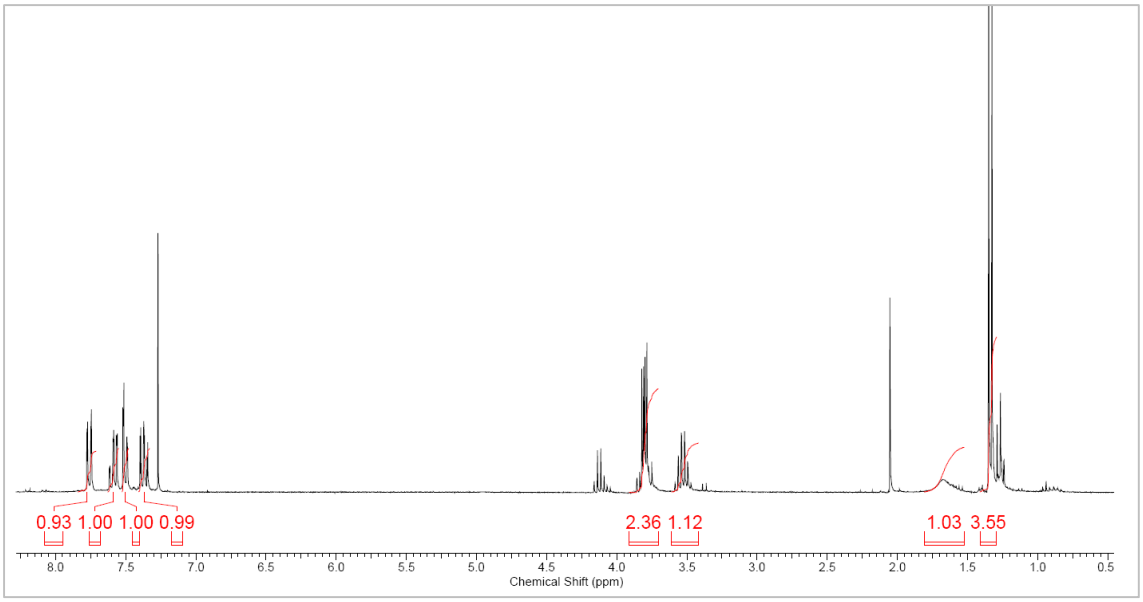

Figure 2.33. ^{1}H NMR of 2-(2 -nitrophenyl)propanol

Preparation of NPPOC chloride : To a solution of 2 -(2 -nitrophenyl)propanol (1 g, 5.5 mmol) in anhydrous THF (5 mL) at 0°C, was added a solution of phosgene (20% in toluene, 0.82 g, 8.33mmol) over a period of 15 min with stirring under a nitrogen atmosphere. After 45 min, the ice bath was removed and stirring was continued at room temperature for 2 h. A stream of N_2 was then bubbled through the solution for 1 h to remove the excess phosgene, after which the mixture was evaporated to dryness under vacuum to give compound (1.28 g, brown oil). Due to the sensitivity of the compound no purification was done. ^{1}H NMR (300 MHz, $CDCl_3$): δ 7.82 (d, 1H), 7.61 (t, 1H), 7.44 (d, 1H), 7.39 (t, 1H), 4.48 (d, 2H), 3.7 (m, 1H), 1.40 (d, 3H)

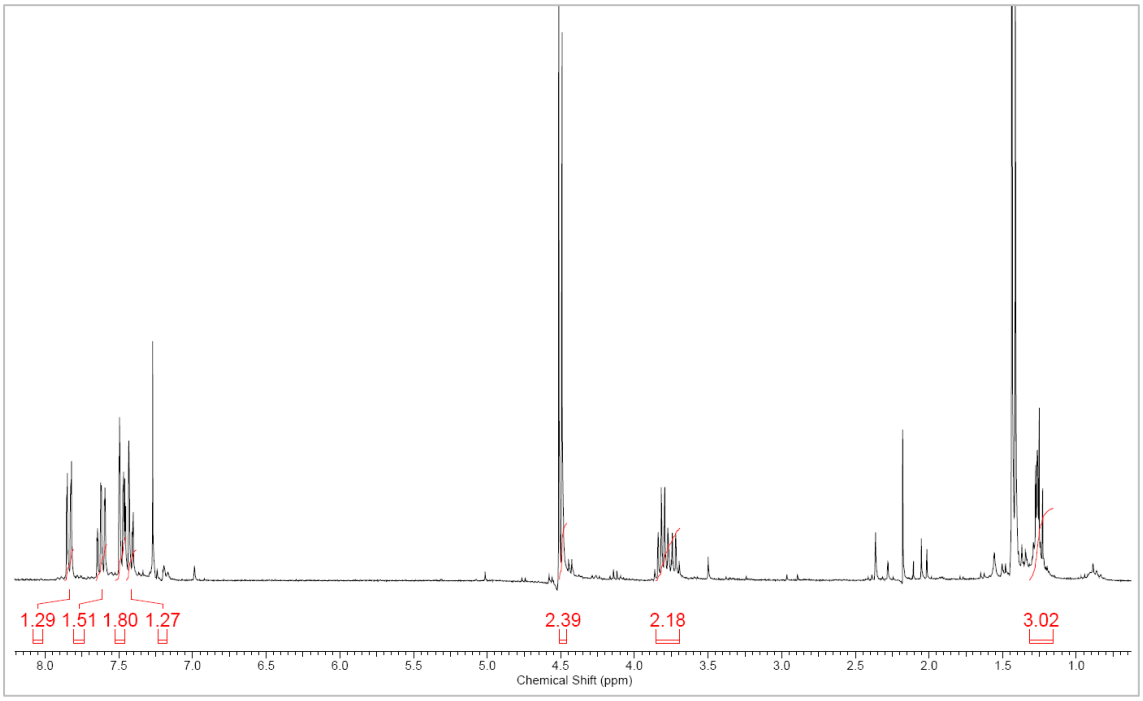

Figure 2.34. ^{1}H NMR of NPPOC Chloride

2.5.6. Synthesis of NPPOC protected diamino disulfide ligand [21]

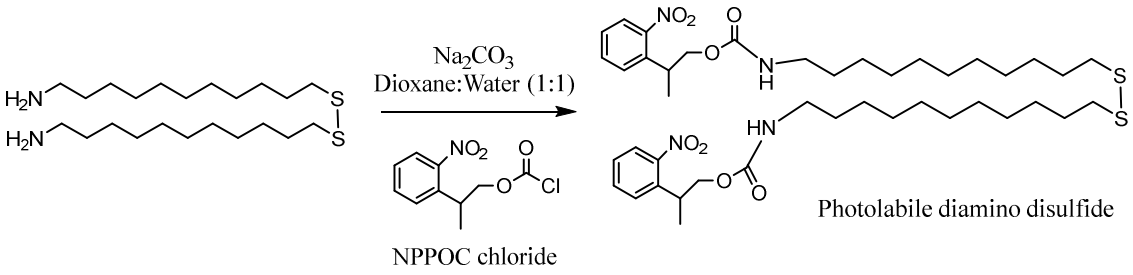

Figure 2.35. Synthesis of NPPOC protected diamino disulfide ligand

Under dark condition Na_2CO_3 (0.23 g, 2.78 mmol) was added to the solution of diamino disulfide (0.4 g, 0.63 mmol) in 6 mL water/1,4-dioxane (1:1) at 0°C, followed by the dropwise addition of NPPOC chloride (0.46 g, 1.9 mmol, in 1 mL THF). After 20 min the ice bath was removed and stirring was continued for 18–24 h. The reaction

mixture was evaporated to dryness, 3 mL of water was added and the mixture was extracted with ethyl acetate (2×5 mL). The aqueous layer was acidified by addition of 5% HCl at 0 °C and extracted with ethyl acetate (3×10 mL); the extracts were dried over Na_2SO_4 and concentrated under vacuum. No purification was done due to the sensitivity of the protected compound. ^{1}H NMR (300 MHz, $CDCl_3$): δ 7.82 (d, 2H), 7.61 (t, 2H), 7.44 (d, 2H), 7.39 (t, 2H), 4.61 (s, 2H) 4.11 and 4.21 (dt, 2H), 3.7 (m, 6H), 3.5 (m, 2H), 3.2 (m, 2H), 2.7 (t, 2H) 1.66 (m, 12H), 1.40 (d, 30H)

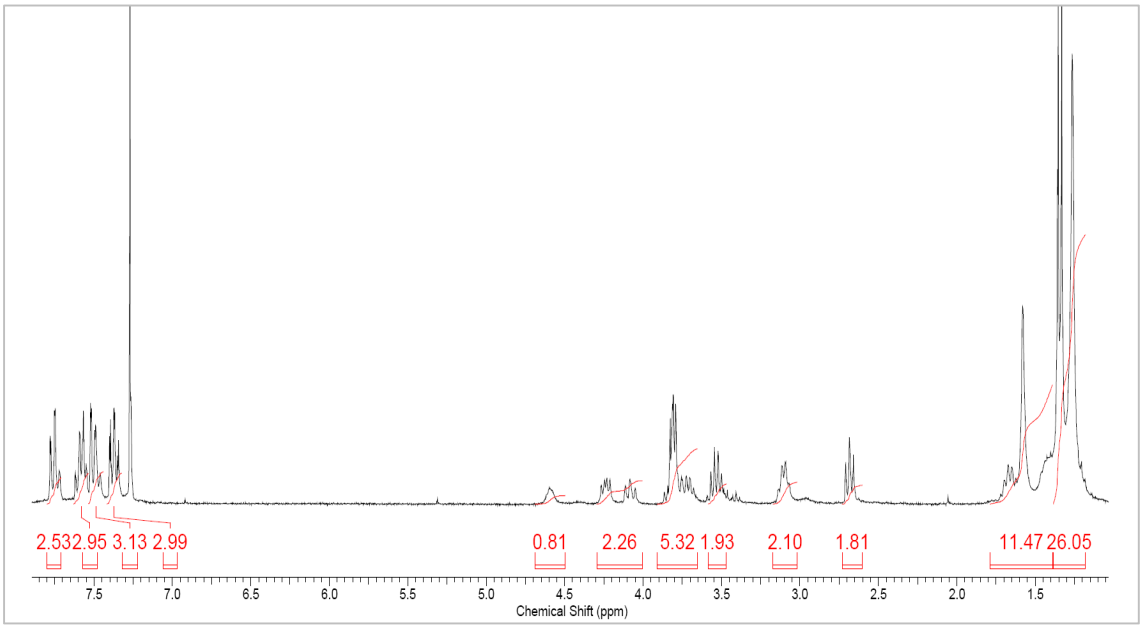

Figure 2.36. ^{1}H NMR of NPPOC protected diamino disulfide

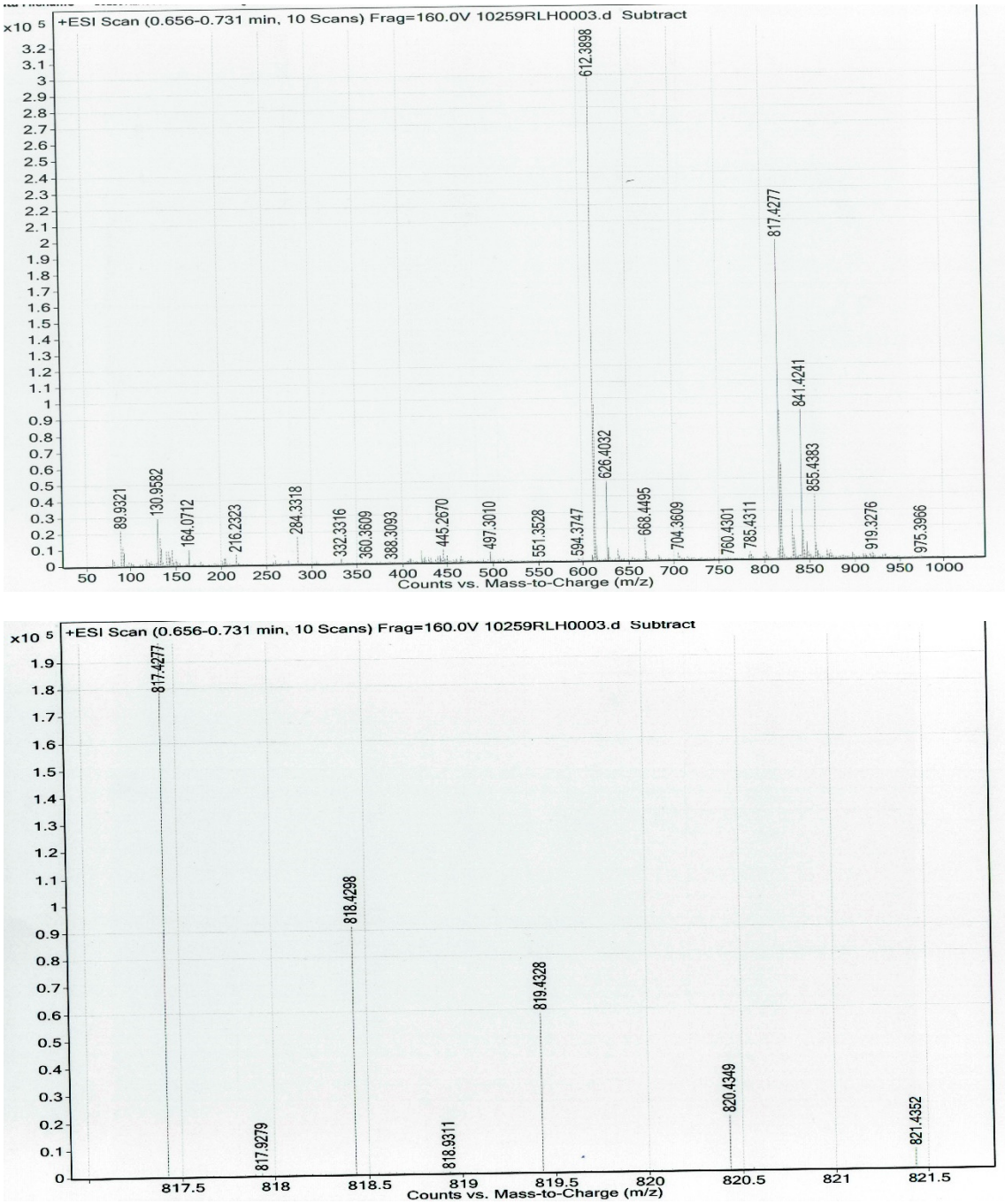

Figure 2.37. Mass spectra of NPPOC protected diamino disulfide.

2.5.7. Place exchange of citrate by thiol and disulfide ligand on GNP surface [8]

By thiol: In different microcentrifuge tubes 200 µL of aqueous suspension of citrate-capped 15 nm GNPs is added to each tube. 1 mM KOH was added to adjust the pH to ~9. Dodecane-1-thiol (200 µL) at different concentrations (0, 0.125, 0.25, 0.5, 1, 2, 3 mM) of in dichloromethane was added to the tubes. The tubes were rotated in rotator for 12 h. The tubes were incubated for 2 h to separate the aqueous and organic phases. Water (800 µL) was added to the biphasic solution to extract the aqueous phase for absorbance measurement.

By disulfide: In different micro centrifuge tubes 200 µL of aqueous suspension of citrate-capped 15 nm GNPs is added to each tube. 1 mM KOH was added to adjust the pH to ~9. 1,2-didodecyldisulfide in dichloromethane (200 µL) at different concentrations (0, 0.02, 0.2, 0.5, 1 mM) of were added to the tubes. The tubes were rotated in rotator for 12 h. The tubes were incubated for 2 h to separate the aqueous and organic phases. Water (800 µL) was added to the biphasic solution to extract the aqueous phase for absorbance measurement.

2.5.8. Place exchange of citrate by water compatible ether thiol [8-9]

The pH of diluted ether thiol solution (prepared by Kalani Gunawadana, 5 mL) was adjusted to ~9.5 by adding KOH (1M) and the solution was added to the citrate-capped gold nanoparticle suspension (15 nm diameter, 10 mL) in a scintillation vial. The sol was incubated overnight to allow the place exchange of citrate by ether thiol to happen.

2.5.9. DTC mediated GNP aggregation using diamino disulfide ligand:

Ether-capped GNP sol (15 nm diameter, 3 mL, ~0.8 nM) was added to four different polystyrene cuvettes, the pH was adjusted to ~8.5. Into one of the cuvettes diamino sulfide dissolved in ethanol (0.5 mM, 200 μL) and CS_2 (1 mM, 200 μL) was added to prepare the sample. There controls were prepared by replacing the ether-capped GNP sol, diamino disulfide, or CS_2 with water respectively. The cuvettes were tightly capped and sealed with parafilm to avoid any evaporation of the solvents. Absorbance spectra were taken without further dilution.

2.5.10. Photo-triggered DTC mediated GNP aggregation:

In a quartz cuvette ethanol:water (1:1) suspension of ether-capped GNP (15 nm diameter, 3 mL, ~0.8 nM) was taken and the pH was adjusted to ~9. The NPPOC protected diamino disulfide in DCM (1 mM, 200 μL) was added to the cuvette. The sample was incubated overnight under dark condition. Absorbance spectra were taken before being exposed to the UV light. To activate the ligand, CS_2 (200 μL,1 mM) was added to the sample in the quartz cuvette and irradiated with UV light source (~350 nm) for 4 h. Then the sample was gently mixed and incubated for 6 h. Absorbance spectra were obtained without further dilution.

2.2.11. Absorbance Measurements

Absorbance measurements were performed using Shimadzu Scientific Instruments UV-2101 PC UV-Vis scanning spectrometer. For each nanoparticle sample the respective solvent was used as the blank. 1.5 mL polystyrene cuvettes with path length 1 cm was used for all measurements. To avoid any variation due to lamp conditions, absorbance of samples and controls were measured without much time interval.

2.6. References

1. Sperling, R. A.; Parak, W. J., Surface modification, functionalization and bioconjugation of colloidal inorganic nanoparticles. *Philos. Trans. R. Soc., A* **2010,** *368* (1915), 1333-1383.

2. (a) Subbiah, R.; Veerapandian, M.; Yun, K. S., Nanoparticles: functionalization and multifunctional applications in biomedical sciences. *Curr. Med. Chem.* **2010,** *17* (36), 4559-4577; (b) Aslan, K.; Gryczynski, I.; Malicka, J.; Matveeva, E.; Lakowicz, J. R.; Geddes, C. D., Metal-enhanced fluorescence: an emerging tool in biotechnology. *Curr. Opin. Biotechnol.* **2005,** *16* (1), 55-62.

3. Kamat, P. V., Photophysical, photochemical and photocatalytic aspects of metal nanoparticles. *J. Phys. Chem. B* **2002,** *106* (32), 7729-7744.

4. Thomas, K. G.; Ipe, B. I.; Sudeep, P. K., Photochemistry of chromophore-functionalized gold nanoparticles. *Pure Appl. Chem.* **2002,** *74* (9), 1731-1738.

5. Love, J. C.; Estroff, L. A.; Kriebel, J. K.; Nuzzo, R. G.; Whitesides, G. M., Self-Assembled Monolayers of Thiolates on Metals as a Form of Nanotechnology. *Chem. Rev. (Washington, DC, U. S.)* **2005,** *105* (4), 1103-1169.

6. Eustis, S.; El-Sayed, M. A., Why gold nanoparticles are more precious than pretty gold: Noble metal surface plasmon resonance and its enhancement of the radiative and nonradiative properties of nanocrystals of different shapes. *Chem. Soc. Rev.* **2006,** *35* (3), 209-217.

7. (a) Singh, A., Cucurbit[7]uril mediated viologen-fluorophore dyad for fluorescence off/on switch. *Dissertation - The University of Oklahoma* **2012**; (b) Singh, A.; Dahanayaka, D. H.; Biswas, A.; Bumm, L. A.; Halterman, R. L., Molecularly Ordered Decanethiolate Self-Assembled Monolayers on Au(111) from in Situ Cleaved Decanethioacetate: An NMR and STM Study of the Efficacy of Reagents for Thioacetate Cleavage. *Langmuir* **2010,** *26* (16), 13221-13226.

8. Gunawardana, K. B., Study of metal-enhanced fluorescence of dye doped silica nanoparticles. *Uinversity of Oklahoma* **2012**.

9. (a) Green, N. S., Plasmonic Properties of Enhanced Fluorescence of Gold and Dye-doped SIlica Nanoparticles Aggregates. **2013**; (b) Gunawardana, K. B.; Green, N. S.; Bumm, L. A.; Halterman, R. L., Metal-Enhanced Fluorescence of Dye-Doped Silica Nano Particles. *J. Fluoresc.* **2015,** *25* (2), 311-317.

10. Turkevich, J.; Stevenson, P. C.; Hillier, J., The nucleation and growth processes in the synthesis of colloidal gold. *Discuss. Faraday Soc.* **1951,** *No. 11*, 55-75.

11. Frens, G., Controlled nucleation for the regulation of the particle size in monodisperse gold suspensions. *Nature (London), Phys. Sci.* **1973,** *241* (105), 20-2.

12. Bastus, N. G.; Comenge, J.; Puntes, V., Kinetically Controlled Seeded Growth Synthesis of Citrate-Stabilized Gold Nanoparticles of up to 200 nm: Size Focusing versus Ostwald Ripening. *Langmuir* **2011,** *27* (17), 11098-11105.

13. Liu, X.; Atwater, M.; Wang, J.; Huo, Q., Extinction coefficient of gold nanoparticles with different sizes and different capping ligands. *Colloids Surf., B* **2007,** *58* (1), 3-7.

14. Bastus, N. G.; Sanchez-Tillo, E.; Pujals, S.; Farrera, C.; Lopez, C.; Giralt, E.; Celada, A.; Lloberas, J.; Puntes, V., Homogeneous Conjugation of Peptides onto Gold Nanoparticles Enhances Macrophage Response. *ACS Nano* **2009,** *3* (6), 1335-1344.

15. Kanemura, S.; Kondoh, A.; Yorimitsu, H.; Oshima, K., Nickel-catalyzed cross-coupling reactions of alkyl aryl sulfides and alkenyl alkyl sulfides with alkyl Grignard reagents using (Z)-3,3-dimethyl-1,2-bis(diphenylphosphino)but-1-ene as ligand. *Synthesis* **2008,** (16), 2659-2664.

16. Navarro, J. R. G.; Plugge, M.; Loumaigne, M.; Sanchez-Gonzalez, A.; Mennucci, B.; Debarre, A.; Brouwer, A. M.; Werts, M. H. V., Probing the interactions between disulfide-based ligands and gold nanoparticles using a functionalized fluorescent perylene-monoimide dye. *Photochem. Photobiol. Sci.* **2010,** *9* (7), 1042-1054.

17. Munechika, K.; Chen, Y.; Smith, J. M.; Ginger, D. S. In *Importance of spectral overlap: fluorescence enhancement by single metal nanoparticles*, John Wiley & Sons, Inc.: 2010; pp 91-118.

18. Bochet, C. G., Photolabile protecting groups and linkers. *J. Chem. Soc., Perkin Trans. 1* **2002,** (2), 125-142.

19. Bhushan, K. R.; DeLisi, C.; Laursen, R. A., Synthesis of photolabile 2-(2-nitrophenyl)propyloxycarbonyl protected amino acids. *Tetrahedron Lett.* **2003,** *44* (47), 8585-8588.

20. Canaria, C. A.; Smith, J. O.; Yu, C. J.; Fraser, S. E.; Lansford, R., New syntheses for 11-(mercaptoundecyl)triethylene glycol and mercaptododecyltriethyleneoxy biotin amide. *Tetrahedron Lett.* **2005,** *46* (28), 4813-4816.

21. Yi, H.; Maisonneuve, S.; Xie, J., Synthesis, glycosylation and photolysis of photolabile 2-(2-nitrophenyl)propyloxycarbonyl (NPPOC) protected glycopyranosides. *Org. Biomol. Chem.* **2009,** *7* (18), 3847-3854.

Chapter III: Synthesis and surface modification of CdSe-ZnS quantum dot incorporated silica nanoparticles

3.1. Chapter Overview

This chapter discusses the advantage of fluorescent nanocrystals with size tunable emission, and our effort to synthesize and encapsulate them in silica nanoparticles. Our interest towards the application of quantum dots (QDs) to explore metal-enhanced fluorescence was driven by the attractive optical properties of QDs such as size tunable emission, high quantum yield, better photostability and the possibility for precise spatial orientation with respect to metal.[1] At the same time we considered that the metal-fluorophore interaction is highly dependent on their spectral overlap and spatial distance between them. We aimed to synthesize various size CdSe-ZnS core-shell quantum dots to match their absorbance wavelengths with the gold nanoparticles' plasmonic scattering wavelength. In order to use the highly hydrophobic quantum dots in aqueous phase it is vital to encapsulated them in hydrophilic shells. Silica scaffolding was chosen to host the quantum dot cores because of its ease of synthesis, ability to functionalize, optical transparency and stability in variety of chemical environments. Additionally the thickness of silica layer can be adjusted to vary the distance between the fluorophore core and metal surface. We adapted the binding method previously established in our lab to achieve the metal-fluorophore aggregation in aqueous solution[2]. Since the dithiocarbamate (DTC) mediated binding between silica and gold nanoparticles was proven to be a robust model[3], we chose to functionalize the surface of QD-doped-silica nanoparticles with organic ligands

containing an amine terminal. Heteroaggregation of gold and silica nanoparticles was promoted by a spontaneous conversion of amine into DTC.

3.2. Introduction

Quantum dots (QDs) are nano size semiconductor crystals composed of hundreds to thousands of atoms and possess interesting optical and electronic properties. The size range of quantum dots is 2 - 10 nm, which is an intermediate between the sizes of bulk materials and atoms. The intermediate size allows the QDs to have properties of both bulk materials and atoms (or molecules). Size tunable emission of QDs is a major variation from their bulk counterpart. QDs not only have a material dependent discrete energy barrier between the conduction and valence band as in bulk semiconductors, but also have size influenced energy levels. The increase in size of quantum dots decreases the energy barrier and thus result in the emission of longer wavelength.[4] Other exotic properties like high photostability, extinction coefficients and photoluminescence are not found in bulk semiconductors.[5] This interesting behavior of QDs promote their uses in various applications which need strong and stable fluorescence with tunable emission.[6]

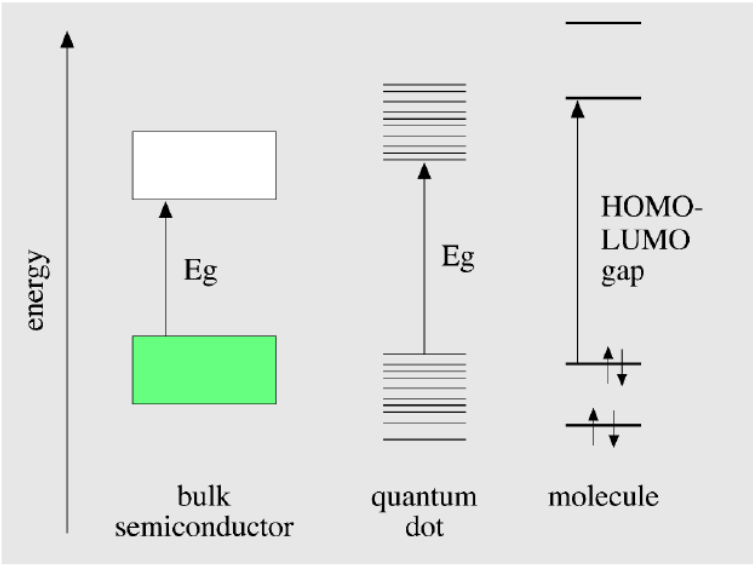

Figure 3.1. Comparison of energy gaps of bulk semiconductors, quantum dots and organic molecules. (Image from Angell)[6]

The electron-hole pair (exciton) created by external energy sources such as light is the attractive phenomenon associated with the quantum dots. In a semiconductor when a photon of energy higher than its energy barrier is absorbed, an electron-hole pair will be created. Since the quantum dots are usually smaller than 10 nm, less than the exciton Bohr radius (typically a few nanometers), the electron-hole pairs are confined and result in a quantum confinement effect (Figure 3.2). The electron-hole pair remains coupled as in the semiconductors, but the energy levels are quantized and dependent on the size of the nanocrystals. The quantum confinement effects are more dominant for smaller size QDs. The recombination of electron-hole happens when the excited electron relaxes back to ground state, and the energy is released as photoluminescence. The emission band of the quantum dots are narrow and symmetric, in contrast to common organic dyes.[7]

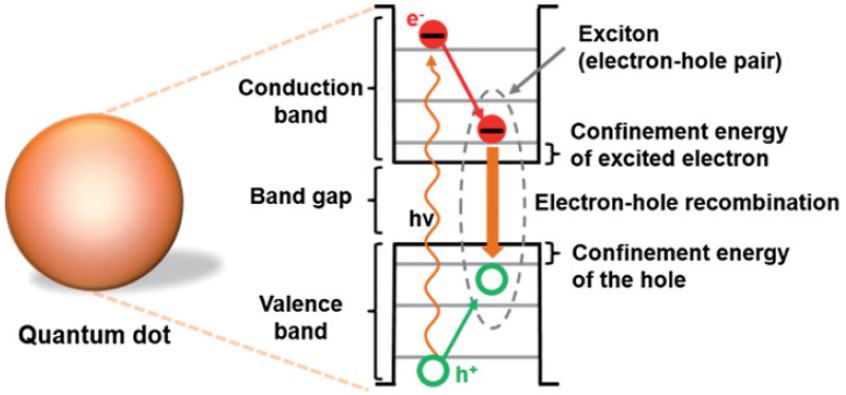

Figure 3.2. Illustration of electrical properties of quantum dots (Image from Pisanic et al.)[5]

The optical spectra of quantum dots are interesting in several aspects compared to that of organic fluorophores. The large Stokes shifts between the broad excitation and narrow emission spectra of quantum dots are remarkable and significant for applications in various fields.[8] The broad excitation spectra range from UV to near IR wavelength; meanwhile the wavelengths of narrow emission spectra depend on the material and size of the quantum dots. Usually larger size QDs emit red color. Due to this exclusive property, a mixed population of different size and material quantum dots can be excited at a single wavelength far from their emission, and still observe multicolor fluorescence[5]. In Figure 3.3 Medinitz et al., show the broad absorbance and narrow emission spectra of different size quantum dots (A) and the narrow absorbance and emission spectra of Cy3 and Cy5 organic dyes (B).

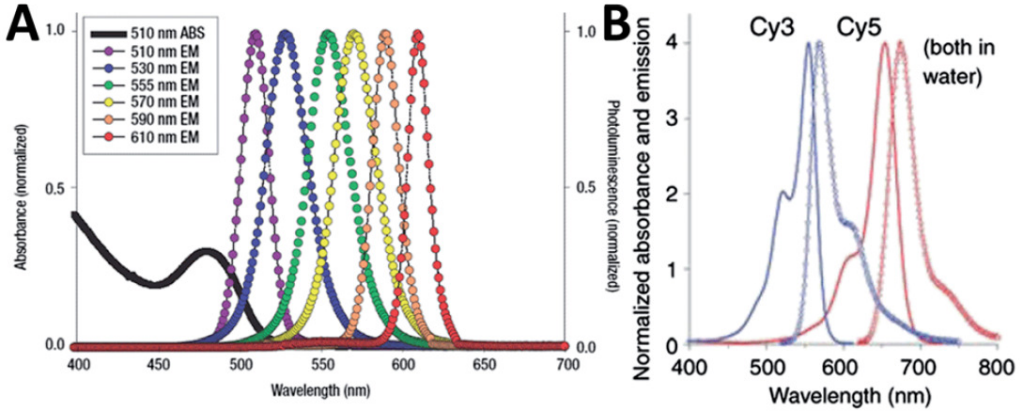

Figure 3.3. Absorbance and emissions spectra of QDs (A) and organic dyes (B). (Image from Medintz et al.)[8]

Quantum dots are also imbued with other remarkable optical properties such as high quantum yield, better photostability, high molar extinction coefficients (10- 100 times more than common organic dyes), and exceptional resistance to photo- and chemical degradation.[9] These features allow us to detect a single quantum dot using a standard fluorescence spectroscopy[10] or a confocal microscopy.[11]

Quantum dots are often integrated in core-shell systems to enhance the photoluminescence and structural stability. Pisanic et al., note that exciton confinement property is highly influenced by the core-shell materials. Two types of core-shell quantum dots commonly prepared are shown in Figure 3.4., where the type-I QD has a shell material with larger energy gap than the core and thus the exciton is confined within the core. These types of core-shell QDs exhibit higher photoluminescence. In type-II QD, since the energy level gap of the shell is smaller than the core, the exciton is confined to both the shell and the core. Therefore, to emit fluorescence by radiative recombination, the charge carriers have to cross the core-shell interface. This type of QDs possess a wide and highly tunable emission wavelength.[5]

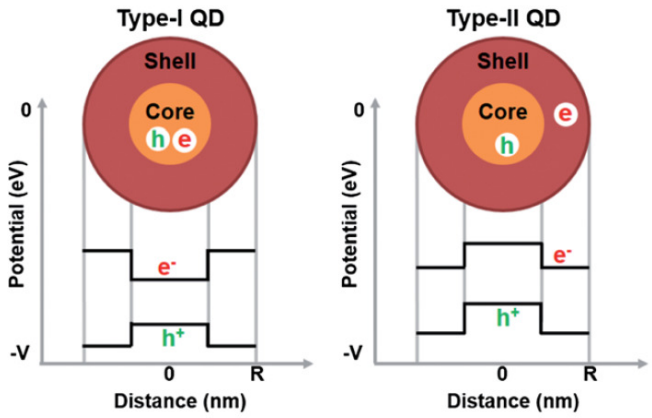

Figure 3.4. Energy level diagram of type-I and type-II QDs,

The optical properties of the quantum dots are sensitive to the presence of charges in their surrounding and on the surface. Non-radiative energy transfer to a nearby charge carrier (Auger recombination) results in a quenching of the quantum dots' fluorescence.[12]

The CdSe-ZnS quantum dot system was an extensively studied type-I core-shell system. The energy bandgap of CdSe core is 1.74 eV and that of ZnS shell is 3.61 eV. Because of this large energy difference the excitons are well confined within the core.[13] Also the addition of ZnS shell increases the fluorescence quantum yield and passivates the surface defects.

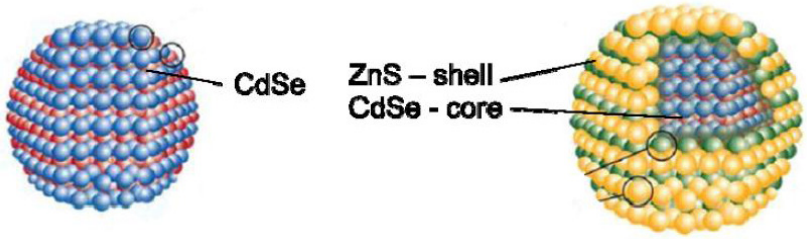

Figure 3.5. Cartoon of CdSe quantum dot core with ZnS shell coating. (Image from Angell)[6]

For our metal-enhanced fluorescence study we synthesized the CdSe cores and coated them with ZnS shells by following the procedure reported by Angell with slight modifications. The CdSe-ZnS quantum dots prepared in octadecene (ODE) medium were hydrophobic and the precipitation was prevented by tributylphosphine (TBP) ligand coating. In order to adapt the hydrophobic QDs for metal-enhanced fluorescence measurements in aqueous solution, a hydrophilic shell was needed. Therefore, we encapsulated each CdSe-ZnS quantum dot in a silica (SiO_2) shell.

Installation of water compatible shells or bioconjugate ligands to the exceptionally photostable, highly photoluminescent and size tunable quantum dots extends the QDs' applications from photovoltaics to bioimaging.[14] Unlike common organic dyes that are chemically distinct and thus require different wavelengths to excite each one of them, CdSe-ZnS QDs of different sizes (infused in different parts of a cell) can be activated by a single excitation source to see different colors.

Brightness, biocompatibility and non-toxic nature should be the properties of an ideal fluorescent marker. In addition to those properties, a multicolor fluorescent marker should have a narrow and symmetric emission spectrum achievable with a single excitation source. Obviously quantum dots possess those properties. Significant efforts have gone into using quantum dots *in vivo* imaging applications. Recent progress in coating or capping quantum dots with biocompatible shells or ligands enable promising steps towards the employment of potential biomarkers. Gao et al., reported an *in vivo* imaging of multicolor quantum dots encapsulated in microbeads and linked to tumor-targeting ligands.[15] Figure 3.6 A. (insets) shows the QD-tagged cancer cells (orange) and the green fluorescent protein (GFP) labelled cancer cells (green). The QD and GFP labelled cancer cells were injected into right and left flank of a mouse respectively. Although both QD and GFP labelled cells were equally bright in cell culture (insets of A), only QD labelled cells were observed *in vivo* (orange fluorescence on the right flank of the mouse, A).

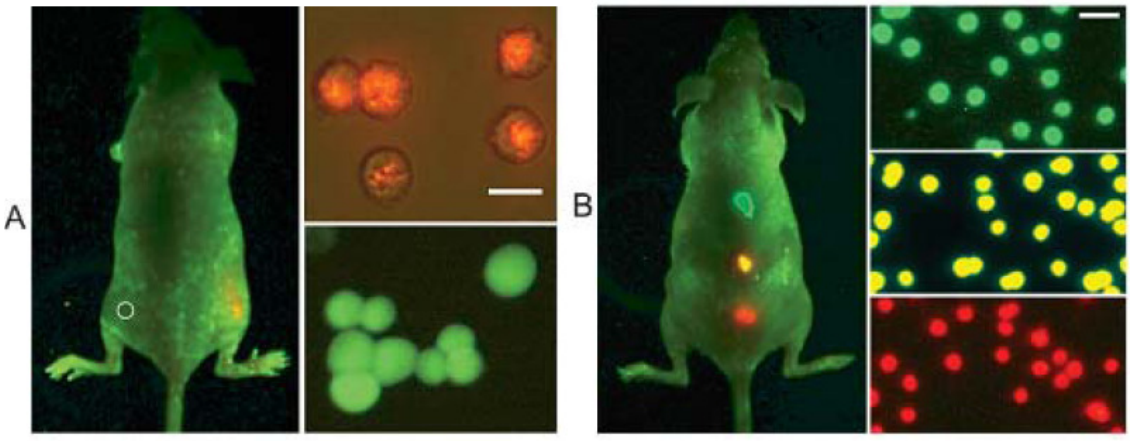

Figure 3.6. Multicolor quantum dots used *in vivo* imaging of cancer cells (Image obtained from Maureen et al.)[15-16]

The authors also explored the use of multicolor QDs *in vivo* imaging (Figure 3.6.B) by ingesting three different color (green, yellow and red) QD-encoded microbeads at three different location in a mouse and exciting the QDs with a single light source. This study shows the execution of toxic quantum dots *in vivo* studies by encapsulating them in non-toxic and biocompatible bioconjugate or microbeads.

Our research group has developed methods of encapsulating organic dyes in silica nanoparticles, and an organic ligand mediated metal-fluorophore aggregate system in order to investigate the metal-enhanced fluorescence in solution. Structurally engineered silica nanoparticle capsules with rhodamine B cores were synthesized in our lab by Kalani Gunawardana and Nathaniel Green.[2-3]

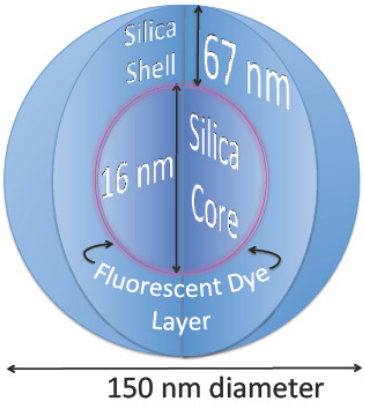

Figure 3.7. Cartoon of a layered dye-doped-silica nanoparticle (Image from Green)[3]

We adapted the same capsule model to employ hydrophobic CdSe-ZnS quantum dots to promote MEF in aqueous solution. The optically transparent silica shell allows the QD core to retain its optical property in aqueous solution. We used the robust dithiocarbamate (DTC) ligands to achieve heteroaggregation of gold and silica nanoparticles.

3.3. Results and Discussion

We synthesized cadmium selenide (CdSe) quantum dot semiconductors to replace the organic fluorophores in the metal-fluorophore aggregate system that was previously developed by our research group. As discussed in the introduction to this section, the quantum dots have size tunable emission, high photostability, and high quantum yield that common organic dyes. In order to increase the quantum dots' fluorescence and passivate the surface defects, the CdSe core was coated with zinc sulfide (ZnS) shell, which shaped the type-1 core-shell quantum dots. The CdSe-ZnS QDs were prepared as colloids in organic solvents, but since we attempt to produce metal-enhanced fluorescence in aqueous solution, these quantum dots were encapsulated in silica shell to introduce the water dispersibility as reported in several literatures.[13, 17] The silica layer can also be used to control the space between the fluorophore core and the metal surface. The surface of the silica nanoparticle was then tethered with organic ligands containing dithiocarbamate moiety. In the following sections we discuss the synthesis of different size quantum dot cores, ZnS coating, silica encapsulation, surface functionalization and heteroaggregation of SiNPs to GNPs.

3.3.1. Synthesis of various size CdSe quantum dot cores

Cadmium selenide quantum dots can be prepared by top-down or bottom-up techniques.[18] The older top-down technique encountered poor reproducibility, poor optical property, large size variations and crystal defects, and that would make the quantum dots unreliable for many applications. But the recent bottom-up nucleation and growth technique made quantum dot synthesis more controllable and highly reproducible.[14] In the bottom-up technique, pyrolysis of organometallic precursors of

cadmium and selenium in a coordinating solvent such as trioctylphosphine (TOP) at a constant high temperature was used to produce hydrophobic and monodisperse quantum dots.[19]

In order to achieve a metal-enhanced fluorescence, the quantum dots should have an optimal spectral overlap with the gold nanoparticles. To achieve an optimal spectral overlap we synthesized various size quantum dot cores with respective emission wavelengths. In the synthesis method a selenium precursor was prepared first and added to cadmium oxide in oleic acid solution. Since the reaction was highly air sensitive we purged all chemical stocks with nitrogen before and during use. A measured amount of selenium powder was taken in a round bottom flask, and the flask was sealed, and purged with nitrogen for 15 min. Then octadecene (ODE) solvent was added to the flask and heated to 210 °C before adding trioctylphosphine (TOP). Since any fluctuation in temperature would affect the uniformity of the core structure, we used a thermostat to maintain a constant temperature throughout the synthesis. The reaction mixture was stirred for 1 hr at 210 °C under N_2 atmosphere. The solution looked green when all of the selenium was dissolved. After1 hr the Se-TOP precursor solution was brought down to 100 °C.

In a separate setup nitrogen flushed cadmium oxide was transferred into a two-neck flask. The flask was charged with a magnetic stir bar and sealed with a thermostat probe. Octadecene was added and the flask was lowered into a hating mantle preheated to 300 °C. Oleic acid was injected into the flask when the temperature was crossing 180 °C. When the temperature reached the constant temperature of 300 °C, previously prepared Se-TOP precursor (which was maintained at 100 °C) was quickly injected into

the flask. Then using glass syringes 1 mL aliquots of the reaction mixture were taken out at every 10 seconds and transferred into separate vials, each containing 9 mL of cold ODE. This process should stop the growth of QD and give mono-disperse QD particle s of increasing size. Figure 3.8 shows the samples of CdSe colloids taken out of the reaction mixture at different reaction times.

Maintaining a constant temperature is important to yield a high monodispersity. After adding the Se-TOP precursor to the Cd in oleic acid solution, the particles immediately nucleate in first few seconds depleting the reactants. Then the particles grow homogeneously due to Ostwald ripening until the colloidal solution is saturated.[6] Any change in the temperature during this particle growth would result in size variations. So to prevent the temperature drop while removing aliquots of reaction mixture every 10 seconds, we kept the flask sealed but inserted a long needle connected to glass syringe to draw out samples. A thermostat was connected to the heating mantle with its probe inserted into the reaction flask in order to correct any temperature variations. We carefully took all safety measures while working with the reaction at high temperature (300 °C) by using heating mantle controlled by thermostat, sealing the reaction flask, and wrapping with aluminium foil.

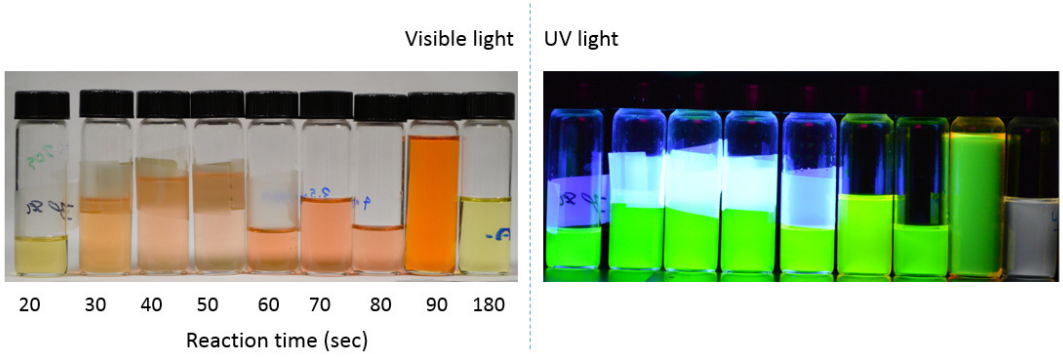

Figure 3.8. Image of different size CdSe quantum dots prepared at different reaction time exposed to visible light and UV light.

Samples (1 mL) taken out at every 10 seconds were immediately diluted with cold ODE solvent (9 mL) to quench the particle growth. Figure 3.8 shows the CdSe quantum dot suspension obtained at different particle growth time. They emit bright green fluorescence under UV light. Octadecene solvent (high boiling point) was used to prepare the highly hydrophobic CdSe colloids. Because of the hydrophobic nature of the quantum dots, it was difficult to prepare TEM samples from the ODE (oil) solvent. So it was not possible to measure the sizes of the QDs directly from the TEM images. However we estimated the diameters using the equation given in the following page.

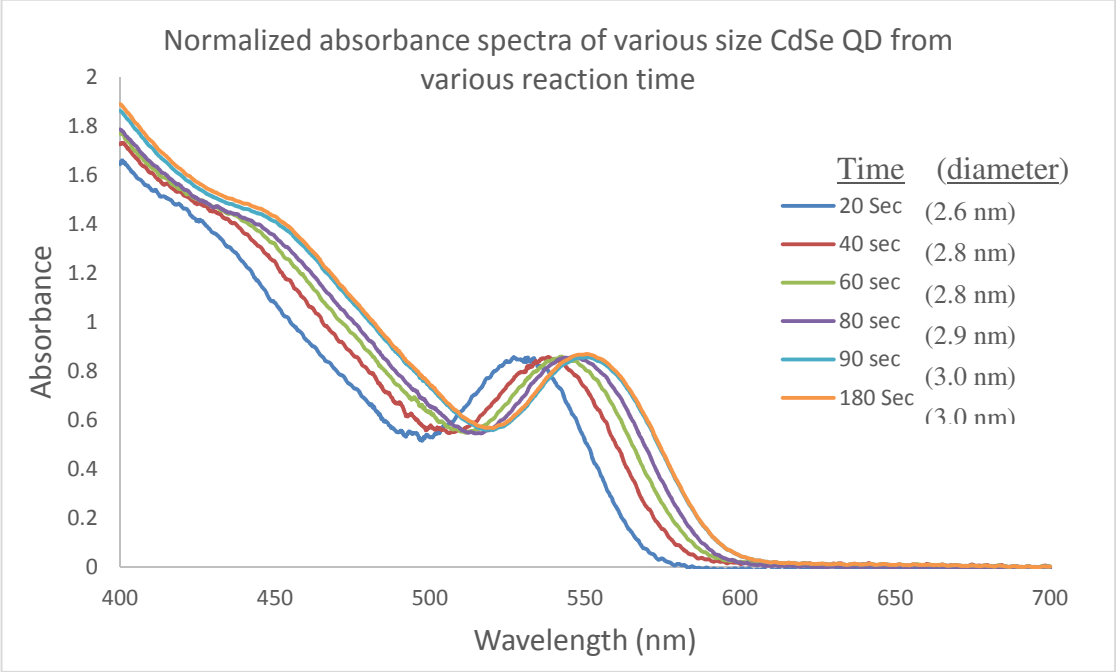

Figure 3.9. Absorbance spectra CdSe quantum dots prepared at various reaction time.

Broad absorbance spectra is one of the characteristics of quantum dots. The QD colloids in ODE solvent, without any further dilution, were transferred into 1.5 mL polystyrene cuvettes for absorbance and fluorescence measurements. Absorbance spectra in Figure 3.9 shows CdSe quantum dots absorb a wide range of light from 400

to 600 nm. Though there are shoulder peaks appeared (between 430-450 nm) in the spectra, the lower energy peaks (between 530-550 nm) are the first excitonic peaks, where the energy gaps between electron and hole are smaller. A gradual red-shift of the absorbance wavelength with increase in reaction times is an evident for the particle growth. Larger size quantum dots have smaller energy gap between valance and conductance band, and thus absorb photons of longer wavelength to excite the electron.[14] Since samples obtained at different reaction times have different particle sizes, concentration of the particle suspension cannot be directly estimated. The difference in concentration resulted in different intensities of absorbance. But we have shown the normalized absorbance spectra to clearly see the energy difference between the different size particles.

Size and extinction coefficient of the quantum dots were calculated using the equation developed by Yu et al.[18] The authors correlated the first excitonic absorbance λ_{max} of the CdSe quantum dots obtained from many literature sources and the diameter of the QDs measured from the respective TEM images. The concentration of the QD sample can be determined from Beer's law.

$$D = (1.16122 \times 10^{-9})\lambda^4 - (2.6575 \times 10^{-6})\lambda^3 + (1.6242 \times 10^{-3})\lambda^2 - (0.4277)\lambda + 41.57$$

$$A = \epsilon C L$$

$$\epsilon = 5857 D^{2.65}$$

Where D = diameter

A = absorbance

C = concentration

L = path length (1 cm)

ϵ = extinction coefficient

Reaction time of CdSe samples	First excitonic λ_{max} (nm)	Absorbance at first excitonic λ_{max}	Calculated diameter (nm)	Extinction Coefficient ($M^{-1}cm-1$)	Concentration (M)
20 sec	527.0	0.1156	2.6	7.779×10^4	1.485×10^{-6}
40 Sec	538.0	0.1315	2.8	9.144×10^4	1.438×10^{-6}
60 Sec	542.4	0.1574	2.8	9.807×10^4	1.605×10^{-6}
80 Sec	545.6	0.1824	2.9	10.34×10^4	1.764×10^{-6}
90 Sec	550.6	0.2613	3.0	11.27×10^4	2.318×10^{-6}
180 Sec	551.0	0.2632	3.0	11.65×10^4	2.319×10^{-6}

Table 3.1. Calculated diameter, extinction coefficient and concentration of CdSe samples obtained at different reaction time.

Based on the calculation the diameter of CdSe quantum dot cores range between 2.654 nm to 3.061 nm. It can be seen that the particle growth due to Ostwald ripening was reduced after 90 sec. The size of 90 sec CdSe is 3.052 nm and the size of 180 sec CdSe is 3.061 nm, so even the 90 sec duration didn't increase the size much. This may be due to the depletion of reactants or a drop in temperature. A drop in temperature could be possible due to the sample acquisition at every 10 sec, because while we removed hot sample from the reaction flask, cold N_2 gas was constantly flushed in. Since the particle growth was nearly quenched at 90 sec, the 180 sec sample doesn't show a significant red-shift from the 90 sec sample.

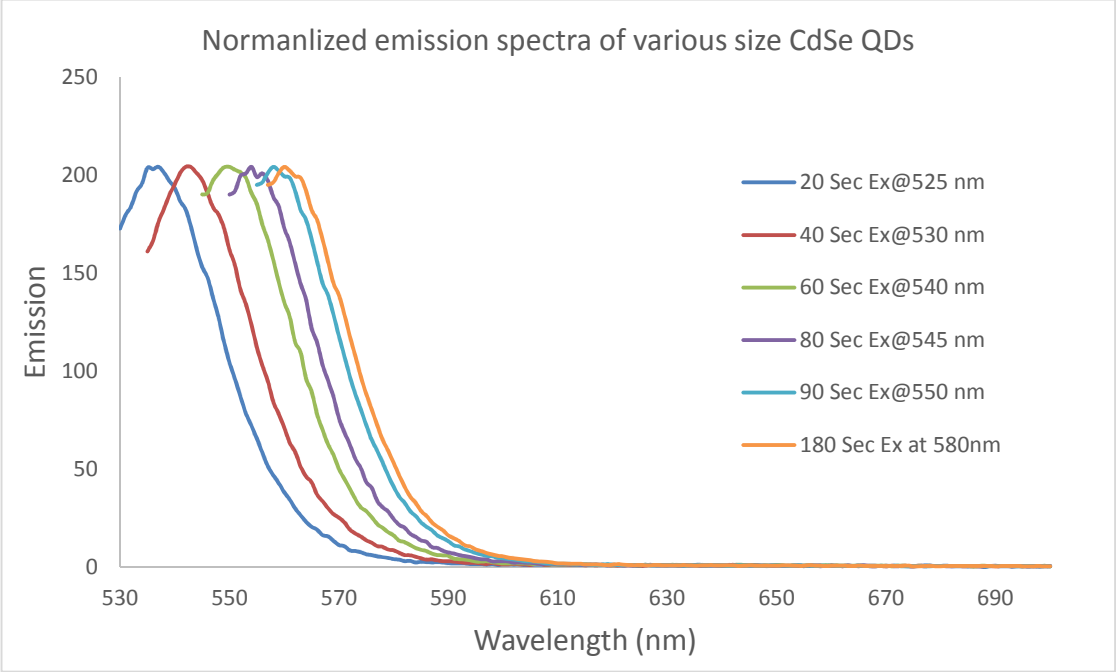

Figure 3.10. Emission spectra CdSe quantum dots prepared at various reaction time.

Fluorescence spectra of the various size QDs were obtained by exciting at their respective absorbance λ_{max}. The normalized fluorescence spectra show a gradual red-shift (535-565 nm) relative to the increase in particle size. A significant Stokes shifts (~10 nm) were absorbed for all size quantum dots, which is crucial to separate the excitation and emission effects during metal-enhanced fluorescence study. In our synthesis we achieved remarkable size-tuned emissions from CdSe quantum dot cores.

Although we were able to synthesize various size CdSe quantum dots in a single pot reaction with prominent size-tuned emissions, the absorbance spectra of those QDs did not overlap with the coupled plasmonic scattering peak of the gold aggregates (>580 nm). The largest QDs (3.061 nm diameter) we synthesized has the first excitonic absorbance λ_{max} ≈550 nm. In MEF studies, to utilize the energy from coupled plasmons

of the gold nanoparticle aggregates, the QDs should have a similar energy level. Hence we attempted to synthesize further larger CdSe particles to extend the absorbance band >580 nm (decreased energy gap).

We followed the same synthetic procedure described above, but this time we increased the temperature to 315 °C and took additional measures to avoid temperature fluctuation during the nucleation and particle growth process. The size of the reaction flask was reduced and necks were sealed tightly to contain a high temperature. Interruption to the constant temperature was minimized by not taking out multiple samples during the particle growth. The Se-TOP precursor was pre-heated to 250 °C before adding to the Cd oleic acid solution. The reaction was allowed to proceed for 4 min at 315 °C to yield larger and monodisperse CdSe particles. Then the particle growth was quenched by swiftly injecting cold ODE solvent in to the flask.

In this synthesis we obtained CdSe core with first excitonic (electron-hole pair) absorbance wavelength at 601 nm, affording optimal overlap with the coupled plasmonic scattering of gold aggregates. From the absorbance spectra (Figure 3.9) and the equation shown above, diameter of the CdSe particles were calculated to be 4.628 nm.

Reaction time of CdSe sample	First excitonic λ_{max} (nm)	Absorbance at first excitonic λ_{max}	Diameter (nm)	Extinction Coefficient ($M^{-1}cm-1$)	Concentration (M)
4 min	601	0.8573	4.6	33.95×10^{4}	2.524×10^{-6}

Table 3.2. Calculated diameter, extinction coefficient and concentration of CdSe samples obtained at 4 min.

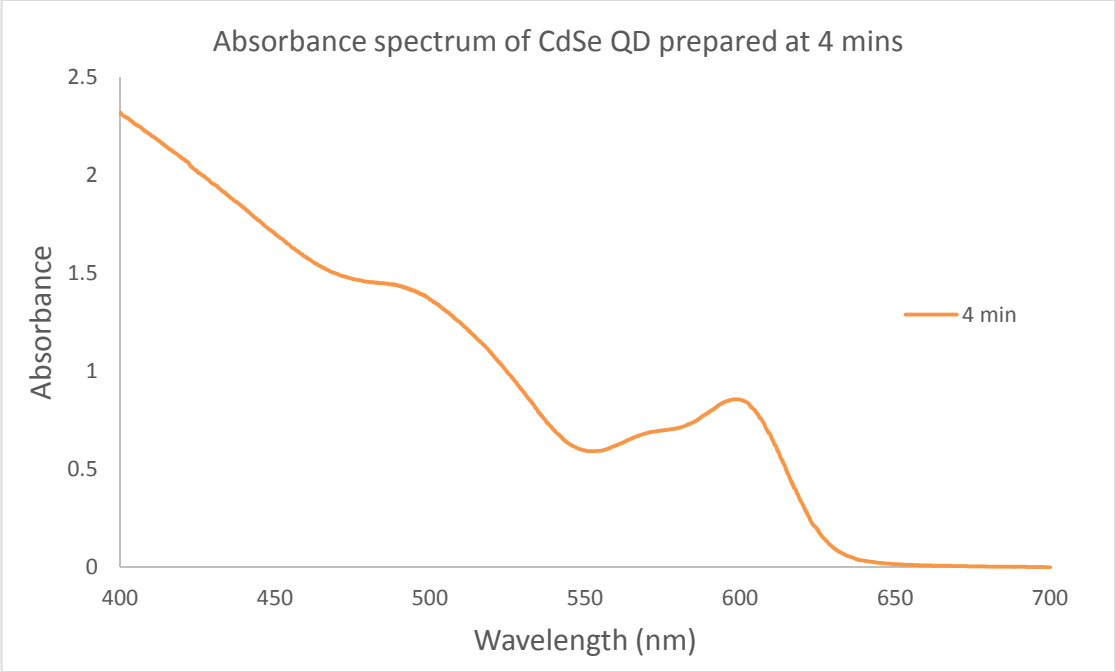

Figure 3.11. Absorbance spectrum of CdSe synthesized at 4 min.

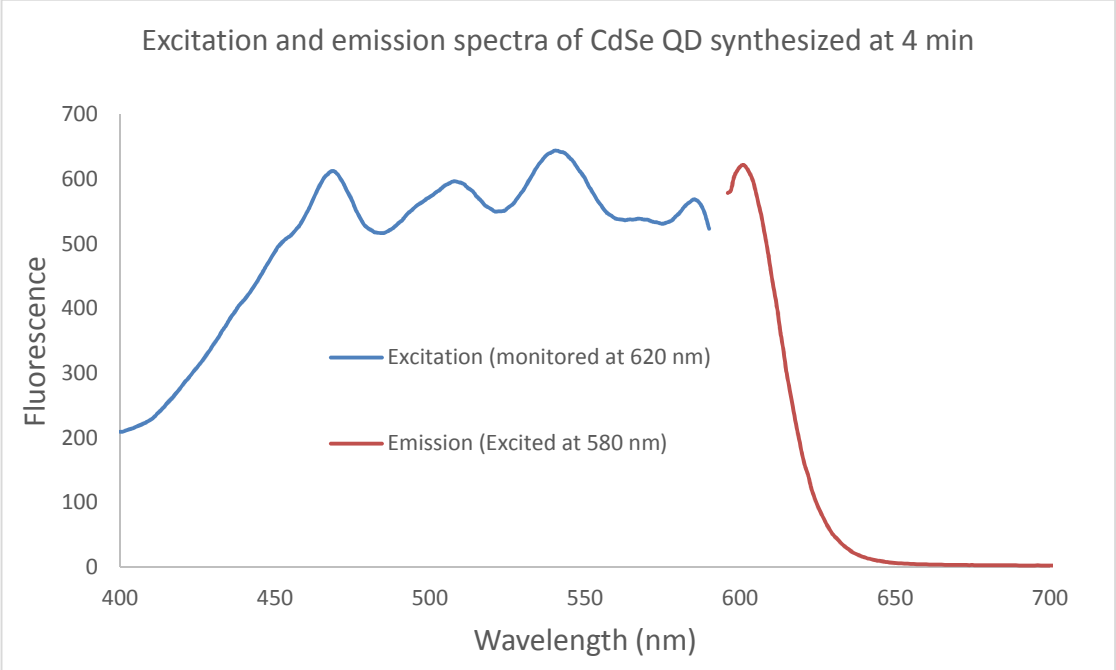

Figure 3.12. Excitation and emission spectra of CdSe QDs synthesized at 4 min.

As discussed in the introduction to this section, the excitation and emission spectra of the CdSe quantum dots displays a broad excitation range (460 – 590 nm) and a narrow emission range (601 nm). This property would allow the QDs to operate with different excitation sources and also adapts to receive energy from individual gold nanoparticles as well as aggregated gold nanoparticle. This larger CdSe core holds a narrow emission wavelength beyond the major absorbance range of gold nanoparticles. This result could help avoid the quenching of the fluorescence by gold re-absorbance. Therefore we used this ~4.6 nm CdSe quantum dot core for our MEF study. To enhance the optical property and to increase the structural stability, we crusted zinc sulfide (ZnS) shell around the CdSe core.

3.3.2. CdSe-ZnS core-shell quantum dot system

Type 1 core-shell quantum dots emit brighter fluorescence as the excitons are confined to the core and also the addition of a shell increases stability of the core. We applied ZnS shell onto the 4.6 nm diameter CdSe core by following the standard procedure developed at California Polytechnic State University.[6] Tributylphosphine (TBP) and diethylzinc ($ZnEt_2$) were purged with N_2 for 15 min before using for the reaction. A round bottom flask with a stir bar was sealed and purged with N_2 for 15 min. TBP was transferred in to the flask and N_2 was constantly flushed into the flask. After 10 min hexamethyldisilathiane $(tms)_2S$ and of $ZnEt_2$, at the molar ratio of 0.8:1, Zn to S, were added into the flask and stirred for 15 min at room temperature. The resulting ZnS precursor was clear and transparent. Any cloudiness would indicate the degradation due to oxygen exposure.

Before adding the ZnS precursor to CdSe coating, the amount of ZnS needed was calculated using the formula given by Reiss et al.[20] It was necessary to know not only the size of CdSe core, but also the concentration and volume of the suspension. To estimate the amount of ZnS precursor needed to add into the CdSe suspension, we should specify the thickness of the ZnS shell. By using the following equations, we estimated the number of moles of ZnS needed to coat a shell of specific thickness on a particular size CdSe core. The reaction yield was assumed to be 100%.

$$V_{ZnS}(ML_x) = \frac{4}{3} \times \pi \times [(r_{CdSe} + X \times d)^3 - r_{CdSe}^3]$$

$$n_{ZnS}(ML_x) = [\rho_{ZnS} \times V_{ZnS}(ML_x)]/m_{ZnS}$$

$$N_{ZnS} = n_{ZnS}(ML_x) \times N_{CdSe}$$

Where,

$V_{ZnS}(ML_x)$	=	volume of the shell comprising x monolayer of ZnS
r_{CdSe}	=	radius of the CdSe core
d	=	thickness of one monolayer ZnS (0.31 nm from literature)
$n_{ZnS}(ML_x)$	=	number of monomer units of ZnS per CdSe particle
ρ_{ZnS}	=	bulk density of ZnS in the wurtzite phase (4090 kg m^{-3} from lit)
m_{ZnS}	=	mass of a shell monomer unit
N_{ZnS}	=	number of moles of ZnS needed to grow x monolayer of ZnS
N_{CdSe}	=	number of moles of CdSe particles in the reaction volume

From literature it was recognized that a ZnS shell of three monolayer thick would yield the greatest quantum yield. Hence calculations were made to find the volume of ZnS precursor required to coat three monolayer thick (9.3 nm) ZnS shell on a 17 mL sample of 4.627 nm diameter CdSe quantum dots at 2.52 μM concentration (from table 3.2). The required number of moles of ZnS molecules was calculated to be 98.7 μmol. So we used 3 mL ZnS solution at 32.9 mM concentration to bring up the number of moles to 98.7 μmol.

Previously synthesized CdSe in ODE suspension (17 mL) was purged with N_2 for 15 min and added into a two-neck reaction flask. The flask with a magnetic stir bar

and a digital thermometer probe was sealed and purged with N_2 for 15 min. The flask was then lowered into an oil bath preheated to about 190 °C. When the reaction mixture was reached a constant temperature, ZnS (3 mL) was added dropwise for 5 min and stirred for 20 min at 185 °C. Then the solution was cooled to 60 °C and 1-butanol was quickly injected to avoid flocculation. Figure 3.13 shows that the fluorescence (orange color) of CdSe quantum dots was increased after the ZnS coating. The figure also compares the fluorescence from a smaller size CdSe sample (20 sec) and an organic dye (BODIPY).

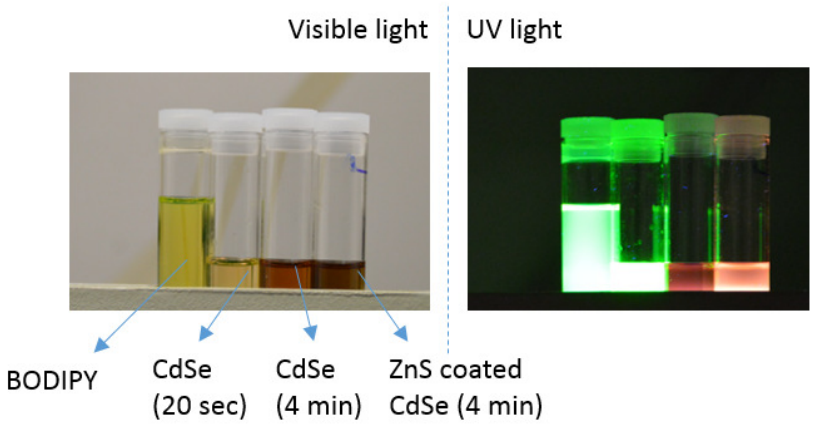

Figure 3.13. Image of an organic dye (BODIPY), CdSe QD synthesized at 20 sec, CdSe QD synthesized at 4 min and CdSe-ZnS core-shell QD under white light and UV light.

The red-shift for the first excitonic absorbance λ_{max} from 600 nm to 609 nm indicates that the size of quantum dots was increased after ZnS coating. Since the volume of ZnS was estimated for three ZnS monolayer, and knowing that each monolayer of ZnS is 0.31 nm thick from the literature,[20] the thickness our ZnS shell should be theoretically 0.93 nm (assuming that the reaction yield was 100%). This should give the overall diameter of the CdSe-ZnS core-shell quantum dots [0.93 + 4.6 =

0.93] = 6.46 nm. The diameter measured from the TEM images (Figure 3.18) was approximately 7 nm and closely matches with the theoretical value.

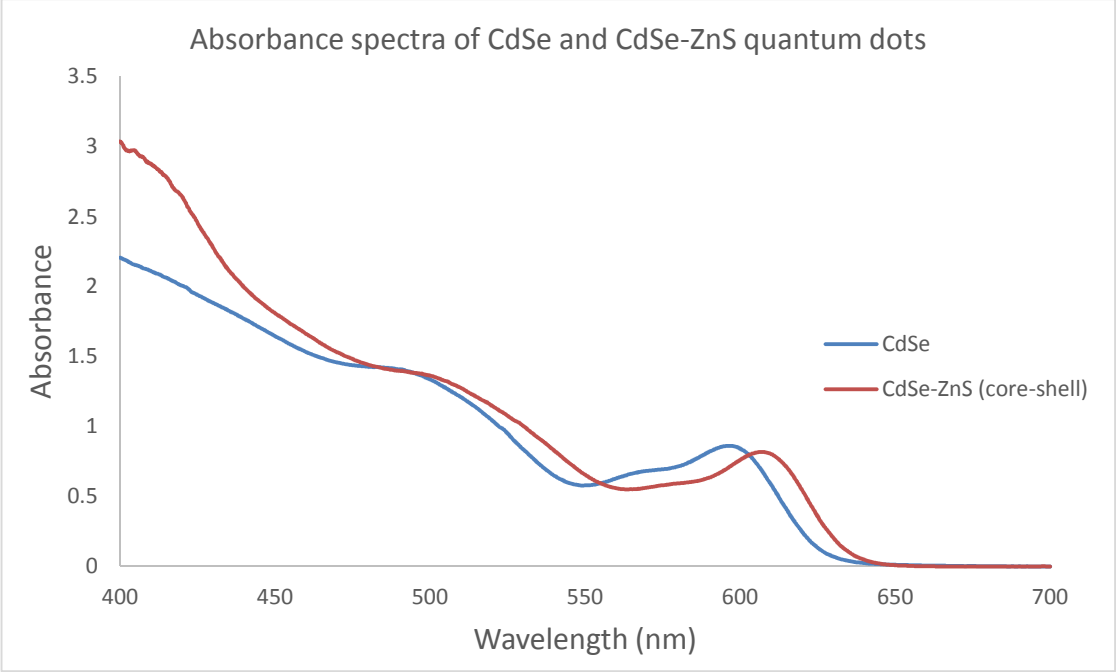

Figure 3.14. Absorbance spectra of CdSe quantum dots before and after ZnS coating.

As a type 1 quantum dots system, CdSe-ZnS QDs should have an increased fluorescence brightness. The fluorescence spectra (Figure 3.15) show the enhanced fluorescence for ZnS coated CdSe QDs. Also the size influenced red-shift of λ_{em} from 601 nm to 615 nm is seen on the spectra. The increased absorbance (λ_{abs}) and emission (λ_{em}) wavelength will be advantageous for the MEF measurements , as the λ_{abs} would overlap better with coupled plasmon scattering of the aggregated gold nanoparticles (>580 nm), while λ_{em} exist beyond the limit of GNP re-absorbance. The excitation spectra (Figure 3.16) also follow the trend seen in absorbance and fluorescence spectra.

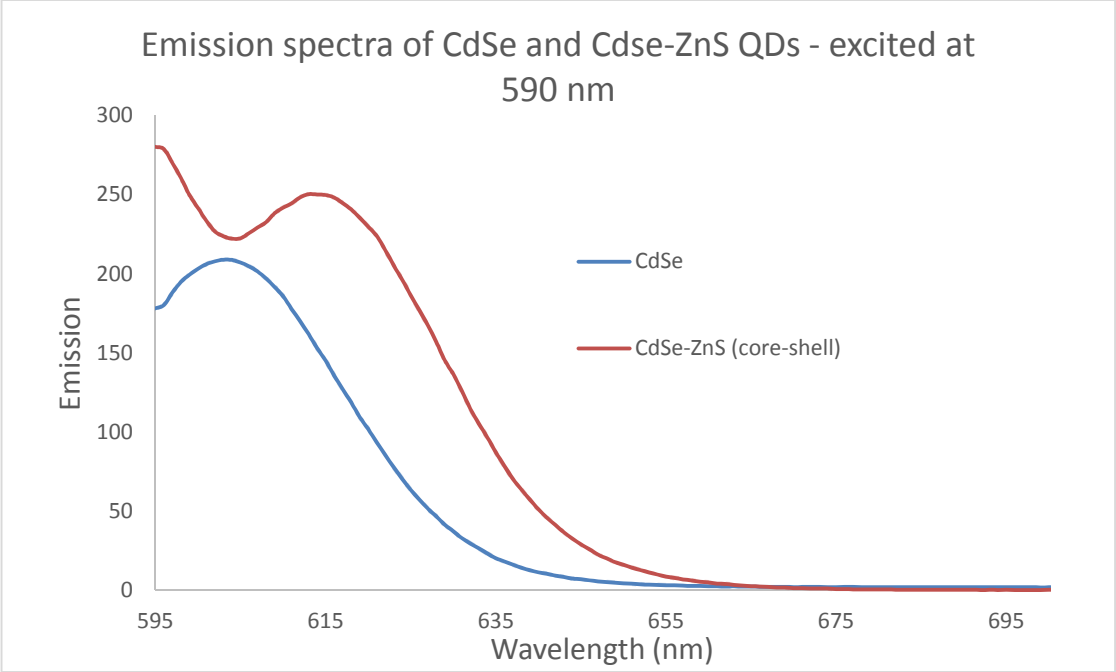

Figure 3.15. Emission spectra of CdSe quantum dots before and after ZnS coating.

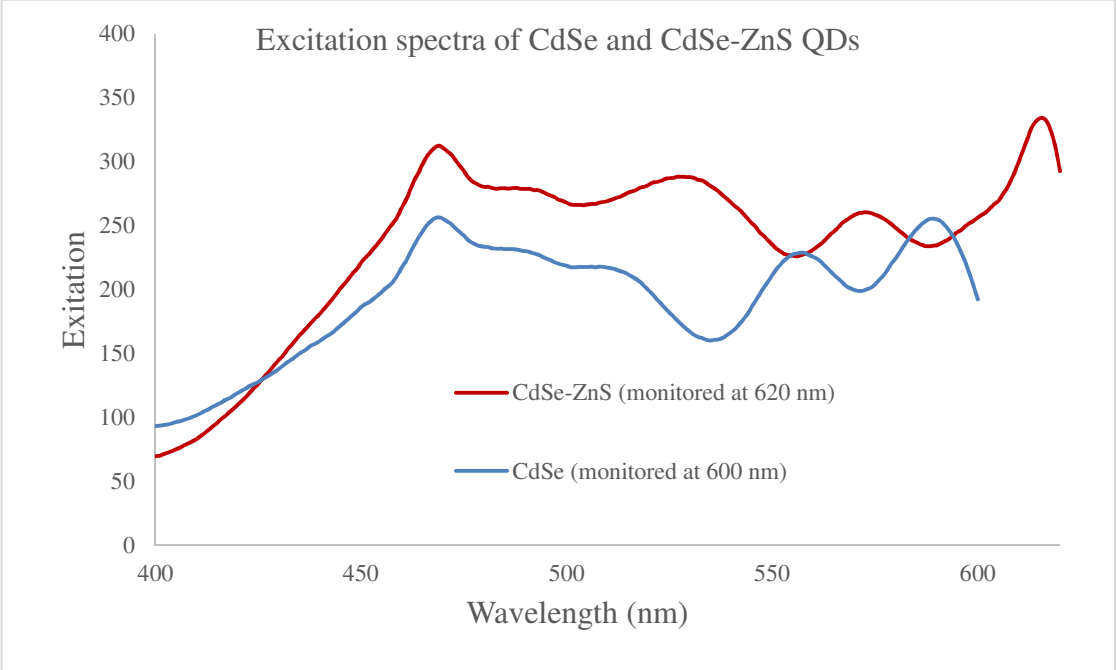

Figure 3.16. Excitation spectra of CdSe quantum dots before and after ZnS coating.

3.3.3. Silica coating on CdSe-ZnS core-shell quantum dots

In the previous step CdSe-ZnS quantum dots were synthesized in organic phase using hydrophobic coordinating ligand tributylphosphine (TBP). Although the quantum dots are better biolabeling agent than common organic dyes, because of QDs' poor water dispersibility, poor biocompatibility, chemical instability and toxicity of heavy metals, they have not been extensively used in biology.[17b] To overcome these drawbacks it is critical to encapsulate the quantum dots with an inert shell. Using silica as coating material is advantageous, because it is nontoxic, easy to functionalize and very stable in aqueous media. And also it is optically transparent with controlled porosity, which allows QD core to receive and emit light.[17a] Additionally, silica coating can be easily engineered and the thickness of the shell can be adjusted to vary the particle size.

The two common methods used for coating metal nanoparticles with silica are the sol-gel method developed by Stöber et al.[21] and the microemulsion method. But the nanoparticles with nonpolar ligands cannot be coated using Stöber method. So we followed microemulsion method reported by Darbandi et al., to coat silica on the hydrophobic QDs.[17a] The method involves base catalyzed hydrolysis of tetraethyl orthosilicate (TEOS), in a microemulsion of water, cyclohexane and surfactant.

$$Si(OC_2H_5)_4 + 2H_2O \rightarrow SiO_2 + 4C_2H_5OH$$

Volume of silica precursor (TEOS) needed to create ~14 nm thick silica shell on 6.46 nm CdSe-ZnS quantum dots were obtained from the literature.

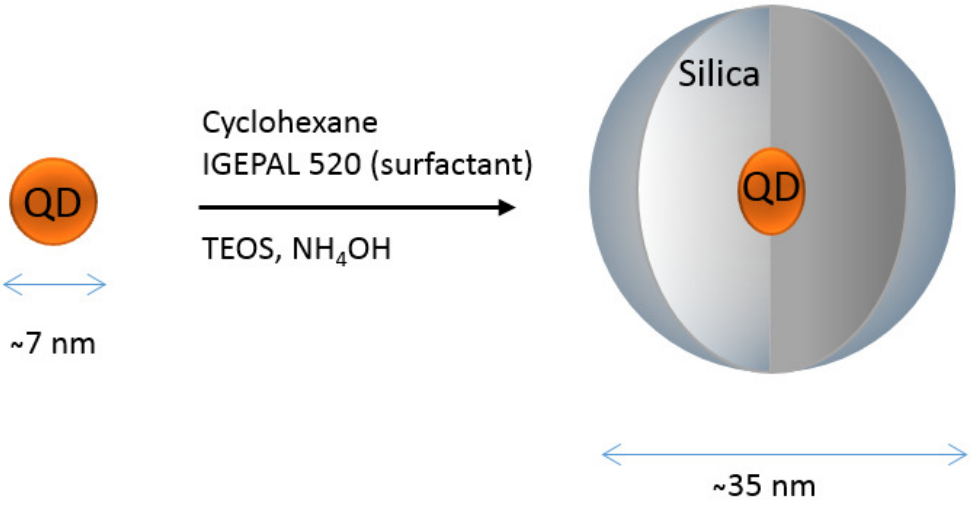

Figure 3.17. Schematic illustration of silica coating on CdSe-ZnS quantum dot

The scheme of encapsulation of QD in silica shell is illustrated in the Figure 3.17. The previously synthesized ~7 nm diameter CdSe-ZnS in octadecene (4.7 mL, 2.66 μM) was added to the mixture of cyclohexane (270 mL) and IGEPAL 520 surfactant (27 mL) in a round bottom flask under vigorous stirring condition. TEOS (2.2 mL) was added to the mixture and vigorously stirred for 30 min, before NH_4OH (4.08 mL) was added. After 20 h of stirring at room temperature, acetone (150 mL) was added to break the microemulsion. Then the particles were cleaned by three centrifugation cycles and the supernatants was replaced with more polar solvent each time (1-butanol, isopropanol and ethanol). Finally the particles were re-suspended in water. To clean the particles further, we dialyzed them with water for 4 days. TEM images (Figure 3.18) show that the produced silica nanoparticles (SiNPs) were spherical and highly monodisperse with single CdSe-ZnS quantum dot core in each SiNP. The average size of the silica nanoparticles was measured to be 35 nm, and the thickness of silica shell was 14 nm. The crystal lattice of CdSe-ZnS core can be seen in the close HR-TEM image of the silica nanoparticles.

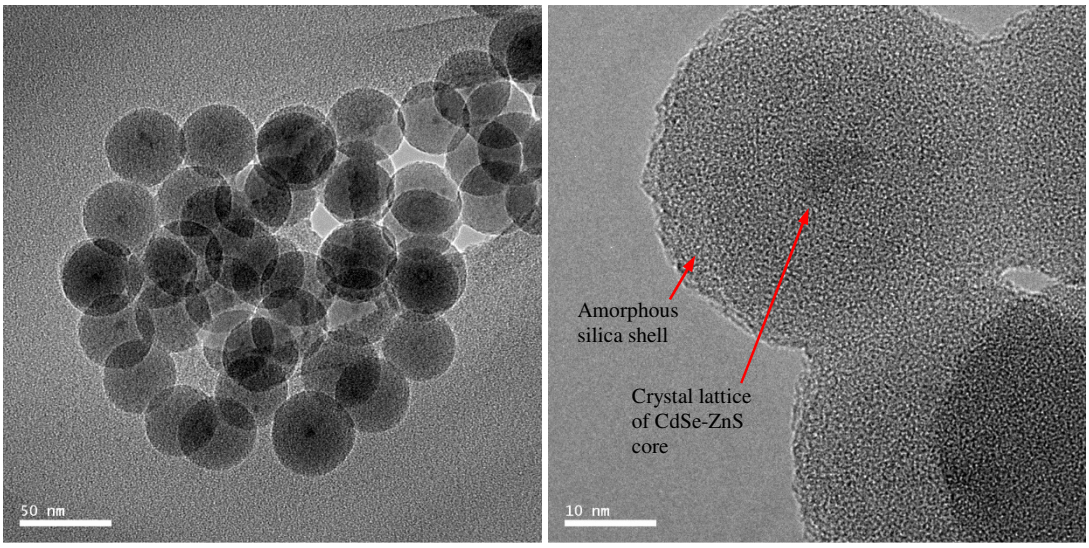

Figure 3.18. HR-TEM images of highly monodisperse QD-doped-silica nanoparticles

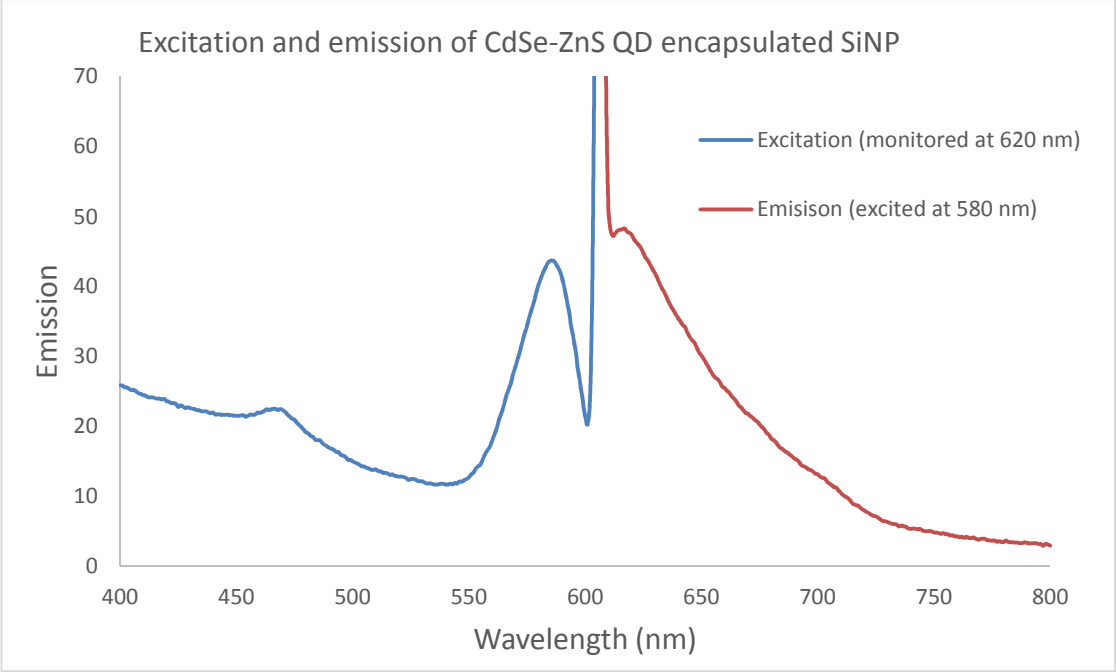

Figure 3.19. Excitation and emission spectra of CdSe-ZnS QD encapsulated silica nanoparticles.

Emission wavelength (λ_{em}) of the silica coated CdSe-ZnS quantum dots was slightly red-shifted from 615 nm to 618 nm, this may be due to the effect of change in solvent (ODE to water) or the increase in size of the particles. But it was not clear why

the excitation spectra was largely blue-shifted from 614 nm to 587 nm. Also the structure of the excitation band was altered with a drop in intensity below 550 nm.

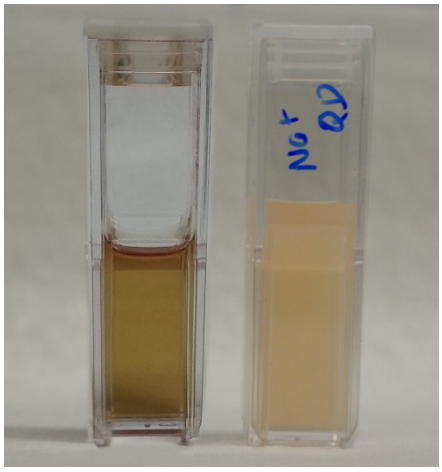

CdSe-ZnS dispersed in octadecene

SiO_2 coated CdSe-ZnS dispersed in water

Figure 3.20. Hydrophobic CdSe-ZnS in octadecene (left) and hydrophilic silica coated CdSe-ZnS in water.

Silica coating on quantum dots introduced water dispersibility to the particles. Figure 3.20 shows the hydrophobic CdSe-ZnS QDs dispersed in octadecene and hydrophilic silica coated QDs dispersed in water. Since the absorbance spectra (not shown) was greatly influenced by the presence of silica, the concentration of SiNPs dispersed in water cannot be calculated using the absorbance intensity. Also the multiple centrifugation cycles, cleaning and dialysis processes made it difficult to track the concentration of QDs before and after the silica coating. So for further studies, we used only the relative concentrations of SiNPs between the controls and samples.

3.3.4. Synthesis of larger size silica nanoparticles

We sought to increase the size of the silica nanoparticles by increasing the amount of TEOS added to the microemulsion silica coating reaction. Adjusting the thickness of silica would vary the distance between fluorophore core and metal surface, so it is critical to make silica shell of different thickness around the QDs to study the effect on MEF. Theoretically the amount of TEOS is directly proportional to the volume of the silica shell. We calculated the volume of silica shell in the 35 nm diameter SiNP synthesized in the previous step and 100 nm diameter SiNP that we attempt to synthesize next. Since the QD core is 7 nm diameter, the thicknesses of the silica hallow spheres in 35 nm and 100 nm SiNPs are 14 and 46.5 nm respectively. The ratio of the volumes of the silica are calculates as shown in the Table 3.3.

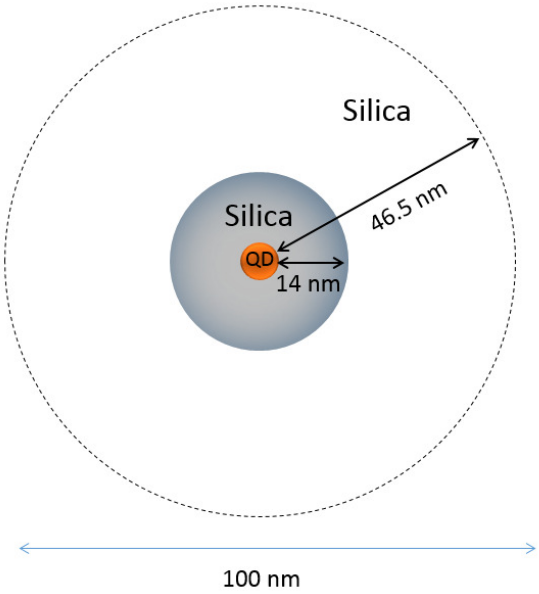

Figure 5.21. Illustration of two different size silica layers around a 7 nm QD core.

	For 35 nm diameter SiNP	For 100 nm diameter SiNP
Thickness of silica hollow sphere	14 nm	46.5 nm
Volume of silica hollow sphere = $\frac{\pi}{6}(D^3 - d^3)$	2.227 x 10^4 nm^3	52.342 x 10^4 nm^3
Volume ratio	1	23.5
Amount of TEOS needed for 0.47 mL of 2.66 μM CdSe-ZnS QDs	0.22 mL	5.17 mL

Table 3.3. Calculation of volume of silica shell and the amount of TEOS needed for microemulsion method.

To synthesize 100 nm silica nanoparticles, 5.17 mL of TEOS (from Table 3.3) was added to the mixture of CdSe-ZnS (0.47 mL, 2.66 μM), cyclohexane (27 mL) and surfactant (2.7 mL) in a round bottom flask under vigorous stirring. After 30 min NH_4OH (0.4 mL) was added and reaction was let to proceed for 20 h at room temperature. The particles were cleaned in centrifugation and dialysis steps and finally re-suspended in water. The TEM image in Figure 3.22.a shows that the silica particles did not gain the desired structure. Instead of monodisperse spherical particles, we see a clumpy silica mass in the image. The fusion of silica occurred may be due to the fact that the microemulsion was not strong enough to support the particle growth beyond certain size limit. The inability to prepare larger SiNP using microemulsion method turned us towards using Stöber method for silica regrowth. As we already mentioned the disadvantage of Stöber method was that the seeds should not be hydrophobic. Instead of using hydrophobic CdSe-ZnS nanoparticle as the seeds in Stöber method we used the hydrophilic 35 nm QD-doped-SiNP (synthesized in microemulsion method).

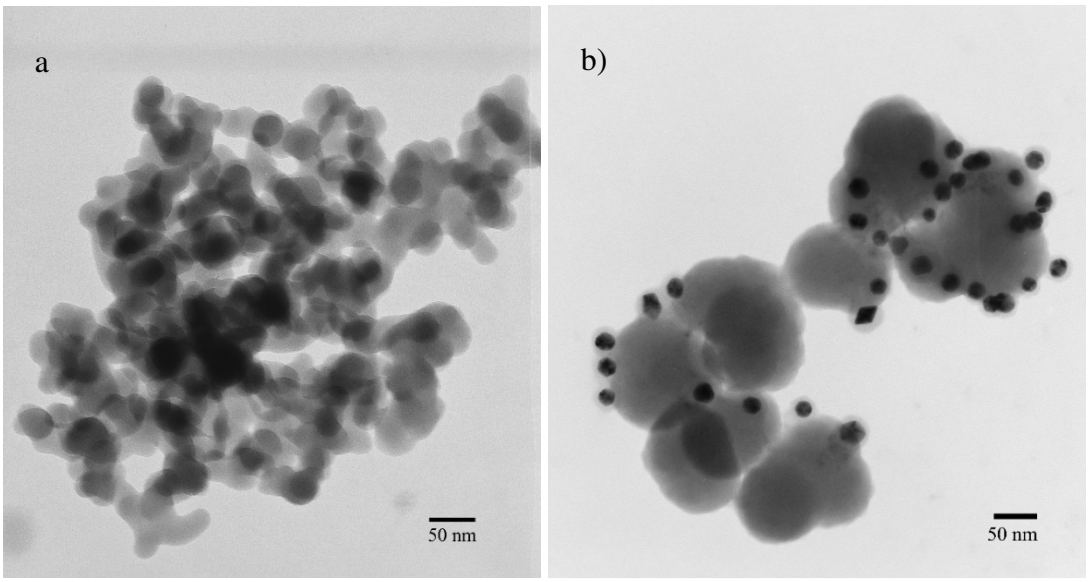

Figure 3.22. TEM images of silica nanoparticles synthesized using a) microemulsion method and b) Stöber method silica regrowth (small black spheres are gold nanoparticles)

A slightly modified Stöber method was used to regrow additional layer of silica on the 35 nm QD-doped-SiNPs. In a scintillation vial QD-doped-SiNP suspension (2 mL, from microemulsion method) was mixed with the solution of L-arginine (3 mg) in water (7.2 mL). Cyclohexane (1 mL) was added and the mixture was heated to 60 °C before adding TEOS (0.8 mL). After 30 h of stirring, the particles were separated by centrifugation, cleaned by washing and dialysis with water. The TEM image (taken after the aggregation of gold nanoparticles in an MEF study) shows that the SiNP particles were roughly spherical and slightly fused at the end of the reaction. The average size of the particles were measured to be 103 nm. Satisfied with our ability to generate QD encapsulated silica nanoparticles, we next examined the surface functionalization of the silica nanoparticles.

3.3.5. Amine functionalization of QD-doped-silica nanoparticles and DTC mediated heteroaggregation

The surface of QD-doped-silica nanoparticles were amine functionalized in order to promote heteroaggregation between gold nanoparticles and silica nanoparticles. Acid hydrolysis of (3-aminopropyl)triethoxysilane (APTES) is the most common method of installing amine onto a silica surface. A mild acid promotes the condensation reaction between the siloxane moieties of APTES and the hydroxyl group on the surface of silica nanoparticles. To an ethanolic suspension of QD-doped-silica nanoparticles, a small amount of glacial acetic acid was added and mixed gently. The mild acid condition was helpful to not affect the structural integrity of the silica nanoparticles. Figure 3.23 illustrates the installation of APTES on the surface a SiNP. The siloxane moiety of APTES condensed on the peripheral hydroxyl groups of silica shell and becomes a part of the shell.

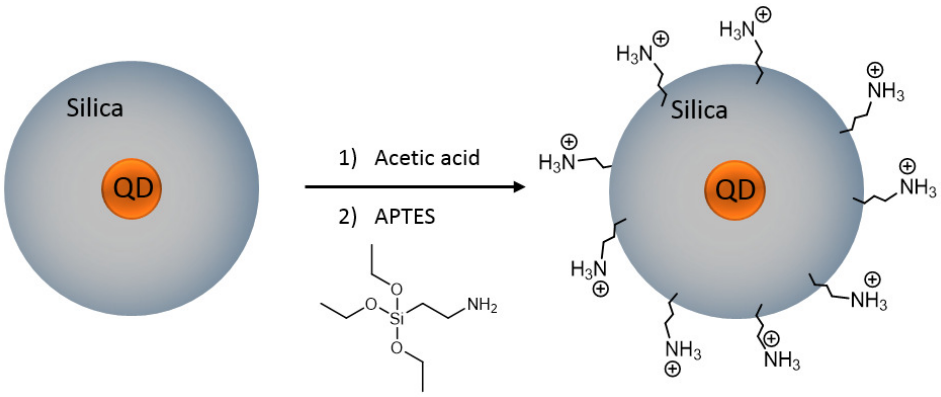

Figure 3.23. Schematic illustration of amine functionalization of QD-doped-silica nanoparticles.

The amine coated silica nanoparticles were centrifuged and the supernatant was replaced with 95% ethanol to wash out the unreacted APTES from the suspension. The centrifugation and washing cycles was repeated three times. Ninhydrin assay was

applied to the supernatant after each washing cycle to qualitatively detect the presence of free APTES. Spotting an aliquot of supernatant on a TLC plate and spraying an ethanolic solution of ninhydrin develops the blue-purple spots on the plate. Figure 3.24 shows the reaction scheme of ninhydrin with primary amine to form Schiff base. The ninhydrin assay shows a gradual decrease in intensity of supernatant spots from first three centrifugation cycle, which indicates the decreased in concentration of unreacted APTES after each cycle. But the intensity of stain form silica nanoparticle was constant and indicated the particles were successfully amine functionalized.

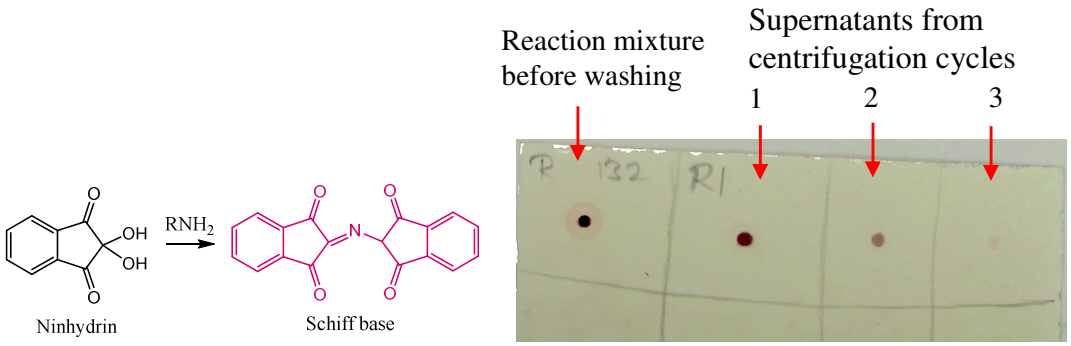

Figure 3.24. Reaction of ninhydrin with primary amine to form colored Schiff base[22] and the ninhydrin assay to monitor the concentration of unreacted APTES during the cleaning process.

Presence of amine on the surface of silica was verified by the morphology change due heteroaggregation of gold nanoparticles to the SiNPs. Although amine moiety by itself could bind to the surface of gold nanoparticles, we used the more robust dithiocarbamate (DTC) linkage. The full negative charge on DTC would be more advantageous than lone pair on amine in binding to positively charged gold surface. We used the spontaneous DTC formation method to connect propyl amine to gold surface. The suspension of amine coated silica nanoparticles was mixed with an ethanolic solution CS_2, and the pH was adjusted to 8.5. After 30 minute, GNP suspension was

added to the mixture and stirred for 6 h before preparing TEM samples on Holey Carbon TEM grids (slimmer than regular TEM grids). Figure 3.25 a) illustrates the scheme of converting terminal amine group on the silica surface into dithiocarbamate to promote a heteroaggregation with GNPs. The TEM image (Figure 3.25.b) of amine functionalized silica nanoparticles (before adding GNP) shows that the morphology of SiNP was not affected by the acid catalyzed amine coating. The heteroaggregation of GNPs to SiNPs can be clearly seen in the TEM image (Figure 25.c.) taken 6 h after the addition of gold to DTC activated SiNPs.

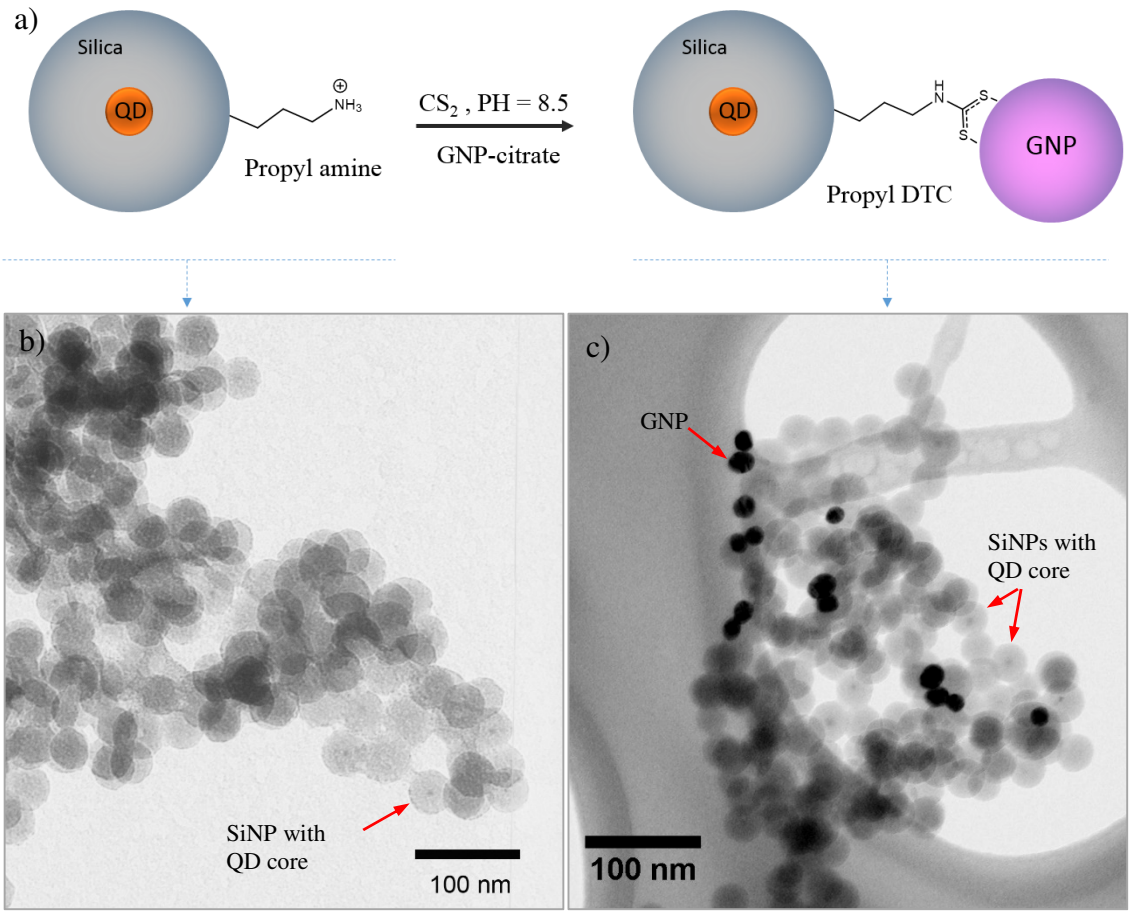

Figure 3.25. a) Schematic illustration of spontaneous DTC formation and gold aggregation on silica surface, b) HR-TEM image of amine functionalized QD-doped-SiNPs and c) HR-TEM image of DTC mediated aggregates of GNPs and QD-doped-SINPs

Amine functionality on the surface of silica nanoparticles is also evident from the following absorbance spectra (Figure 3.26). A significant shoulder peak appeared for the sample containing amine functionalized SiNP, CS_2 and GNPs (blue line). The increase in absorbance at >600 nm corresponds to the propyl-DTC mediated heteroaggregation of gold nanoparticle to the surface of silica nanoparticles. At same time the absorbance drop ~540 nm indicates the decrease in concentration of free gold nanoparticles in the sample. These changes were not seen for the control that has no APTES (purple line).

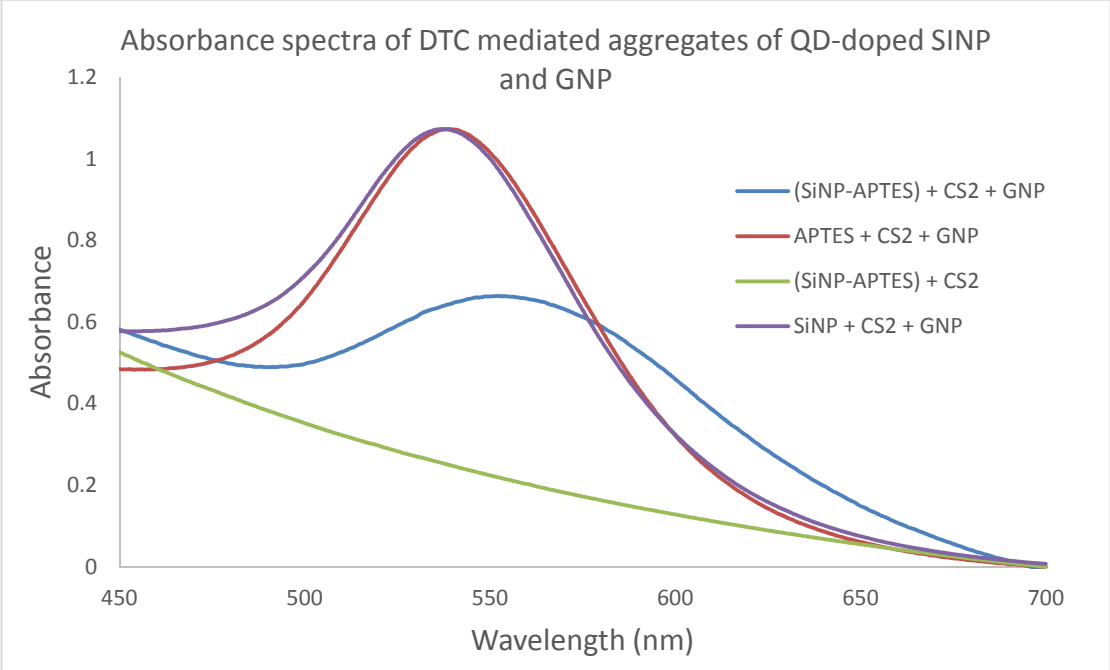

Figure 3.26. Absorbance spectra of propyl-DTC mediated aggregates of QD-doped-SiNP and GNP

Therefore propyl-amine ligand shows a great promise as a precursor of DTC binding between silica and gold nanoparticles. In Chapter IV we discussed the application of propyl-amine as well as a longer TEG chain with terminal amine to investigate the effect of aggregation on fluorescence enhancement.

3.4. Chapter Summary

In this chapter we discussed the need for CdSe-ZnS core-shell quantum dots and our effort to synthesize and integrate them into silica nanoparticles. We also discussed the application of QDs in fluorophore-metal aggregate system in order to facilitate metal-enhanced fluorescence. To achieve an optimal spectral overlap with the gold nanoparticles, we synthesized various size CdSe quantum dot cores using bottom-up technique. The pyrolysis of cadmium and selenium in a coordination solvent trioctylphosphine (TOP) at a constant high temperature produced highly hydrophobic nanocrystals of CdSe. Aliquots of reaction mixture were taken out at every 10 s during the Ostwald ripening particle growth process to get different size CdSe particles. Sizes of the particles were measured from the first excitonic absorbance wavelength using the equation developed by Yu et al.[18] The diameters of the CdSe particles ranged from 2.6 nm to 3.0 nm, and these particles showed broad excitation and narrow emission bands. Size tunable emission is one the major attraction of QDs in contrast with the commonly used organic dyes. The different size CdSe cores (2.654 nm to 3.061 nm) that we synthesized have respective absorbance wavelength from 527 to 551 nm, and respective emission wavelength from 537 to 561 nm, with 10 nm Stokes shifts. To obtain even larger QDs, we focused on optimizing the reaction conditions. In a separate synthesis, by maintaining constant temperature during the particle growth, we were able to synthesize 4.627 nm diameter CdSe particles with absorbance λ_{max} at 601 nm, which could overlap better with the coupled plasmonic scattering of gold aggregates (>580 nm).

We built type-1 core-shell CdSe-ZnS quantum dot system in order to passivate the surface defects of the QDs and increase the fluorescence brightness by confining the electron-hole pair to the core. The amount of reactants needed to coat three monolayers of ZnS shell on 4.627 nm CdSe core was determined using the equation developed by Reiss et al.[20]. With that we synthesized the CdSe-ZnS core-shell quantum dots of diameter ~7 nm. We observed a 9 nm red-shift of the λ_{abs} due to the size increase by ZnS coating and an enhanced fluorescence brightness due to the exciton confinement effect. The λ_{em} was red-shifted to 614 nm beyond the major absorbance limit of gold nanoparticles, which could be beneficial during the metal-enhanced fluorescence study to avoid the re-absorbance of MEF by gold.

The CdSe-ZnS quantum dots were highly hydrophobic and incompatible for MEF study in aqueous solution unless they were coated with hydrophilic shell or ligands. We integrated the quantum dots into optically transparent, easy to functionalize and hydrophilic amorphous silica shell. We found that the microemulsion method best accomplished the effective encapsulation of hydrophobic QDs in silica shells without altering the photophysical properties of the QDs. We produced silica nanoparticles with excellent uniformity and monodispersity. The diameter of the QD-doped-silica nanoparticles were measured to be ~35 nm based on the TEM images. The thickness of the silica layer was adjusted in order to appropriately position the QD fluorophores away from the gold surface, which is a key factor to establish metal-enhanced fluorescence. To overcome the size limitations of microemulsion method, we used Stöber method to regrow of additional layer of silica on the ~35 nm SiNPs. Using this method we produced QD-doped-silica nanoparticles of 100 nm diameter. This process

is attractive due to the discrete control over the location of QDs within the silica matrix. The fluorophore incorporated SiNPs that we produced in our lab represent an exciting frontier for investigating the metal-fluorophore interaction in aqueous solution.

The surface of QD-doped-silica nanoparticles were amine functionalized with the aim of promoting heteroaggregation to gold nanoparticles. Propyl amines with siloxane moieties were condensed on to the silica surface by acid catalyzed reaction. The terminal amine was then converted into dithiocarbamate (DTC) in favor of robust binding towards gold nanoparticles. The propyl-DTC (organic ligand) tethered on the silica surface could ensure a controlled linkage of gold to silica nanoparticles in solution phase. The TEM images and the absorbance spectra clearly showed the heteroaggregation of 25 nm GNPs to 35 nm QD-doped-SiNPs. This promising model of metal-fluorophore aggregates in aqueous solution produced in our lab could be further developed to adapt to various applications such as biolabeling, imaging and targeted delivery. Also replacing the common organic dyes with quantum dots would be a beneficial not only due to QDs' high quantum yield, photostability and size tunable optical property, but also due to the needless of a proper spatial orientation of the fluorophore with respect to metal.

3.5. Experimental and Methods

3.5.1. Synthesis of CdSe quantum dot core[6]

Synthesis of Se-TOP precursor: An oil bath was preheated to 210 °C, meanwhile octadecene (ODE) and trioctylphosphine (TOP) stock were purged with nitrogen for 15 min. In the fume hood, 44.9 mg of selenium powder (Se) was weighed and transferred into a 10 mL round bottom flask. The flask was charged with a magnetic stir bar and sealed with a rubber septum, which was then purged with N_2 for 15 min. Then a 6 mL of ODE was transferred under N_2 atmosphere into the flask, and the flask was lowered into the hot oil bath. When the reaction mixture reached the constant temperature of 210 °C, 0.45 mL of TOP was added and stirred for 1 hr at 210 °C. The reaction mixture looked green when all of the Se was dissolved. After 1 hr, the mixture was cooled to100 °C. Throughout this process the reaction mixture was purged with N_2 to avoid any degradation due to oxygen.

Synthesis of various size CdSe particles: A heating mantle connected to a thermostat was preheated to 300 °C, meanwhile ODE, oleic acid and Se-TOP precursor were purged with N_2 for 15 min. In the fume hood, 17 mg of cadmium oxide (CdO) was weighed and transferred into a two-neck 50 mL flask. The flask was charged with a stir bar and sealed with a septum and a thermostat probe. ODE (14 mL) was transferred under N_2 atmosphere into the flask, and the flask was lowered into the hot mantle. Oleic acid (0.75 mL) was added to the mixture when the temperature was crossing around 180 °C. When the temperature was constant at 300 °C, 1.2 mL of Se-TOP precursor (which was maintained at 100 °C) was added quickly into the flask. Then using glass syringes with long needle 1 mL aliquots of reaction mixture were taken out every 10 seconds up

to 90 seconds and transferred to separate vials containing 9 mL of cold ODE. At 180 seconds 10 mL of ODE was injected in to the reaction flask to stop the particle growth. Absorbance and fluorescence spectra were taken without further dilution. Sizes of the particles were calculated from the absorbance spectra as shown in **Section 3.3.1.**

Synthesis of larger size CdSe particles: A heating mantle connected to a temperature controller was preheated to 315 °C, meanwhile ODE, oleic acid and Se-TOP precursor were purged with N_2 for 15 min. In the fume hood, 17 mg of cadmium oxide (CdO) was weighed and transferred into a two-neck 25 mL flask. The flask was charged with a stir bar and sealed with a septum and a thermostat probe. ODE (14 mL) was transferred under N_2 atmosphere into the flask, and the flask was lowered into the hot mantle. Oleic acid (0.75 mL) was added to the mixture when the temperature was crossing around 180 °C. When the temperature was constant at 315 °C, 1.2 mL of Se-TOP precursor (which was maintained at 250 °C) was added quickly into the flask. At 4 minutes, 10 mL of cold ODE was injected in to the reaction flask to quench the particle growth.

3.5.2. Synthesis of CdSe-ZnS core-shell quantum dots[6]

Synthesis of ZnS precursor: Tributylphosphine (TBP) and diethylzinc ($ZnEt_2$) stock were purged with N_2 for 15 min. A 10 mL round bottom flask charged with a magnetic stir bar was sealed and purged for 15 min. TBP (3.2 mL) was transferred to the flask under nitrogen atmosphere and continued to flush with N_2. After 10 min 0.06 mL of hexamethyldisilathiane $(tms)_2S$ and 0.2 mL of $ZnEt_2$ (molar ratio of Zn to S was 0.8:1) were added into the flask and stirred for 15 min at room temperature. The resulting mixture was clear and transparent. Any cloudiness indicates the degradation due to oxygen, and that should be disposed.

ZnS shell coating on CdSe core: The amount of ZnS need to coat three monolayer on the particular concentration and volume of CdSe was calculated using the formula given by Reiss et al., and was show in the **Section 3.3.2.** Coating procedure given in Angell thesis was followed. Briefly, an oil bath was preheated to 190 °C, meanwhile CdSe in ODE was purged with N_2 for 15 min. A 25 mL two-neck flask with a magnetic stir bar was sealed with a digital thermometer probe and purged for 15 min. Then a 17 mL of CdSe (4.627 nm diameter, 2.52 μM) solution was added and the flask was lowered in to the hot oil bath. When the reaction mixture reached a constant temperature around 185 °C, 2.7 mL of ZnS precursor was added dropwise for 5 min and stirred for 20 more minutes at 185 °C. After 20 min, the reaction mixture was cooled and 3 mL of 1-butanol was quickly injected when the temperature was around 65 °C, to avoid flocculation. Absorbance and fluorescence spectra were taken without further dilution.

3.5.3. Silica coating on CdSe-ZnS core-shell quantum dots[17]

Microemulsion method silica coating: Amount of silica precursor (TEOS) needed to create ~15 nm thick silica shell on 6.46 nm CdSe-ZnS quantum dots were calculated to match the literature value.[17a] In a 500 mL RB flask, 270 mL of cyclohexane was taken. NP-5 (IGEPAL 520) surfactant (27 mL) was added to the solvent under vigorous stirring. The mixture was sonicated briefly, and 4.7 mL of CdSe-ZnS quantum dots in ODE was added under vigorous stirring and sonicated again. Then 2.2 mL of TEOS was added and stirred vigorously for 30 min. Finally 4.08 mL of ammonium hydroxide was added and the mixture was stirred for 20 h at room temperature. After 20 h of stirring the reaction mixture (150 mL) was taken out into a four centrifuge tubes, and 50 mL of acetone was added, vortexed, sonicated and centrifuged. The orange precipitate was

washed with 1-butanol, isopropanol and 95% ethanol in sonication bath and centrifuged each time. Finally the CdSe-ZnS quantum dots doped-silica nanoparticles were re-suspended in 30 mL of milipore water. TEM samples were prepared after dialysis step. TEM confirms the resulting clean silica nanoparticles are 35 nm diameter in average and had 7 nm diameter QD core.

Microemulsion method synthesis of larger silica coating: Amount of silica precursor (TEOS) needed to create ~46.5 nm thick silica shell on ~6.46 nm CdSe-ZnS quantum dots were determined as shown in **Section 3.3.3.** Volume of silica hollow sphere with thickness ~14 nm (from previously synthesis) and 46.5 nm (required in this synthesis) were calculated to be (2.227×10^4 nm^3) and (52.342×10^4 nm^3) respectively. Then we applied the ratio between the volumes to derive the amount of TEOS. We used the same procedure reported above but the volumes were changed cyclohexane (27 mL), IGEPAL 520 surfactant (2.7 mL), CdSe-ZnS quantum dots in ODE (0.47 mL), TEOS (5.17 mL) of TEOS and NH_4OH (0.4 mL). The orange precipitate was washed with 1-butanol, isopropanol and 95% ethanol in sonication bath and centrifuged each time. Finally the CdSe-ZnS quantum dots doped-silica nanoparticles were re-suspended in 3 mL of milipore water. TEM samples were prepared without further cleaning.

Silica shell re-growth:[3] Modified Stöber preparation was used to regrow additional layer of silica on the 35 nm silica particles prepared in microemulsion method. 20 mL scintillation vial was charged with QD-doped-SiNP (2 mL, 35 nm diameter) from previous step, water (7.2 mL), and a magnetic bar. L-arginine (3 mg) was added to the mixture. Cyclohexane (1 mL) was added to create a top organic layer. The vial was heated to about 60° before TEOS (0.8 mL) was added to the top layer. The vial was

sealed and stirred slowly to avoid any perturbation of the top organic layer as much as possible, for 30 h at 60°. The resulted cloudy solution was cleaned via centrifugation, spinning at 15,000 rpm for 5 min and replacing the supernatant with milipore water (5 mL, 17.8 MΩ). This cleaning cycle was repeated for three times. Finally the particles were re-suspended in milipore water. TEM confirms the resulting silica particles had an average diameter of ~103 nm.

Dialysis:[3] For further cleaning, all previously synthesized silica nanoparticles were dialyzed in milipore water using molecularporous membrane tubing MWCO : 12-14,000 (from Spectra/Por). The QD-doped-SiNP suspensions were added to 5-6 inch strip of membrane tubing (one end was sealed with dialysis clamp) after it had been soaked in water for 15 min. After excess air was removed from the tubing, the second end was sealed with another dialysis clamp. To float the dialysis tube a small strip of Styrofoam was added to the top clamp. The assembly was then placed in a 4 L beaker filled with 3 L of milipore water and a magnetic stir bar. For every 12 h the water was replaced. After 4 days the freshly cleaned particles from the membrane tubing were suspended in 10 mL of water. TEM images showed the resulting silica particles are highly monodisperse.

3.5.4. Amine functionalization of QD-doped-silica nanoparticles

Amine functionalization:[17b] 15 mL centrifugation tube was charged with 35 nm diameter QD-doped-SiNP in 95% ethanol (8 mL), glacial acetic acid (20 μL) and (3-aminopropyl)-triethoxysilane (20 μL)and rotated for 20 h. The resulting mixture was centrifuged and the supernatant was replaced with 95% ethanol three times. Ninhydrin

assay was used to monitor the concentration of amine in the supernatant each time as show in **Section 3.3.5.** Finally the particles were re-suspended in 95% ethanol.

Verification of amine coating by aggregation of GNP to QD-doped-SiNP: Amine functionalized QD-doped-SiNP (35 nm diameter) in 95% ethanol (2 mL) was taken in a scintillation vial and the pH was raised to 8.5-9 by adding concentrated KOH solution. A 1.5 mL slim polystyrene cuvettes was charged with 100 µL of this solution. In a separate vial 1mM of CS_2 was prepared by dissolving CS_2 solution in 95% ethanol and the pH was raised to 8.5-9 by adding concentrated KOH. Then 50 µL of the CS_2 solution was added to the amine functionalized SiNP solution in the cuvette. The mixture was rotated for 30 min for DTC activation. Then to these cuvettes 400 µL of GNP (25 nm diameter) citrate stabilized in water solution was added, and the final volume was made up to 1 mL by adding milipore water. In separate cuvettes three controls were made as shown in the table. The cuvettes were then tightly capped and sealed with parafilm. The samples and controls were gently rotated for 6 h in dark at room temperature. TEM samples were prepare on holey carbon grids.

Sample ID	QD-doped-SiNP (35 nm diameter)	APTES	1 mM CS_2	GNP (25 nm diameters)	Millipore water
Sample 1	100 µL (APTES tethered)	0 µL	50 µL	400 µL	450 µL
Control 1	100 µL (no APTES tether)	0 µL	50 µL	400 µL	450 µL
Control 2	0 µL	5 µL	50 µL	400 µL	545 µL
Control 3	100 µL (APTES tethered)	0 µL	50 µL	0 µL	850 µL

Table3.4. Amounts of QD-doped-SiNPs, APTES, CS_2 and GNPs for MEF study.

3.6. References

1. Zhang, C.-Y.; Yeh, H.-C.; Kuroki, M. T.; Wang, T.-H., Single-quantum-dot-based DNA nanosensor. *Nat. Mater.* **2005,** *4* (11), 826-831.

2. Gunawardana, K. B., Study of metal-enhanced fluorescence of dye doped silica nanoparticles. *Uinversity of Oklahoma* **2012**.

3. Green, N. S., Plasmonic Properties of Enhanced Fluorescence of Gold and Dye-doped SIlica Nanoparticles Aggregates. **2013**.

4. Alivisatos, A. P., Semiconductor clusters, nanocrystals, and quantum dots. *Science (Washington, D. C.)* **1996,** *271* (5251), 933-7.

5. Pisanic, T. R., II; Zhang, Y.; Wang, T. H., Quantum dots in diagnostics and detection: principles and paradigms. *Analyst (Cambridge, U. K.)* **2014,** *139* (12), 2968-2981.

6. Angell, J. J., Synthesis and characterization of CdSe-ZnS core-shell quantum dots for increased quantum yield *Thesis - California Polytechnic State University* **2011**.

7. Michalet, X.; Pinaud, F. F.; Bentolila, L. A.; Tsay, J. M.; Doose, S.; Li, J. J.; Sundaresan, G.; Wu, A. M.; Gambhir, S. S.; Weiss, S., Quantum Dots for Live Cells, in Vivo Imaging, and Diagnostics. *Science (Washington, DC, U. S.)* **2005,** *307* (5709), 538-544.

8. Medintz, I. L.; Uyeda, H. T.; Goldman, E. R.; Mattoussi, H., Quantum dot bioconjugates for imaging, labelling and sensing. *Nat. Mater.* **2005,** *4* (6), 435-446.

9. Alivisatos, P., The use of nanocrystals in biological detection. *Nat. Biotechnol.* **2004,** *22* (1), 47-52.

10. Zhang, L.; Song, Y.; Fujita, T.; Zhang, Y.; Chen, M.; Wang, T.-H., Large Enhancement of Quantum Dot Fluorescence by Highly Scalable Nanoporous Gold. *Adv. Mater. (Weinheim, Ger.)* **2014,** *26* (8), 1289-1294.

11. Michalet, X.; Pinaud, F.; Lacoste, T. D.; Dahan, M.; Bruchez, M. P.; Alivisatos, A. P.; Weiss, S., Properties of fluorescent semiconductor nanocrystals and their application to biological labeling. *Single Mol.* **2001,** *2* (4), 261-276.

12. Klimov, V. I.; Mikhailovsky, A. A.; McBranch, D. W.; Leatherdale, C. A.; Bawendi, M. G., Quantization of multiparticle Auger rates in semiconductor quantum dots. *Science (Washington, D. C.)* **2000,** *287* (5455), 1011-1013.

13. Dabbousi, B. O.; Rodriguez-Viejo, J.; Mikulec, F. V.; Heine, J. R.; Mattoussi, H.; Ober, R.; Jensen, K. F.; Bawendi, M. G., (CdSe)ZnS Core-Shell Quantum Dots: Synthesis and Optical and Structural Characterization of a Size Series of Highly Luminescent Materials. *J. Phys. Chem. B* **1997,** *101* (46), 9463-9475.

14. Biju, V.; Itoh, T.; Anas, A.; Sujith, A.; Ishikawa, M., Semiconductor quantum dots and metal nanoparticles: syntheses, optical properties, and biological applications. *Anal. Bioanal. Chem.* **2008,** *391* (7), 2469-2495.

15. Gao, X.; Cui, Y.; Levenson, R. M.; Chung, L. W. K.; Nie, S., In vivo cancer targeting and imaging with semiconductor quantum dots. *Nat. Biotechnol.* **2004,** *22* (8), 969-976.

16. (a) Gao, X.; Nie, S., Quantum Dot-Encoded Mesoporous Beads with High Brightness and Uniformity: Rapid Readout Using Flow Cytometry. *Anal. Chem.* **2004,** *76* (8), 2406-2410; (b) Walling, M. A.; Novak, J. A.; Shepard, J. R. E., Quantum dots for live cell and in vivo imaging. *Int. J. Mol. Sci.* **2009,** *10* (2), 441-491.

17. (a) Darbandi, M.; Thomann, R.; Nann, T., Single quantum dots in silica spheres by microemulsion synthesis. *Chem. Mater.* **2005,** *17* (23), 5720-5725; (b) Darbandi, M.; Urban, G.; Krueger, M., Bright luminescent, colloidal stable silica coated CdSe/ZnS nanocomposite by an in situ, one-pot surface functionalization. *J. Colloid Interface Sci.* **2012,** *365* (1), 41-45.

18. Yu, W. W.; Qu, L.; Guo, W.; Peng, X., Experimental Determination of the Extinction Coefficient of CdTe, CdSe, and CdS Nanocrystals. *Chem. Mater.* **2003,** *15* (14), 2854-2860.

19. Murray, C. B.; Norris, D. J.; Bawendi, M. G., Synthesis and characterization of nearly monodisperse CdE (E = sulfur, selenium, tellurium) semiconductor nanocrystallites. *J. Am. Chem. Soc.* **1993,** *115* (19), 8706-15.

20. Reiss, P.; Protiere, M.; Li, L., Core/shell semiconductor nanocrystals. *Small* **2009,** *5* (2), 154-168.

21. Stoeber, W.; Fink, A.; Bohn, E., Controlled growth of monodisperse silica spheres in the micron size range. *J. Colloid Interface Sci.* **1968,** *26* (1), 62-9.

22. Friedman, M.; Sigel, C. W., A kinetic study of the ninhydrin reaction. *Biochemistry* **1966,** *5* (2), 478-85.

Chapter IV: Aggregation of quantum dot incorporated silica nanoparticles and gold nanoparticles to produce metal-enhanced fluorescence in solution

4.1 Chapter Overview

Metal-enhanced fluorescence (MEF) is of great interest due to its transformative effects on medicine and material chemistry. So for the MEF on solid surface to produce surface enhanced Raman spectroscopy (SERS) has been proved to dramatically enhance the fluorescence brightness of molecules near the surface of a metal.[1] Considering the limitations of using solid phase substrates in medicine, we attempted to produce similar dramatic increase of fluorescence signal in aqueous solution. Producing metal-enhanced fluorescence in solution without requiring a solid phase substrate would provide a path to new and sensitive biosensors[2] and potential applications in light harvesting systems.[3] This chapter describes our effort to produce metal-enhanced fluorescence (MEF) of CdSe-ZnS quantum dot incorporated silica particles in aqueous solution by aggregating to gold nanoparticles

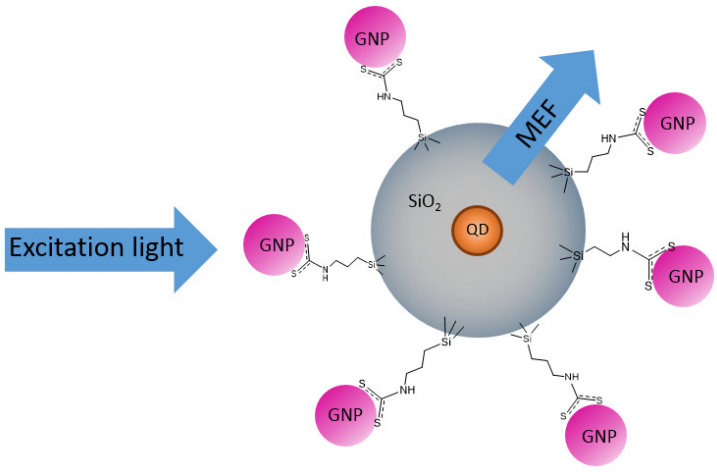

Figure 4.1. Overview of the MEF produced from QD-doped-silica particle aggregated with gold nanoparticles.

4.2 Introduction

Recent advancement of metal-enhanced fluorescence suggest that it could be a potential tool in creating ultra-bright fluorescence probes with increased photostability.[4] MEF has been intensively studied over the last decade as a method for greatly increasing the fluorescence brightness when brought a fluorophore close to surface of a metal nanostructures. The enhancement of fluorescence relies on the increased excitation events of the fluorophore and introduction of additional emission pathways.[5] Metal nanoparticles can interact with the incident light and cause a collective oscillation of surface electrons that results in concentrated local electric field confined to a nanometer scale. Placing a fluorophore in that region would increase the number of excitation events of fluorophore and thus cause a faster excitation-emission cycles, which enhances the brightness of the fluorescence.[6] Figure 4.2 displays the local electric field of a metal nanostructure and the increased excitation of fluorophore placed near the surface of the metal.

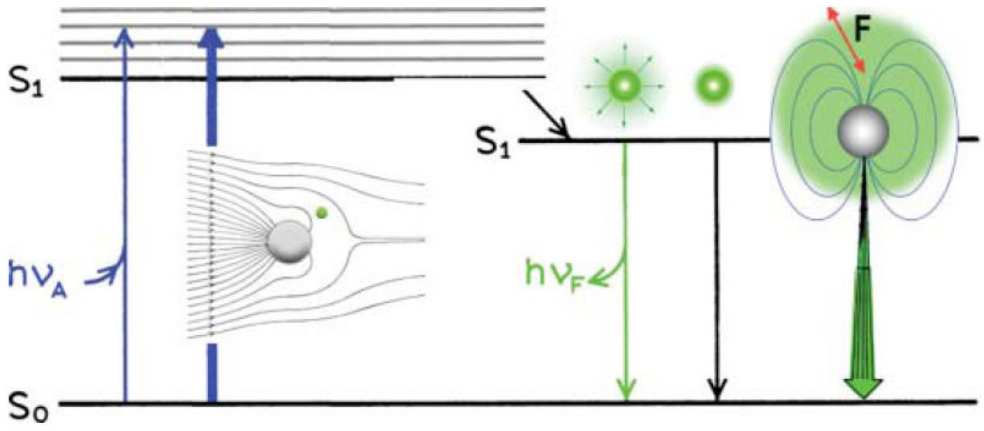

Figure 4.2. Placing the fluorophore (tiny green sphere) in the concentrated electric field around the metal nanostructure increases the excitation events and enhances the fluorescence.

Keeping a fluorophore near a metal nanoparticle surface also decreases the fluorescence lifetime and offers additional emission pathways leading to increased turnover of excitation/emission cycles. Figure 4.3 displays a Jablonski diagram depicting the increased excitation and emission pathways of a fluorophore near the surface of a metal.

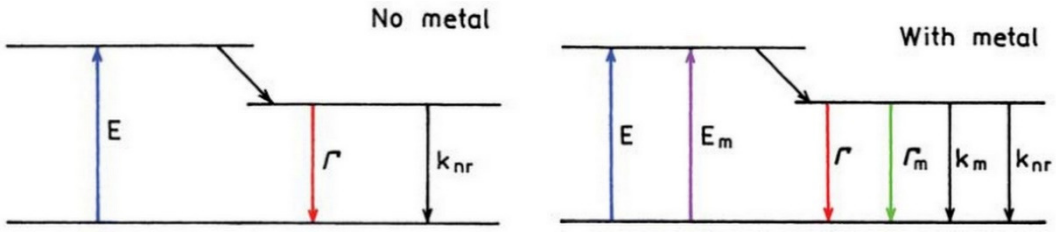

Figure 4.3. Jablonski diagram of the excitation/emission process of a fluorophore near the surface of a metal nanostructure.

Equation (1) represents the fluorescence lifetime (τ) of a free fluorophore in solution

$$\tau = \frac{1}{\Gamma + k_{nr}} \qquad (1)$$

Where Γ is the rate of radiative decay and k_{nr} is the rate of non-radiative decay. The introduction of an emission pathway by interacting with a metal (Γ_m) increases the number of radiative pathways and decreases the fluorescence lifetime of the fluorophore. Equation (2) represents the lifetime of fluorophore near a metal surface (τ_m)[7]

$$\tau_m = \frac{1}{\Gamma + \Gamma_m + k_{nr}} \qquad (2)$$

The surface plasmon resonance of the metal nanostructures is effective within certain nanometer scale region, hence the metal-enhanced fluorescence is highly dependent on distance between fluorophore and metal surface. Placing the fluorophore

too close to the metal results in fluorescence quenching while being too far results in no interaction at all. Recent findings show that the optimum distance of 0.5–200 nm yields a significant MEF.[8]

The overlap of multiple plasmonic resonance of nearby metal nanostructures is called plasmon coupling that strongly intensifies the electric field between multiples nanostructures and creates a hotspot for the fluorophore.[6b] Acuna et al., measured the dependence of fluorescence enhancement on the number of metal nanoparticles and converted it to a numerical values. A 117-fold fluorescence enhancement was reported for a dye molecule positioned at the hot spot between two gold nanospheres of 80 nm diameter with 23 nm interparticle distance.[9] Figure 4.4 shows the hotspot (intensified electric field) due to plasmon coupling of two gold nanoparticles.

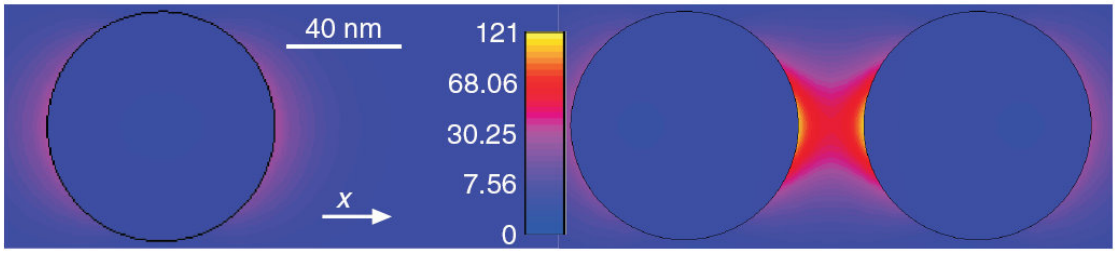

Figure 4.4. Numerical simulation of electric filed intensity of a single 80 nm diameter gold nanosphere (left) and two gold nanoparticles with 23 nm gap between them (right). (Image from Acuna et al)[9]

A similar study conducted on the aggregation of multiple 13 nm gold nanoparticles showed the coupling of plasmons would redshift the scattering component of the aggregates.[10] Scattering is an elastic reflection of incident light that was shown to be increased upon aggregation.[11] This increase in scattering intensity is significant because the rate of emission due to energy transfer between fluorophore and gold depends on the metal scattering component .[11-12]

Therefore, a fluorophore placed in the coupled plasmonic hotspot emits brighter fluorescence due the increased probability of excitation in the intensified electric field.

M

.+oreover the fluorophore can predominantly emit by coupling to the increased plasmon scattering. Lakowicz et al., recently observed that a single molecule fluorescence of Cy5 dye showed a 7-fold enhancement when coupled with a monomer silver nanoparticle and a 13-fold enhancement when placed between a dimer of silver nanoparticles[13]. In the below absorbance spectrum, the silver dimer show increase in scattering at ~500 nm and is responsible for the 13-fold fluorescence enhancement.

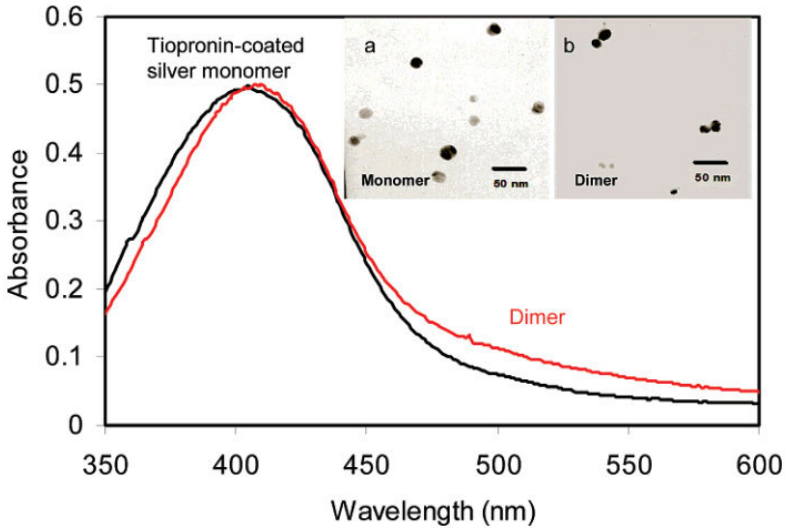

Figure 4.4. Absorbance spectra shows a redshift for dimer silver nanoparticles, and increased scattering around 500 nm. The insets are the TEM images of the monomer and dimer silver nanoparticles. (Image from Lakowicz et al)[13]

Metal-enhanced fluorescence has been broadly studied on solid phase substrates where the fluorophores can be easily placed at a controlled distance from metal surface.[1-2, 5, 7, 14] Acuna et al., measured the fluorescence enhancement of a single fluorescence dye placed in a plasmonic hotspot between two 100 nm gold nanoparticles attached to self-assembled nanoantennas of DNA origami.[9] Nanolithography technique

was used to construct DNA origami pillars of 220 nm length and 15 nm diameter with docking sites for gold nanoparticles. A dye-labeled DNA strand and three capturing strands were constructed at the docking sites. After the construction of the pillars, DNA functionalized gold nanoparticles were immobilizes at the docking site by hybridization to capturing strands (Figure 4.6). This technique allowed to place the dimer nanoparticles at a precise interparticle distance (23 nm) with nanometer accuracy. Based on this solid state platform a fluorescence enhancement of single dye molecule up to 117-fold was achieved for 100 nm dimer with 23 nm interparticle.

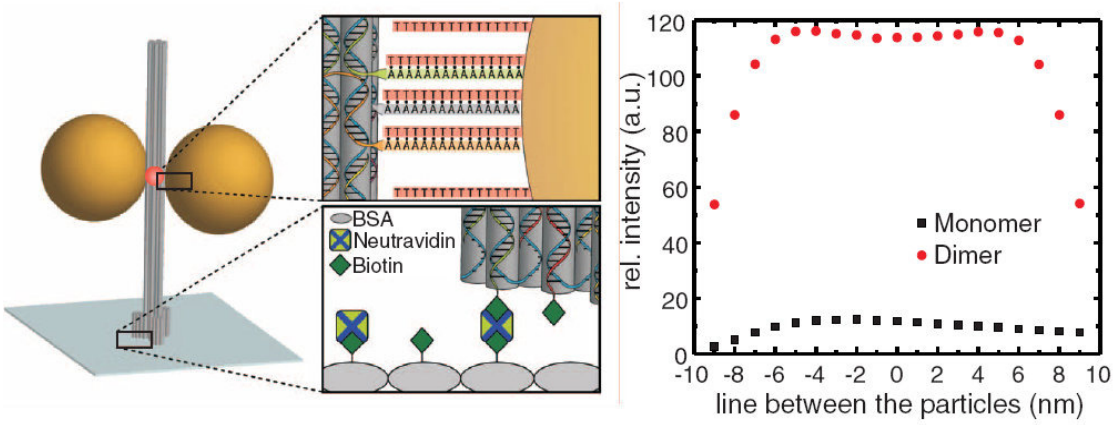

Figure 4.6. A schematic illustration of gold nanoparticle dimer (yellow spheres) docked on self-assembled DNA origami pillar with the dye (red sphere in the left image) located at the plasmonic hot spot. The insets represent the binding of NP to origami pillar and the binding of the origami to a base. The graph shows a smaller fluorescence enhancement of the dye next to a monomer and a larger fluorescence enhancement in the hotspot between dimer gold nanoparticles. (Images from Acuna et al)[9]

Lakowicz et al., measured the effect of distance between a fluorophore and a metal surface on the fluorescence enhancement.[5] When each polymer monolayer was added to the silver island films, the distance between the fluorophore N,N[1]-(dipropyl)-tetramethylindocarbocyanine (Cy5) and silver surface was increased by 1 nm. Placing Cy5 dye within the previously discussed optimal distance from metal surface increases

the excitation while diminishing fluorescence quenching. The greatest enhancement was observed when the Cy5 was a single biotin monolayer away from the silver surface, which is roughly 1 nm distance. Figure 4.7 displays the effect of distance on emission of the fluorophore-doped polymer when they were added on silver islands.

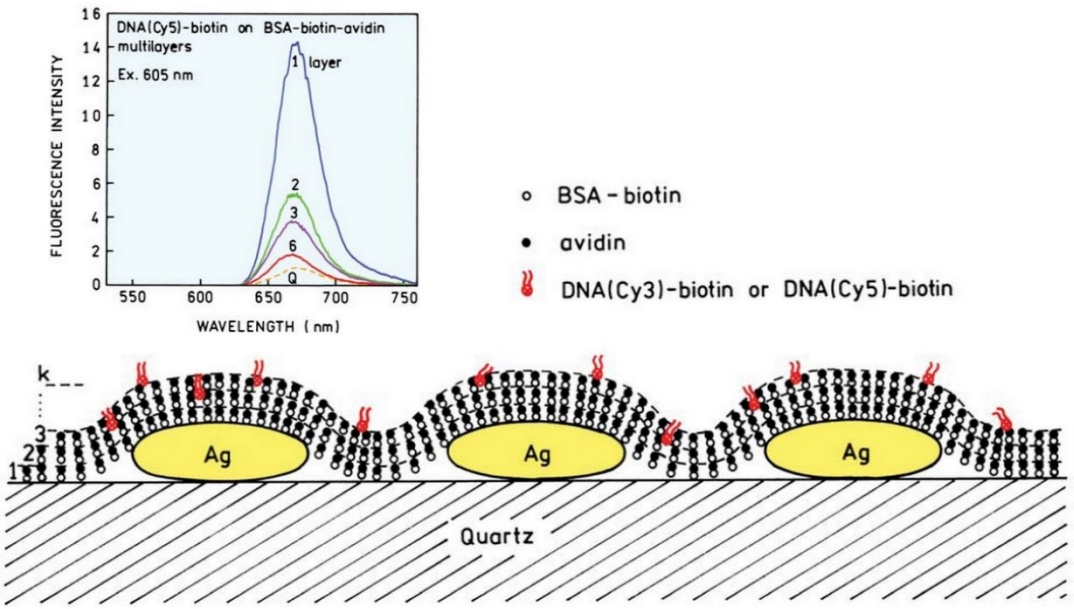

Figure 4.7. Schematic illustration of Cy5 dye bound polymer in multiple layers on the surface of silver island film. (Image from Lakowicz et al)[5]

An increase in the number of layers resulted in a significant drop in the fluorescence brightness due to the fact that the fluorophore was not in interaction with the surface plasmon of the silver to increase the emission pathway and thus a slower rate of excitation/emission cycles. The method of deposition of silver island on a glass surface offers the control over the metal aggregation and coating of dye bound polymer layer controls the distance between the dye and the metal surface.

These solid substrate platforms provide an excellent insight to the underlying factors like plasmonic hotspots and distance dependency of metal-enhanced

fluorescence. However solid substrates have strong limitations in biological applications.[15]

Our research group has been developing methods to achieve the metal-enhanced fluorescence in aqueous solution by aggregating fluorophore doped silica nanoparticles to metal nanoparticles using organic linkers. Kalani Gunawardana accomplished a 200-fold fluorescence enhancement from the propyl dithiocarbamate (DTC) mediated aggregates of rhodamine B doped silica nanoparticles and gold nanoparticles.[6a]

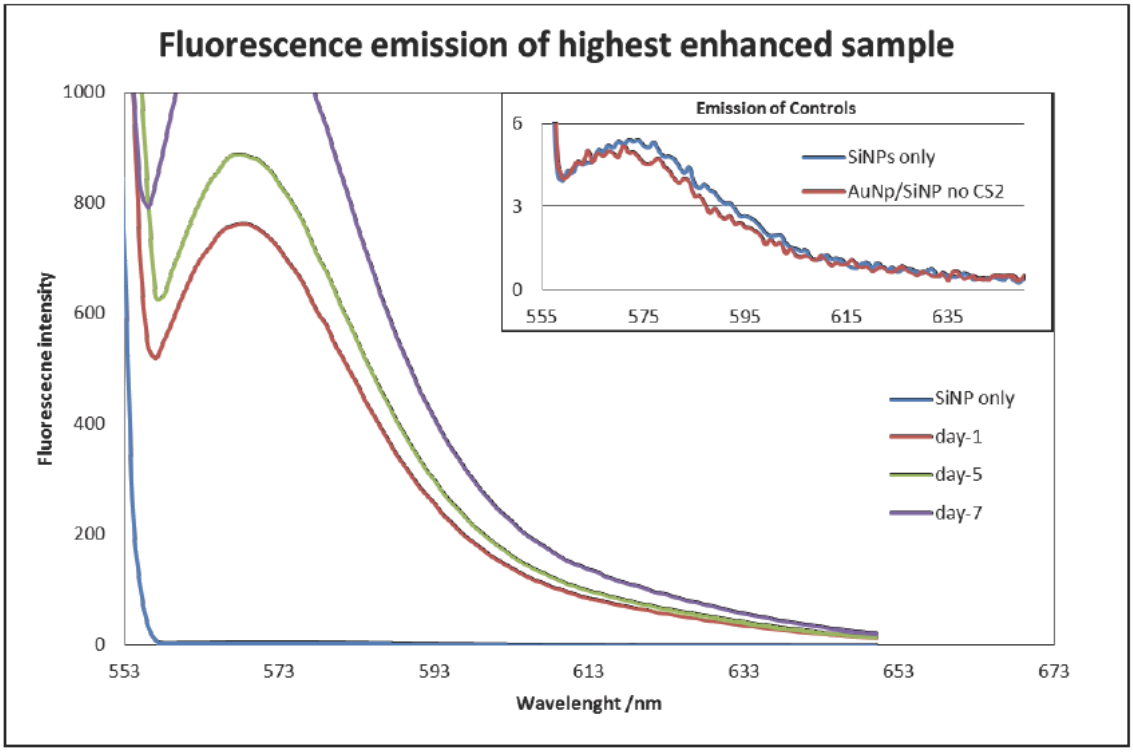

Figure 4.8. Emission spectra from the aggregates of rhodamine B doped silica nanoparticles and gold nanoparticles in aqueous solution. (Image from Gunawardana)[6a]

Nathan Green in our group demonstrated a robust method of aggregating 13 nm size gold nanoparticles on 120 nm diameter dye-doped silica nanoparticle using propyl amine as a linker in aqueous solution. TEM images in Figure 4.9 shows a well ordered heteroaggregation of GNP to SiNP.[16]

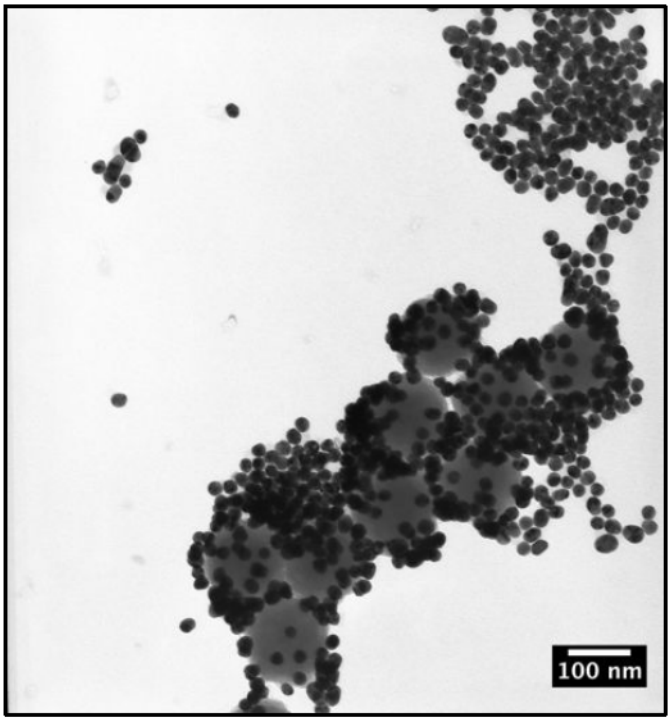

Figure 4.9. TEM image of gold nanoparticles aggregated with 120 nm diameter amine coated silica nanoparticles in aqueous solution. (Image from Green)[16]

These results shaped the model of amine and DTC facilitated aggregation in aqueous solution that utilizes the plasmonic scattering to increase excitation-emission events and thus promote the metal-enhanced fluorescence. With this proof-of-concept from the previous work of Gunawardana, Green, Bumm and Halterman, the current work focus on our effort to produce metal-enhanced fluorescence from inorganic fluorophores by applying the same model. We used CdSe-ZnS quantum dot (QD) semiconductors as our fluorophores since they possess a broad excitation band while retaining a narrow emission band. Switching to QDs would allow us to excite the system with a wide range of wavelengths where the plasmonic scattering of GNP is more pronounced and measure a narrow emission from QDs. Hence the excitation and emission factors can be decoupled and quenching can be minimized.

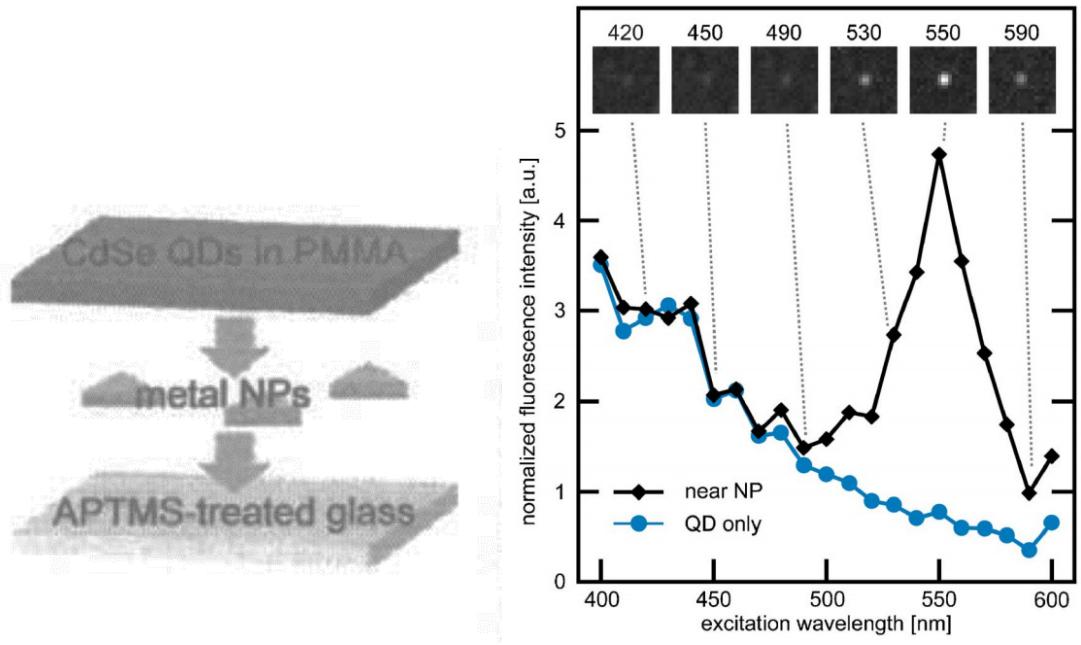

Figure 4.10. Metal enhancement fluorescence from CdSe quantum dots near metal nanoprism on glass substrate. (Image from Chen et al) [17]

Chen et al., reported 3 to 10-fold fluorescence enhancement of CdSe quantum dots coated on a solid substrate with gold nanoprisms of different scattering wavelength.[17] The excitation spectrum of the QDs closely follows the surface plasmon resonance scattering spectrum of those gold nanoparticles. When they excited the assembly with different excitation wavelengths, they observed fluorescence enhancement only from the quantum dots that were placed near the metal nanoprims whose scattering wavelength matches with the excitation wavelength.

We anticipate the metal-enhanced fluorescence of quantum dots can be attained in aqueous solution by aggregating QD-doped-silica nanoparticles and gold nanoparticles via DTC linkage. Investigation of the interaction between quantum dots and gold nanoparticles in solution will provide a path for application of MEF in bio-sensing and light harvesting systems.

4.3 Results and Discussion

4.3.1 Investigating the spectral overlap of gold nanoparticles and CdSe-ZnS quantum dots

Understanding the wavelength dependence of metal-enhanced fluorescence (MEF) would help to choose the right structure, size and composite for the metal and fluorophore complex. It is apparent that a strong interaction between metal and fluorophore will occur only when the plasmon scattering spectrum of the metal and the excitation spectrum of the fluorophore have an optimum overlap. Because of the factor that both fluorescence enhancement and fluorescence quenching by metal are wavelength dependents,[18] different degrees of spectral offset are needed for different applications such as biological sensing (maximum fluorescence), photochemistry (maximum excitation), improved photostability (minimum lifetime), etc.[19]

We investigated the overlap of absorbance spectra of different size gold nanoparticles and the excitation/emission spectra of different size CdSe-ZnS quantum dots in order to choose the right size GNP and QD to aggregate. Gold nanoparticles not only alter the radiative decay pathway of the QD fluorophore, but also opens up a new non-radiative decay pathway through energy transfer to GNP, which can be re-scattered back in to far-field.[20] Simply the energy of the excited state QD can be quenched by loss to GNP's non-radiative decay pathway. Since GNP can either increase or decrease the fluorescence quantum efficiency of the nearby fluorophore, it's important to separate the enhanced emission spectrum of the aggregates away from the absorbance spectrum of the GNPs. Even though the separation of the emission and absorbance spectra is

difficult, both of these are extremely sensitive to the shape and size of the GNP and the QD and the distance between them.

The spectral overlap can be optimized by synthesis and optical characterization of gold nanoparticles and quantum dots. We selected to use gold nanospheres as our metal because of their simple surface plasmon resonance profile (a single scattering peak seen in the absorbance spectrum) compared to gold nanorods having two scattering peaks corresponding to their length and width. Plasmon scattering wavelength of gold nanospheres can be tunable across the visible spectrum by altering their size. We synthesized different size citrate capped gold nanospheres via kinetically controlled seeded growth method following the Bastus et al., procedure with slight modifications.[21] Gold nanospheres with different diameter between 10 nm - 65 nm were synthesized in different generations of seeded growth. The scattering λ_{max} of different size gold nanospheres were ranged between 515 - 540 nm. In some cases the full width half maximum (FWHM) of the scattering spectrum spreads above 90 nm. To avoid the quenching of quantum dots by the far-field energy transfer to gold nanoparticles, it is better to keep the scattering peak of the GNP to a narrow range of wavelength.

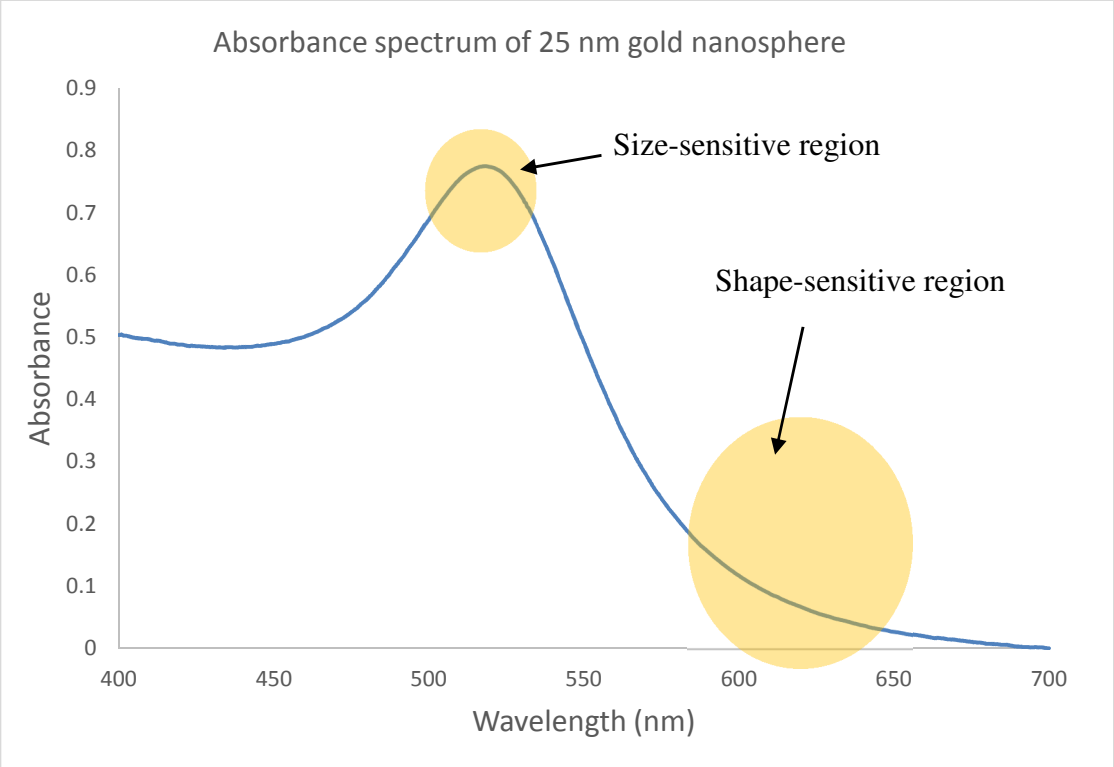

Figure 4.11. Absorbance spectrum of 25 nm diameter gold nanospheres shows the plasmon scattering peak with size-sensitive region around 515 nm and shape-sensitive region around 600-650 nm.

Gold nanoparticle of different size and shape absorb photons of different energy that causes the surface plasmon resonance. Thus the scattering spectrum of gold nanoparticles has a size-sensitive region and a shape sensitive region (Figure 4.11). The increase in size of the GNP would result in red-shift of the λ_{max} of scattering peak. Figure 4.12 shows a range of scattering λ_{max} for different size GNPs. This would allow us to choose the right size GNP for the optimal spectral overlap with the quantum dots.

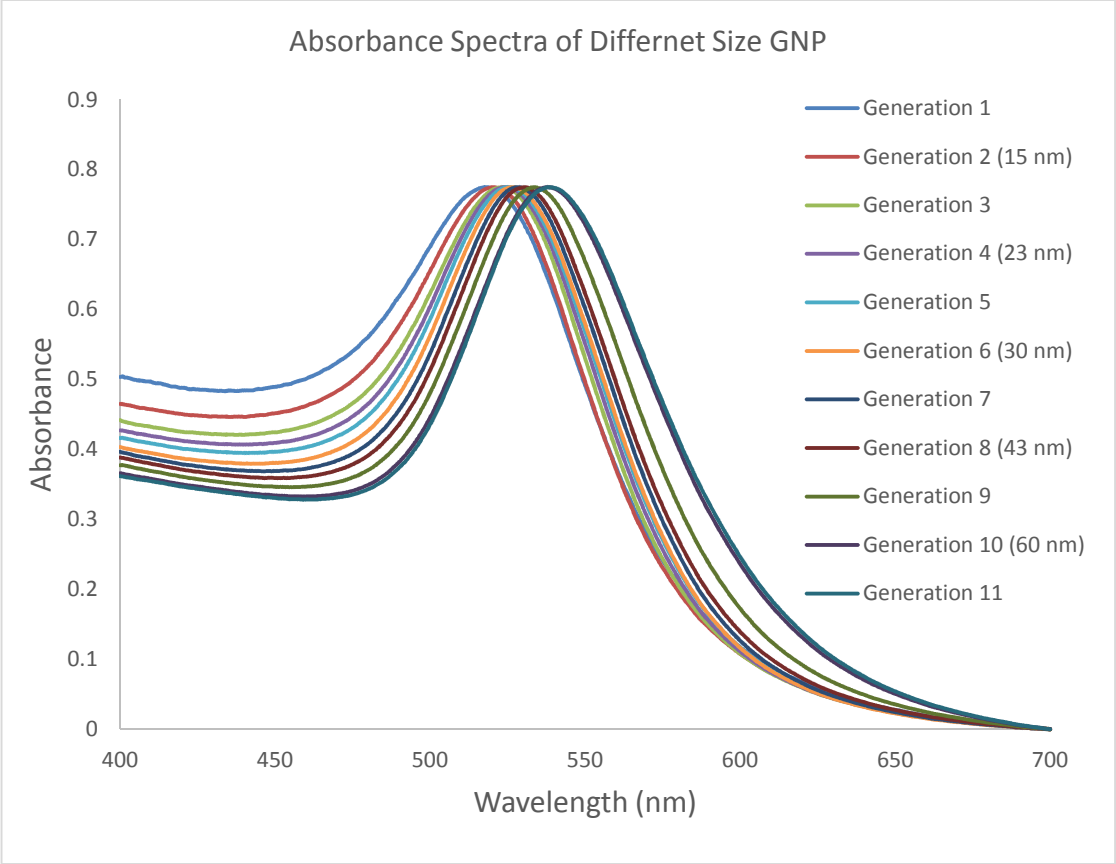

Figure 4.12. Normalized absorbance spectra of different size gold nanoparticles show the increase in size of the particles causes the red-shift of the λ_{max} of the scattering peak.

The shape of gold nanoparticles strongly influences the absorbance. A change in shape due to clustering of multiple small gold nanoparticles would also influence the absorbance intensity >600 nm. Aggregation of multiple gold nanoparticle would create a region of plasmonic hotspot where the plasmon resonance of individual particles are coupled to produce an enhanced scattering >600 nm. In order to assess the plasmonic coupling of different size GNPs, they were bound to 100 nm silica nanoparticles (SiNP) tethered with propyl-DTC.

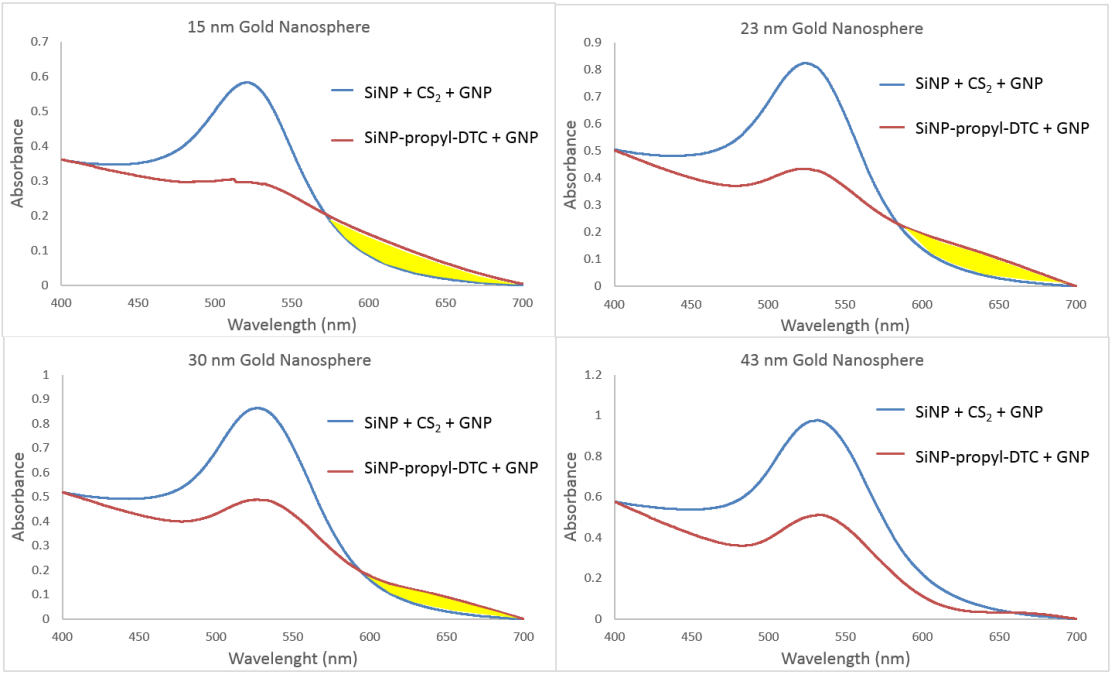

Figure 4.13. Absorbance spectra of aggregates of different size gold nanoparticles to 100 nm SiNPs. Yellow band represents the different degree of scattering enhancement due to coupled plasmonic resonance.

In Figure 4.13 absorbance spectra of the aggregates of the different size GNPs to 100 nm SiNPs show a decrease in absorbance λ_{max} between 515-540 nm corresponds to decrease in number of free GNP in the solution. At the same time the increase in absorbance between 575-700 nm indicates the enhancement of scattering due to coupled plasmonic resonance. This enhanced absorbance infer that multiple GNP were aggregated in proximity on the surface of SiNP. Also it is clearly seen that the aggregation was better for smaller GNPs (15 and 23 nm) that the larger GNPs (30 and 43 nm). This may be due the fact that more number of smaller GNP can occupy the surface of relatively larger size SiNP. Figure 4.14 shows the TEM image of aggregation of 23 nm GNP to 100 nm SiNP. The better aggregation of smaller GNP was also evident from the color change from pink to purple for the sample.

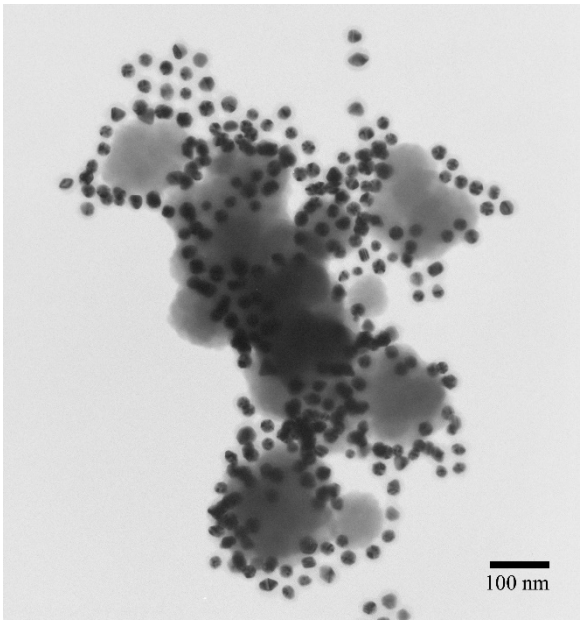

Figure 4.14. TEM image of aggregates of 23 nm GNP on the surface of 100 nm SiNP with propyl-DTC coating.

Minimum scattering from free GNPs and maximum scattering of aggregated GNP in a sample would allow us to utilize much of the coupled plasmonic scattering for fluorescence enhancement. When the system was excited between 575 – 700 nm the contribution of coupled plasmonic scattering from aggregated GNP to enhance the fluorescence would dominate the contribution of normal scattering from free GNPs. Although 15 nm GNP demonstrates increased aggregation to SiNPs and a better coupled plasmonic scattering, we chose 23 nm GNPs to study the MEF because of its optimal spectral with quantum dots.

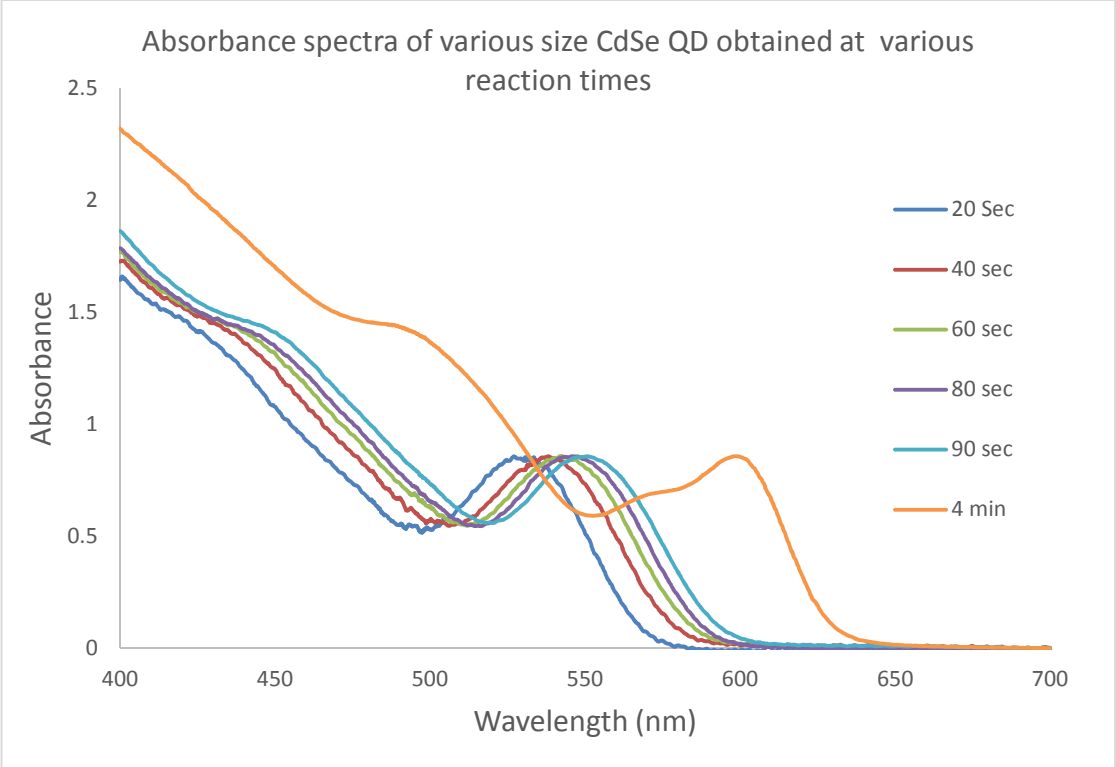

Figure 4.15. Normalized absorbance spectra of different size CdSe quantum dots synthesized at different reaction times.

One of the advantages of quantum dots over organic fluorophores is the tunable emission. The size dependent emission allows us to synthesize QDs of specific size that could effectively absorb energy from the concentrated electric field around the gold nanoparticles and emit beyond the absorbance limit of GNP. In order to obtain a better spectral overlap with 15 or 23 nm size GNPs' scattering profile we synthesized different sizes of CdSe quantum dos and picked up the one with optimal excitation/emission profile. CdSe quantum dots of different size were synthesized by varying the reaction time of particle growth.[22] Figure 4.15 shows the normalized absorbance spectra of QDs obtained at various reaction time (20 sec to 4 min). Red-shift of the λ_{max} from 520 – 600 nm corresponds to the increase in size of CdSe.

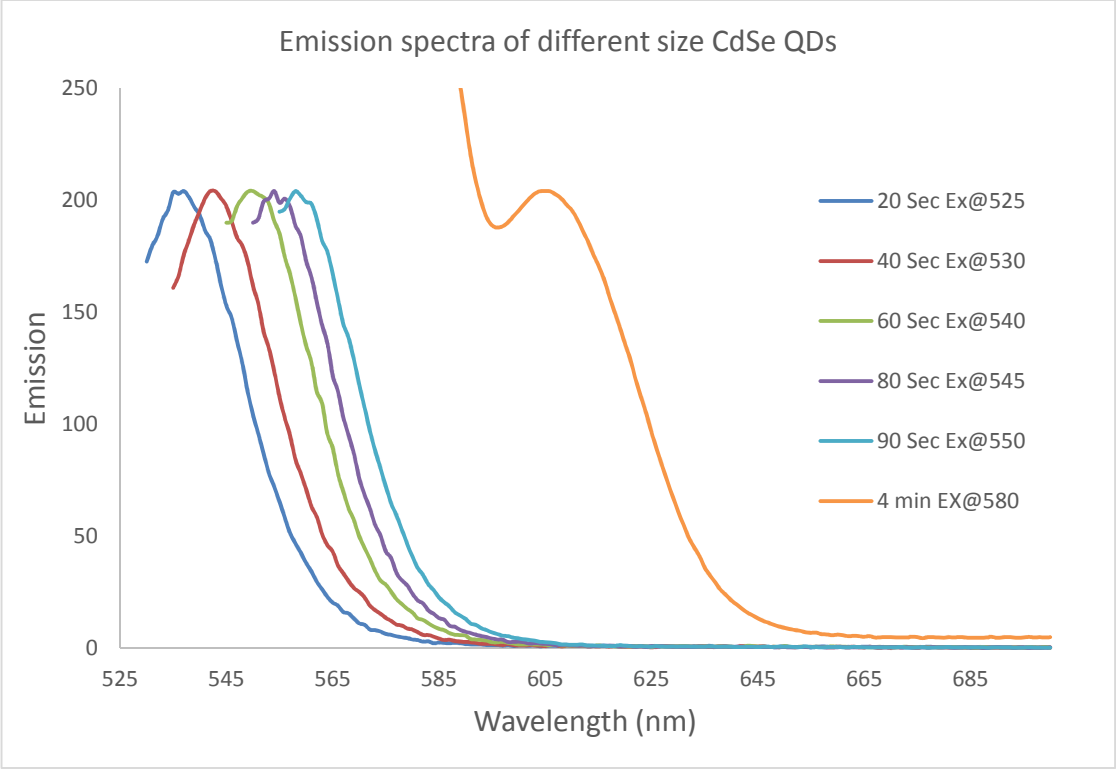

Figure 4.16. Normalized emission spectra of different size CdSe quantum dots synthesized at different reaction times.

Emission spectra of CdSe quantum dots are shows in Figure 4.16. The increase in particle size caused a red-shift of the emission λ_{max}. The largest size quantum dots that we synthesized at reaction time 4 min emits florescence around 605 nm. The emission band of the largest CdSe quantum dot is beyond the absorbance limit of 13 nm and 25 nm GNP. Moreover, when placing in the hotspot of the aggregated GNP, they can receive the scattering of combine plasmon. Thus we picked this largest size CdSe core and coated with ZnS shell to gain structural stability and photostability. Adding ZnS shell resulted in further red-shift of the emission of CdSe-ZnS core-shell quantum dots to 620 nm, and the size was measured to be 7 nm.

Organic fluorophores exhibit narrow absorption peaks that partially overlap its emission peak because of the small Stokes shift. Therefore it is difficult to separate the excitation and emission effects. However semiconductor quantum dots have a broad absorption range while reserving a narrow emission range. This enables us to excite the quantum dots at different wavelengths and spectrally decouple the excitation and emission effects. This contrast with organic fluorophores makes quantum dots more attractive towards studying the fluorescence enhancement. Figure 4.17 displays constant narrow emission spectra of 7 nm CdSe-ZnS QD at 620 nm when excited between 425 – 600 nm.

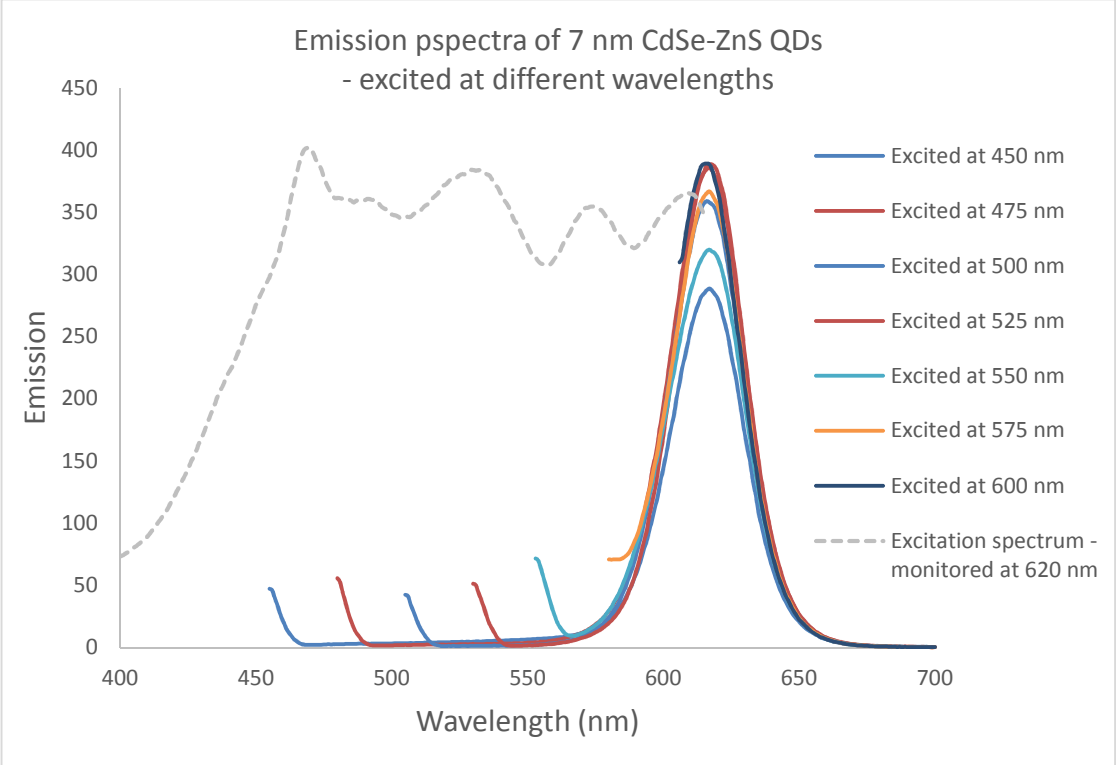

Figure 4.17. Emission spectrum of 7 nm CdSe-ZnS QDs, when excited at different wavelengths.

The broad excitation spectrum between 425 - 610 nm of 7 nm size CdSe-ZnS quantum dots can comfortably comprise the scattering spectrum of 23 nm GNP. Also when placed at the plasmonic hotspot of GNP aggregates, the QD's excitation can be amplified by the enhanced scattering (610 – 620 nm) of GNP aggregates, that in turn can produce fluoresce enhancement. The yellow band in Figure 4.18 represents the enhanced scattering from aggregates of GNP and SiNP. Also the emission λ_{max} of 7 nm CdSe-ZnS quantum dots is beyond the major absorbance peak of GNPs, so it can prevent the fluorescence quenching due to far-filed energy transfer.

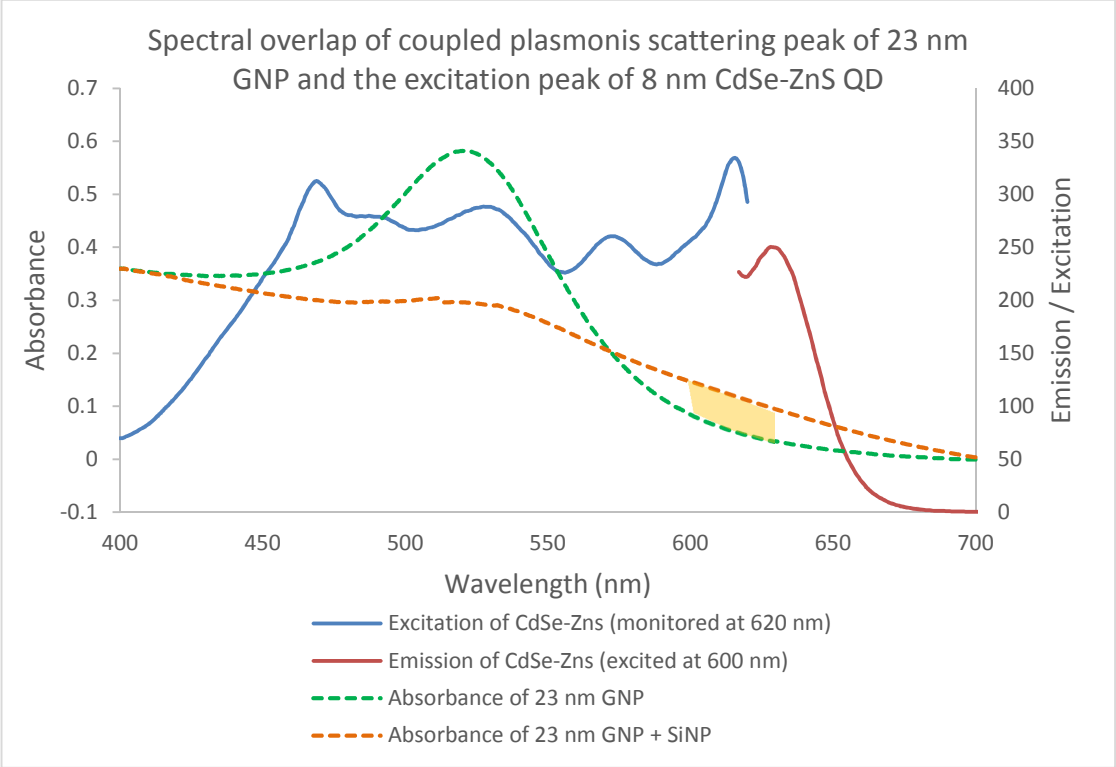

Figure 4.18. Spectral overlap of 7 nm CdSe-ZnS quantum dots and 23 nm gold nanoparticles

Different sizes of gold nanoparticles and CdSe-ZnS quantum dots were synthesized to investigate their spectral overlap in order to achieve maximum fluorescence enhancement. GNP of 23 nm diameter, upon aggregation to SiNP showed increased scattering around >600 nm. CdSe-ZnS quantum dots of 7 nm possess a broad excitation band between 425 – 610 nm and a constant narrow emission band at 620 nm. Since these particular sizes of GNPs and QDs hold the optimal spectral overlap, we selected that to proceed with further aggregation studies down the path to metal-enhanced fluorescence.

4.3.2 Investigation of gold nanoparticle and silica nanoparticle aggregation effect on fluorescence intensity

We investigated the effects of aggregation of gold nanoparticles to quantum dot incorporated silica nanoparticles via organic linkage in order to produce metal-enhanced fluorescence. QD-doped-silica nanoparticles (SiNPs) were constructed by coating a silica layer on CdSe-ZnS quantum dots using a microemulsion method, followed by growth of additional layer of silica using a seeded silica re-growth method. Although one purpose of adding a silica layer is to improve water solubility of the quantum dots, it also acts as a spacer between the fluorophore and metal surface. Construction of 45 nm thick silica layer around the 7 nm CdSe-ZnS quantum dot brought about 100 nm diameter to the silica nanoparticles. QD-doped-silica nanoparticles were thoroughly washed in dialysis process before coating with (3-aminopropyl)triethoxysilane (APTES) ligand. Presence of APTES on the surface of SiNP was confirmed using ninhydrin test. Then CS_2 was added to the SiNP-APTES solution at pH = 8.5 to form dithiocarbamate (DTC) terminals. Finally 400 μL of citrate capped GNP solution was added to 100 μL of the SiNP-propyl-DTC solution. Figure 4.19 is the schematic representation of aggregation of GNPs to the DTC functionalized SiNP.

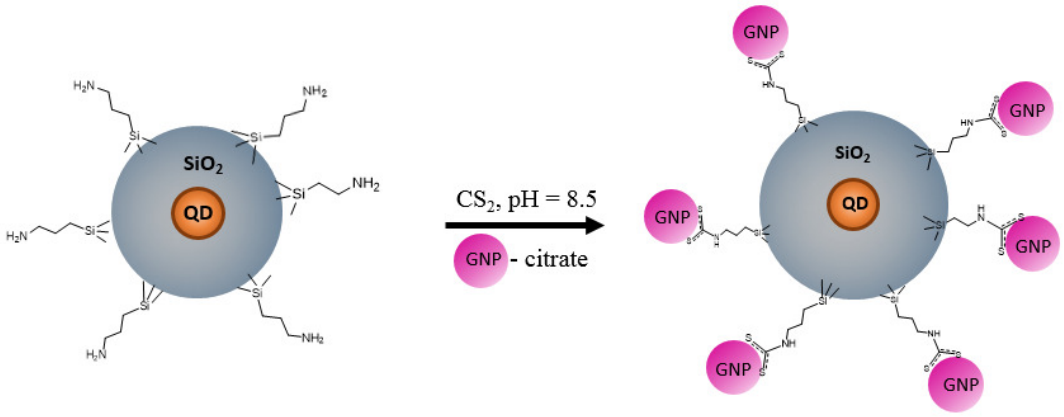

Figure 4.19. Schematic illustration of multiple gold nanoparticles aggregated to propyl-DTC tethered silica nanoparticles.

Figure 4.20 shows the absorbance spectra recorder at 6 h after mixing the GNPs and DTC functionalized SiNPs. These spectra are dominated by the gold absorbance curves as the solutions contain only trace amount of silica nanoparticles. Thus the control contains only SiNP-propyl-DTC (purple line) is featureless due to masking by the overwhelming higher concentration of GNPs in the samples, but this effect will be taken into consideration with the emission spectra. The addition of GNP to the solution of SiNP-propyl-DTC has a clear aggregation compared to the controls. A shoulder appeared at ~ 650 nm correspond to the GNP aggregation can be seen in the sample (blue line). Also the decrease in concentration of unbound GNP is evident from the decrease in absorbance around 550 nm. Remarkably and not surprisingly, the control that has no APTES (red line) but just GNP and SiNP with CS_2 doesn't show any aggregation.

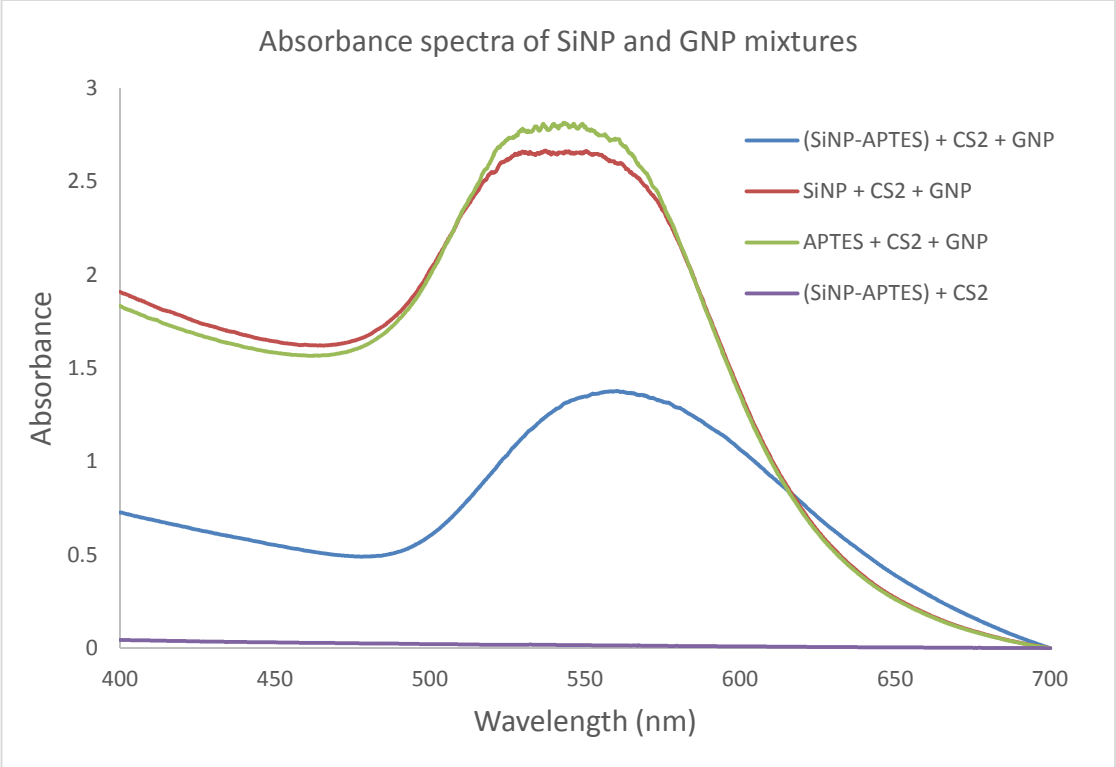

Figure 4.20. Absorbance spectra provides evidence to the aggregation of GNP to DTC functionalized SiNP. The shoulder at ~650 nm (blue line) shows the increased plasmonic scattering from the aggregated GNP.

The heteroaggregation of gold nanoparticles to the DTC functionalized silica nanoparticles was also evident from the TEM images and the photograph of the samples. The TEM image (Figure 4.21.a) clearly shows the heteroaggregation of multiple GNPs per SiNP in the presence of APTES and CS_2 and the cause for the increased scattering seen in the absorbance spectrum at ~ 650 nm (blue line). Also, the very less concentration of free GNP seen in the same TEM image accounts for the decreased absorbance at ~550 nm. The reason for unexpected fusion of silica particles was not yet clear. Figure 4.21.b corresponds to the control SiNP + CS_2 + GNP without APTES (red line in absorbance spectra) shows no heteroaggregation between silica and gold nanoparticles occurred.

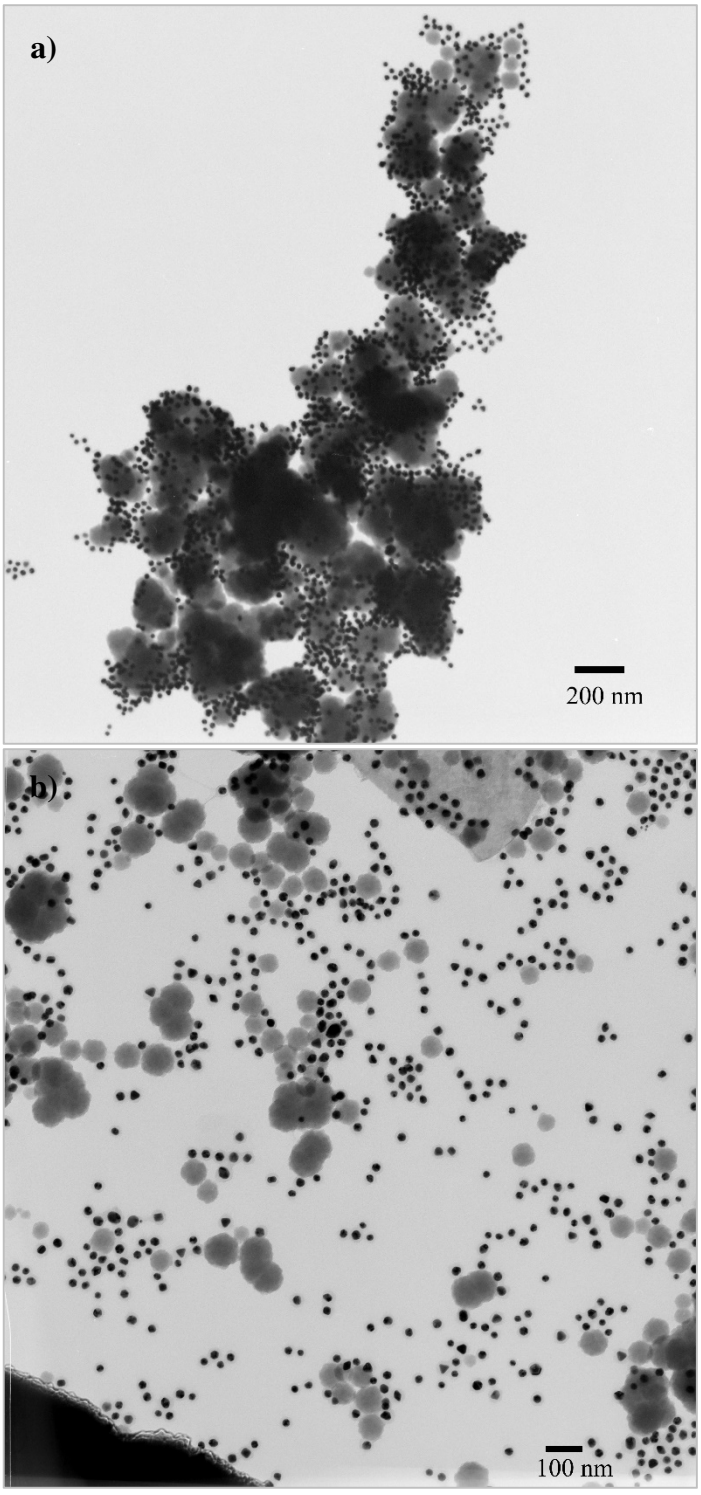

Figure 4.21. TEM images show a) heteroaggregation of multiple GNPs on silica nanoparticles in the presence of propyl-DTC, but b) no aggregation of GNPs on silica nanoparticles when there was no APTES (aminopropyl precursor).

The photograph of sample and controls (Figure 4.22) shows that when GNP was added to the solution of DTC functionalized SiNP, the color changed from pink (color of free GNP) to purple (color of aggregated GNP).

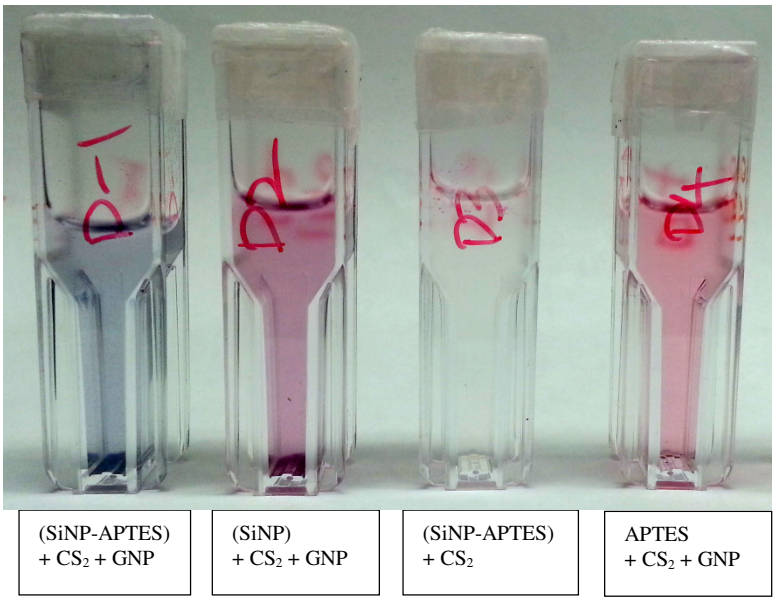

Figure 4.22. Photograph of sample and controls from aggregation study. Purple color of the sample (D-1) accounts for the aggregation of GNP to DTC-functionalized SiNP.

Fluorescence from the SiNP-GNP aggregates was recorded and it was originally dimmer than the SiNP controls because of the inner-filtering effect from gold nanoparticles (far-filed quenching). Gold nanoparticles are not fluorescent, but they are known for quenching and filtering fluorescence in several ways. Inner-filtering was a major problem in obtaining correct fluorescence data in our case. Primary and secondary inner-filtering are the artifacts associated with the extremely sensitive fluorescence spectroscopy. Hence correction for these inner-filtering artifacts was necessary to eliminate the effect of re-absorption by GNP.

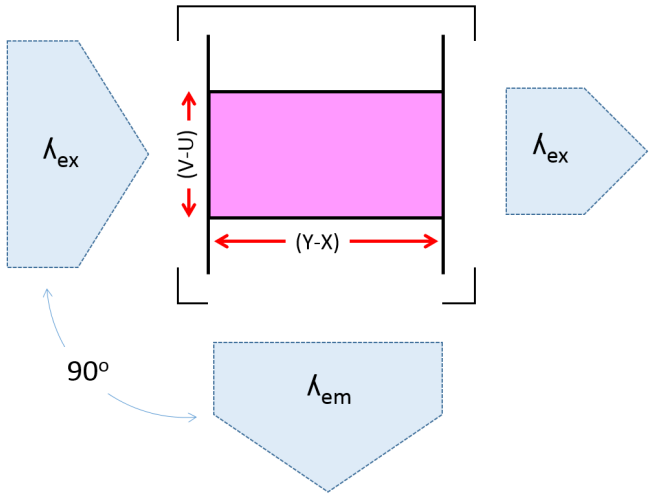

Figure 4.23. Typical cell configuration of right-angle fluorometry. Window parameters (Y-X) and (V-U) were determined by measuring the sides of the cuvettes.

The intensity of the fluorescence from SiNP-GNP aggregate sample can be affected by the GNPs blocking the excitation light (λ_{ex} = 575 nm) along the (Y-X) interrogation zone of the cuvette. This is called the primary inner-filtering effect. The intensity of fluorescence emitted by SiNP-GNP aggregates (λ_{ex} = 620 nm) at 90° angle can also be diminished by GNP re-absorbing the light along the (V-U) interrogation zone. This is called secondary inner-filtering effect. These artifacts can be corrected by following the procedure reported by Tucker et al., and as shown below.[23]

$$I_F^{corr} = f_{prim} \times f_{sec} \times I_F^{obs}$$

Where,

$$f_{prim} = I_F^{corr}/I_F^{obs} = [2.303\ A\ (Y - X)]\ /[10^{-AX} - 10^{-AY}]$$

I_F^{corr} = corrected emission signal

I_F^{obs} = observed emission signal

A = absorbance (b = 1 cm) at λ_{ex}

$$f_{sec} = I_F^{corr}/I_F^{obs} = [(V - U)\ (1/b) \ln T]/[T_{at\ V/b} - T_{at\ U/b}]$$

I_F^{corr} = corrected emission signal

I_F^{obs} = observed emission signal

T = transmittance (b = 1 cm) at λ_{em}

$T_{at\ V/b}$ and $T_{at\ U/b}$ are the transmittance values calculated using Beer's law. To apply the above correction factors, the length of the excitation and emission window of the cuvette was measure. It was found that (Y-X) is equal to 0.9 cm and (V-U) is equal to 0.4 cm. Detailed calculation is shown in the experimental section 4.5.2.

Figure 4.24 shows the inner-filtering corrected emission spectra of SiNP-GNP aggregate samples and controls. A significant 3-fold fluorescence enhancement for aggregates of GNP to DTC functionalized SiNP (blue line) compared to the SiNP control (purple line) was observed when excited at 575 nm. It is remarkable that we were able to produce metal-enhanced fluorescence in aqueous solution from the organic linker mediated heteroaggregation of GNP to QD-doped-SiNP.

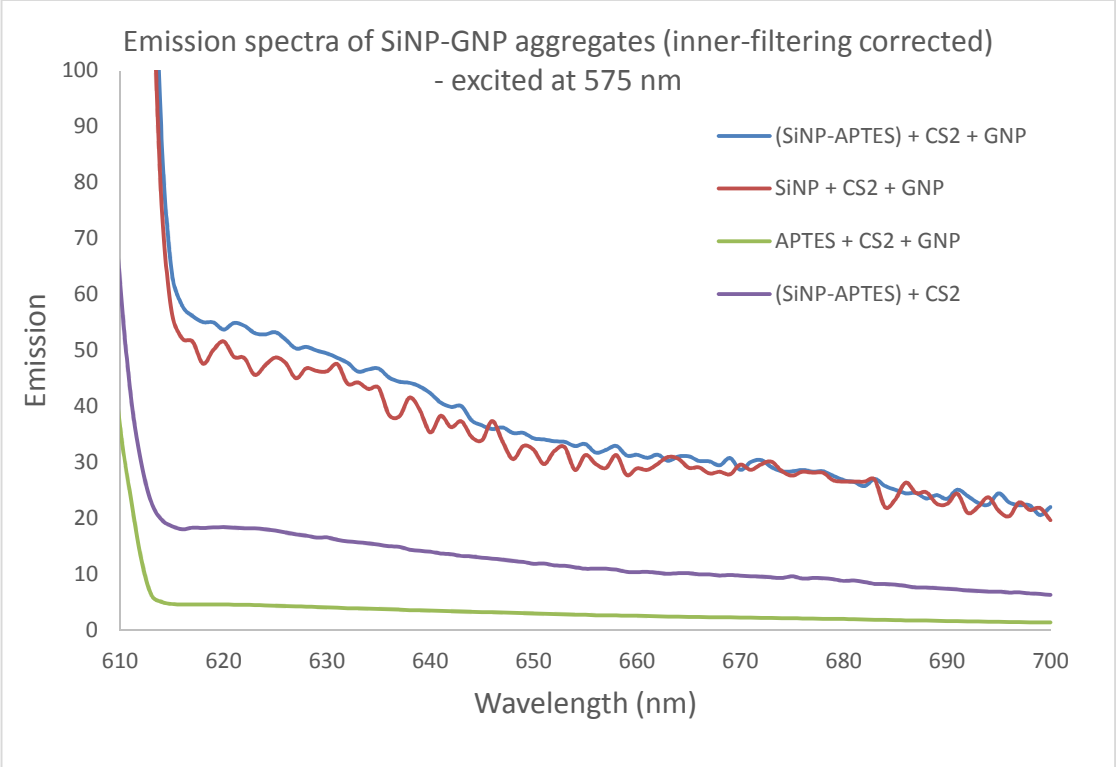

Figure 4.24. Emission spectra show the 3-fold florescence enhancement of SiNP-GNP aggregates compared to SiNP control.

It is a notable MEF for inorganic fluorophore (CdSe-ZnS quantum dots) that we observed for the first time in our lab. However the control with no APTES but just SiNP + GNP + CS_2 (red line) also shows similar enhancement. Figure 4.25 shows the comparison fluorescence enhancement of the sample and the controls, before and after inner-filtering correction. Considering that the excitation wavelength is 575 nm, this fluorescence enhancement at 620 nm may be possible by the interaction with uncoupled plasmonic resonance of gold nanoparticles. Higher concentration of free gold nanoparticles may account for this similar fluorescence enhancement (red line) in the control.

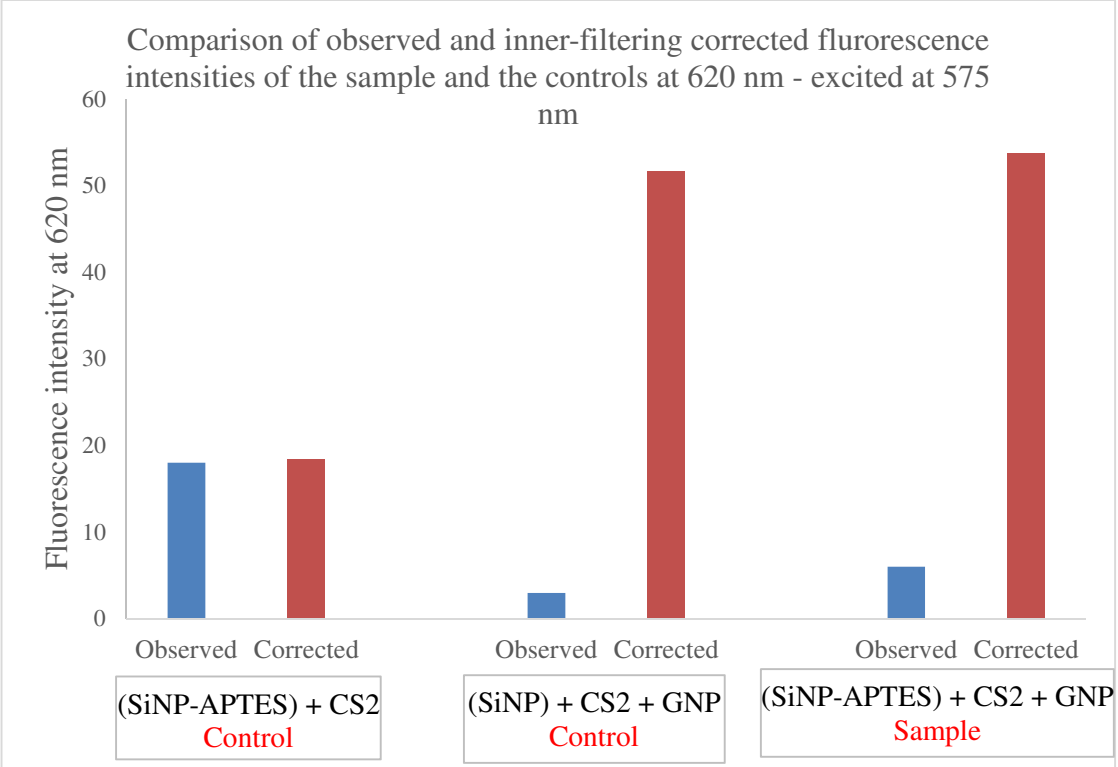

Figure 4.25. Comparison of fluorescence intensities show the 3-fold enhancement of SiNP-GNP aggregates relative to SiNP controls after inner filtering correction.

Figure 4.25 also shows that the inner-filtering correction increased the fluorescence intensity from the observed value up to 9 times for the sample and 17 times for the control with no APTES. Presence of higher concentration of free GNP may be the reason for the larger filtering effect in the control. This can be seen in the excitation spectra measured at 620 nm (Figure 4.26), where the relative fluorescence intensity of control is higher than that of the sample when excited at ~580 nm. The excitation spectra reflect the absorbance spectra. There is a clear connection between the addition of GNP to SiNP and the overall increase in fluorescence.

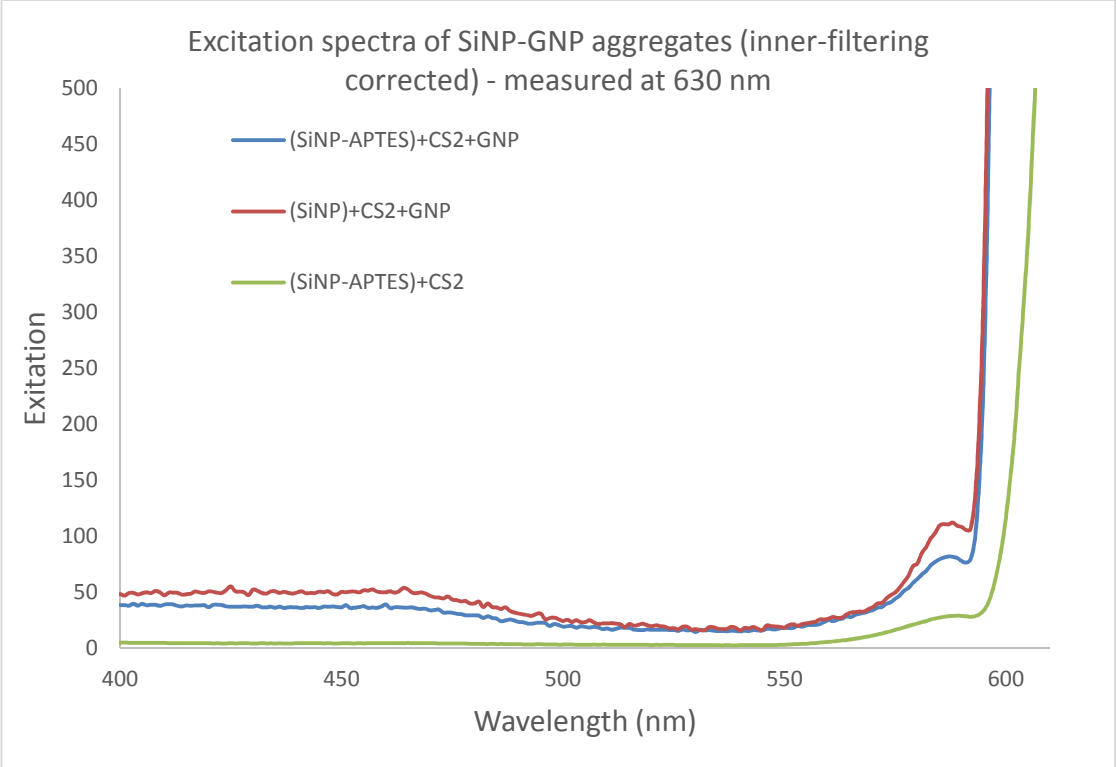

Figure 4.26. Excitation spectra of SiNP-GNP aggregates monitored at 630 nm

To avoid the effect of interaction with free GNP it is better to use an excitation wavelength beyond their absorbance limit. Also we can examine the effect of coupled plasmonic resonance by exciting the sample at 650 nm, where the scattering due to aggregation is most pronounced in the absorbance spectrum. But emission spectra (Figure 4.27) shows an unexpected drop in fluorescence (blue line) for the sample containing aggregates of GNP to SiNP-propyl-DTC. It is not immediately clear what causes this decrease in intensity, but we assumed that any undesired quenching (near field) may be occurring within the sample. Figure 4.28 show the comparison of fluorescence intensity at

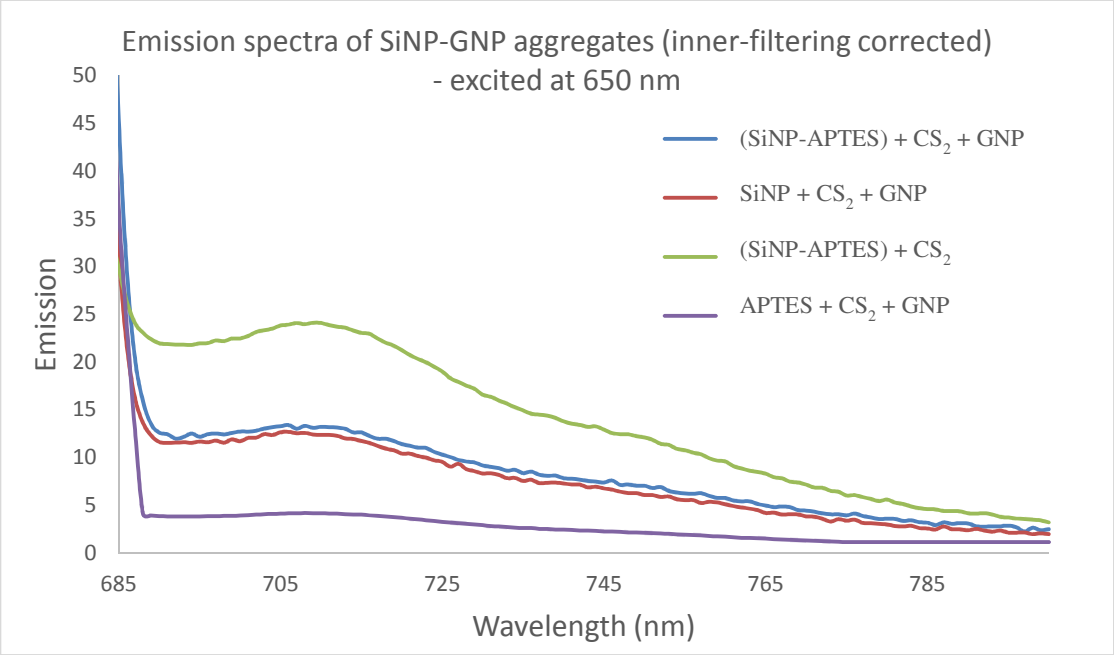

Figure 4.27. Emission spectra show the decrease in fluorescence of SiNP-GNP aggregates compared to the SiNP control.

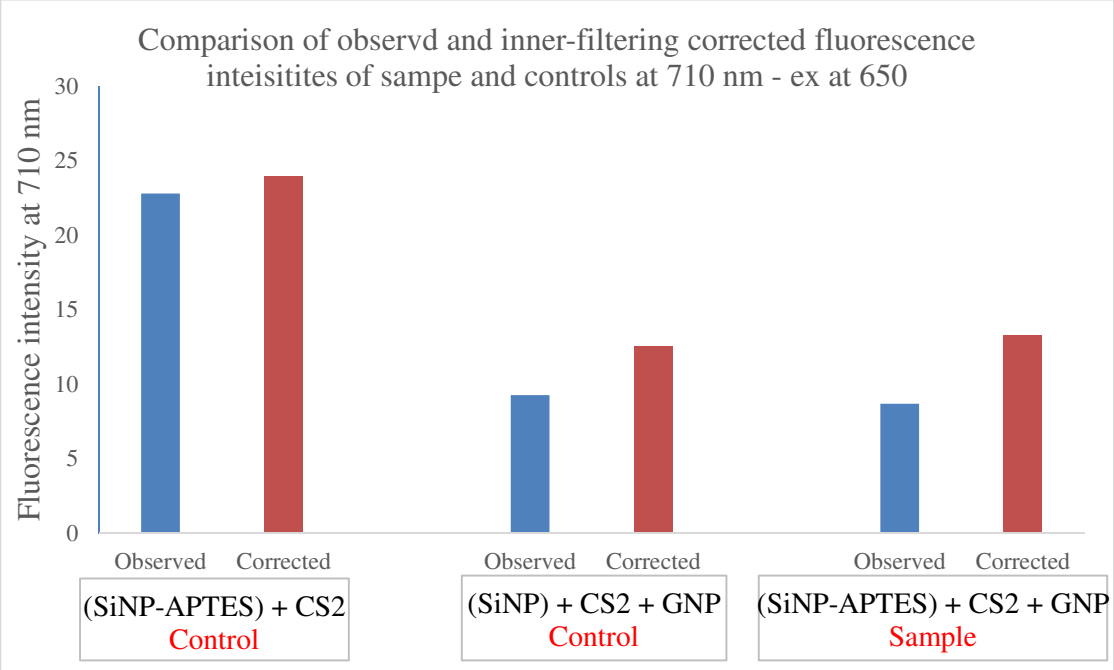

Figure 4.28. Comparison of fluorescence intensities show decrease in fluorescence of SiNP-GNP aggregates relative to SiNP controls even after inner filtering correction.

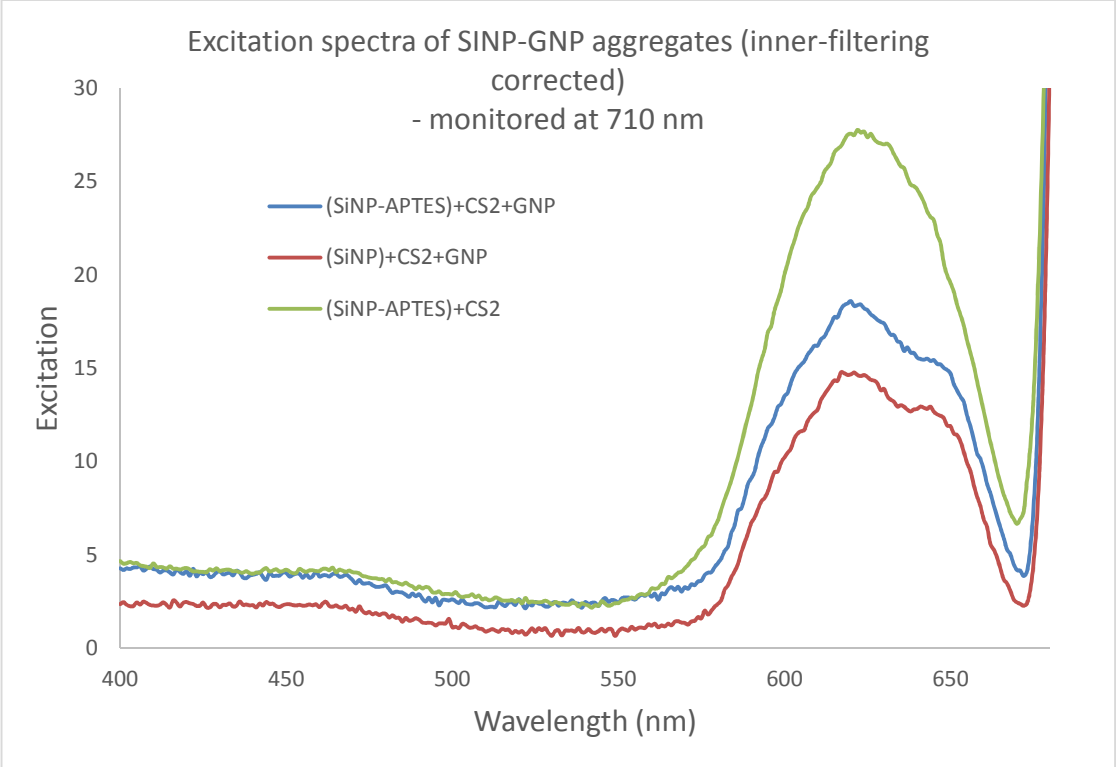

Figure 4.29. Excitation spectra of SiNP-GNP aggregates monitored at 710 nm show shoulder peaks around 650 nm

It is interesting to note that the excitation spectra of the sample (blue line) and the control (red line) containing SiNP and GNP clearly show a shoulder at ~ 650 nm, which is absent for the control (green line) that has no GNP. The taller excitation peak at ~ 620 nm accounts for the direct excitation of CdSe-ZnS quantum dots. The shoulder at ~ 650 nm matches with the scattering peak from coupled plasmonic resonance of GNP aggregation. It is promising to see the clear connection between GNP aggregation and the structure of excitation/emission spectra, although no fluorescence enhancement from coupled plasmonic resonance was observed.

4.3.3 Investigation of relative concentration effect between silica nanoparticles and gold nanoparticles on fluorescence intensity

To further promote the fluorescence enhancement, we investigated the fluorescence from various relative concentration of GNP to SiNP. Since the size of GNP (23 nm) is smaller than the SiNP (100 nm), the increase in relative concentration of GNP to SiNP was expected to promote the heteroaggregation. Binding more number of GNPs on the surface a SiNP would increase the excitation events for CdSe-ZnS quantum dots that are encapsulated in the SiNP. For this study we prepared propyl-amine coated QD-doped-SiNPs using previously described method. The solution was diluted to very low concentration in order to clearly quantify any difference in percentage of enhancement. In the sample preparation, various amount of SiNP-propyl-amine solution (50 μL, 100 μL, 200 μL, 400 μL) in ethanol was taken in four different cuvettes. Then 1M concentration CS_2 (20 μL) was added and the pH was raised to 8.5 by adding KOH solution. Then cuvettes were capped and rotated for 30 min for DTC activation. After 30 min, 400 μL of a highly concentrated GNP (citrate capped) solution was added to each samples. The final volume was raised to 1 mL by adding milipore water. One set of controls were prepared by adding SiNP without propyl amine coating and another set of controls were prepared by replacing GNP with ethanol-water. The samples were rotated for 6 h before measuring the absorbance and fluorescence. The TEM samples were prepared the fluorescence measurements.

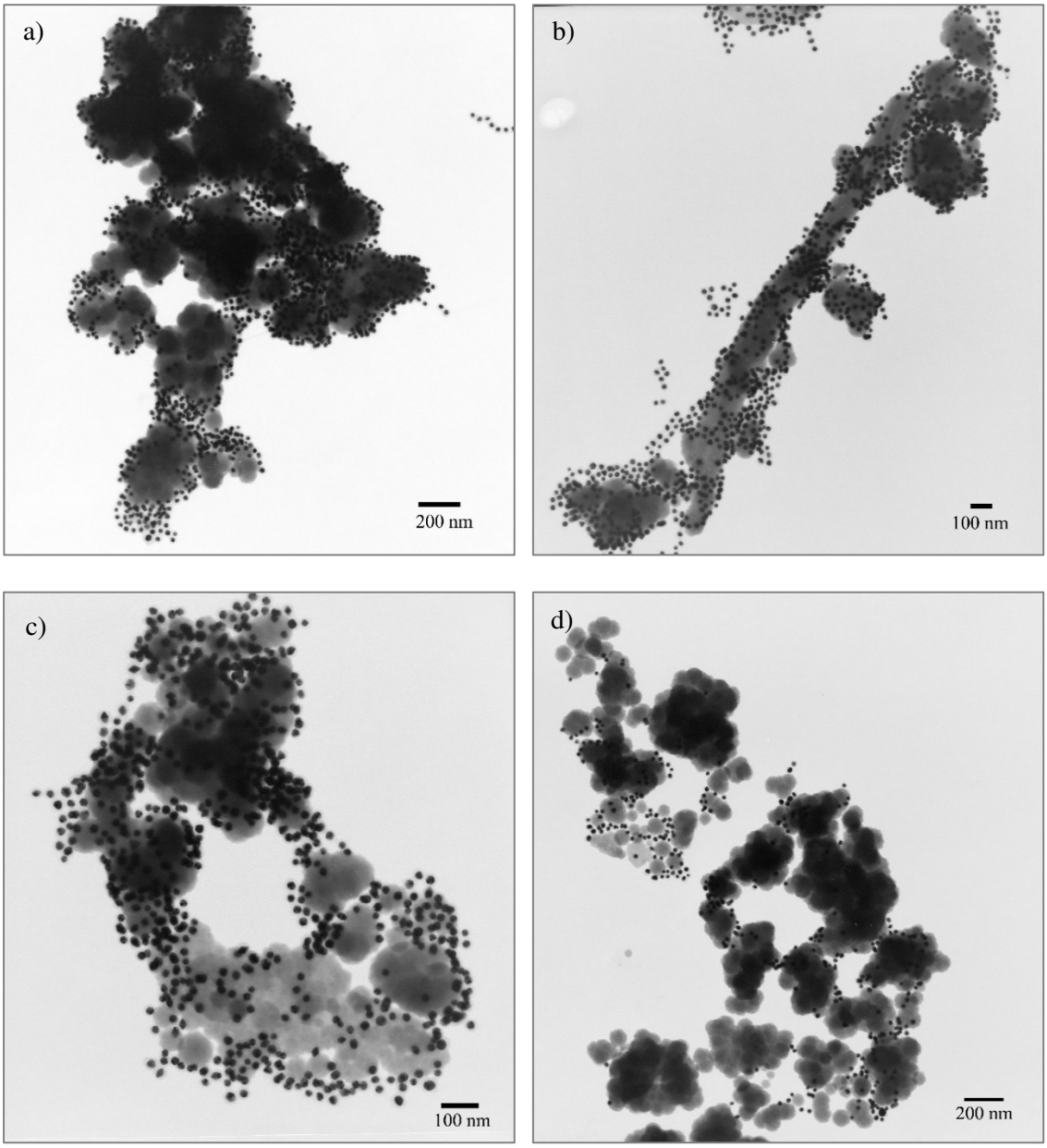

Figure 4.30. TEM images of SiNP-GNP aggregates. TEM samples were prepared at 6 h after the addition of a) 50 µL b) 100 µL c) 200 µL d) 400 µL of SiNP-propyl-DTC solutions to constant amounts of GNP solution.

TEM image (Figure 4.30.a) for the sample containing higher relative concentration of GNP to SiNP shows higher degree of aggregation. Whereas the sample containing lower relative concentration of GNP to SiNP indicates lower number of GNPs aggregated on the surface of SiNPs (Figure 4.30.d). But in all cases, it is optimistic to see very low concentration of unbound gold nanoparticles and that ensures the possibility of robust heteroaggregation via propyl-DTC linker. But undesirably the silica nanoparticles were fused together to form clusters, that may not help each SiNP gets access to the GNPs. Nevertheless the absorbance spectra were all good.

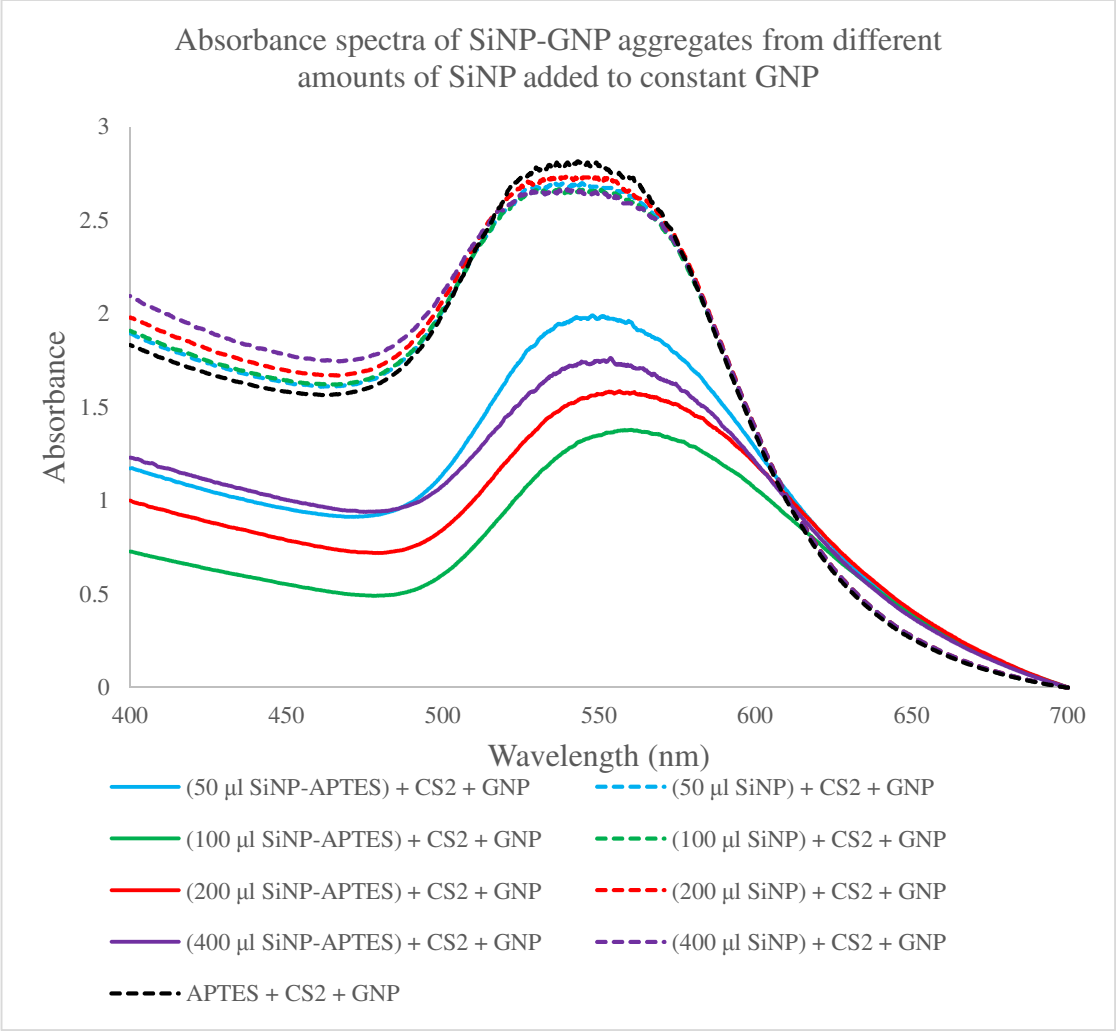

Figure 4.31. Absorbance spectra of SiNP-GNP aggregates via propyl-DTC linkage from various relative concentration of GNP to SiNP and the controls.

Absorbance spectra taken at 6 h indicates a clear heteroaggregation of GNP to SiNP for all samples that contain propyl-DTC linker (solid lines). The shoulder at ~650 nm corresponds to the coupled plasmonic resonance is seen only for the samples but not for the controls (broken lines). The decrease in absorbance at ~550 nm accounts for the decrease in concentration of free GNPs in all samples, and also evidence for the heteroaggregation.

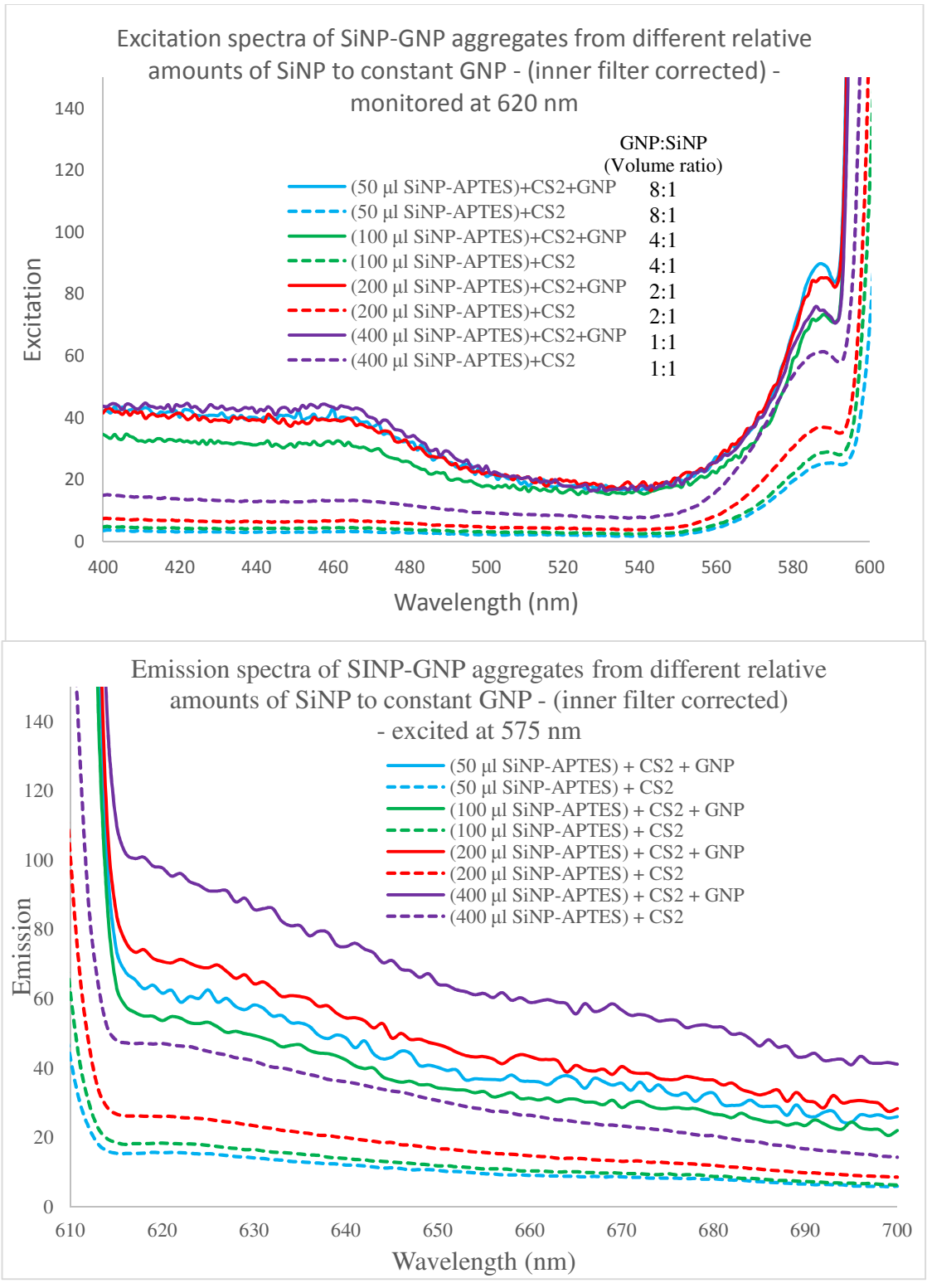

Figure 4.32. Emission and excitation spectra of SiNP-GNP aggregates via propyl-DTC linkage from various relative concentration of SiNP to GNP.

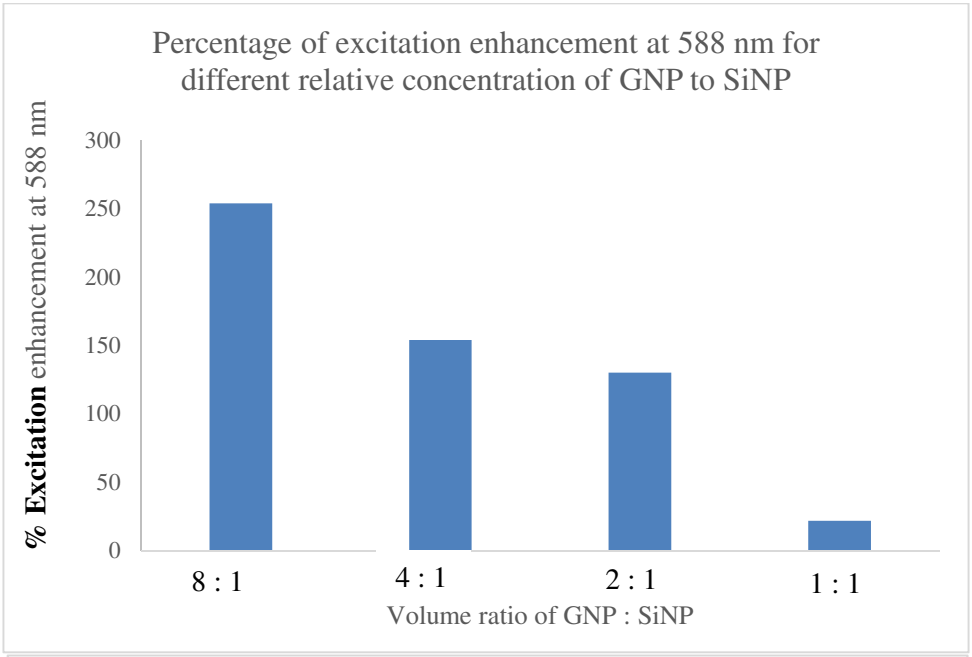

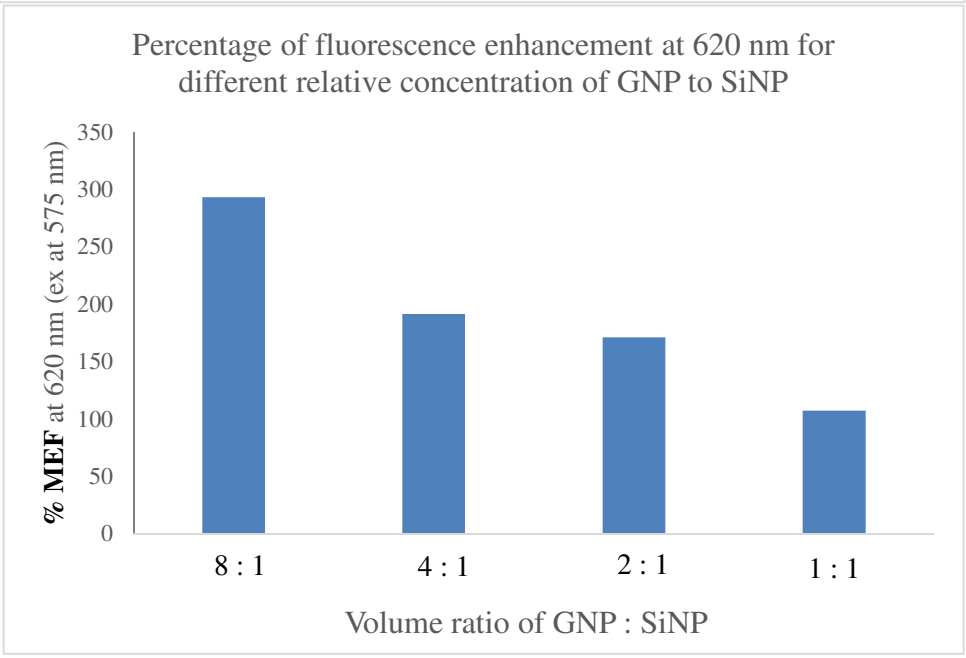

Figure 4.33. Percentage of metal-enhanced fluorescence and percentage of excitation from aggregates of different relative amounts of GNP to SiNP

Examination of the emission and excitation spectra (Figure 4.32) indicates that the fluorescence enhancement is possible by interaction of multiple GNPs with fewer

QD-doped-SiNP. That bar graphs (Figure 4.33) show that fluorescence and excitation enhancement has a proportional relationship with the relative amount of GNP to SiNP in the solutions. As anticipated the increase in concentration of gold nanoparticles within the sample increased the metal-enhanced fluorescence. A 3-fold (or 294%) fluorescence enhancement for 8:1 volume ratio of GNP:SiNP was observed. This enhancement more or less gradually decreased to 1-fold (or 107%) enhancement for 1:1 volume ratio of GNP:SiNP. This trend of increase in fluoresce brightness with increase in GNP:SiNP ratio matches with the trend in excitation spectra and the degree of aggregation seen in TEM images, which verifies that the MEF seen in the emission spectra is not an artifact. The reason for enhanced excitation and emission events should be due to the increase in number of metal-fluorophore nanoparticle aggregates.

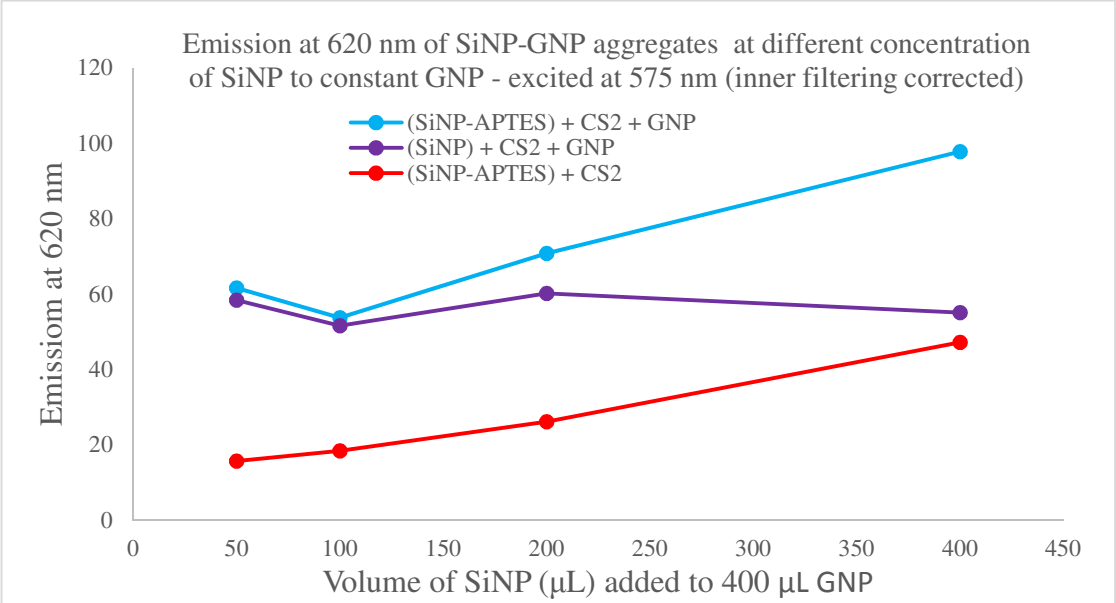

Figure 4.34. Emission at 620 nm against various amounts of SiNP to constant GNP

It is also significant to consider the enhancement from the controls that contains no ATPES, but just SINP + GNP + CS_2 solution (purple line in Figure 4.34). The purple line in the above chart indicates that the SiNP and GNP mixture without APTES linker

also shows similar enhancement with a higher concentration of GNP in the solution. This indicates that the enhancement may also be possible with SiNP interacting with the higher concentration of free GNP in the solution. But this interaction may not be possible for the lower concentration of GNP near the SiNP. It is interesting to see the % enhancement drastically drops (purple line) with the decrease in ratio of GNP:SiNP in the solution. Thus the fluorescence enhancement for 1:1 volume ratio of GNP to SiNP-propyl-DTC, even though it is less, it could be purely from the GNP aggregated on the surface of QD-doped-SiNP.

4.3.4 Investigation of effect of silica nanoparticle size on fluorescence intensity of SiNP-GNP aggregates

We investigated smaller diameter (35 nm) silica nanoparticles as a means of adjusting the distance between the CdSe-ZnS quantum dot and the surface of metal in order to measure the metal-enhanced fluorescence. The smaller silica nanoparticles were prepared by growing 14 nm think silica layer around the 7 nm size quantum dot using microemulsion method. The silica particles were thoroughly washed in dialysis process before functionalizing the surface with amines and then DTC. Then 400 µL of highly concentrated gold nanoparticle solution was added to 50 µL of SiNP-propyl-DTC. Then TEM samples were prepared 6 h after the mixture and images were recorded to examine the extent of aggregation and especially the number of GNPs to a SiNP.

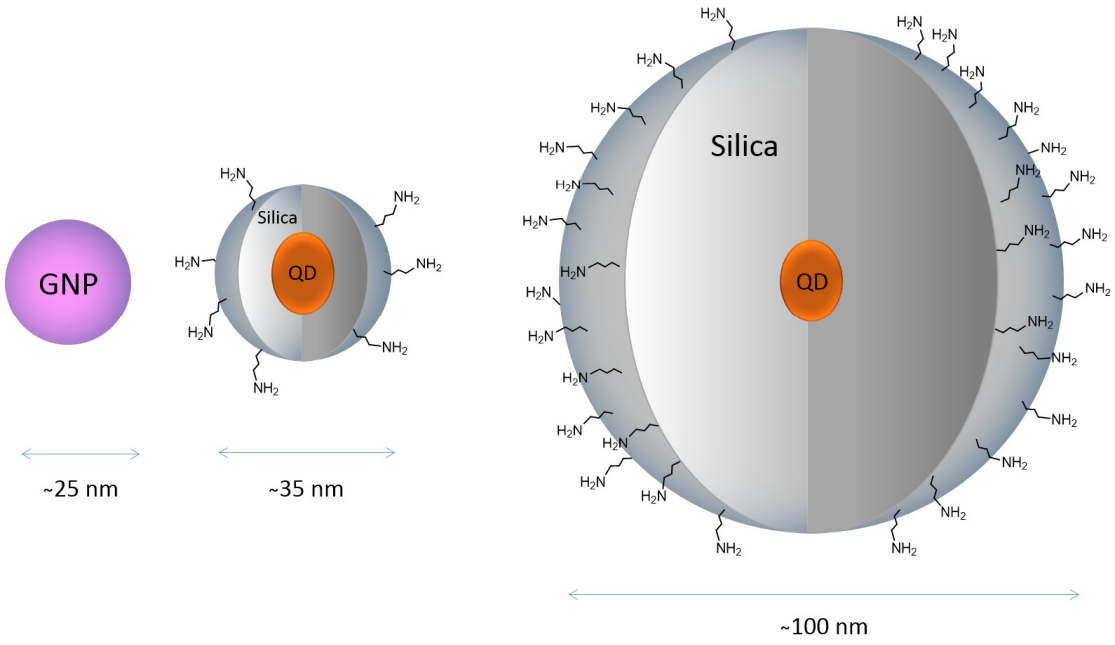

Figure 4.35. Size comparison of GNP (~25 nm), and QD-doped-SiNP with propyl amine coating (~35 and ~100 nm)

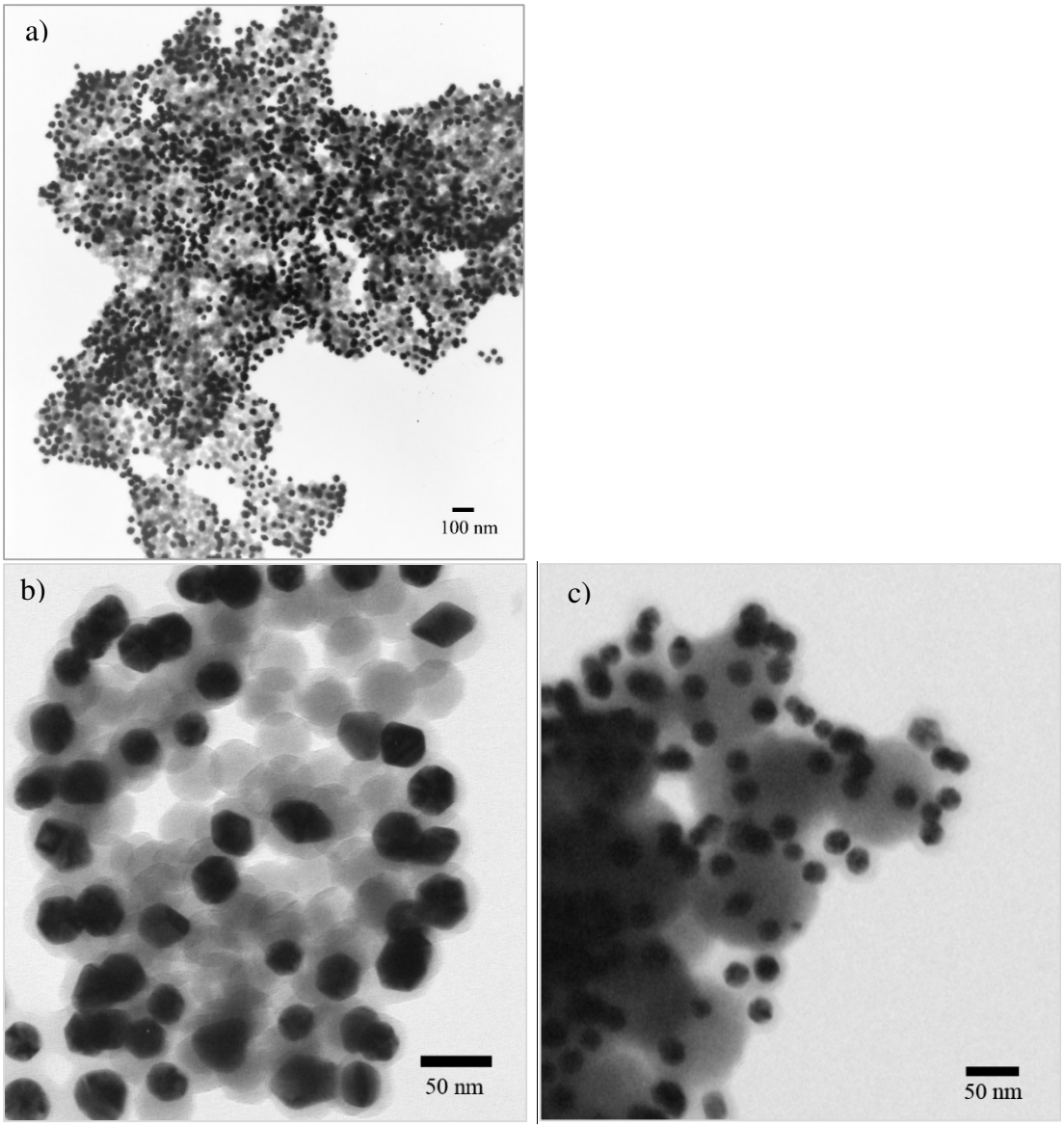

Figure4.36. TEM images show aggregates of 25 nm GNPs to 35 nm SiNPs (a) and (b), and 100 nm SiNP (c).

It is interesting to see the robust aggregation of 25 nm GNPs to 35 nm SiNPs in the TEM image (Figure 4.36.a). But as anticipated the number to GNPs aggregated per 35 nm SiNP is less compared to 100 nm SiNP. The smaller surface area of the 35 nm SiNP accommodates not more than one or two GNPs, as clearly seen in the magnified

TEM image (Figure 4.36.b). But the larger SiNP accommodates significantly more number of GNPs (Figure 4.36.c) to aggregate on its surface.

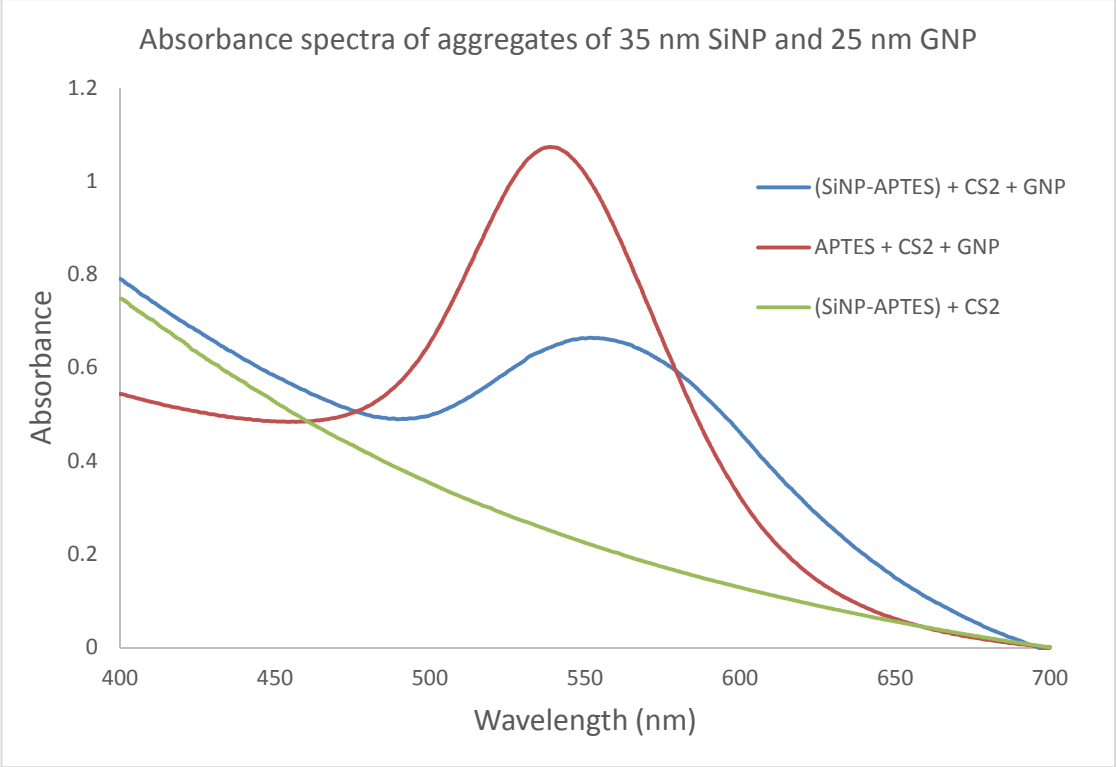

Figure 4.37. Absorbance spectra show coupled plasmon scattering (~620 nm) for the aggregates of 25 nm diameter GNP and 35 nm diameter SiNP.

The above absorption spectra show an increased scattering at >590 nm (blue line) for the sample containing 35 nm SiNP-propyl-DTC and 25 nm GNP. The change in scattering profile of the sample matches with its TEM image. The robust aggregation of GNPs to SiNPs accounts for the increased scattering at >590 nm and the low concentration of free GNPs within the sample supports the overall loss of scattering at ~550 nm. Note that the absorbance curves of the sample and controls are once again dominated by the overwhelming concentration of GNPs. The green line for the control containing only SiNP doesn't show any notable absorbance curve because of very low concentration of QD-doped-SiNP in the solution.

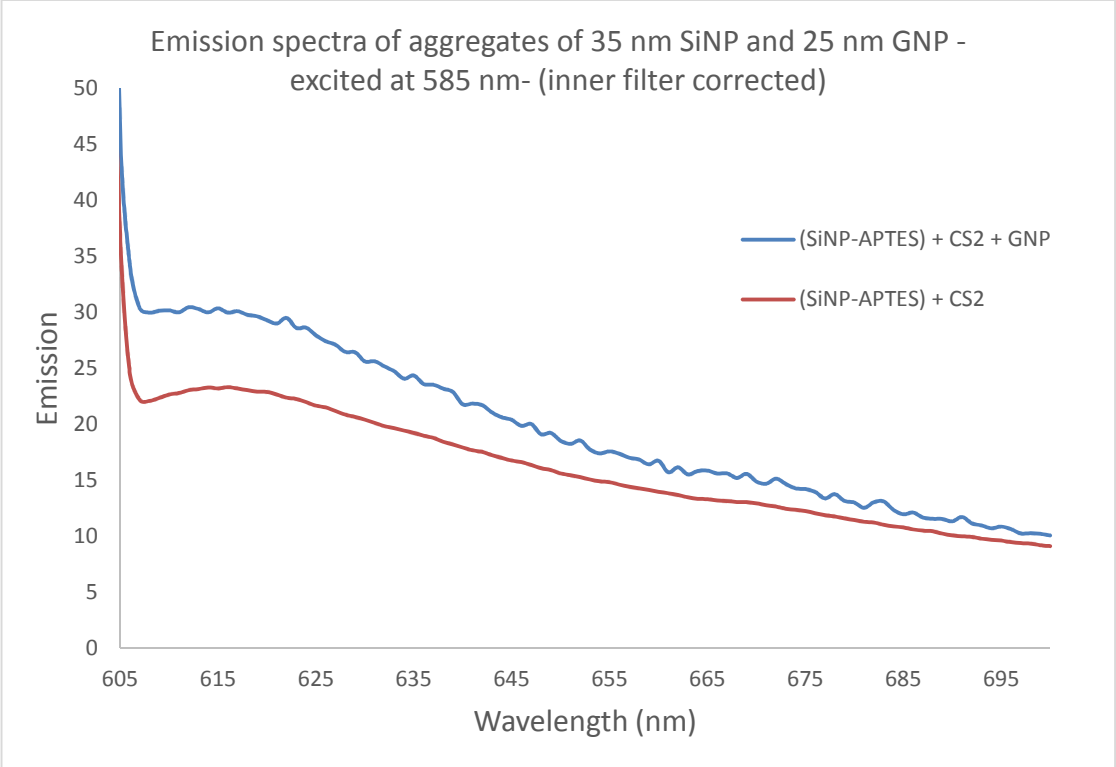

Figure 4.38. Emission spectra show slight increase in fluorescence brightness for aggregates of 35 nm SiNP and 25 nm GNP.

The emission spectra were recorded in order to investigate the effect of change in thickness of silica shell on the degree of aggregation and changes in the fluorescence brightness of CdSe-ZnS quantum dots encapsulated in the SiNP. The samples demonstrate a slight increase in fluorescence intensity as seen in previous experiments. The blue line in emission spectra corresponds to the sample with SiNP-propyl-DTC and GNP aggregates is notably raised from the control that has no GNP. However, we were unable to directly compare the fluorescence intensities from 35 nm and 100 nm SiNPs because of the difference in concentration caused by the difference in particle sizes.

The effect of distance between fluorophore and metal surface on the fluorescence enhancement was well investigated by many researchers and by our lab mates Nathan Green and Kalani Gunawardana. It was known that placing a fluorophore

within the range of 0.5 - 200 nm from a metal surface would promote MEF. But there was no previous report of optimal distance for inorganic fluorophores such as CdSe-ZnS quantum dots. For organic fluorophores, because of their molecular sizes, the distance between the fluorophore site within the molecule and metal surface can be precisely measured. But for the inorganic fluorophores such as our CdSe-ZnS quantum dots with 7 nm diameter, the distance could only be measured from the center of the QD to the surface of the GNP. For the two different size SiNPs (35 nm and 100 nm diameter) that we prepared, the distances between the center for QD core and the surface of GNP are 17.5 nm and 50 nm respectively. In Figure 4.39 we compared the percentage fluorescence enhancement caused by the different size SiNP particles when aggregated to 25 nm GNPs. It is apparent that the 100 nm SiNP produce 10 times more fluorescence enhancement than the 35 nm SINP. But apart from the effect of distance, the effect of number of participating GNPs should also be considered. The larger surface area of 100 nm SiNP affords significantly more number of GNPs to aggregate on and gives 3-fold (294%) fluorescence enhancement, whereas the 35 nm SiNP gives only 0.3 fold (28%) enhancement.

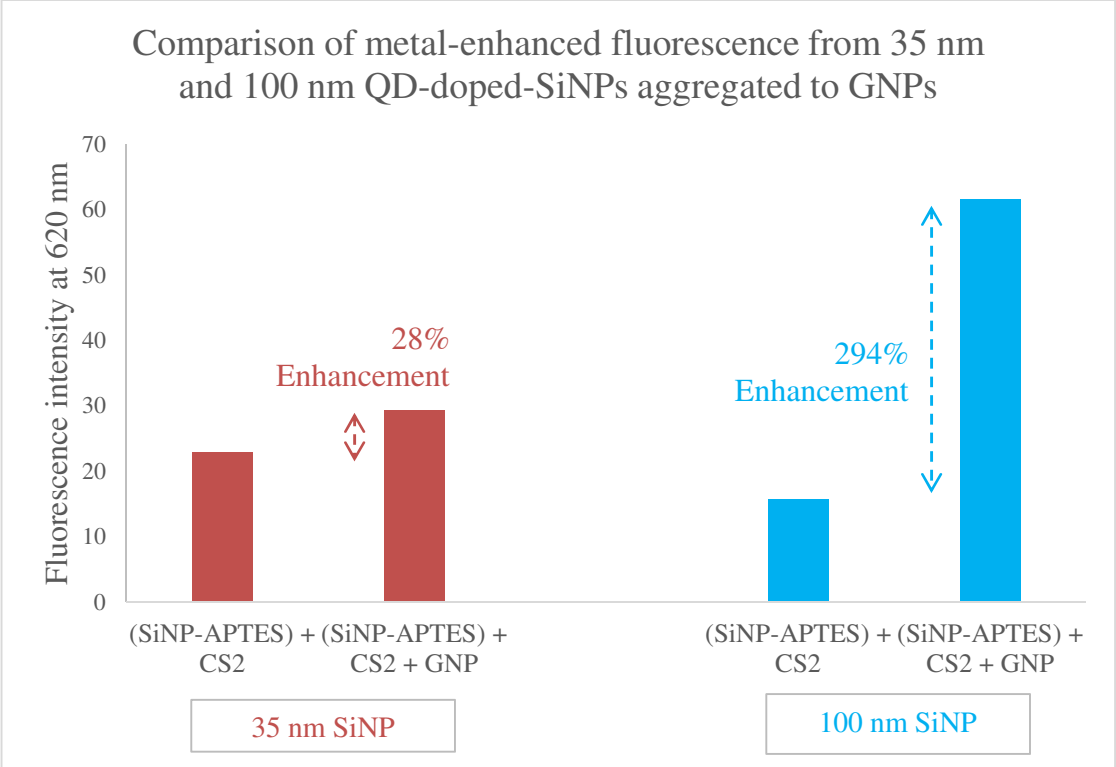

Figure 4.39. Comparison of gold-enhanced fluorescence of 35 nm diameter SiNP and 100 nm diameter SiNP.

The excitation spectra from aggregates of 35 nm SiNPs and 25 nm GNPs (Figure 4.40) show that maximum fluorescence brightness (at 620 nm) was recorded with the excitation light of 590 nm. At this wavelength the plasmonic scattering of aggregated GNPs is more than that of free GNP. Hence, from the absorbance and the excitation spectra we can say that the coupled plasmonic resonance from aggregated GNP contributed for the observed MEF.

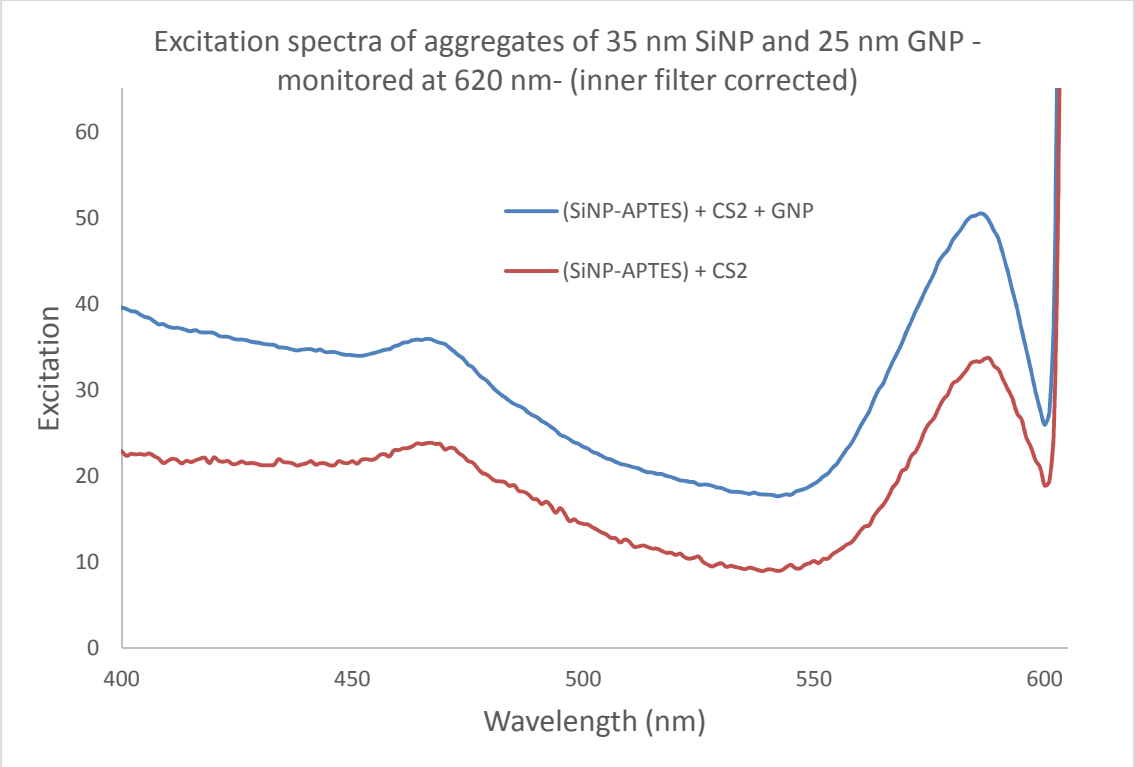

Figure 4.40. Excitation spectra monitored the fluorescence intensity of 35 nm SiNP and 25 nm GNP aggregates (at 620 nm) indicates the major contribution of 590 nm light.

4.3.5 Investigation of effect of linkage between silica nanoparticles and gold nanoparticles on fluorescence intensity

We investigated the effect of a different organic linker on the degree of heteroaggregation and the fluorescence enhancement. Also we attempted to fuse the quantum dots and the gold nanoparticle in silica clusters order to measure any change in the enhancement that was previously observed for propyl-DTC linkage.

Coating long-chain ether on gold nanoparticle increased the water stability and prevented the homoaggregation of GNPs (Chapter 2). This longer and more stable ether ligand on gold nanoparticles are theoretically difficult to displace with the short propyl-DTC ligand on silica nanoparticles. Nathan Green from our lab reported the difficulties in promoting the silica-gold aggregation because of the inability of the shorted propyl-DTC ligand on the surface of silica nanoparticles to interdigitate with the long chain ether surrounding the gold nanoparticle.[16] He also observed the rate of aggregation was slow as the ether displacement by propyl-DTC was a kinetically disfavored approach. Because of this reason we examined the effect of coating a longer chain DTC ligand on silica particle to overcome the distance restrictions of the shorter ligands. We synthesized and coated a long chain tetraethylene glycol (TEG) siloxane derivative on silica nanoparticles. The longer chain tether consisted of a modified TEG skeleton with a propyl siloxane precursor attached to one end and amine on the other end to form dithiocarbamate moiety. Figure 4.41 show the synthetic scheme of the long chain tethered SiNP and aggregation to water stabilized GNP.

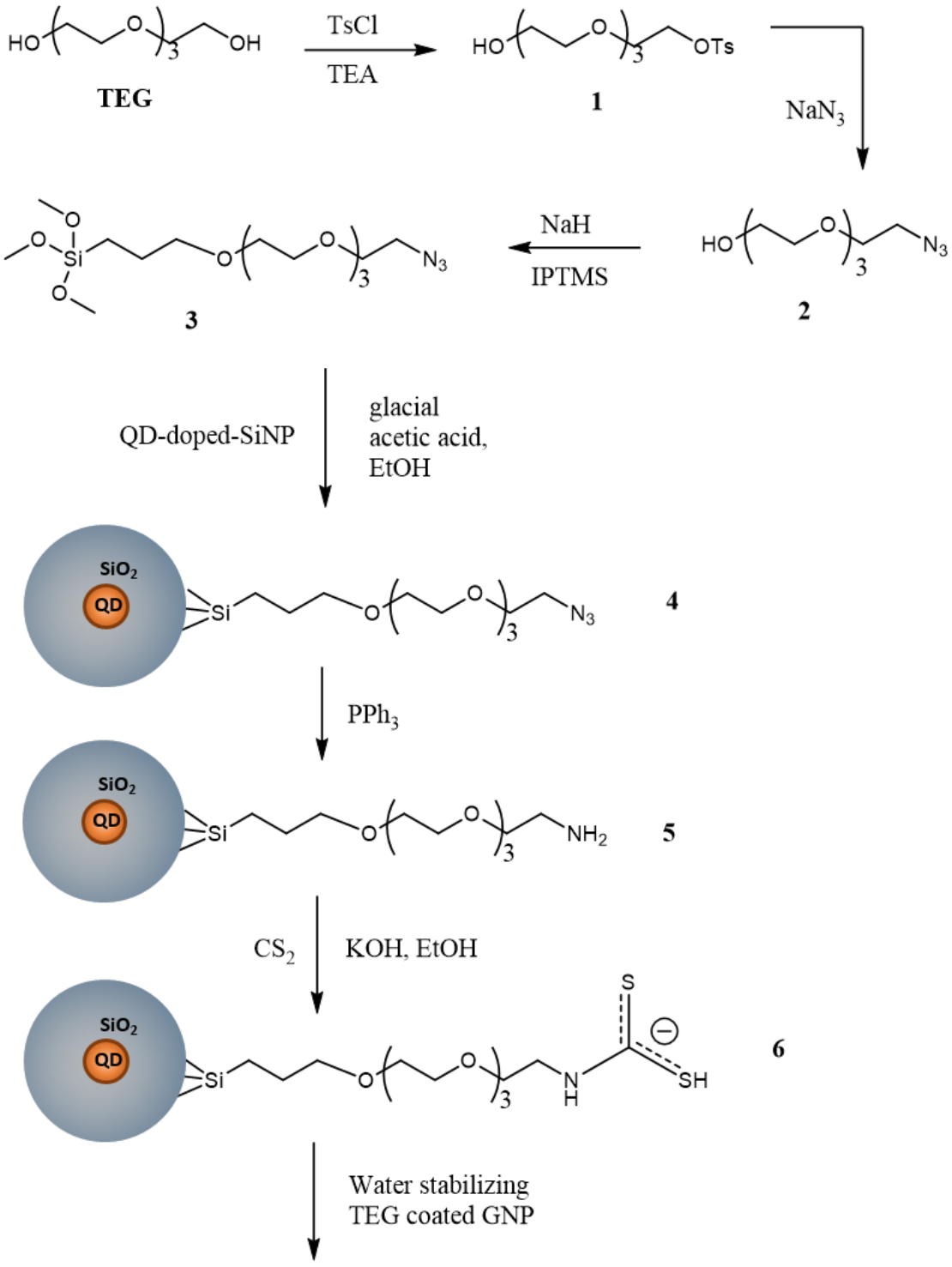

Figure 4.41. Synthetic scheme to produce long chain TEG tethered SiNP and its aggregation to water stabilizing ligand tethered gold nanoparticles.

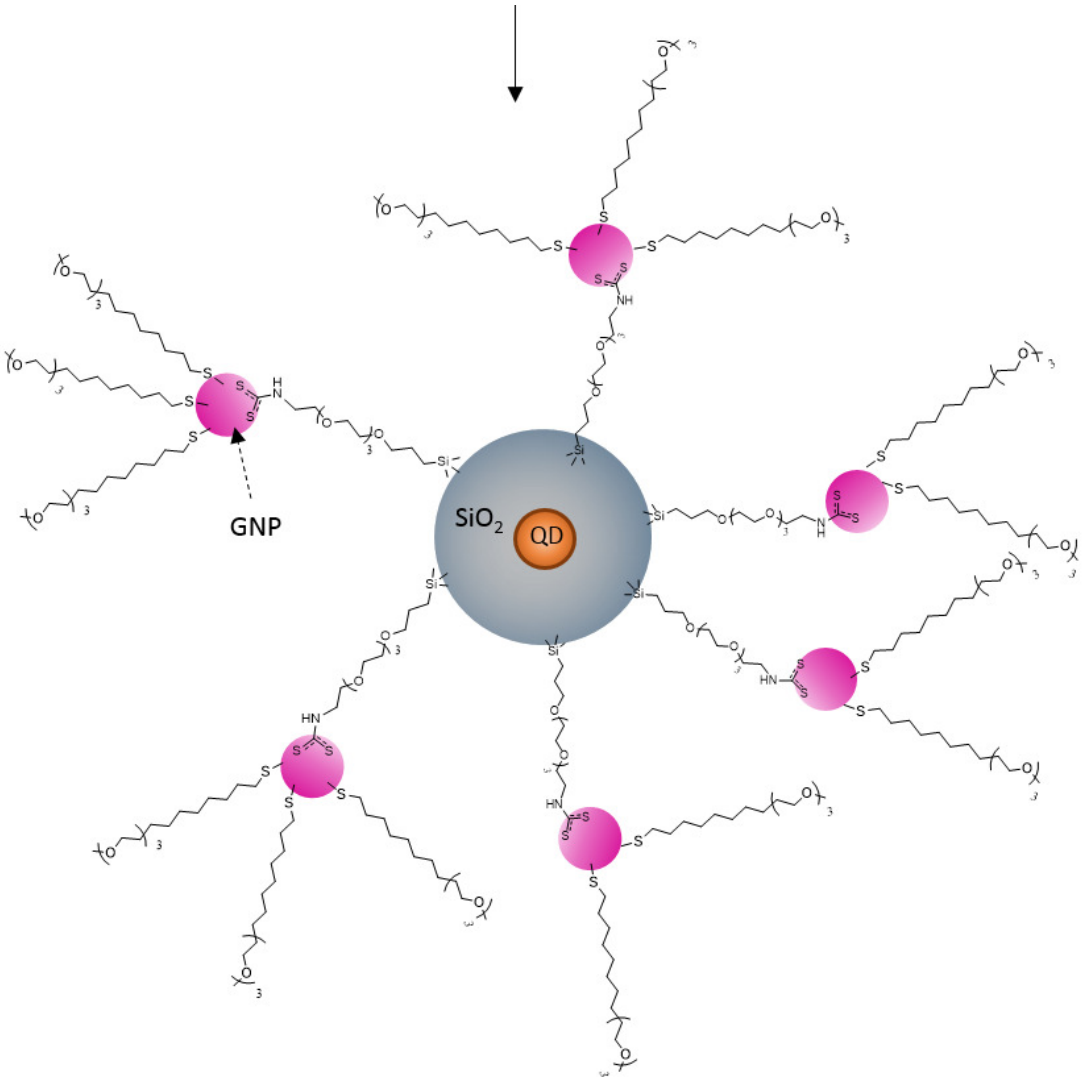

Figure 4.41.cont. Synthetic scheme to produce long chain TEG tethered SiNP and its aggregation to water stabilizing ligand tethered gold nanoparticles.

Monotosyl-TEG **1** was prepared by monotosylation of tetraethylene glycol and purified by column chromatography. Then the tosyl group was converted into azide by reacting with sodium azide. The azide-TEG **2** was carried out without further purification to substituted with siloxane precursor **3** by nucleophilic substitution of (3-iodopropyl)trimethoxysilane (IPTMS). The siloxane was sensitive to air and water, so without further purification **3** was condensed onto the surface of 100 nm QD-doped-SiNP by acid hydrolysis.

The azide terminal was then converted into amine via Staudinger reaction to produce amine functionalized QD-doped-SiNP **5.** The particles were washed multiple times with water and ethanol. The presence of amine on SiNP was confirmed by ninhydrin test. Then a portion of amine-functionalized SiNP sample was take for DTC activation by adding CS_2 at pH 8.5 before mixing with TEG capped gold nanoparticles. TEM samples were prepared 24 h after the mixture of SINP and GNP solutions.

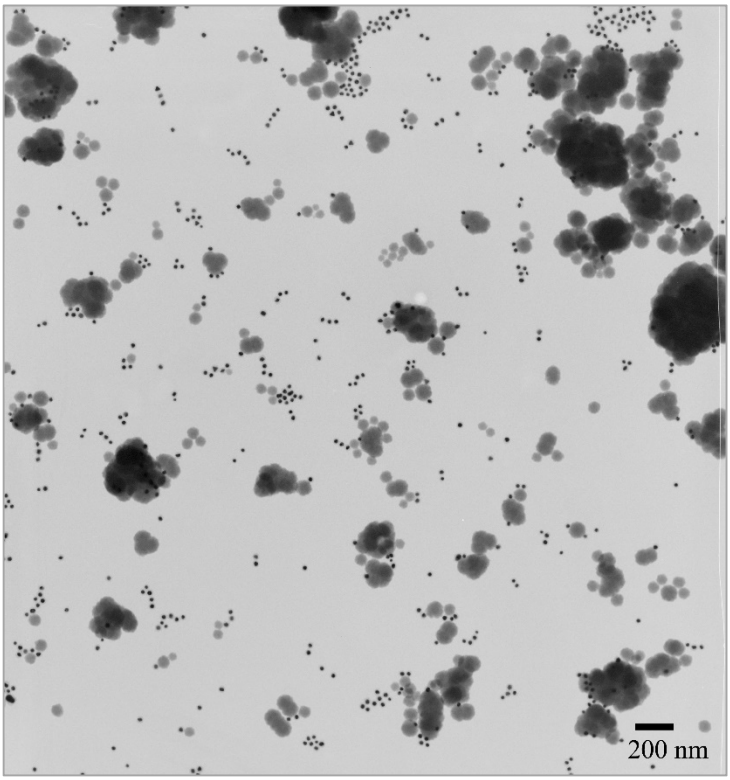

Figure 4.42: TEM image of the mixture of SiNP-TEG-DTC and GNP-TEG

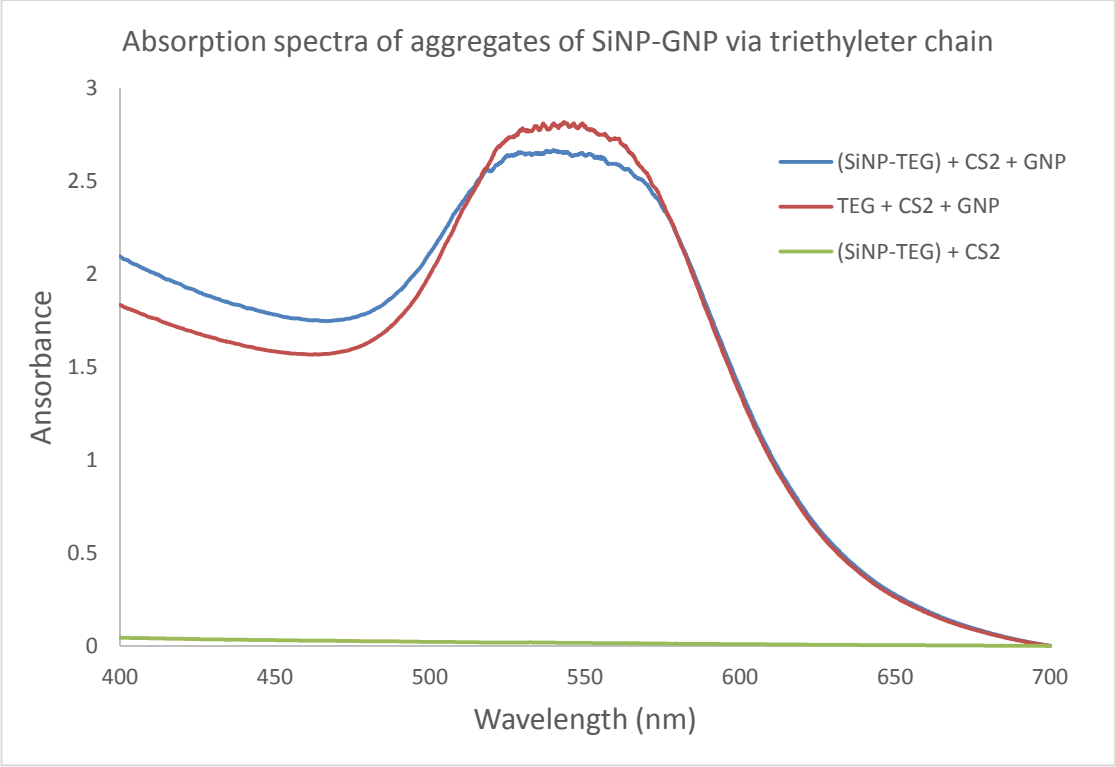

Figure 4.43. Absorbance spectra of SiNP-GNP aggregates via longer chain TEG-derived ligand.

TEM image of the sample shows no significant heteroaggregation of SiNP to GNP via the longer organic liker. It is not immediately clear what interrupted the aggregation. The above absorption spectra of the sample doesn't show the increase in scattering at > 600 nm that was previously observed from the heteroaggregation of SiNP-GNP via propyl-DTC ligand. Long chain TEG derived ligand on SiNP was expected to be a better replacement of shorter APTES in order to overcome the distance restrictions with aggregation to GNP coated with water stabilizing ether-thiol. But the heteroaggregation using long chain DTC ligand was not accomplished so far.

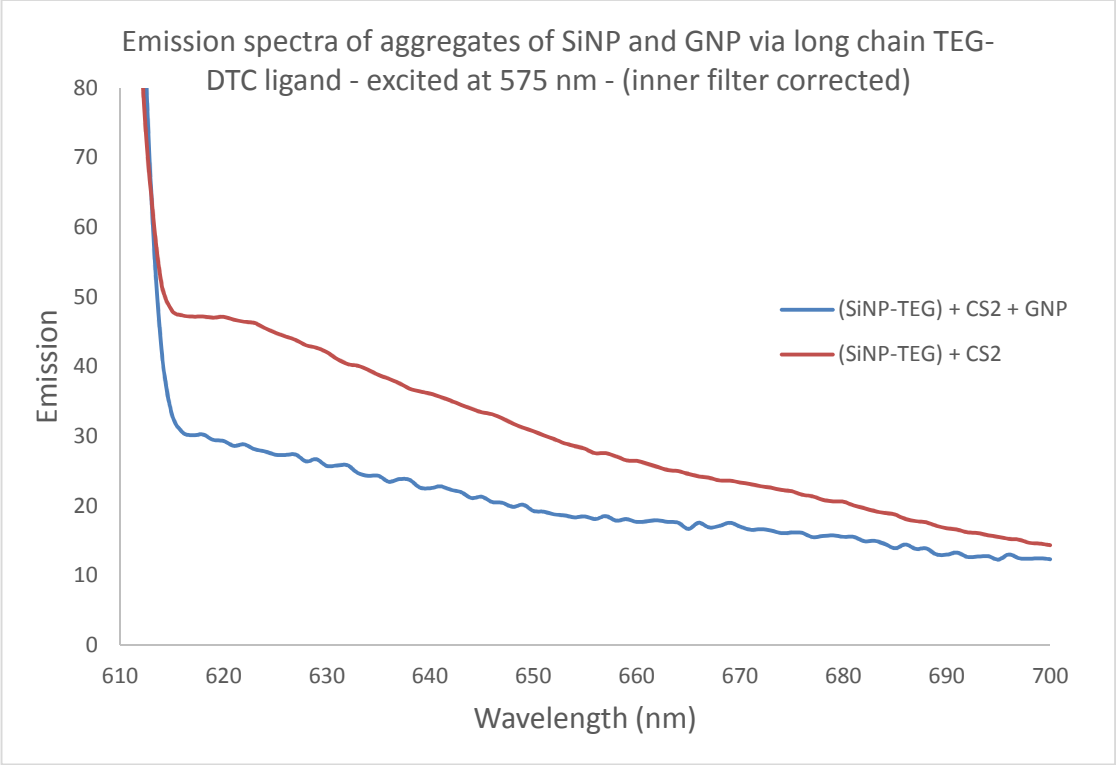

Figure 4.44. Emission spectra of SiNP-GNP aggregates via longer chain TEG-derived ligand.

Not surprisingly the emission spectra shows a drop in emission of SiNP-GNP aggregates from the SiNP only control sample. The lower emission intensities indicates that there may be a quenching (near filed / far field) from the high concentration of highly water stabilized free GNPs. In our attempt to reproduce the metal-enhanced fluorescence, that was previously seen for propyl-DTC mediated SINP-GNP aggregates, using a longer organic linker, we faced the symptoms of poor heteroaggregation.

In our effort to bring the fluorophore and metal nanoparticles close to each other in solution phase, we applied various linkers and spacers to bind the particles. Here we investigated the efficiency of silica to fuse the quantum dots and the gold nanoparticles

in a cluster. Replacing the organic linkers with silica would lose the advantage of controlled aggregation, but it is worth to see any change in fluorescence enhancement.

We used two methods to prepare the silica cluster that encapsulates both quantum dots and gold nanoparticles. In the first method we used modified reverse microemulsion technique by Darbandi et al., to co-encapsulate the QD and GNP in SiNP in a single pot. Briefly, to a mixture of CdSe-ZnS quantum dots and IGEPAL 520 surfactant in cyclohexane, tetraethylorthosilicate (TEOS) was added and stirred vigorously for 30 min to form microemulsion. Then gold nanoparticles was added under vigorous stirring. Finally ammonium hydroxide was added to convert TEOS into amorphous silica polymer around QD and GNP. The volume ratio of QD to GNP was 1:4 in the mixture. After 20 h of stirring at room temperature acetone was added to break the microemulsion, and the particles were cleaned by washing with 1-butanol, isopropanol and ethanol and finally dispersed in milipore water. TEM images were recorded to see the effectiveness of this single pot reverse microemulsion method to co-encapsulate QD and GNPs in amorphous silica. Figure 4.45.a illustrates the anticipated geometry of the SiNP. But the TEM image of the sample (Figure 4.45.b and c) shows that there was no definite structure of silica particles with QD and GNP incorporation, but seen a large mist of silica with GNPs glued to it. In the preparation process, though we formed microemulsion around the QD seeds before adding GNP, the position of QD was uncertain from the TEM images. Thus the uniformity of distance between QD and GNP was unfixed.

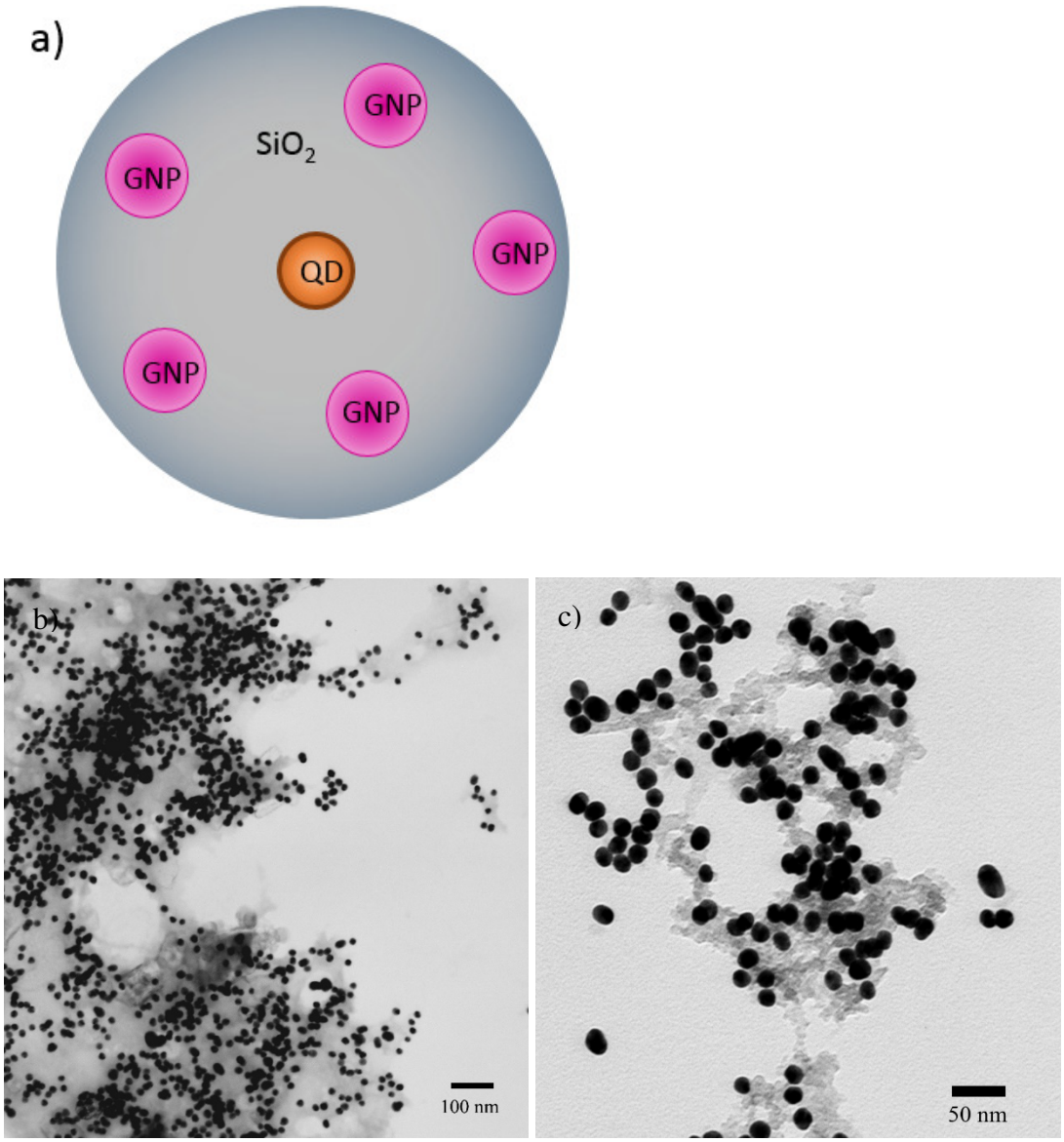

Figure 4.45. Schematic illustration of QD and GNP co-encapsulated in SiNP prepared in a single pot microemulsion method (a) and the TEM images of the sample (b and c).

Absorbance spectra (not shown) of the single pot reverse microemulsion SiNP preparation exposed an increased scattering at >600 nm, which supports the aggregation of GNPs seen in the TEM images. But emission spectra (not shown) were not promising. There was a substantial drop in the fluorescence intensity, may be due to the

poor dispersion of QDs in the sample. To overcome this inability of controlled silica growth to bind QD and GNP together, we used a different method of forming silica.

Coating QD with silica before adding GNP would grant the co-encapsulation of QD and GNP in larger silica particle. For our second method, we prepared well-ordered capsules of silica nanoparticles with QD cores using reverse microemulsion method as described previously. The particles were thoroughly washed in dialysis process and dispersed in water. Then TEM samples were prepared on holey carbon grids in order to clearly expose the QD core of SiNP. We obtained HR-TEM image (Figure 4.46.a) that shows the 7 nm QDs were perfectly encapsulated in 35 nm silica nanoparticles. So in our next step 25 nm GNPs were added along with TEOS to grow additional layer of silica (Stöber method). Briefly, to the solution of QD-doped-SiNP (35 nm) in ethanol, citrate capped GNPs, tetraethylorthosilicate (TEOS) and ammonium hydroxide were added and the mixture was stirred at room temperature for 5 h. A control sample was prepared by adding same amount of water instead of GNP in the Stöber preparation. The resulting particles were centrifuged, cleaned and dispersed in water before preparing TEM samples. Figure 4.46.b shows the schematic illustration of QD and GNP co-encapsulated in a silica nanoparticle. TEM images (Figure 4.47) of the sample show that the QD-doped-SiNP and the GNPs are fused in a larger silica cluster. Here, unlike the previous microemulsion method, we were able to keep the QDs in 35 nm spherical SiNPs and bind 25 nm GNP close to it. But we were still unable to govern the number of GNPs per SiNPs in these larger silica clusters.

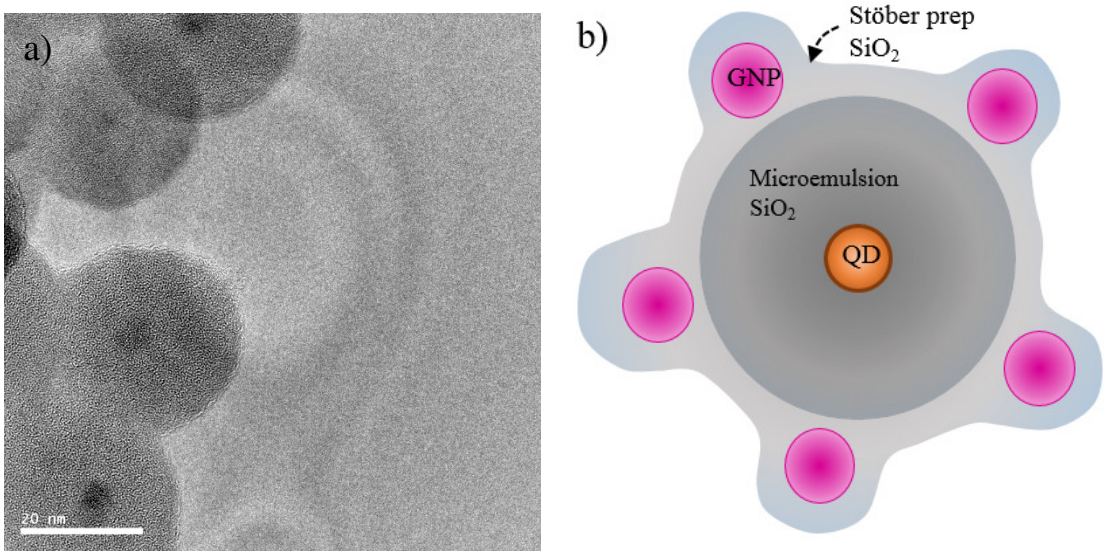

Figure 4.46. a) HR-TEM image of QD-doped-SiNP. b) Schematic illustration of aggregates of gold nanoparticles and quantum dots via additional growth of silica layer around the QD-doped-SiNP

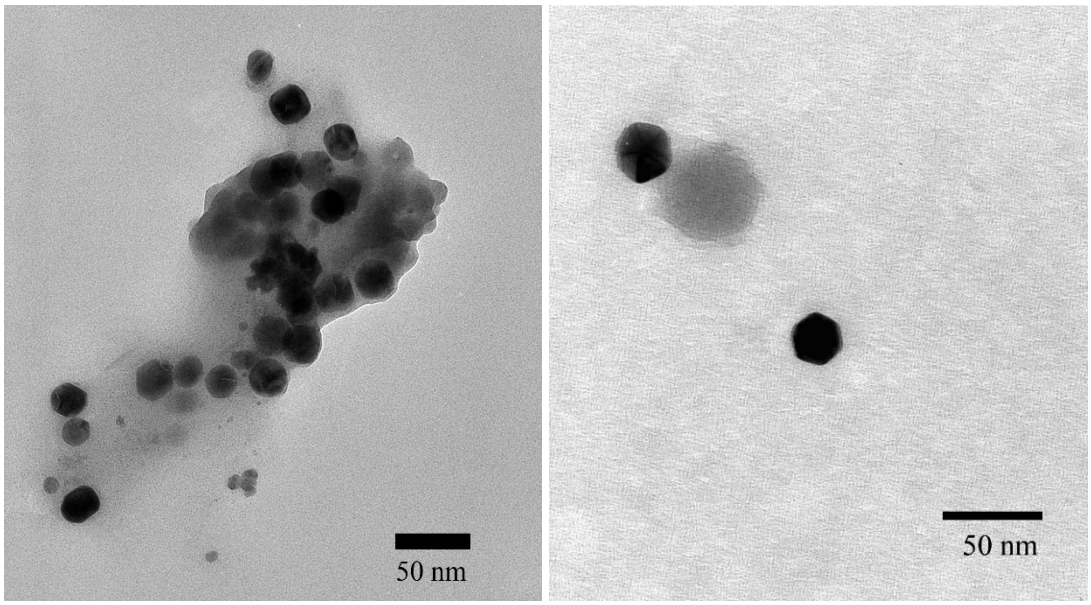

Figure 4.47. TEM images of GNPs aggregated on a QD-doped-SiNPs by additional growth of silica layer.

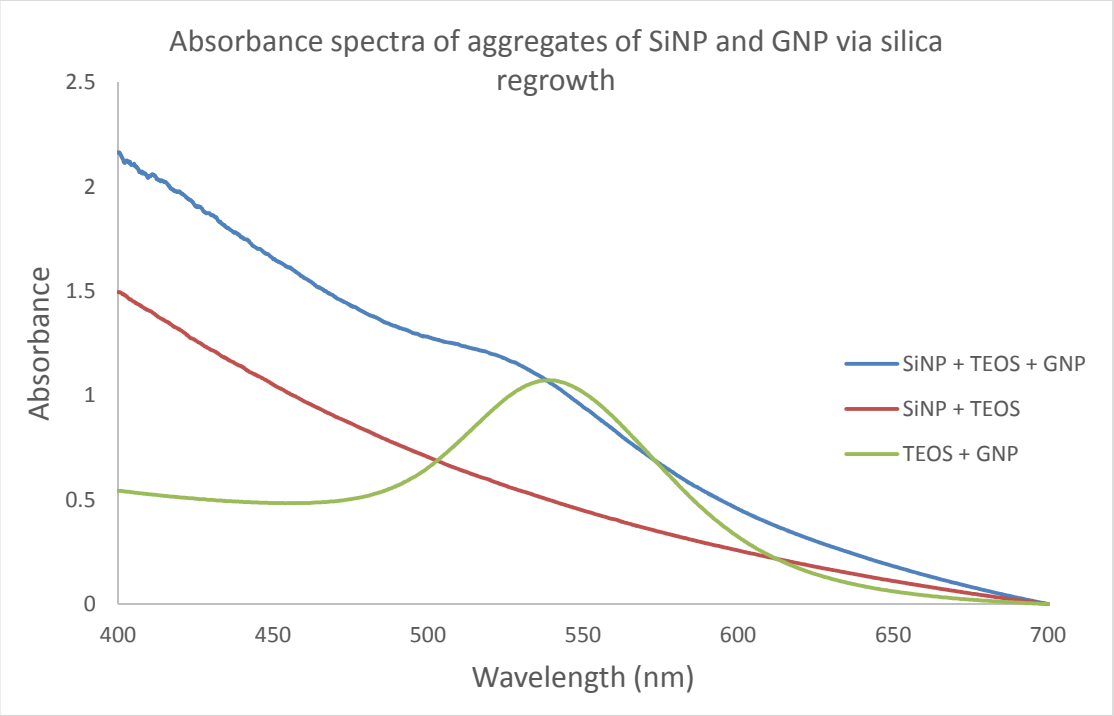

Figure 4.48. Absorbance spectra of GNPs aggregated on a QD-doped-SiNPs by additional growth of silica layer.

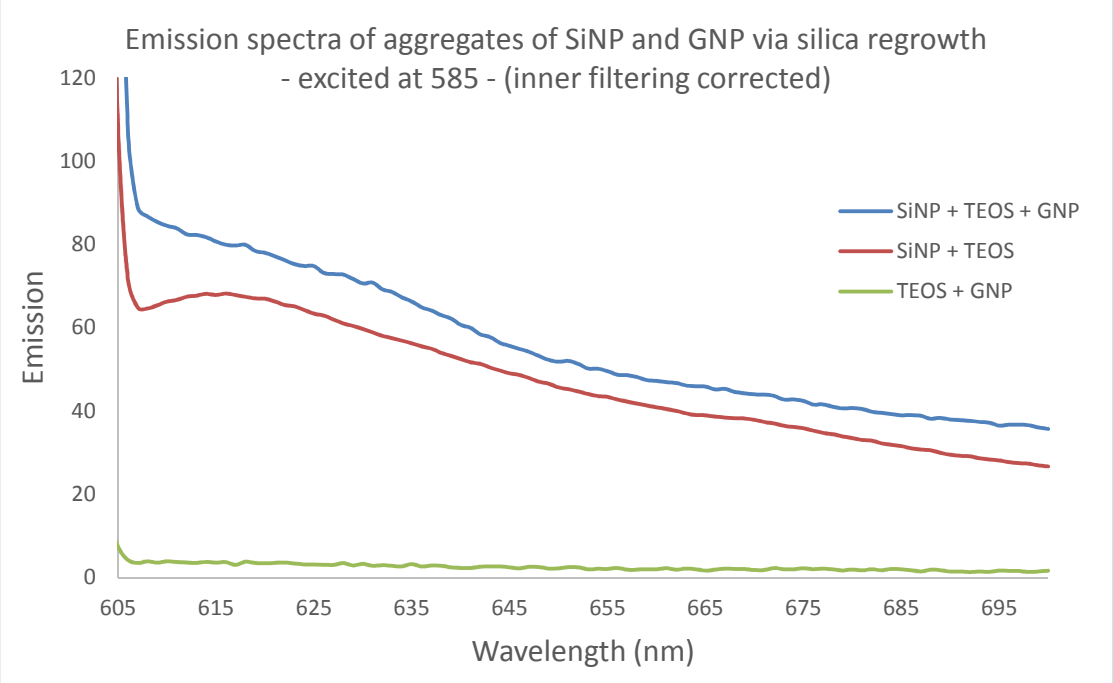

Figure 4.49. Emission spectra of GNPs aggregated on a QD-doped-SiNPs by additional growth of silica layer.

Absorbance spectra show an increase in absorbance at >600 nm (blue line in Figure 4.48) corresponds to the aggregation of GNPs. But it is uncertain what caused the blue shift of the free GNP's λ_{max} from ~540 to ~520 nm. We suspect that a thick silica coating around the GNP's surface might slightly affect the optical property of GNP. Emission spectra of the sample (blue line in Figure 4.49) shows a slight increase (16%) in fluorescence intensity when excited at 585 nm. This very less enhancement compared to that of propyl-DTC mediated aggregates may be due to the less number of GNPs per QD-doped-SiNP in the silica cluster.

We also investigated the effect of aggregating QD-doped-SiNP to a larger size GNP using Stöber type silica regrowth on the fluorescence intensity. For that we took the QD-doped-SiNPs previously synthesized by microemulsion method dissolved in ethanol and added 60 nm diameter GNPs in water, TEOS and ammonium hydroxide. The mixture was stirred at room temperature for 24 h and then centrifuged, cleaned and dispersed in water. Two controls were prepared by replacing QD-doped-SiNP solution with equal amount of ethanol in one control and GNP replacing with equal amount of milipore water in the other. Zoomed in TEM image (Figure 4.51) shows that the 35 nm QD-doped-SiNP were aggregated on the surface of 60 nm GNP as anticipated in the illustration (Figure 4.50). But this scene was not observed in the zoomed out view (Figure 4.51.b), rather a lack of uniform binding of SiNP and an unrestrained nature of aggregation were seen as the overall outcome. Once again we were unable to control the ratio of large GNP to QD-doped-SiNP in the silica mediated aggregates.

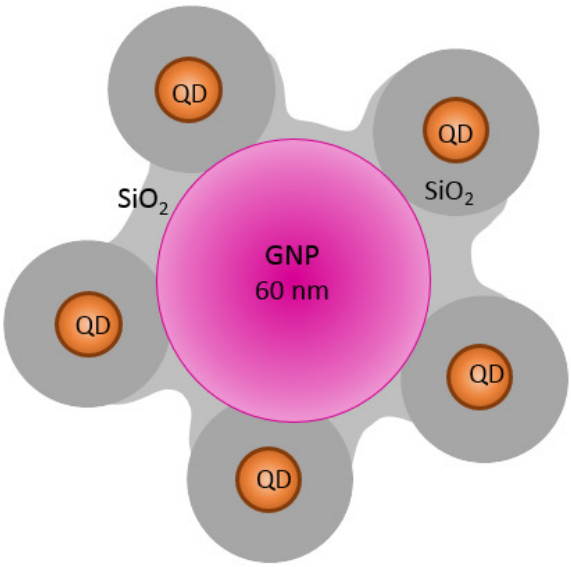

Figure 4.50. Schematic illustration of multiple quantum dots aggregated via silica layer growth on the silica coated 60 nm gold nanoparticle

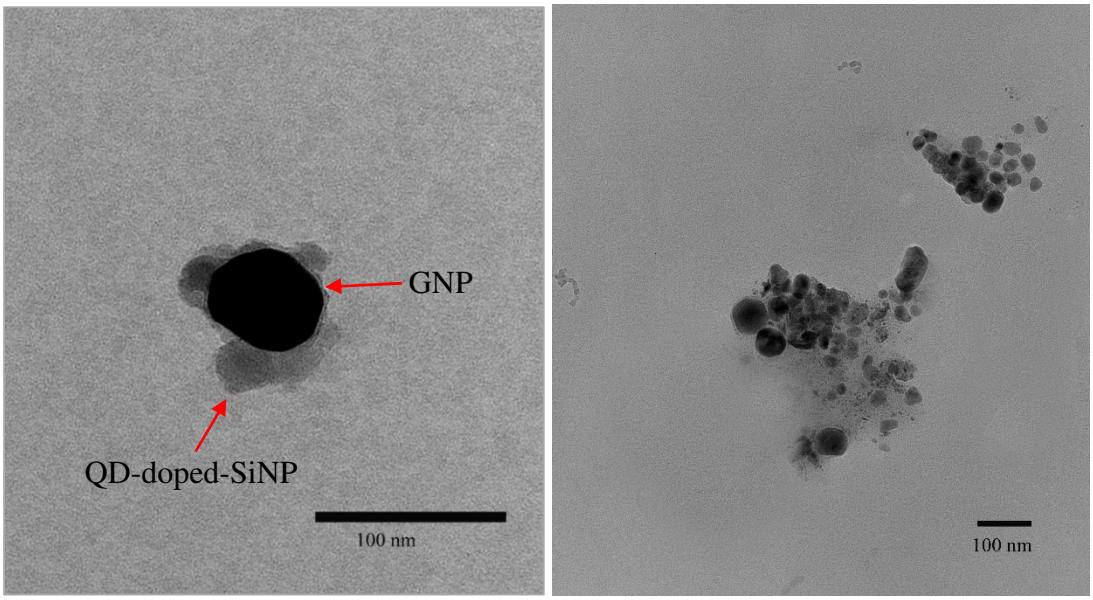

Figure 4.51. TEM images of aggregates of 60 nm GNP and previously synthesized QD-doped-SiNP via silica regrowth.

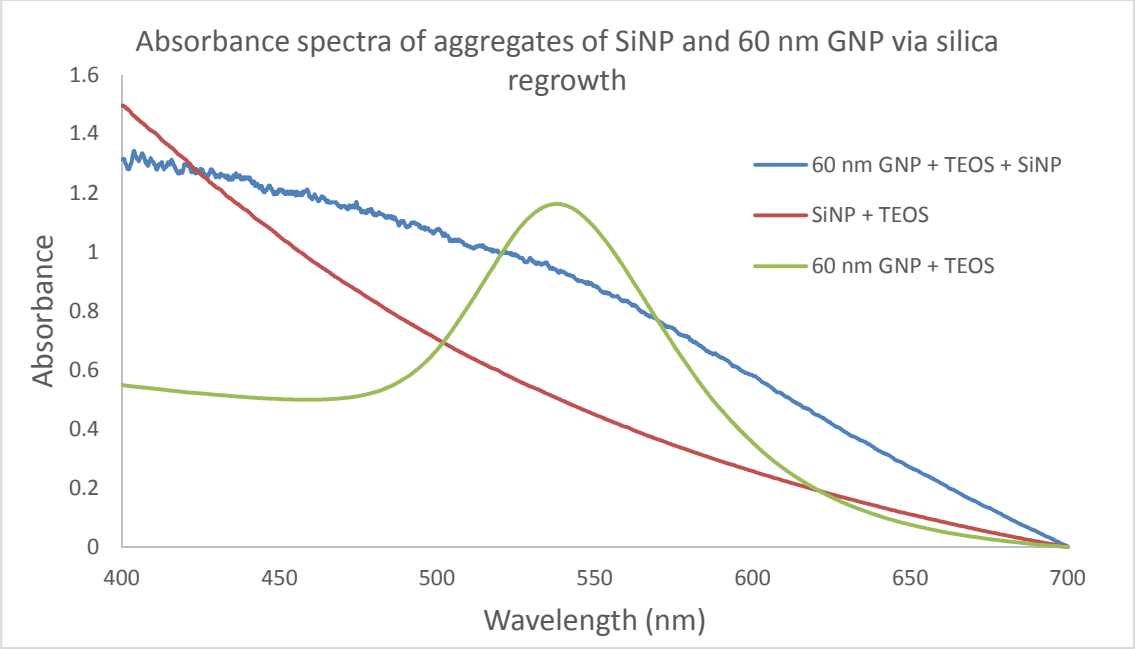

Figure 4.52. Absorbance spectra of aggregates of 60 nm GNP and previously synthesized QD-doped-SiNP via silica regrowth.

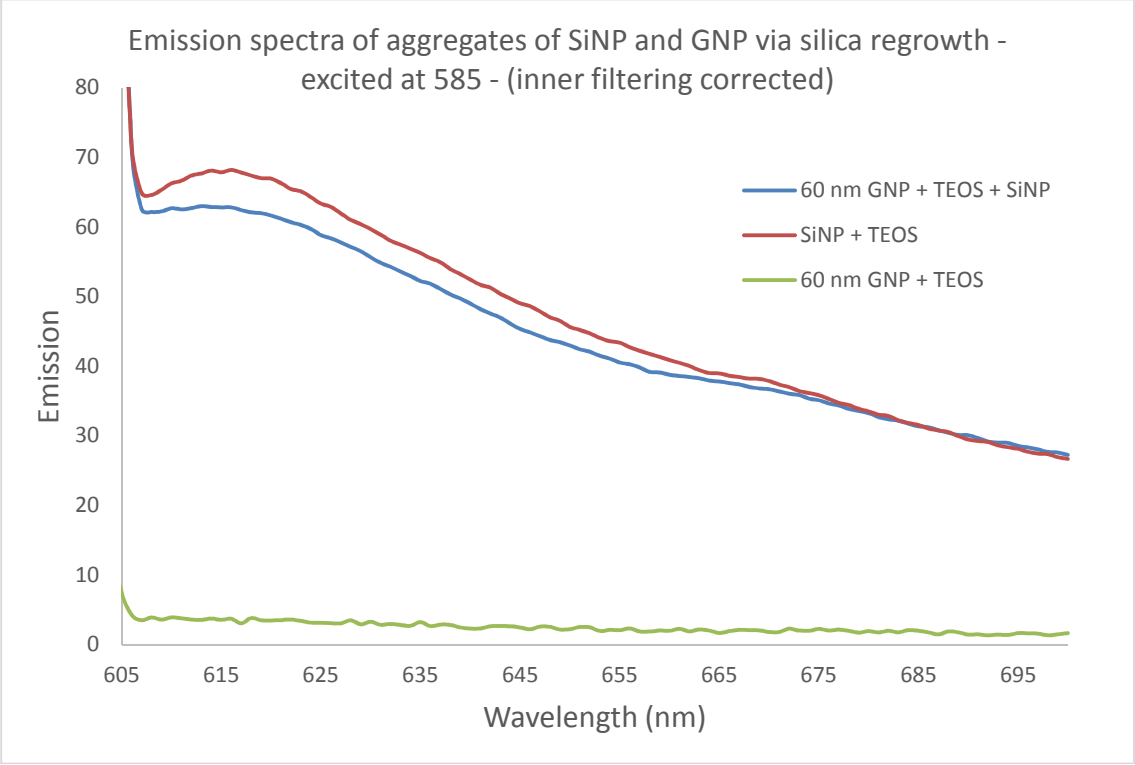

Figure 4.53. Emission spectra of aggregates of 60 nm GNP and previously synthesized QD-doped-SiNP via silica regrowth.

Larger gold nanoparticles possess stronger electric filed and should increase the enhancement to a large extend. Acuna et al., reported a 117-fold fluorescence enhancement from a dimer of 100 nm GNPs.[9] Compared to our previously reported enhancements from 25 nm GNPs, we expected a relatively higher degree of enhancement from 60 nm diameter GNPs. Absorption spectra show the increase in scattering at >600 nm the characteristic of aggregated GNPs, and decrease in scattering at ~550 nm that indicates a decrease in concentration of free GNPs (blue line). However the emission spectra show a slight drop in fluorescence intensity. That once again indicates the problem of uncontrolled aggregation. The silica regrowth to combine QD-doped-SiNP to larger size GNPs using Stöber method was not effectively creating best geometry throughout the solution.

4.4 Chapter Summary

This chapter details our effort to produce a metal-enhanced fluorescence (MEF) of gold nanoparticle and CdSe-ZnS quantum dot incorporated silica nanoparticle aggregates in aqueous solution. Our research group previously established a robust method of aggregating organic dye-doped-silica nanoparticles with gold nanoparticles via dithiocarbamate (DTC) linkage in aqueous solution and demonstrated a substantial florescence enhancement. [6a, 16] We investigated various parameters to produce a similar enhancement from CdSe-ZnS quantum dots, an inorganic fluorescent semiconductor. A notable enhancement of fluorescence brightness (3-fold) was measured after correcting the inner-filtering effects caused by the overwhelming concentration of gold nanoparticles in the samples.

We investigated the effect of relative concentration of gold nanoparticles to QD-doped-silica nanoparticles on the heteroaggregation in order to produce MEF. The TEM analysis of different volume ratios of GNP : QD-doped-SiNP, 8:1, 4:1, 2:1 and 1:1 suggests that the increase in relative concentration of GNP:SiNP increases the heteroaggregation. Absorbance spectra for all of those GNP:SiNP relative concentrations showed the appearance of shoulder peak >600 nm corresponds to the heteroaggregation of GNP with SiNP. The inner-filtering corrected emission spectra showed 294%, 192%, 171% and 107% fluorescence enhancement respectively for those different relative concentrations of GNP to SiNP. This results revealed that excess of gold to silica nanoparticle is needed to maximize the MEF.

We investigated different sizes of silica nanoparticles as a means of varying distance between the fluorophore core of SiNP and the GNP surface. Also SiNPs with

different surface area would accommodate different amounts of GNPs. TEM images revealed that SiNPs with 100 nm diameter aggregates to more number of GNPs (25 nm) compared to 35 nm SiNP. A significantly less fluorescence enhancement (0.3-fold) was obtained from the aggregates of 35 nm SiNPs with GNPs, compared to that (3-fold) of 100 nm SiNP with GNP.

We investigated various binding methods of quantum dots and gold nanoparticles to measure the change in MEF. QD-doped-silica nanoparticles were bound to GNPs using long-chain tetraethylene glycol (TEG) derivative with DTC moiety. TEM images showed that this long chain DTC binding did not form a robust aggregates, unlike the short chain propyl ligand. In our next method we attempted to co-encapsulate the quantum dots and GNPs in same silica nanoparticles by growing amorphous silica around them in a single pot. The reverse microemulsion method formed thin clouds of silica but the presence of QD in them was uncertain. The emission spectra showed a drop in fluorescence brightness due to the poor QD dispersion in the silica coating. The Stöber method of silica re-growth produced clusters of silica that contained both GNPs and QD-doped-SiNPs but in unrestrained ratio. However, the Stöber method showed only a slight enhancement of fluorescence (0.16 fold). Then we examined the effect of large gold nanoparticles on the MEF by aggregating the QD-doped-SiNPs to 60 nm diameter GNPs via silica regrowth. But again we were unable to control the ratio of SiNPs to GNPs in this method of aggregation and thus no fluorescence enhancement was observed.

Our experiments outlined in this chapter lay the foundation to produce metal-enhanced fluorescence in aqueous solution by creating high quality fluorophore to metal

heteroaggregates. The future study will focus on separating the metal-enhanced fluorescence (the signal) from the fluorescence of unbound QDs (the background) by optimizing the cleaning procedures and gaining more control over the aggregation process.

4.5 Experimental and Methods

4.5.2. Investigation of coupled plasmonic resonance of various size gold nanoparticles

QD-doped-SiNP preparation:[24] In a 500 mL RB flask, 270 mL of cyclohexane was taken. NP-5 (IGEPAL 520) surfactant (27 mL) was added to the solvent under vigorous stirring. The mixture was sonicated briefly, and 4.7 mL of CdSe-ZnS quantum dots in ODE was added under vigorous stirring and sonicated again. Then 2.2 mL of TEOS was added and stirred vigorously for 30 min. Finally 4.08 mL of ammonium hydroxide was added and the mixture was stirred for 20 h at room temperature. After 20 h of stirring the reaction mixture (150 mL) was taken out into a four centrifuge tubes, and 50 mL of acetone was added, vortexed, sonicated and centrifuged. The orange precipitate was washed with 1-butanol, isopropanol and 95% ethanol in sonication bath and centrifuged each time. Finally the CdSe-ZnS quantum dots doped silica nanoparticles were re-suspended in 30 mL of milipore water. TEM confirms the resulting clean particles had average diameter of 35 nm and had 7 nm diameter QD core

Silica shell re-growth:[16] Modified Stöber preparation was used to regrow additional layer of silica on the 35 nm silica particles. 20 mL scintillation vial was charged with QD-doped-SiNP (2 mL, 35 nm diameter) from previous step, water (7.2 mL), and a magnetic bar. L-arginine (3 mg) was added to the mixture. Cyclohexane (1 mL) was added to create a top organic layer. The vial was heated to about 60° before TEOS (0.8 mL) was added to the top layer. The vial was sealed and stirred slowly to avoid any perturbation of the top organic layer as much as possible, for 30 h at 60°. The resulted cloudy solution was cleaned via centrifugation, spinning at 15,000 rpm for 5 min and

replacing the supernatant with milipore water (5 mL, 17.8 MΩ). This cleaning cycle was repeated for three times. Finally the particles were re-suspended in milipore water.

Dialysis:[16] For further cleaning, the particles were dialyzed in milipore water using molecularporous membrane tubing MWCO : 12-14,000 (from Spectra/Por). The entire portion of QD-doped-SiNP from previous Stöber preparation was added to 5-6 inch strip of membrane tubing (one end was sealed with dialysis clamp) after it had been soaked in water for 15 min. After excess air was removed from the tubing, the second end was sealed with another dialysis clamp. To float the dialysis tube a small strip of Styrofoam was added to the top clamp. The assembly was then placed in a 4 L beaker filled with 3 L of milipore water and a magnetic stir bar. For every 12 h the water was replaced. After 4 days the freshly cleaned particles from the membrane tubing were diluted with water to 10 mL. TEM confirms the resulting silica particles had an average diameter of 100 nm.

Amine functionalization:[25] 15 mL centrifugation tube was charged with 100 nm diameter QD-doped-SiNP in 95% ethanol (8 mL), glacial acetic acid (20 μL) and (3-aminopropyl)-triethoxysilane (20 μL)and rotated for 20 h. The resulting mixture was centrifuged and the supernatant was replaced with 95% ethanol three times. Ninhydrin assay was used to monitor the concentration of amine in the supernatant each time. Finally the particles were re-suspended in 95% ethanol.

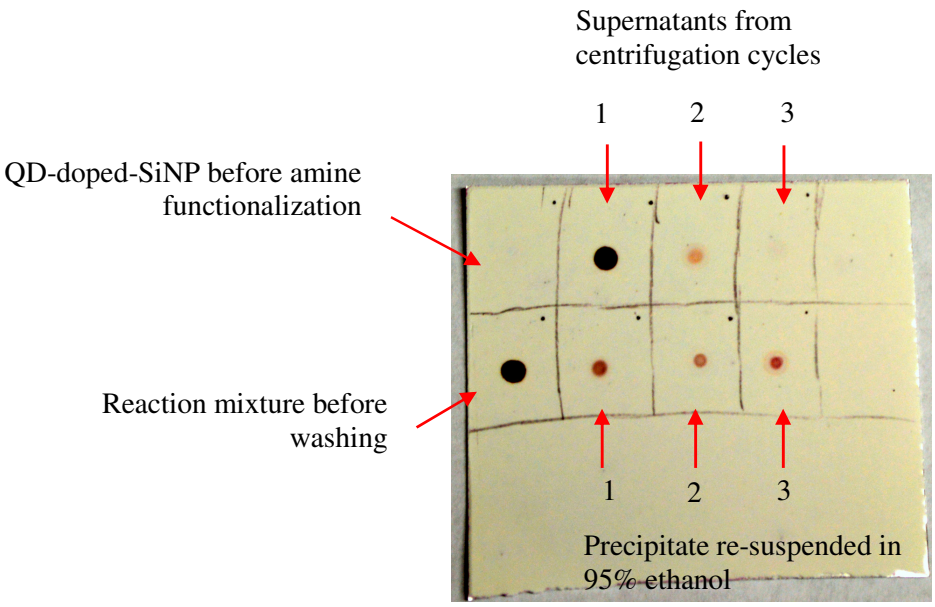

Figure 4.54. Ninhydrin assay to monitor the concentration of amine coating on 100 nm QD-doped-SiNP.

Aggregation of various size gold nanoparticle: A portion of amine functionalized QD-doped-SiNP (100 nm diameter) in 95% ethanol (2 mL) was taken in a scintillation vial and the pH was raised to 8.5-9 by adding concentrated KOH solution. Four 1.5 mL slim polystyrene cuvettes were charged with 100 µL of this silica particle solution. In a separate vial 1mM of CS_2 was prepared by dissolving CS_2 solution in 95% ethanol and the pH was raised to 8.5-9 by adding concentrated KOH. Then 50 µL of the CS_2 solution was added to the amine functionalized SiNP solution in each cuvette. The mixture was rotated for 30 min for DTC activation. Then to these cuvettes 400 µL of various size GNP (15 nm, 23 nm, 30 nm and 43 nm diameter) citrate stabilized in water solution was added, and the final volume was made up to 1 mL by adding milipore water. In separate cuvettes controls for this experiment were made by adding same amount of various size GNPs and CS_2 solution, but 100 µL of 95% ethanol instead of SiNP solution. The cuvettes were then tightly capped and sealed with parafilm. The

samples and controls were gently rotated for 6 h in dark at room temperature. Absorbance measurements were performed using Shimadzu Scientific Instruments UV-2101 PC UV-Vis scanning spectrometer.

Sample ID	APTES tethered QD-doped-SiNP (100 nm diameter)	APTES	1 mM CS_2	GNP (various diameters)	Milipore water
Sample 1	100 µL	0 µL	50 µL	400 µL (15 nm)	450 µL
Sample 2	100 µL	0 µL	50 µL	400 µL (23 nm)	450 µL
Sample 3	100 µL	0 µL	50 µL	400 µL (30 nm)	450 µL
Sample 4	100 µL	0 µL	50 µL	400 µL (43 nm)	450 µL
Control 1	0 µL	5 µL	50 µL	400 µL (15 nm)	545 µL
Control 2	0 µL	5 µL	50 µL	400 µL (23 nm)	545 µL
Control 3	0 µL	5 µL	50 µL	400 µL (30 nm)	545 µL
Control 4	0 µL	5 µL	50 µL	400 µL (43 nm)	545 µL

Table 4.1. Amounts of various sizes of GNPs added to SiNP.

4.5.2. Investigation of aggregation effect on fluorescence enhancement

Aggregation of GNP to QD-doped-SiNP: Amine functionalized QD-doped-SiNP (100 nm diameter) in 95% ethanol (2 mL) was taken in a scintillation vial and the pH was raised to 8.5-9 by adding concentrated KOH solution. A 1.5 mL slim polystyrene cuvettes was charged with 100 µL of this solution. In a separate vial 1mM of CS_2 was prepared by dissolving CS_2 solution in 95% ethanol and the pH was raised to 8.5-9 by adding concentrated KOH. Then 50 µL of the CS_2 solution was added to the amine functionalized SiNP solution in the cuvette. The mixture was rotated for 30 min for DTC activation. Then to these cuvettes 400 µL of GNP (23 nm diameter) citrate stabilized in water solution was added, and the final volume was made up to 1 mL by

adding milipore water. In separate cuvettes three controls were made as show in the table. The cuvettes were then tightly capped and sealed with parafilm. The samples and controls were gently rotated for 6 h in dark at room temperature. Absorbance measurements were performed using Shimadzu Scientific Instruments UV-2101 PC UV-Vis scanning spectrometer and fluorescence measurements were performed using Schimadzu Scientific Instruments RF 5301 PC spectrofluorophotometer. The excitation source of the instrument was a 150 W Xenon lamp.

Sample ID	QD-doped-SiNP (100 nm diameter)	APTES	1 mM CS_2	GNP (23 nm diameters)	Millipore water
Sample 1	100 µL (APTES tethered)	0 µL	50 µL	400 µL	450 µL
Control 1	100 µL (no APTES tether)	0 µL	50 µL	400 µL	450 µL
Control 2	0 µL	5 µL	50 µL	400 µL	545 µL
Control 3	100 µL (APTES tethered)	0 µL	50 µL	0 µL	850 µL

Table 4.2. Amounts of QD-doped-SiNPs, APTES, CS_2 and GNPs for MEF study.

Correction of inner-filtering effect: Primary and secondary inner filtering effects were corrected using the formulas obtained from the literature [tucker lit]. All fluorescence spectra shown in this dissertation are inner-filtering corrected.

$$I_F^{corr} = f_{prim} \times f_{sec} \times I_F^{obs}$$

Where,

$f_{prim} = I_F^{corr}/I_F^{obs} = [2.303\ A\ (Y - X)]\ /[10^{-AX} - 10^{-AY}]$

I_F^{corr} = corrected emission signal

I_F^{obs} = observed emission signal

A = absorbance (b = 1 cm) at λ_{ex}

$f_{sec} = I_F^{corr}/I_F^{obs} = [(V - U)\ (1/b) \ln T]/[T_{at\ V/b} - T_{at\ U/b}]$

I_F^{corr} = corrected emission signal

I_F^{obs} = observed emission signal

T = transmittance (b = 1 cm) at λ_{em}

$T_{at\ V/b}$ and $T_{at\ U/b}$ are the transmittance values calculated using Beer's law.

$T_{at\ v/b} = 10^{-A(v/b)}$ and $T_{at\ u/b} = 10^{-A(u/b)}$

To apply the above correction factors, the length of the excitation and emission window of the cuvette was measure. It was found that X = 0.05 cm, Y = 0.95 cm, and Y-X = 0.9 cm for the excitation path. And U = 0.3 nm, V = 0.7 nm, and V-U = 0.4 nm. Inner-filtering correction for fluorescence intensities of the samples and controls at 620 nm are shown below.

Sample ID	Absorbance at λ_{ex} = 575 nm	f_{prim}	Absorbance at λ_{em} = 620 nm	Transmittance at λ_{em} = 620 nm	f_{sec}
Sample 1	1.3227	3.4126	0.8653	0.1363	2.6376
Control 1	2.3478	6.4261	0.8984	0.1264	2.7345
Control 2	2.3821	6.5423	0.7288	0.1867	2.2713
Control 3	0.0128	1.0150	0.0083	0.9811	1.0096

Table 4.3. Calculation of primary and secondary inner-filtering effect

Sample ID	Sample Contains	Observed fluorescence I_F^{obs} at λ = 620 nm	Corrected fluorescence I_F^{corr} at λ = 620 nm
Sample 1	(SiNP-APTES) + CS_2 +GNP	5.9690	53.7289
Control 1	SiNP + CS_2 + GNP	2.9374	51.6176
Control 2	GNP + APTES + CS_2	0.4621	5.3806
Control 3	(SiNP-APTES) + CS_2	17.979	18.4238

Table 4.4. Correction of inner-filtering effect of observed fluorescence

4.5.3. Investigation of relative concentration effect between SiNP and GNP on fluorescence intensity

Amine functionalized QD-doped-SiNP (100 nm diameter) in 95% ethanol (4 mL) was taken in a scintillation vial and the pH was raised to 8.5-9 by adding concentrated KOH solution. Four 1.5 mL polystyrene cuvettes were charged with 50 µL, 100 µL, 200 µL and 400 µL of this solution. In a separate vial 1mM of CS_2 was prepared by dissolving CS_2 solution in 95% ethanol and the pH was raised to 8.5-9 by adding concentrated

KOH. Then 50 μL of the CS_2 solution was added to the amine functionalized SiNP solution in the cuvette. The mixture was rotated for 30 min for DTC activation. Then to these cuvettes 400 μL of GNP (23 nm diameter) citrate stabilized in water solution was added, and the final volume was made up to 1 mL by adding milipore water. In separate cuvettes three controls were made as show in the table. The cuvettes were then tightly capped and sealed with parafilm. The samples and controls were gently rotated for 6 h in dark at room temperature.

Sample ID	APTES tethered QD-doped-SiNP (100 nm diameter)	1 mM CS_2	GNP (various diameters)	Milipore water
Sample 1	50 μL	50 μL	400 μL	500 μL
Sample 2	100 μL	50 μL	400 μL	450 μL
Sample 3	200 μL	50 μL	400 μL	350 μL
Sample 4	400 μL	50 μL	400 μL	150 μL
Control 1a	50 μL (no APTES)	50 μL	400 μL	500 μL
Control 2a	100 μL (no APTES)	50 μL	400 μL	450 μL
Control 3a	200 μL (no APTES)	50 μL	400 μL	350 μL
Control 4a	400 μL (no APTES)	50 μL	400 μL	150 μL
Control 1b	50 μL	50 μL	0 μL	900 μL
Control 2b	100 μL	50 μL	0 μL	850 μL
Control 3b	200 μL	50 μL	0 μL	750 μL
Control 4b	400 μL	50 μL	0 μL	550 μL
Control 5	0 μL	50 μL	400 μL	550 μL

Table 4.5. Various amounts of SiNP added to constant amounts of GNP for investigating relative concentration effect on MEF

4.5.4. Investigation of effect of silica nanoparticle size on fluorescence intensity of SiNP-GNP aggregates

A portion of amine functionalized QD-doped-SiNP (35 nm diameter) in 95% ethanol (2 mL) was taken in a scintillation vial and the pH was raised to 8.5-9 by adding concentrated KOH solution. A 1.5 mL slim polystyrene cuvettes was charged with 100 µL of this solution. In a separate vial 1mM of CS_2 was prepared by dissolving CS_2 solution in 95% ethanol and the pH was raised to 8.5-9 by adding concentrated KOH. Then 50 µL of the CS_2 solution was added to the amine functionalized SiNP solution in the cuvette. The mixture was rotated for 30 min for DTC activation. Then to these cuvettes 400 µL of GNP (25 nm diameter) citrate stabilized in water solution was added, and the final volume was made up to 1 mL by adding milipore water. In separate cuvettes three controls were made as show in the table. The cuvettes were then tightly capped and sealed with parafilm. The samples and controls were gently rotated for 6 h in dark at room temperature.

Sample ID	APTES tethered QD-doped-SiNP (35 nm diameter)	APTES	1 mM CS_2	GNP (25 nm diameters)	Millipore water
Sample 1	50 µL	0 µL	50 µL	400 µL	500 µL
Control 1	0 µL	5 µL	50 µL	400 µL	545 µL
Control 2	50 µL	0 µL	50 µL	0 µL	900 µL

Table 4.6. Amounts of 35 nm SiNP and 25 nm GNP

4.5.5. Investigation of effect of linkage between silica nanoparticles and gold nanoparticles on fluorescence intensity

Synthesis of mono-tosyl TEG:

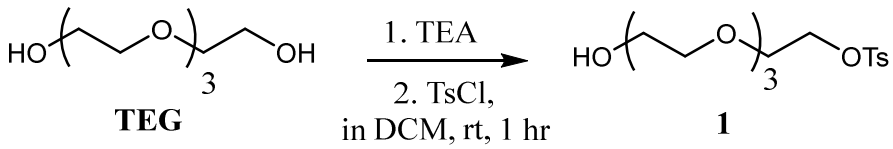

In a 200 mL round bottom flask equipped with a magnetic stir bar, triethylamine (TEA) (17.8 mL, 0.05 mol), tetraethylene glycol (TEG) (20 g, 0.1 mol) and dichloromethane (DCM) (75 mL) were added. The mixture was stirred for about 5 min before the addition of tosyl chloride (TsCl) (1.9 g, 10 mmol) dissolved in DCM (20 mL). The reaction mixture was stirred for 1 h at room temperature. After the reaction was completed the organic material was extracted using saturated $NaHCO_3$ solution (~30 mL) with DCM (15 mL, 3X). The extracted organic portion was washed with NaCl solution (~20 mL) and the organic portion (DCM) was collected and dried over anhydrous sodium sulfate (Na2SO4). The solvent was removed under vacuum to get a yellow oil. The product was purified by flash silica column chromatography (2% methanol in DCM) (Rf= 0.2) to give a pure monotosylated TEG (5.2 g, 57%). ^{1}H NMR (300 MHz, $CDCl_3$): δ 7.80 (d, 2H, J = 8 Hz), 7.35 (d, 2H, J = 8 Hz), 4.16 (t, 2H, J = 10 Hz, 5 Hz), 3.65 (m, 14H), 2.56 (s, 1H) and 2.44 (s, 3H).

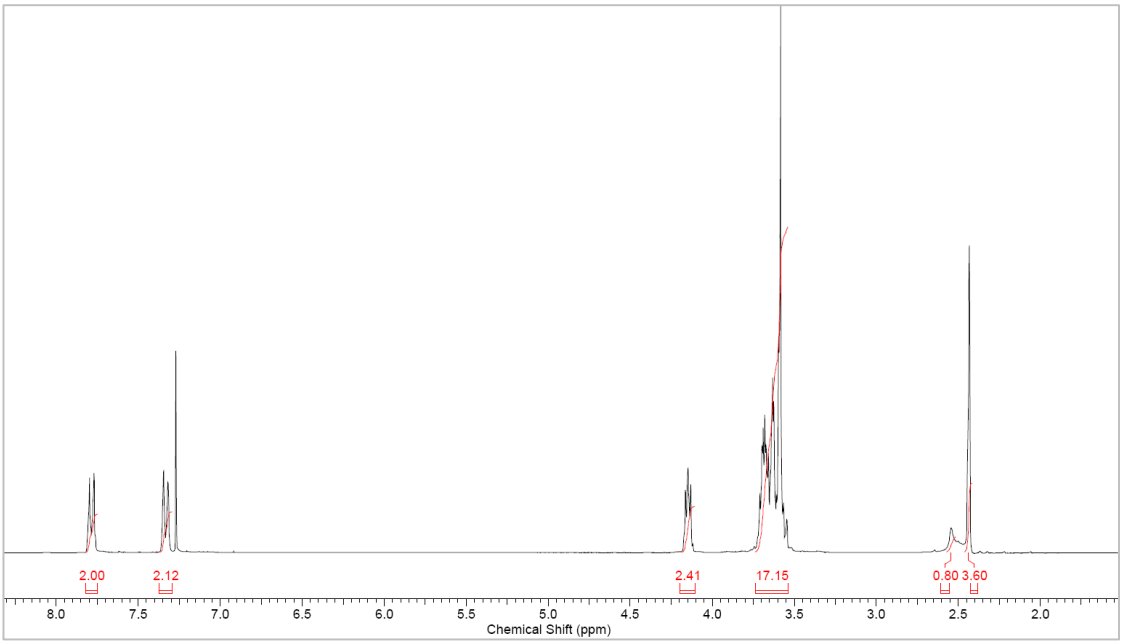

Figure 4.55. ^{1}H NMR of monotosyl TEG (300 MHz).

Synthesis of azide TEG:[26]

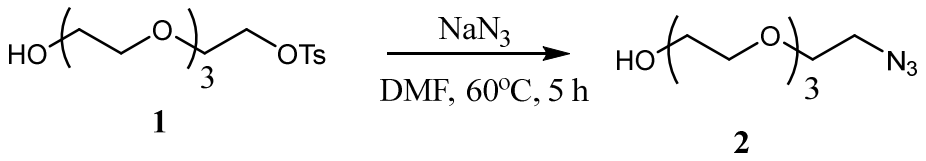

1 **2**

A 100 mL round bottom flask was charged with a magnetic stir bar and monotosyl TEG **1** (4.6 g, 0.013 mol) dissolved in anhydrous dimethylformamide (DMF) (50 mL). To the mixture sodium azide (NaN3) (4.29 g, 0.066 mol) was added and heated the reaction flask to 60 ºC under N_2 atmosphere. After 5 h of reaction the DMF was removed in vacuum. Organic material was extracted by saturated $NaHCO_3$ solution (~30 mL) with DCM (15 mL, 3X). The extracted organic portion was washed once with NaCl solution (~15 mL) before the organic portion was dried over anhydrous sodium sulfate (Na_2SO_4). Then the solvent was removed under vacuum to yield the azide TEG as a yellow oil (1.8 g, 63%). ^{1}H NMR (300 MHz, $CDCl^3$): δ 3.67 (m, 14H), 3.39 (t, 2H, J = 10 Hz, 5 Hz) and 2.22 (s, 1H).

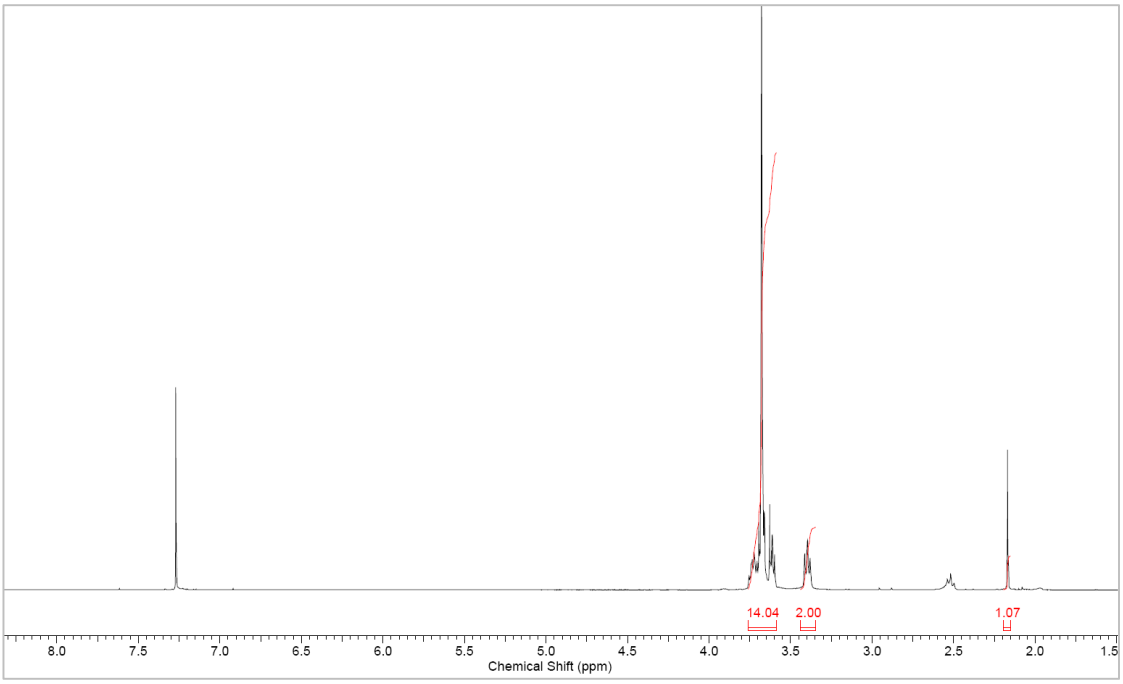

Figure 4.56. ^{1}H NMR of azide TEG (300 MHz)

Synthesis of azide TEG siloxane and silica coating:[27]

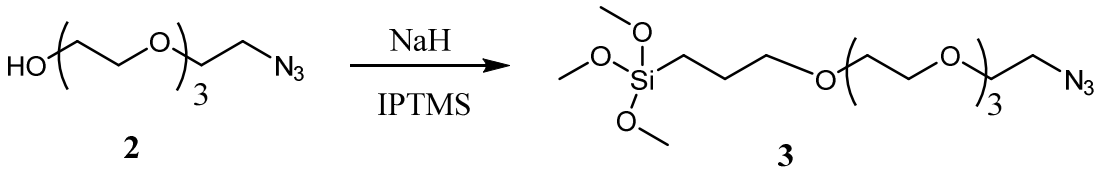

2 **3**

Sodium hydride (2 mg, 0.045 mmol, 60% mineral oil) was cleaned by washing with petroleum ether (2 mL) three times under N_2 atmosphere in a flame dried 50 mL round bottom flask. Previously synthesized azide TEG (10 mg, 0.045 mmol) dissolved in THF (18 mL) was added to the flask containing a magnetic stir bar and the clean NaH. The mixture was stirred for 10 min at room temperature before (3-iodopropyl)-trimethoxysilane (IPTMS) (0.19 mL, 0.95 mmol) was added. Then the reaction mixture was heated to 70 °C for 20 h under N_2 atmosphere. After the reaction was over THF was removed by vacuum to yield a dark green oil. The product was silica and air sensitive. So without further purification the product was carried out to attach with

silica nanoparticles. Previously synthesized QD-doped-SiNP (1 mL, 100 nm) was taken in a microcentrifuge tube, and glacial acetic acid (20 µL) was added to that. The mixture was gently shaken before adding the azide TEG siloxane (20 µL). The tube was rotated for 12 h at room temperature in dark. Then the azide-TEG coated SiNP were cleaned by centrifugation three times and the supernatant was replaced with 95% ethanol each time. Finally the particles were re-suspended in 95% ethanol (1.5 mL).

Amine functionalization of TEG SiNP:

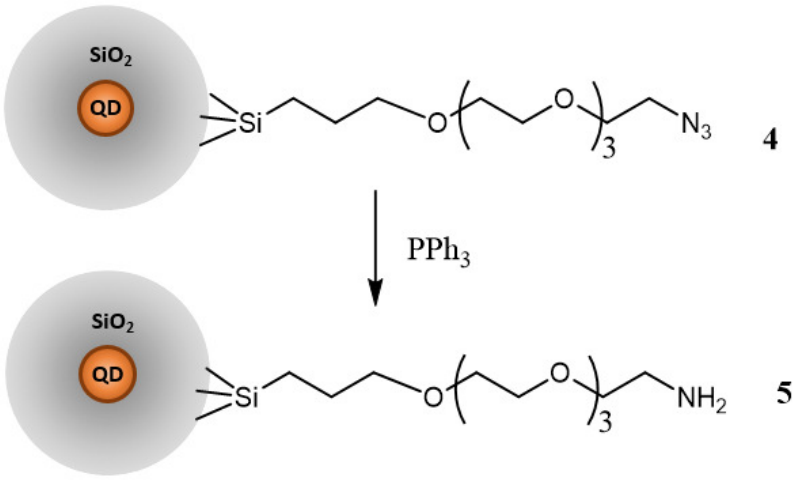

Azide TEG-coated SiNP (1 mL) suspended in 95% ethanol was taken in a 10 mL round bottom flask, charged with a magnetic stir bar and added triphenylphosphine (TPP) (26 mg, 0.095 mmol) dissolved in 95% ethanol (5 mL). An air condense was attached to the flask and refluxed at 70 ºC under N_2 atmosphere for 2 h. Solvent was removed in vacuum and added two drops of HCl (1M) and toluene (250 µL) to yield the free amine. The particles were centrifuged three times for 10 min at 15,000 rpm. Each time the supernatant was removed and the particles were re-suspended in 95% ethanol (1.5 mL). Ninhydrin assay was performed to confirm the presence of free amine on the particles.

Aggregation of GNP to SiNP using modified longer TEG ligand: Procedure given in section **4.5.2** was followed using the materials and amounts given in the table to prepare the sample and controls. The reaction was allowed to go for 24 h since the slow rate of displacing the long chain on GNP by DTC.

Sample ID	TEG coated QD-doped-SiNP (100 nm diameter) pH = 8.5-9	1 mM CS_2 pH = 8.5-9	Water stabilized GNP (25 nm diameters)	Millipore water
Sample 1	100 μL	50 μL	400 μL	450 μL
Control 1	0 μL	50 μL	400 μL	550 μL
Control 2	100 μL	50 μL	0 μL	850 μL

Table 4.7. Amounts of TEG-coated-SiNP and water stabilized GNPs

Aggregation of GNP to QD via single pot microemulsion method: A 25 mL round bottom flask was charged with cyclohexane (5 mL), previously synthesized CdSe-ZnS quantum dots (0.1 mL) and a magnetic stir bar. Then IGEPAL 520 surfactant (0.5 mL) was added to the flask and vigorously stirred to form microemulsion. Tetraethlyorthosilicate (TEOS) (0.05 mL) was added to them mixture and vigorously stirred for 30 min. Then gold nanoparticles (25 nm diameter, 0.4 mL) was added to the same flask and finally ammonium hydroxide (33%, 0.4 mL) was added to condense the silica precursor to form amorphous silica polymer around the QD and GNP. The reaction was stirred for 24 h in dark at room temperature Acetone was added to the reaction mixture to break the microemulsion, and the particles was washed cleaned by

centrifugation for 20 min at 4000 rpm. Supernatant was removed and the particles were suspended in pure solvents. The process were repeated for two times in each different solvents 1-butanol, isopropanol, and ethanol. Finally the clean particles were suspended in milipore water (1.5 mL, 17.8Ω). Controls were made by adding the same amount of milipore water instead of GNP solution.

Aggregation of GNP to SiNP via silica regrowth: QD-doped-SiNPs (35 nm diameter, 0.5 mL) previously synthesized by microemulsion method were suspended in ethanol and taken in a scintillation vial. Gold nanoparticles (25 nm diameter, 0.5 mL) and tetraethylorthosilicate (TEOS, 50 μL) were added to the vial. Then finally ammonium hydroxide (100 μL) was added to condense the silica precursor encapsulating the QD-doped-SiNP and GNP. There mixture was mixed for 24 h in a shaker at room temperature in dark condition. Then the particles were cleaned in three cycles of 10 min centrifugation at 15,000 rpm and the supernatant was replaced with ethanol each time. Finally the clean particles were re-suspended in milipore water (1.5 mL).

Aggregation of SiNP to larger size GNP: Gold nanoparticles (60 nm diameter, 0.5 mL) previously synthesized by microemulsion method were suspended in ethanol and taken in a scintillation vial. QD-doped-SiNPs (35 nm diameter, 0.5 mL) and tetraethylorthosilicate (TEOS, 50 μL) were added to the vial. Finally ammonium hydroxide (100 μL) was added to condense the silica precursor encapsulating the QD-doped-SiNP and GNP. There mixture was mixed for 24 h in a shaker at room temperature in dark condition. Then the particles were cleaned in three cycles of 10 min centrifugation at 15,000 rpm and the supernatant was replaced with ethanol each time. Finally the clean particles were re-suspended in milipore water (1.5 mL).

4.5.6. TEM parameters and sample preparation

Transition electron microscopy (TEM) imaging was performed on two different microscopes at University of Oklahoma Samuel Roberts Nobel Electron Microscopy Laboratory. Most of the images were obtained from Ziess 10A Conventional microscope operating at 80 kV from a tungsten filament source were uses. High resolution TEM images were obtained from JEOL 2010-F operating at 200 kV from Field Emission Gun (FEG) source. Samples from aggregation studies were prepared by drop coating 4 μL of diluted sample onto a 300 mesh formvar coated copper TEM gird (from Ted Pella Corp.) and allowing to air dry. Samples form surface modification of quantum dots were prepared by drop coating 4 μL of diluted samples onto a 200 mesh Lacey F/C gird (Ted Pella Corp.) and allowing to air dry.

4.6. References

1. (a) Jackson, J. B.; Halas, N. J., Surface-enhanced Raman scattering on tunable plasmonic nanoparticle substrates. *Proc. Natl. Acad. Sci. U. S. A.* **2004,** *101* (52), 17930-17935; (b) Moula, G.; Aroca, R. F., Plasmon-Enhanced Resonance Raman Scattering and Fluorescence in Langmuir-Blodgett Monolayers. *Anal. Chem. (Washington, DC, U. S.)* **2011,** *83* (1), 284-288.

2. Dragan, A. I.; Golberg, K.; Elbaz, A.; Marks, R.; Zhang, Y.; Geddes, C. D., Two-color, 30 second microwave-accelerated Metal-Enhanced Fluorescence DNA assays: A new Rapid Catch and Signal (RCS) technology. *J. Immunol. Methods* **2011,** *366* (1-2), 1-7.

3. Deceglie, M. G.; Ferry, V. E.; Alivisatos, A. P.; Atwater, H. A., Design of Nanostructured Solar Cells Using Coupled Optical and Electrical Modeling. *Nano Lett.* **2012,** *12* (6), 2894-2900.

4. (a) Aslan, K.; Gryczynski, I.; Malicka, J.; Matveeva, E.; Lakowicz, J. R.; Geddes, C. D., Metal-enhanced fluorescence: an emerging tool in biotechnology. *Curr. Opin. Biotechnol.* **2005,** *16* (1), 55-62; (b) Sweatlock, L. A.; Maier, S. A.; Atwater, H. A.; Penninkhof, J. J.; Polman, A., Highly confined electromagnetic fields in arrays of strongly coupled Ag nanoparticles. *Phys. Rev. B: Condens. Matter Mater. Phys.* **2005,** *71* (23), 235408/1-235408/7.

5. Lakowicz, J. R.; Geddes, C. D.; Gryczynski, I.; Malicka, J.; Gryczynski, Z.; Aslan, K.; Lukomska, J.; Matveeva, E.; Zhang, J.; Badugu, R.; Huang, J., Advances in Surface-Enhanced Fluorescence. *J. Fluoresc.* **2004,** *14* (4), 425-441.

6. (a) Gunawardana, K. B., Study of metal-enhanced fluorescence of dye doped silica nanoparticles. *Uinversity of Oklahoma* **2012**; (b) Hao, E.; Schatz, G. C., Electromagnetic fields around silver nanoparticles and dimers. *J. Chem. Phys.* **2004,** *120* (1), 357-366.

7. Lakowicz, J. R.; Ray, K.; Chowdhury, M.; Szmacinski, H.; Fu, Y.; Zhang, J.; Nowaczyk, K., Plasmon-controlled fluorescence: a new paradigm in fluorescence spectroscopy. *Analyst (Cambridge, U. K.)* **2008,** *133* (10), 1308-1346.

8. Lakowicz, J. R.; Gryczynski, I.; Malicka, J.; Gryczynski, Z.; Geddes, C. D., Enhanced and localized multiphoton excited fluorescence near metallic silver islands: metallic islands can increase probe photostability. *J. Fluoresc.* **2002,** *12* (3/4), 299-302.

9. Acuna, G. P.; Moeller, F. M.; Holzmeister, P.; Beater, S.; Lalkens, B.; Tinnefeld, P., Fluorescence Enhancement at Docking Sites of DNA-Directed Self-Assembled Nanoantennas. *Science (Washington, DC, U. S.)* **2012,** *338* (6106), 506-510.

10. Lazarides, A. A.; Schatz, G. C., DNA-Linked Metal Nanosphere Materials: Structural Basis for the Optical Properties. *J. Phys. Chem. B* **2000,** *104* (3), 460-467.

11. Halas, N. J., Plasmonics: An Emerging Field Fostered by Nano Letters. *Nano Lett.* **2010,** *10* (10), 3816-3822.

12. Hartland, G. V.; Schatz, G., Virtual Issue: Plasmon Resonances - A Physical Chemistry Perspective. *J. Phys. Chem. C* **2011,** *115* (31), 15121-15123.

13. Zhang, J.; Fu, Y.; Chowdhury, M. H.; Lakowicz, J. R., Metal-Enhanced Single-Molecule Fluorescence on Silver Particle Monomer and Dimer: Coupling Effect between Metal Particles. *Nano Lett.* **2007,** *7* (7), 2101-2107.

14. Folmar, M.; Shtoyko, T.; Fudala, R.; Akopova, I.; Gryczynski, Z.; Raut, S.; Gryczynski, I., Metal enhanced fluorescence of Me-ADOTA·Cl dye by silver triangular nanoprisms on a gold film. *Chem. Phys. Lett.* **2012,** *531*, 126-131.

15. Geddes, C. D., Metal-enhanced fluorescence. *Phys. Chem. Chem. Phys.* **2013,** *15* (45), 19537.

16. Green, N. S., Plasmonic Properties of Enhanced Fluorescence of Gold and Dye-doped SIlica Nanoparticles Aggregates. **2013**.

17. Chen, Y.; Munechika, K.; Jen-La Plante, I.; Munro, A. M.; Skrabalak, S. E.; Xia, Y.; Ginger, D. S., Excitation enhancement of CdSe quantum dots by single metal nanoparticles. *Appl. Phys. Lett.* **2008,** *93* (5), 053106/1-053106/3.

18. Bharadwaj, P.; Novotny, L., Spectral dependence of single molecule fluorescence enhancement. *Opt. Express* **2007,** *15* (21), 14266-14274.

19. Munechika, K.; Chen, Y.; Smith, J. M.; Ginger, D. S. In *Importance of spectral overlap: fluorescence enhancement by single metal nanoparticles*, John Wiley & Sons, Inc.: 2010; pp 91-118.

20. Aslan, K.; Malyn, S. N.; Geddes, C. D., Angular-dependent metal-enhanced fluorescence from silver island films. *Chem. Phys. Lett.* **2008,** *453* (4-6), 222-228.

21. Bastus, N. G.; Comenge, J.; Puntes, V., Kinetically Controlled Seeded Growth Synthesis of Citrate-Stabilized Gold Nanoparticles of up to 200 nm: Size Focusing versus Ostwald Ripening. *Langmuir* **2011,** *27* (17), 11098-11105.

22. Hardison, D.; Deepthike, H. U.; Senevirathna, W.; Pathirathne, T.; Wells, M., Temperature-sensitive microcapsules with variable optical signatures based on incorporation of quantum dots into a highly biocompatible hydrogel. *J. Mater. Chem.* **2008,** *18* (44), 5368-5375.

23. Tucker, S. A.; Amszi, V. L.; Acree, W. E., Jr., Primary and secondary inner filtering: effect of potassium dichromate on fluorescence emission intensities of quinine sulfate. *J. Chem. Educ.* **1992,** *69* (1), A8, A11-A12.

24. Darbandi, M.; Thomann, R.; Nann, T., Single quantum dots in silica spheres by microemulsion synthesis. *Chem. Mater.* **2005,** *17* (23), 5720-5725.

25. Darbandi, M.; Urban, G.; Krueger, M., Bright luminescent, colloidal stable silica coated CdSe/ZnS nanocomposite by an in situ, one-pot surface functionalization. *J. Colloid Interface Sci.* **2012,** *365* (1), 41-45.

26. Shirude, P. S.; Kumar, V. A.; Ganesh, K. N., BisPNA targeting to DNA: Effect of neutral loop on DNA duplex strand invasion by aepPNA-N7GlaepPNA-C substituted peptide nucleic acids. *Eur. J. Org. Chem.* **2005,** (24), 5207-5215.

27. Zamadar, M.; Ghosh, G.; Mahendran, A.; Minnis, M.; Kruft, B. I.; Ghogare, A.; Aebisher, D.; Greer, A., Photosensitizer Drug Delivery via an Optical Fiber. *J. Am. Chem. Soc.* **2011,** *133* (20), 7882-7891.